DEVELOPMENT AND CHARACTERISATION OF NOVEL STRUCTURAL COMPOSITES FROM RECYCLED MATERIALS

By

Adeayo Olubunmi Sotayo BEng (Hons)

This thesis is submitted in partial fulfilment of the requirements for the degree of Doctor of Philosophy

October 2016

Engineering Department, Lancaster University

This project was supported by the Centre for Global Eco-Innovation and is partly financed by the European Regional Development Fund.

EUROPEAN UNION
Investing in Your Future
European Regional Development Fund 2007-13

www.cgeinnovation.org

Declaration

I declare that this thesis is my own work and has not been submitted in substantially the same form for the award of a higher degree elsewhere.

Adeayo Olubunmi Sotayo

Abstract

Carpets are composite materials and, like many composite materials, waste carpet is both difficult and expensive to recycle because of the complicated, multi-stage processes involved. In the UK, approximately 400,000 tonnes of carpet waste are sent to landfill annually. However, the landfill option is becoming uneconomic due to increasing landfill charges, the reduction in landfill sites and changes in environmental legislation.

This project, in collaboration with ECO2 Enterprises, aimed to avoid the landfill option and develop novel structural composites from carpet waste, which could be used to replace timber and PVC posts and rails in equestrian fencing. The development of these composites is a recycling approach that makes use of carpet waste which would otherwise be sent to landfill thereby increasing environmental pollution. The study encompasses the investigation of relevant material and mechanical properties and processing characteristics of the prototype novel waste carpet composites both as a structural beam and an assembled fencing system. Details of the manufacturing processes of the novel waste carpet structural composites are described. Extensive experimental testing has been carried out to determine and compare the mechanical properties of the novel waste carpet structural composites to timber and PVC materials.

In addition, experimental load tests and Finite Element (FE) analysis on typical equestrian timber and PVC post and rail fencing structures (benchmark data) were carried out to evaluate their stiffness characteristics against corresponding characteristics for a similar fencing structure comprised of the novel waste carpet structural composites. Design optimisation via geometric changes and FE analyses showed that a 69 % increase in the depth (from 71 to 120 mm) of the novel waste carpet composite posts resulted in a transverse stiffness similar to that of the timber fence. The results obtained from this study has demonstrated that the mechanical properties of the novel structural composites could potentially serve as an alternative/replacement for some common materials used in structural applications, such as timber and PVC fencing.

Publications

Sotayo, A., Green, S. and Turvey, G., (2016). Experimental and Finite Element (FE) Modelling of Timber Fencing for Benchmarking Novel Composite Fencing. Composite Structures, 158, pp 44-55

Sotayo, A., Green, S. M., & Turvey, G. J. (2016). Benchmark testing and Finite Element (FE) analysis of timber fencing for replacement by novel composite materials. In A. Ferreira, A. Neves, E. Viola, F. Tornabene, & N. Fantuzzi (Eds.), 2nd International Conference on Mechanics of Composites, Porto. July 2016.

Sotayo, A., Green, S. and Turvey, G., (2016). Mechanical Investigation of Novel Composites Fabricated from Waste Materials. Lancaster University Postgraduate Research Conference. May 2016.

Sotayo, A., Green, S. and Turvey, G., (2016). Experimental Investigation of Recycled Carpet Composites for Barrier Structures. Proceeding of the 18th Young Researchers' Conference, Institution of Structural Engineers, London. April 2016.

Sotayo, A., Green, S. and Turvey, G., (2015). Carpet recycling: a review of recycled carpets for structural composites. Environmental Technology & Innovation, 3, pp.97-107.

Sotayo, A., Green, S. and Turvey, G., (2014). Developing Novel Structural Composites from Recycled Materials. Faculty of Science and Technology, Lancaster University, Christmas Conference. December 2014. Poster Presentation (Dean's Poster Competition Award – Runner Up)

Acknowledgments

I would like to express my gratitude, first and foremost to my two supervisors Dr Sarah Margaret Green and Dr Geoffrey John Turvey for their guidance, support and highly satisfying assistance that they have provided at all stages of this PhD research. Their patience, knowledge and technical abilities have allowed me to learn tremendously and enhance several skills during this project. The detailed feedbacks and encouragement are also greatly appreciated.

I am indebted to my PhD sponsors – the Centre for Global Eco-Innovation, ECO2 Enterprises LLP, Dowager Countess Eleanor Peel Trust and the Lancaster University Engineering Department for the financial support. Appreciation also goes to the William Ritchie and Friend's Programme Travel Fund, Lancaster University Graduate College and Graduate School Travel Grant for the financial contributions towards the trip to Porto for the 2nd International Conference on Mechanics of Composites.

I am also grateful to the academic staff at Lancaster University Engineering Department, especially Professor Jianqiao Ye and Dr Allan Rennie for their discussions and feedbacks during the appraisal stages. Special appreciation also goes to Mark Salisbury, and the other technicians at the Engineering Department for their technical support with the comprehensive experimental work carried out during this research.

I will also like to acknowledge the support of David Joliffe, Kim Miller, Rob Harper and James Harper (Equestrian Surfaces Ltd) for the provision of the necessary technical details about the waste carpet structural composites analysed in this study. Thanks to Dr Richard Wilbraham for his assistance and advice with Scanning Electron Microscopy (SEM) analysis. Also thanks to Aaron Aboshio, Koralia Karaoli, Jonathan Milburn, Charles Odijie, Yakubu Tsado, Michael Fagbohungbe and Adam Sutch.

Finally, I would like to thank my family and friends for their moral support. To my Mother, thank you very much for the continued love, prayers and encouragements. Abiodun Adeoye – Thanks for the patience and support during those tough and demoralising times.

Table of Contents

List of Figures

List of Tables

1. Chapter One - Introduction

1.1. Background

Waste is a component that plays a key role in the issue of climate change, particularly as its disposal produces several greenhouse gas emissions that contribute to global climate change (United Nations Environment Programme, 2002). According to the Department for Environment, Food and Rural Affairs (DEFRA), England generates about 177 million tonnes of waste annually (Department for Environment Food and Rural Affairs, 2014). The most common route for disposal of waste has been to landfill and incineration. However, these waste management options cause the release of methane (CH_4) and carbon dioxide (CO_2) to the atmosphere, and methane emissions are more harmful (by a factor of 20) than carbon dioxide emissions (United Nations Environment Programme, 2002). Hence, the issue of waste is a major environmental concern and increasing recycling is a major goal of the current environmental agenda. DEFRA (Department for Environment Food and Rural Affairs, 2011) estimates that one tonne of general waste re-used or recycled saves over 3 tonnes of CO_2 equivalent. Hence, the European Union's seventh framework programme aims at finding innovative ways of utilising waste as a resource (European Union, 2010).

Carpets, which are typically used as floor coverings, are composite materials that are difficult and costly to separate mechanically and reprocess at the end of their useful lives (Miraftab and Mirzababaei, 2009, Realff et al., 2005). This is because carpets are multilayer mixtures of different polymers and inorganic fillers (Realff et al., 2005). In waste streams, carpets are classified as textiles, and textiles account for about 2 - 5 % of all waste going to landfill in the UK (Miraftab and Mirzababaei, 2009). Although this appears to be a small quantity, it is worth noting that carpet waste has low bulk density, and hence occupies a large volume of landfill. According to Carpet Recycling UK (Bird, 2014), 400,000 tonnes of carpets are sent to landfill in the UK annually. However, the landfill option is becoming increasingly impractical given the rising landfill costs, and the physical limitations on the number of landfill sites available in the UK (Bird, 2013). The landfill tax associated with the disposal of carpet waste to landfill was £24 in 2007 and has increased to £84 in 2016 reflecting a 250% increase over nine years (Gardner, 2016). The UK government (2016) have also stated that the landfill tax will increase to £89 in 2018 to meet environmental

objectives by reducing the amount of waste produced and the use of alternative waste management options. It is expected that, by 2025, carpet waste will be banned from UK landfill, because it is non-biodegradable and reduces the availability of landfill for other uses (Bird, 2014). Furthermore, effective waste management is vital in attaining a sustainable environment. Figure 1.1 shows the carpet waste management hierarchy according to Carpet Recycling UK (Bird, 2014). The hierarchy shows that the prevention option is the 'most favoured option'. The prevention option can be achieved through the use of fewer raw materials where possible in the design and manufacturing process, which, in turn, reduces the waste generated as well as the greenhouse gas emissions associated with the fabrication of carpets. Also, prevention of carpet waste can be achieved through the use of reduced carpet volume, and/or by increasing carpet longevity through adequate maintenance or repair (United States Environmental Protection Agency, 2003).

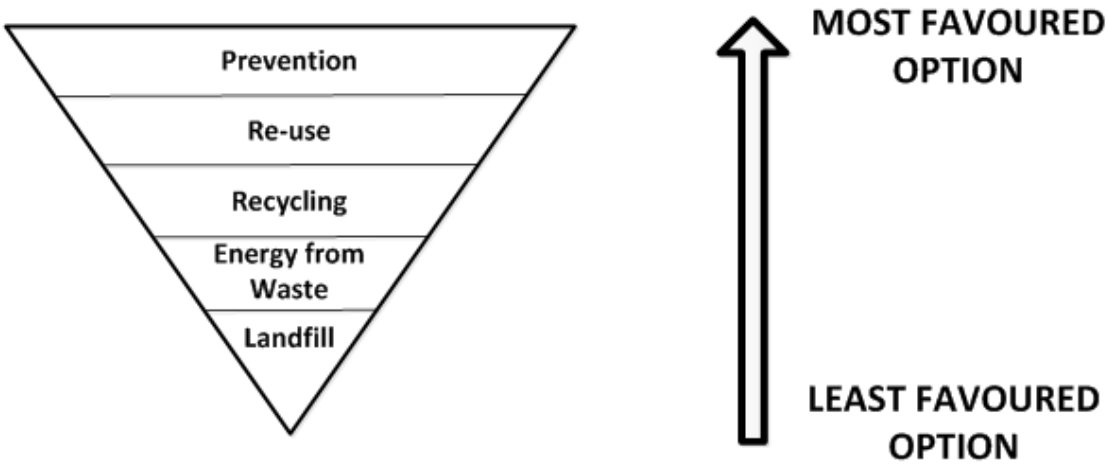

Figure 1.1: Carpet Waste Management Hierarchy (Bird, 2014)

According to Peoples (2006), an important approach to carpet recycling is the development of non-carpet products containing carpet waste. In view of this, the materials embodied in carpet waste may be suitable as raw materials for the development of load-bearing structural composites. Furthermore, this recycling approach can be highly economical, relatively cheap and environmentally friendly depending on the manufacturing processes involved (Vaidyanathan et al., 2013, Mihut et al., 2001, Wang, 2006a). To date, only a few studies have been carried out on the development of structural composites from carpet waste. If successful, such developments will create a stable pathway for carpet waste and provide new materials for low/medium load-bearing applications such as fencing, decking,

flooring and furniture. Additionally, one tonne of recycled carpet waste saves 4.2 tonnes of CO_2 emissions (Carpet Recycling UK, 2010). Thus, carpet recycling could potentially have a substantial and positive impact on the environment through a reduction in greenhouse gas emissions.

This work forms part of a wider ambition to recycle carpet waste through the development and characterisation of novel waste carpet structural materials, which can be used for equestrian fencing. The benefits of this innovative approach could include the reduction of carpet waste sent to landfill annually by replacement of common equestrian fencing materials (timber and PVC) which is expected to yield economic and environmental benefits. (NOTE: The words 'wood' and 'timber' are used interchangeably in this thesis). Timber is a very common material used for equestrian fencing (see Figure 1.2a). However, global forest loss is occurring at a rate of 13.7 million hectares (137,000 km^2) per year and deforestation accounts for about 12 % of global CO_2 emissions (Van der Werf et al., 2009, Smith 2013). Furthermore, plastic materials (specifically PVC) are increasingly being used as alternative structural materials to timber for equestrian fencing (see Figure 1.2b). These plastic materials are typically derived from non-renewable fossil fuels and involve multi-stage production processes which are energy intensive.

(a) (b)

Figure 1.2: Image of equestrian fence: (a) timber and (b) PVC

This research project is in partnership with a small local (SME) industry, ECO2 Enterprises. ECO2 Enterprises specialises in carpet waste management and recycling, and is a sister company to Equestrian Surfaces Ltd, which supplies to the equestrian market. ECO2 Enterprises receives about 6000 tonnes of carpet waste annually and aims to recycle this waste into useful products which can be utilised by Equestrian Surfaces Ltd in the design and installation of equestrian fencing arenas. As one tonne of recycled carpet waste saves

4.2 tonnes of CO_2 emissions (Carpet Recycling UK, 2010), ECO2 Enterprises could potentially save about 25,200 tonnes of CO_2 emissions annually through recycling carpet waste. In addition, about 400,000 tonnes of carpet waste are sent to landfill annually in the UK, therefore, annual estimate savings of about 1,680,000 tonnes of CO_2 emissions could be demonstrated through the sustainable recycling of carpet waste. However, there are limitations associated with these estimates such as greater energy related to multi-stage processing stages of carpet waste, which may reduce the environmental benefits.

1.2. Scope and Limitations

1.2.1. Scope

This project comprises the investigation of fundamental material and mechanical properties alongside the manufacturing processes of recycled novel waste carpet structural composites both as a structural beam and as the posts/rails of an equestrian fencing structure. Details of the manufacturing process of several prototype samples of recycled waste carpet structural composites are described, and the project seeks to determine their fundamental mechanical properties relative to those of typical equestrian fencing materials (i.e. timber and PVC). These mechanical properties are also part of the information required to determine and analyse the load-deformation response of fencing structures.

Furthermore, this study investigates experimental load tests on two-bay timber and PVC post and rail fences, which are representative of typical multi-bay fencing systems. The scope of the project was extended through the application of Finite Element (FE) modelling to supplement comprehensive experimental work. The FE models of the timber and PVC fences are validated by comparison with the experimental results. The FE models are also used to investigate the load-deformation response of fencing structures comprised of novel waste carpet structural composite posts and rails, whilst varying their overall geometry and the geometric properties of the posts and rails.

The experimental load tests and FE analyses carried out on the timber and PVC fences are restricted to linear elastic responses. Although the nonlinear deformation, collapse testing and dynamic response of the fencing structures are also important, linear elastic analysis can predict the serviceability deformations of timber and PVC fencing accurately. It is also

worth noting that there have been no load tests or FE analyses reported on timber or PVC fencing in the open literature. Therefore, this project gives an improved scientific understanding of the load-deformation response of timber and PVC fencing which may be transformed into useful structural design guidance. Several authors (Bakis et al., 2002, Satasivam and Bai, 2014) have also highlighted that the serviceability design (i.e. deflection limits) of structures is often more critical than the strength design.

1.2.2. Limitations

- The load tests on the representative timber and PVC fences were limited to static incremental loading without failing the fences.
- All the mechanical tests were carried out in the laboratory at ambient temperature, and the effect of changes in weather conditions (i.e. changes in temperature) was not investigated.
- Experimental tests were not carried out on a representative fencing structure made of the novel waste carpet structural composite posts and rails.

1.3. Aim and Objectives

1.3.1. Aim

The aim of this research is the development and characterisation of novel structural composites fabricated from carpet waste, which can be used to replace timber and PVC posts and rails used in equestrian fencing.

1.3.2. Objectives

The specific objectives include:

i. Review and analysis of waste carpet structural composites reported in the literature alongside common equestrian structural fencing materials, specifically timber and PVC.
ii. Fabrication of prototype structural composites from carpet waste and an investigation of their processing characteristics.
iii. Experimental testing to determine and compare the mechanical properties of novel prototype waste carpet structural composites, timber and PVC materials.

iv. Computational modelling and experimental testing of representative timber and PVC equestrian fences to evaluate their load-deformation responses.

v. Investigation of the load-deformation response of a fence structure fabricated from waste carpet structural composite and evaluation of its stiffness properties relative to those of similar equestrian timber and PVC fences.

vi. Structural analysis and design optimisation of the waste carpet structural composite sections and overall geometry of the fence structure to enable it to achieve stiffness properties similar to those of equestrian timber and PVC fences.

1.4. Thesis Structure

This thesis comprises of eight chapters. Chapter one gives the introduction, background, aim and objectives of the study.

Chapter Two – Literature Review

This chapter gives an overview of the composition of carpets and the classification of carpet waste. Also, the different carpet waste processing options in the UK are discussed. This chapter also focuses on studies that have been carried out on the fabrication of waste carpet structural composites using different manufacturing processes. The mechanical properties of these composites are presented and compared. Furthermore, Chapter two gives an overview and description of the properties of timber and PVC fencing materials. Their end-of-life options and carbon footprints are also presented and discussed. A section on fencing which covers the design and assembly methods for typical equestrian timber and PVC fencing is also included in this chapter.

Chapter Three - Materials and Manufacturing Methods

This chapter gives details of the manufacturing processes for the novel waste carpet structural composites. In addition, the chapter gives a brief description of typical timber and PVC post and rail sections used for equestrian fencing.

Chapter Four - Experimental Characterisation of Fencing Materials

This chapter describes the experimental setup and methods used to determine the mechanical properties of the fencing materials. These fencing materials include timber, PVC and the novel waste carpet structural composites. The results of the experimental tests are

analysed and discussed. Details of the statistical analyses carried out are presented. Furthermore, failure modes of the materials are identified and reported where applicable. The mechanical properties of the waste carpet structural composites are presented and compared with those of timber and PVC used for equestrian fencing.

Chapter Five – Experimental Characterisation of Fencing Structures

This chapter covers the experimental setup and testing of representative equestrian timber and PVC fencing structures with their results analysed and discussed. Furthermore, comparisons of the load-deformation responses of the fencing structures are carried out and presented. The experimental test results provide useful benchmark data for assessing the structural stiffness requirements of the novel waste carpet structural composites.

Chapter Six - Finite Element Modelling of Timber and PVC Fencing Structures

This chapter gives an introduction and brief review of literature on finite element modelling of beams and structures. The finite element modelling of timber and PVC fencing structures are carried out and validated against the experimental results from Chapter five. This chapter also provides a useful analysis for evaluating the stiffness of the novel waste carpet structural composites.

Chapter Seven - Finite Element Modelling of Novel Carpet Structural Composite Fencing Structure

Chapter seven gives details of the finite element modelling of a fencing structure comprised of the novel waste carpet structural composite post and rail sections. The chapter also includes an investigation of the load-deformation response of the fencing structure using the elastic properties of the novel waste carpet structural composite material given in Chapter Four. In addition, this chapter contains design optimisations and structural analyses undertaken to enable the carpet composite structure to achieve load-deformation responses similar to those of the equestrian timber fences described in Chapters Five and Six.

Chapter Eight – Conclusion

Chapter eight gives an overall conclusion of the thesis and recommendations for further study.

2. Chapter Two - Literature Review

2.1. Introduction

This chapter gives details of the different carpet waste processing options in the UK and the challenges associated with each of the options. Also, a review of the manufacturing processes and mechanical properties of different recycled waste carpet structural composites is carried out and discussed. This chapter also gives details of timber and PVC materials used for equestrian fencing. A brief review of their end-of-life options and environmental assessment is given. Details of assembly methods, geometry and structural connections for equestrian timber and PVC fencing are presented.

2.2. Composition and Classification of Carpet Waste

A typical carpet consists of four layers: face fibre, primary backing, adhesive and secondary backing (see Figure 2.1). The top layer, which is the face fibre, can either be nylon, polypropylene, polyethylene terephthalate (PET), mixed synthetics or natural fibres such as wool, cotton and jute (Jain et al., 2012, Bird, 2014, Miraftab et al., 1999, Hayles, 2015). The primary backing is the layer into which the yarns of the face fibres are bonded. Elastomeric adhesive is applied to the underside of the primary backing to hold the face fibres together (The Carpet and Rug Institute, 2003). The elastomeric adhesive is typically made of styrene butadiene rubber (SBR), which can be filled with inorganic materials such as calcium carbonate ($CaCO_3$) or barium sulphate ($BaSO_4$) (Mihut et al., 2001). The secondary backing is the layer bonded to the back of the carpet pile. The primary and secondary backings can be made of polypropylene, nylon, polyurethane or jute (Miraftab and Mirzababaei, 2009). According to Helms and Hervani (2006), nylon and polypropylene are the most commonly used materials for the backings and face fibres of carpets.

Carpets can be classified according to the type of manufacturing process - tufting, weaving, knitting, bonding and needle punching (The Carpet and Rug Institute, 2003). However, tufting is the most common method of manufacturing carpets, representing about 76 % of all carpets manufactured in the UK (Miraftab et al., 1999). The high volume of tufted carpets in the UK is mainly due to their low cost and high production rate. It involves sewing strands of face fibre yarns into the backing material and thereby creating thousands of yarn loops

(The Carpet and Rug Institute, 2003). Tufted carpets have two main style classifications – cut-pile and level-loop (see Figure 2.1) (Jain et al., 2012, Vaidyanathan et al., 2013). Cut-pile carpets have face fibres that are cut at the top to give a smooth surface, whereas, level-loop pile carpets have their fibres wound in a loop fashion. However, other styles, which combine one or more different styles, can be manufactured.

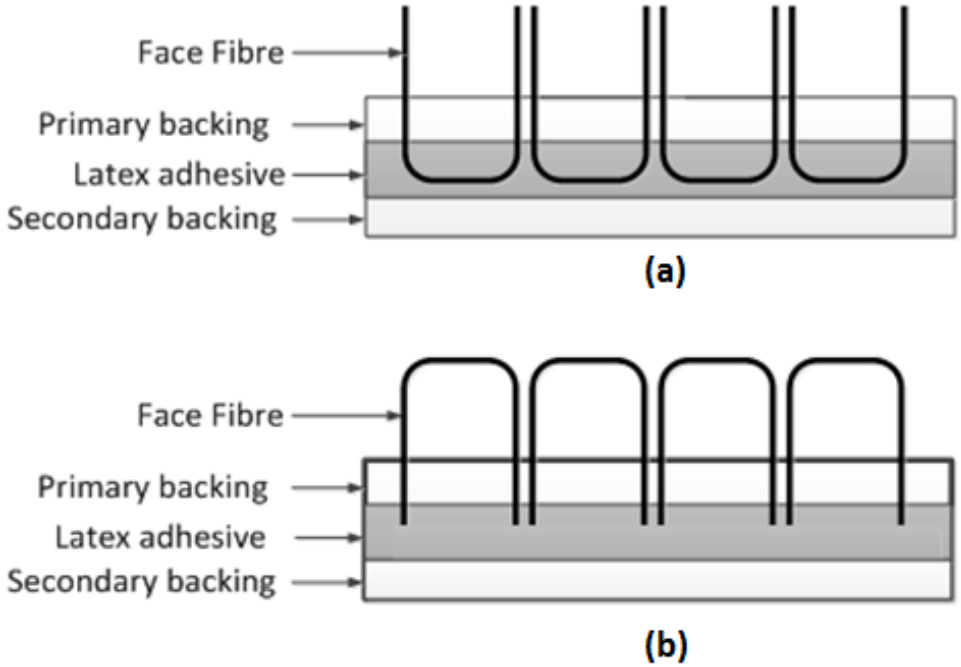

Figure 2.1: Typical construction of carpet: (a) cut-pile (b) level-loop

Carpet waste can be divided into two classes based on their source of origin: (1) pre-consumer and (2) post-consumer. Pre-consumer carpet waste includes scraps or offcuts generated during their manufacture and/or installation, whereas, post-consumer carpet waste includes carpets from end-of-life waste streams (Vaidyanathan et al., 2013, Bird, 2014). A typical carpet has a lifespan of 5 – 11 years (Jain et al., 2012). Furthermore, carpet has an approximate areal density of 2.3 kg/m^2, with the face fibre constituting almost half of its weight (Peoples, 2006). Table 2.1 shows the approximate component percentages in carpets with a polypropylene and SBR construction, which represents more than half of all carpet waste in the UK. Post-consumer carpet waste generally contains dirt, chemicals and other materials, which accumulate in-service and make them about 30 % heavier than new carpets (Mihut et al., 2001).

Table 2.1: Percentage composition of carpet components with polypropylene and SBR construction (Data extracted from Vaidyanathan et al. (2013), Wang et al. (2003) and Lave et al. (1998))

Component Type	Weight Percentage [wt. %]
Face fibre	46
Primary backing	6
Secondary backing	4
Latex adhesive (with fillers)	44

According to Bird (2013), post-consumer carpet waste accounts for 94 % of the total carpet waste in the UK, whereas, pre-consumer carpet waste accounts for the remaining 6 % (see Figure 2.2a). Figure 2.2b also shows that synthetic/man-made fibres (nylon, polypropylene and mixed synthetics) account for about 83 % of post-consumer carpet waste and natural fibres (wool blends) account for the remainder.

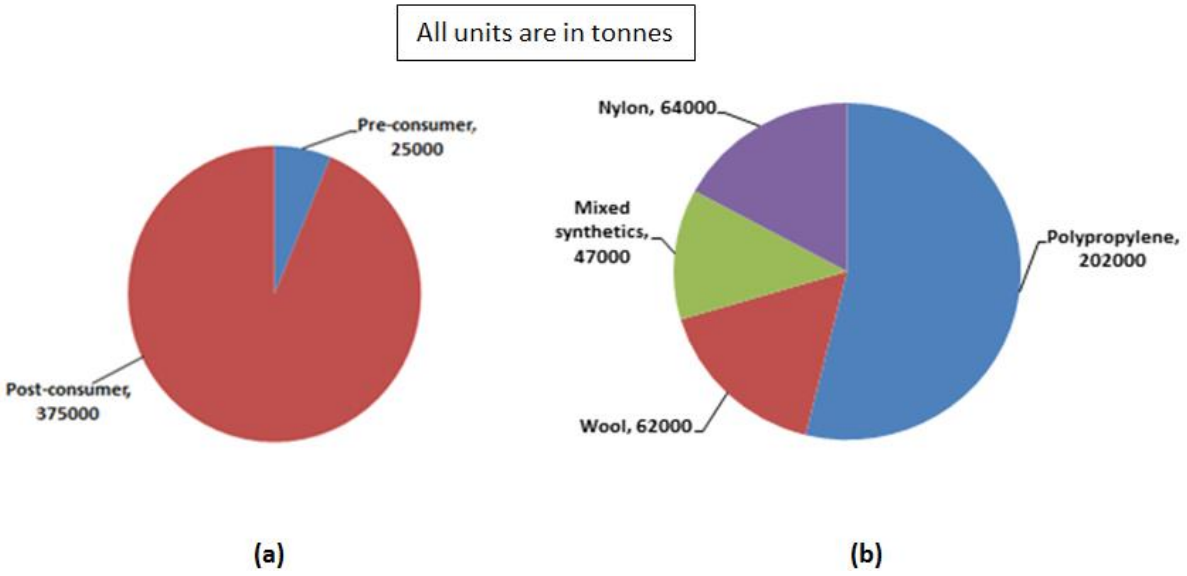

Figure 2.2: (a) Classification of carpet waste according to their source of origin (b) Face fibre classification of post-consumer carpet waste (Data extracted from (Bird, 2014))

2.3. Carpet Waste Processing Options

Figure 2.3 shows the different processing options for carpet waste diverted from landfill in the UK in 2013. They include energy recovery (via incineration), carpet re-use, equestrian surface applications, fibre reprocessing and plastics reprocessing.

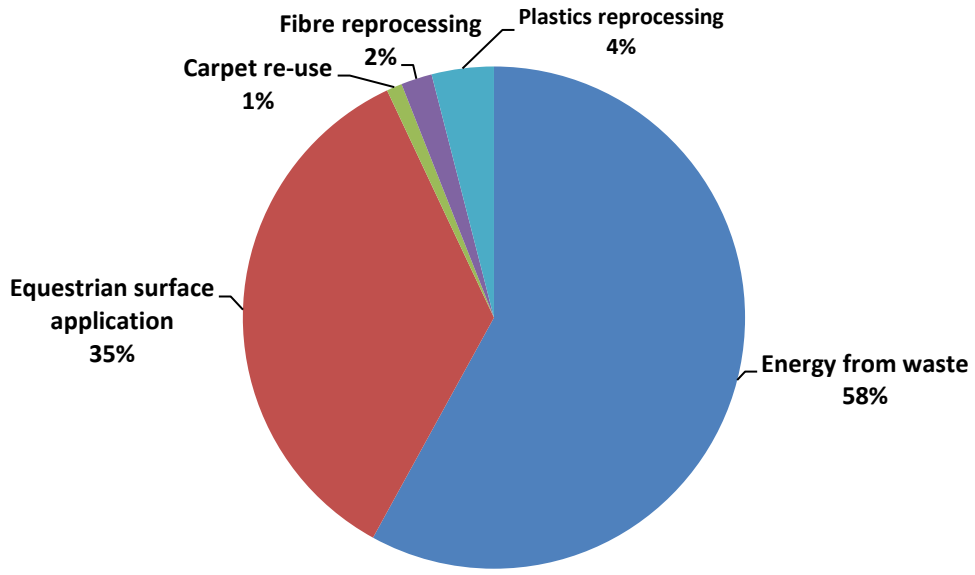

Figure 2.3: Carpet waste processing options in 2013 (Bird, 2014)

2.3.1. Carpet Waste to Energy (via Incineration)

Energy recovery from carpet waste via incineration involves shredding of the carpets, which are subsequently used as fuel to replace traditional sources, such as coal, for use in cement kilns or boilers (Bird, 2013, Miraftab et al., 1999, Tousey, 2011, Bolden et al., 2013). Energy recovery represented the highest percentage (58 %) among the carpet waste processing options (see Figure 2.3). The fuel obtained from carpet waste is known as Carpet Derived Fuel (CDF) (Jain et al., 2012). Table 2.2 shows a list of calorific values for different fibres compared to common fuels.

Table 2.2: Calorific values of fuels (Data extracted from (Miraftab et al., 1999, Wang, 2010, Wang et al., 2003)

Fuel source	Calorific value [MJ/kg]
Nylon	29
Polypropylene fibre	46
Polyethylene	46
Polyester fibre	19 - 30
Diesel	46
Wood	16-21
Naphtha	42-46
Coal	30

It is evident that the calorific energy values of polypropylene and polyethylene fibres are similar to those of diesel and naphtha. Furthermore, the calorific value of polyester fibres is similar to that of wood. Moreover, the calorific value of nylon is roughly equal to that of coal, which is used in cement kilns. These values show that carpet fibres represent useful sources of fuel as they have comparable calorific values to common fuels.

Although energy recovery may be feasible for all types of carpet waste, the problem associated with the utilisation of carpet waste in the production of CDF is the generation of ash waste and toxic gases (Jain et al., 2012, Miraftab et al., 1999). The ash waste generated is due to the high fraction (37 %) of calcium carbonate in carpets (Tousey, 2011). The ash waste is sent to landfill which can lead to groundwater and soil pollution due to the presence of heavy metals such as lead and cadmium (Siddique et al., 2008). However, if the carpet waste is used as a fuel source in cement kilns, the ash waste generated can be utilised as a raw material in the production of cement (Lemieux et al., 2004). Bolden et al. (2013) and Jain et al. (2012) highlighted that waste incinerators generate more toxic gas emissions than coal, oil, or natural gas-fuelled power plants. A study carried out by Lemieux et al. (2004) showed a 110 % increase in NO_x emissions from nylon face fibre carpets compared to coal. These higher NO_x emissions are as a result of higher nitrogen content in nylon carpets compared to coal. Realff et al. (2005) also carried out studies that indicate that carbon emissions from carpets are about two to three orders of magnitude greater than from coal. Nevertheless, combustion helps to divert carpet waste from landfill, which reduces the amount of methane generated (United Nations Environment Programme, 2002). DEFRA (Department for Environment Food and Rural Affairs, 2013) also states that energy recovery poses more environmental benefits compared to landfilling.

2.3.2. Carpet Waste Re-Use

Carpets are removed from homes and businesses for various reasons which include: being stained, worn out, dirty, fire damaged or a change of style (Wang et al., 2003). However, Biehl et al. (2007) also stated that disposed carpets are rarely worn out and that they can still be re-used. The re-use process usually involves cleaning, trimming and re-colouring for 'second life' usage. Re-use is regarded as the most cost-effective approach to recycling, and is considered the 'most favoured' option among the carpet waste processing options (Bird, 2014), because it leads to substantial savings in the consumption of raw materials, energy

and significant reductions in greenhouse gas emissions. Nevertheless, carpet re-use represented only 1 % of the total carpet waste processing options in 2013 (see Figure 2.3). Their re-use depends on the in-service physical condition of the carpet waste, and accessibility to re-use processing centres (Waste and Resources Action Programme, 2012). The geographical location of the carpet waste is important, as transportation costs to local re-use facilities are meant to be minimised.

2.3.3. The Use of Carpet Waste for Equestrian Surface Applications

The use of carpet waste for fibres based equestrian surfaces (see Figure 2.4) represented 35 % of the total carpet waste processing options in 2013 (Bird, 2014).This application involves shredding synthetic carpet waste fibres, and mixing them with silica sand and/or rubber crumbs (from waste tyres) (Fatahi et al., 2012). It also involves sorting the carpet waste into natural and synthetic face fibres, this is because natural fibres (i.e. wool) decompose, hence only carpets with synthetic fibres are used for equestrian surfaces (Waste and Resources Action Programme, 2014). The benefits of using fibres based equestrian surfaces include greater stability and cushioning effect for the horses (Blundell, 2010) (see Figure 2.4).

Figure 2.4: Images showing: (a) carpet fibres based equestrian surfaces and (b) close-up view (Mansfield, 2012)

2.3.4. Fibre Reprocessing of Carpet Waste

Fibre reprocessing of carpet waste represented 2 % of the total carpet waste processing options in 2013 (Bird, 2014). This carpet waste processing option pertains to depolymerisation, which involves carpet being dissolved in a solvent at a high temperature which causes separation of the face fibres from the other carpet components (Jain et al., 2012). Different depolymerisation techniques were discussed by Mihut et al. (2001), all of which result in the recovery of the nylon from the carpet waste; it has the same quality as the original nylon used. The depolymerisation processes involve the recovery of caprolactam (monomer of nylon) which is then re-polymerised by linking the monomer units into new nylon products (Strong, 2008). The recycled nylons are then used in the production of new carpets. The shortcoming with this recycling option is that only the nylon face fibre is recycled which is about half of its weight (Fishbein, 2000), while the remaining constituents of the carpet (i.e. backings and adhesive) are sent to landfill or incinerated (Miraftab and Mirzababaei, 2009). Also, the regeneration of nylon face fibres is a costly process which includes a pre-process that involves sorting the carpet waste according to their face fibres (Mihut et al., 2001). Furthermore, Miraftab et al. (1999) stated that the process of utilising recycled face fibres through depolymerisation in the production of new carpets may be more costly than a typical carpet manufacturing route.

Fibre reprocessing of carpet waste also pertains to the development of textile products such as felt used as carpet underlay. Studies (Miraftab et al., 2005, Rushforth et al., 2005) have confirmed that carpet underlays with good sound insulation properties can be fabricated from a mixture of styrene butadiene rubber (SBR) binder with granulated waste carpet tiles that have PVC backing and nylon/polypropylene face fibre.

It is also worth noting that the addition of synthetic carpet fibres to soil and concrete enhances their structural load-bearing properties. For example, studies (Ucar and Wang, 2011, Wang et al., 1994) show that the addition of carpet waste fibres (nylon and polypropylene) to concrete increased its toughness and ductility. Furthermore, studies (Miraftab and Lickfold, 2008, Murray et al., 2000, Wang, 2006b) show that recycled carpet waste fibres in reinforced soil significantly increases its compression strength.

2.3.5. Plastics Reprocessing of Carpet Waste

Plastics reprocessing involves the use of carpet waste in engineered plastic solutions. Plastics reprocessing represented about 4 % of the total carpet waste processing options in 2013 (Bird, 2014). This approach is cost effective compared to costly separation and fibre reprocessing procedures (Vaidyanathan et al., 2013, Wang et al., 2003). The process involves shredding of carpet waste at high temperatures, which is then extruded to form a blended mixture used in the fabrication of injection moulded thermoplastics. However, the blended mixture may consist of different immiscible plastics such as nylon and polypropylene which results in poor mechanical properties (i.e. tensile strength) compared to those of pure plastics (Wang et al., 2003). However, polymeric binding agents (sometimes referred to as compatibilizers, compatibilizing agents or coupling agents) may be used to improve the mechanical properties of the resultant composite. Conventional plastic processing techniques include injection moulding, vacuum bagging, extrusion and compression moulding (Strong, 2008). Several types of manufacturing processes utilising carpet waste as a raw material in the fabrication of composites have been developed (Gowayed et al., 1995, Xanthos and Dey, 2001, Xanthos et al., 2002, Kotliar, 1999, Kiziltas and Gardner, 2012, Young et al., 1998, David et al., 1996, Murdock et al., 2011, Jain et al., 2012, Muzzy, 2006, Zhang et al., 1999). Section 2.4 focuses on some of the innovative approaches in the fabrication of waste carpet structural composites. The mechanical properties of these composites are also presented and discussed.

2.4. Waste Carpet Structural Composites

Composite materials are typically composed of a binder or matrix that surrounds and holds the reinforcement in place (Strong, 2008). The different properties of the matrix and reinforcements contribute to the overall properties of the composite. Furthermore, the rule of mixtures can be used to estimate the Young's modulus of a composite in the longitudinal direction; $V_f E_f + V_m E_m = E$. E is the longitudinal Young's modulus of the composite; V_f is the volume fraction of the fibre reinforcement; V_m is the volume fraction of the matrix; E_f is the Young's modulus of the fibre reinforcement, and E_m is the Young's modulus of the matrix. However, the rule of mixture is based on the following assumptions: fibres and matrix are linear elastic and homogeneous; both the fibre reinforcement and matrix are free of voids; complete interface adhesion between the fibres and the matrix (Strong, 2008).

In addition, a strong bond between the fibre reinforcement and the matrix interface is vital; this is because load applied on the composites is transmitted to and distributed among the fibres through the matrix (Callister and Rethwisch, 2008). Other factors that may affect the properties of a composite include orientation of the reinforcement, manufacturing process and processing conditions (Callister and Rethwisch, 2007). The direction of the fibre reinforcement is an important factor in evaluating the properties of composites; this is because optimal strength and stiffness can be achieved in a composite by aligning the fibres parallel to the direction of loading. On the other hand, the strength and stiffness of the composite are weaker when the load is applied perpendicular to the fibres. Therefore, these composites will be highly anisotropic. An alternative orientation of fibre reinforcement is the random orientation of the fibres, which makes it isotropic, thereby making the mechanical properties independent of the loading direction (Sheikh-Ahmad, 2009).

A major goal in the fabrication of carpet based composites is to achieve a resultant composite suitable for load-bearing applications. The development of these composites with good structural properties will enhance a steady recycling option for carpet waste and provide new materials for low/medium load-bearing applications such as fencing, decking, flooring and furniture, etc.

The strength and modulus are two vital structural properties in load-bearing applications. The strength of a material is the maximum stress it can withstand before fracture whereas the modulus is a measure of the stiffness or a material's resistance to elastic deformation (Callister and Rethwisch, 2007). Carpet may include materials such as polypropylene, nylon, polyethylene, polyvinyl chloride (PVC), polyethylene terephthalate (PET), wool, polyurethane, wool and styrene-butadiene rubber (SBR). The tensile strengths and Young's moduli of these raw carpet materials, as well as other commonly used matrix materials, are given in Table 2.3.

Table 2.3: Tensile strength and Young's modulus of different materials found in carpets (Ashby and Jones, 2006, Callister and Rethwisch, 2007, Cambridge Engineering Selector 3.1, 2000)

Polymer	Tensile strength [MPa]	Young's modulus [GPa]
Polypropylene	50 - 70	1.2 - 1.7
Nylon	60 - 110	2.0 - 3.5
Low density polyethylene	7 - 17	0.15 - 0.24
High density polyethylene	20 - 37	0.55 - 1.0
Polyvinyl chloride (PVC)	30 - 70	2.4 – 3.0
Polyethylene terephthalate (PET)	50 - 80	2.2 - 3.5
Wool	40 - 200	3.9 - 5.2
Polyurethane	25 - 51	0.002 - 0.03
Styrene-butadiene rubber (SBR)	12 - 21	0.002 - 0.010
Epoxies*	40 - 85	2.1 - 5.5
Phenol formaldehyde*	35 - 55	8.0

***Other commonly used matrix materials that are not usually constituents of a typical carpet**

There are only a few studies that have examined the mechanical properties of carpet based structural composites. This section reviews the mechanical properties and the manufacturing process of such composites. Key structural properties such as the flexural modulus, flexural strength, tensile modulus and tensile strength of the carpet-based composites reviewed are compared in Figure 2.5 - Figure 2.8. Some of the studies included a second phase addition such as glass fibre reinforcement, binding agents or other fillers. The carpet based structural composites from literature with and without second phase additions are indicated with an '(a)' and '(b)' respectively, in Figure 2.5 - Figure 2.8. Their range of measured values is also indicated in the aforementioned figures. The variations in the mechanical properties of the carpet based composites (see Figure 2.5 - Figure 2.8) may be attributed to the factors discussed below:

- **Properties and volume fraction of the polymer/matrix and reinforcement** - The properties of the composite depend on the interfacial adhesion between the polymer/matrix and the reinforcement. Good interfacial adhesion results in composites with good mechanical properties. Also, their different distinct properties contribute to the properties of the resultant composite (Strong, 2008). Furthermore, the volume fraction of the matrix or reinforcement can affect the properties of the

carpet based composites, thus complying with the rule of mixtures. For example, studies (Muzzy, 2006, Zhang et al., 1999) have shown that increasing the volume of rigid reinforcement such as glass fibres results in an increase in the stiffness and strength properties of carpet based composites.

- **Compatibility and miscibility of the polymers involved** - As discussed earlier, carpets are multilayer mixtures of different polymers. During extrusion or melt blending of carpets, two immiscible polymers such as polypropylene and nylon may lead to composites with low mechanical properties. However, the addition of a binding agent, a matrix or reinforcement can be used to improve the mechanical properties of the resultant composite.
- **Manufacturing and processing conditions** – Different manufacturing processes exist for the production of carpet based composites, including injection moulding, extrusion, hand lay-up, compression moulding and resin transfer moulding. These processes are carried out at different temperatures and pressures which may lead to variations in the mechanical properties of carpet based composites. The presence of flaws (such as voids) may also be attributed to the processing conditions, which in turn affect the mechanical properties of the composite**.**
- **Type/source of carpet waste** – carpet waste comes from different sources which are exposed to different in-service physical conditions. These lead to variations in different carpet wastes (such as the presence of dirt particles, impurities or chemicals) used as raw materials in the fabrication of composites, which, in turn, leads to variations in the mechanical properties of the resultant composite. Furthermore, carpets can be made from different materials which have different mechanical properties (see Table 2.3). Hence, the mechanical properties of the resultant waste carpet structural composite are affected by the composition and mechanical properties of the constituents of the carpet used.

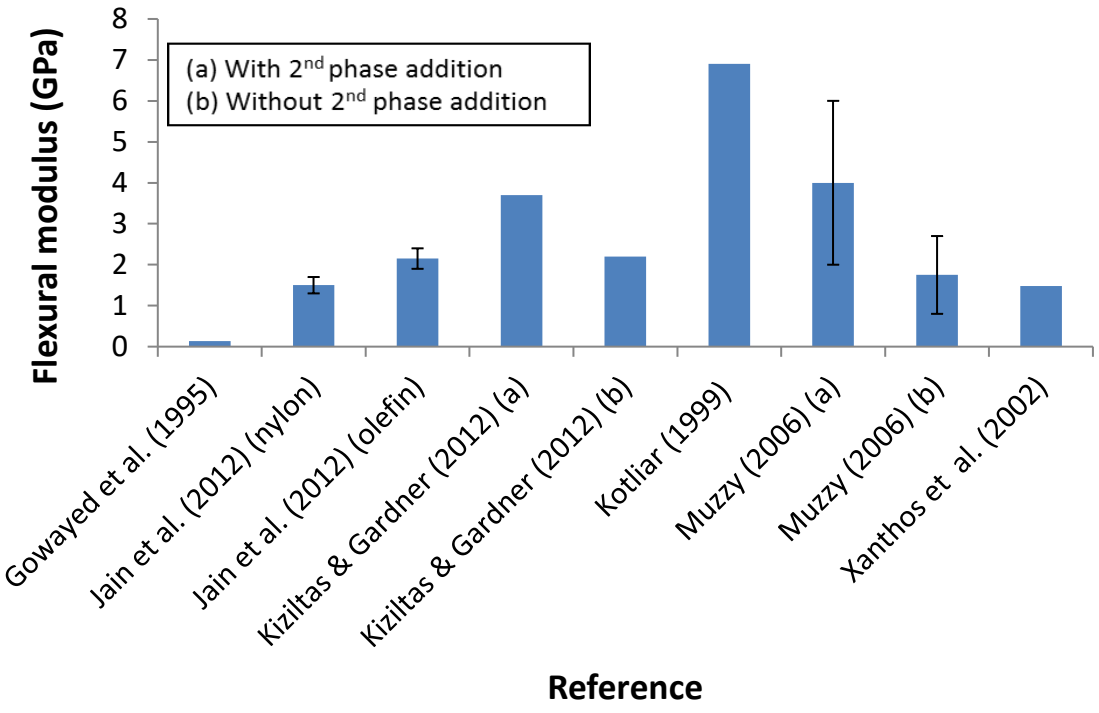

Figure 2.5: Comparison of the flexural modulus of carpet based composites

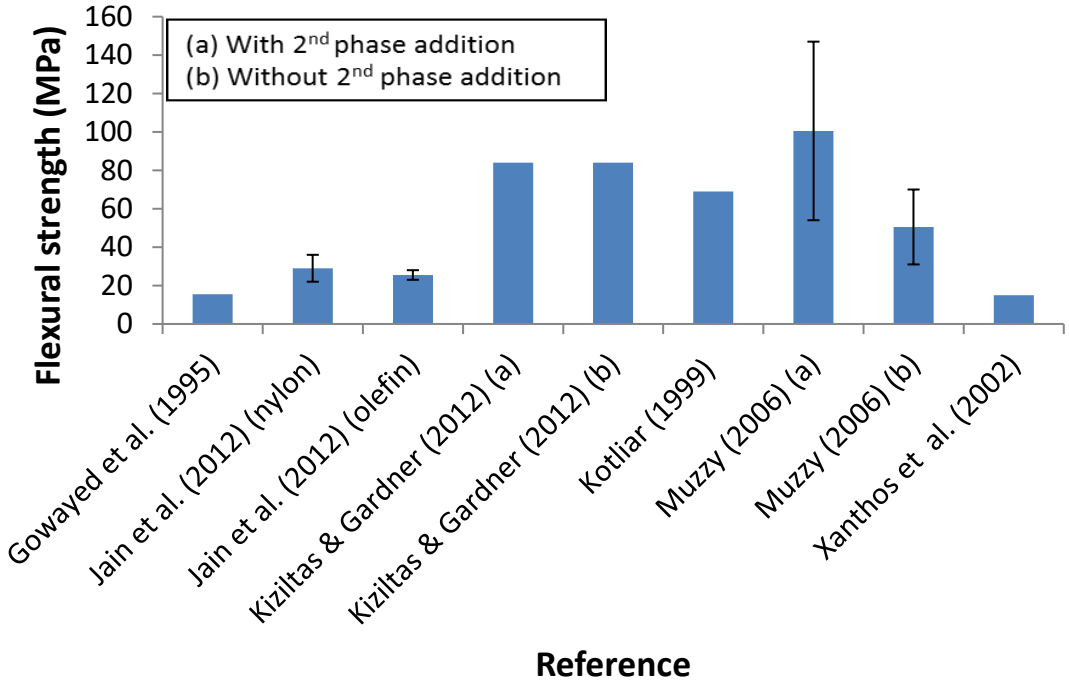

Figure 2.6: Comparison of the flexural strength of carpet based composites

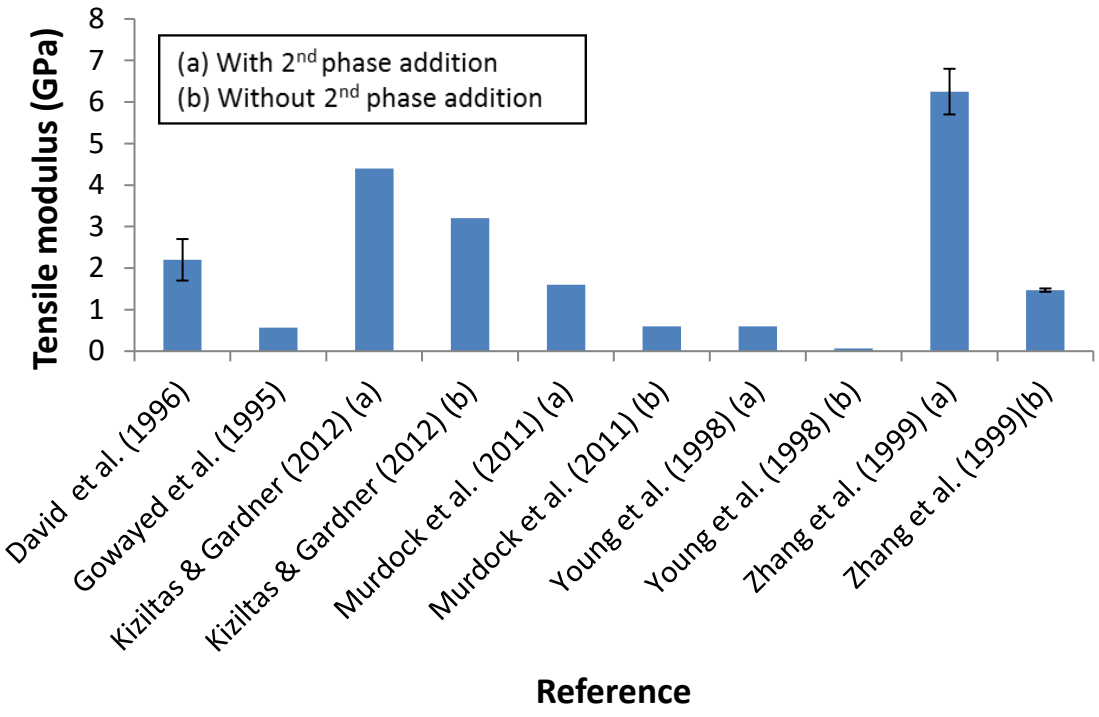

Figure 2.7: Comparison of the tensile modulus of carpet based composites

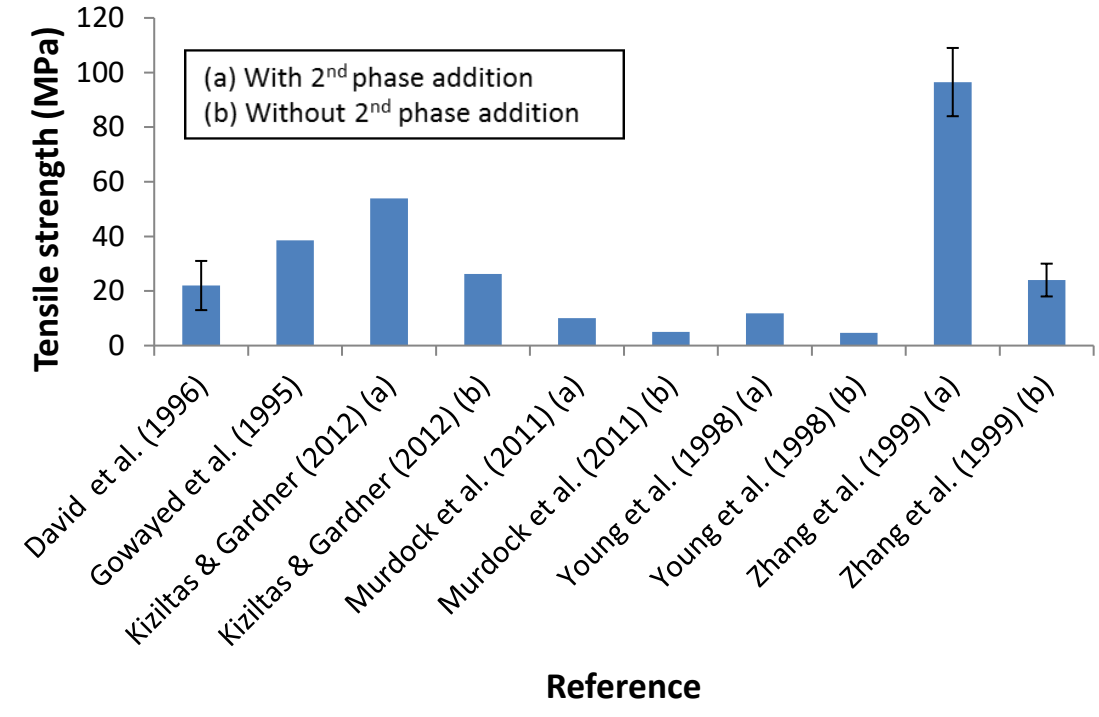

Figure 2.8: Comparison of the tensile strength of carpet based composites

Gowayed et al. (1995) fabricated composites utilising polypropylene backings from pre-consumer carpet waste and a polyethylene matrix. The composite samples were compression moulded with a 25 % fibre volume fraction of carpet waste. Flexural and tensile tests were carried out on a pure polyethylene matrix as well as the carpet based composite samples. The average flexural modulus for the carpet composite was 0.137 GPa with an average flexural strength of 15.50 MPa, whereas the average flexural modulus of the pure polyethylene matrix was 0.086 GPa and its average flexural strength was 13.80 MPa. The average tensile modulus for the carpet composite was 0.57 GPa with an average tensile strength of 38.5 MPa, whereas the average tensile modulus of the pure polyethylene matrix was 0.15 GPa and average tensile strength was 9 MPa. The study shows that the addition of 25 % polypropylene backings from carpet waste to the polyethylene matrix gave a significant increase in the mechanical properties compared to pure polyethylene. The relatively low flexural and tensile moduli are due to the low Young's modulus of the low density polyethylene matrix (see Figure 2.5 and Figure 2.7). Furthermore, this approach is not economically viable as it only utilises a fraction (backings) of the carpet waste which accounts for only about 10 wt. % of a typical carpet (see Table 2.1). Also, the process involves the pre-processing step of mechanical separation of the backings which is costly (Mihut et al., 2001).

Xanthos et al. (2002) developed a method of fabricating a structural composite utilising the residue compound obtained as a by-product in the recovery of nylon fibres from carpet waste. This residue compound contains about 63 – 65 wt. % of calcium carbonate, 15 – 18 wt. % of polypropylene and 12 – 15 wt. % of SBR. The matrix used was low density polyethylene. The manufacturing process involves 'Intrusion' moulding which is a combination of extrusion and injection moulding to fill a mould cavity (Xanthos et al., 2002). The flexural strength and flexural modulus of the composite (residue compound – 80 wt. %, low density polyethylene – 20 wt. %) were 15 MPa and 1.48 GPa, respectively. Xanthos et al's paper (Xanthos et al., 2002) attributes the relatively higher modulus of the composite to the high content of calcium carbonate (which has a modulus of 35 GPa) in the residue compound compared to the low density polyethylene matrix (Hugo et al., 2011). However, the flexural properties of the composite were still low when compared to the other carpet based composites (see Figure 2.5 and Figure 2.6) due to the relatively lower mechanical

properties of the low density polyethylene matrix (see Table 2.3). A major criticism of this manufacturing process is that it uses an energy intensive and costly pre-processing stage which requires the mechanical separation of nylon fibres from carpets (Mihut et al., 2001).

Kotliar (1999) produced composite samples from waste textiles and carpets. The process involved shredding of carpet waste and cotton, which were then coated with a high modulus phenol formaldehyde resin matrix (20 wt. %). The test results showed that a flexural modulus of about 6.9 GPa and flexural strength of about 69 MPa was achieved. The high composite modulus could be attributed to the relatively high Young's modulus of the phenol formaldehyde matrix (see Table 2.3). In addition, the relatively high flexural modulus of the composite is partly as a result of the composite laminates having a honeycomb sandwich structure for the benefit of increased flexural stiffness and low weight.

A research study that was carried out by Kiziltas and Gardener (2012) investigated the effect of adding natural filler (microcrystalline cellulose (MCC)) to recycled nylon from carpet waste. MCC is cellulose that is obtained from refined wood pulp. However, the mechanical property of the MCC filler used was not reported. The composite samples were injection moulded. Flexural and tensile tests were carried out on the injection moulded samples. The recycled nylon composite without filler reinforcement showed a flexural strength and flexural modulus of 84.3 MPa and 2.2 GPa, respectively. However, the addition of 30 wt. % MCC filler showed an increase in flexural modulus to 3.7 GPa with no significant change in the flexural strength. Furthermore, the addition of 30 wt. % MCC filler showed an increase in the tensile strength from 26.2 MPa to 53.9 MPa and an increase in the tensile modulus from 3.2 GPa to 4.4 GPa. The relatively higher mechanical properties of the composites fabricated by Kiziltas and Gardener (2012) (see Figure 2.5 - Figure 2.8) may be attributed to the effect of the lubricant (with a trade name of TPW113) used in the manufacturing process to improve the processing conditions. Additionally, the study utilised only recycled nylon from carpet waste which was supplied in the form of pellets from a commercial source. The study also indicates that MCC-filled composites are suitable for high temperature applications in the automotive industry.

Young et al. (1998) utilised automotive carpet waste scraps which consisted of nylon and polyester face fibres. These types of carpet are different from conventional post-consumer

carpet as they have an increased amount of inorganic fillers (such as $BaSO_4$ and $CaCO_3$ to levels of 71 wt. %) for improved sound insulation in automotive applications (Mihut et al., 2001). The manufacturing process involved shredding, granulation, and extrusion before being injection moulded. The injection moulded samples had a tensile strength and tensile modulus of 4.7 MPa and 0.062 GPa, respectively. The relatively low Young's modulus and tensile strength may be due to incompatibility of the two different polymers. Subsequently, Young et al. (1998) used a binding agent (an acrylic acid modified polypropylene polymer under the trademark PolyBond 1001) to improve the mechanical properties of the carpet waste composite. The addition of the binding agent (20 wt. %) increased the tensile strength and tensile modulus of the composite to 11.8 MPa and 0.6 GPa, respectively.

David et al. (1996) also fabricated composites from post-consumer carpet waste. Their tensile test results showed a tensile modulus ranging from 1.7 – 2.7 GPa and tensile strength from 13 – 31 MPa. Their study only utilised nylon, polypropylene and polyester face fibre carpet waste. The manufacturing process used by David et al. (1996) is similar to that of Young et al. (1998), which involves extrusion at a high temperature and pressure. However, no additives or binding agents were added to the composite samples fabricated by David et al. (1996), in view of this, the tensile properties of David et al. (1996) appear to be significantly higher than those of Young et al. (1998) (see Figure 2.7 and Figure 2.8). The higher tensile properties may be due to added processing steps which include the passage of the melt blended samples through a strand die, water bath and chopper to produce pellets of superior quality before being injection moulded.

Murdock et al. (2011) fabricated composites using a technique that incorporated chopping and shredding the carpet waste followed by mixing with Methylene Diphenyl Diisocyanate (MDI) as the binding agent. The method involved shredding the carpet waste and coating the shredded carpet waste with the binding agent (5 wt. %) before being extruded. Tensile tests were carried out on the resultant composite samples. The tensile strength and tensile modulus of the composite samples were 5 MPa and 0.6 GPa, respectively. The tensile modulus of the composite samples fabricated by Murdock et al. (2011) was the same as that of Young et al. (1998) (with PolyBond binding agent), whereas the tensile strength of the former is about half of the latter. The difference in the tensile strengths may be attributed to the difference in the type and volume of the binding agents used. In addition, the

difference in tensile strength could also be attributed to the type of carpet waste used; this is because the carpet waste used by Young et al. (1998) was different from conventional carpet waste as it had a higher quantity of inorganic filler. Subsequently, Murdock et al. (2011) added wood filler (about 25 wt. %) to the composite, which showed a significant increase in tensile strength and tensile modulus from 5 MPa to 10 MPa, and 0.6 GPa to 1.6 GPa, respectively (see Figure 2.7 and Figure 2.8).

Jain et al. (2012) used vacuum-assisted resin transfer moulding to fabricate a structural composite from post-consumer carpet waste. The process involved the infusion of epoxy resin into the carpet layers, which were then cured under pressure to form laminates. Two types of carpet were used in the study; the first type had nylon face fibres with a cut – loop construction and the second type had olefin (polypropylene) face fibres with a level-loop construction. The flexural modulus of the nylon based carpet composite samples ranged from 1.3 – 1.7 GPa, while the flexural strength ranged from 22 – 36 MPa. The flexural modulus of the olefin (polypropylene) based carpet composite samples ranged from 1.9 – 2.4 GPa, while the flexural strength ranged from 23 – 28 MPa. The olefin face fibre carpet composite had an average flexural modulus which was about 40 % greater than the nylon face fibre carpet composite. Jain et al's paper (Jain et al., 2012) suggests that the difference in flexural modulus is due to the differences in construction (level-loop versus cut-loop) and fibre-matrix adhesion. The process utilised in this study (Jain et al., 2012) was simpler than those used in the other studies reviewed, and did not require any energy intensive preparation steps. However, the study only focused on carpet waste with nylon and olefin (polypropylene) face fibres.

2.4.1. Studies Investigating the Effect of Glass Fibre Addition

Glass fibres are used as reinforcement in structural load-bearing applications due to their high strength and stiffness properties. Glass fibres have tensile strengths ranging from 3500 – 4600 MPa and tensile moduli ranging from 69 – 83 GPa (Strong, 2008). Studies (Muzzy, 2006, Zhang et al., 1999) have been carried out to investigate the effect of glass fibre addition to carpet based composites. Zhang et al. (1999) used two different processes to fabricate composite from carpet waste – (1) injection moulding and (2) compression moulding (with glass mat). The injection moulding process involved shredding, de-bulking and drying of the carpet waste before injection moulding, whereas the compression

moulding process involved de-bulking and interleaving with glass mat, before being moulded. The tensile strength of the injection moulded composites ranged from 18 to 30 MPa, whereas the tensile modulus ranged from 1.43 – 1.51 GPa. The tensile strength of the compression moulded composite samples with 40 wt. % glass ranged from 84 -109 MPa, while the tensile modulus ranged from 5.7 – 6.8 GPa. The compression moulded samples' tensile properties are significantly greater than those of the injection moulded samples due to the glass fibre reinforcement. It is worth noting that this study focused mainly on carpet waste that had a very high content of polypropylene. Also, flexural tests were not carried out on the composite samples.

Zhang et al. (1999) also investigated the effect of the glass mat fraction on the tensile properties of compression moulded samples. Table 2.4 gives the tensile strength and tensile modulus of the composite with different glass fibre reinforcement percentages. The test results showed that an increase in the volume of glass mat led to a significant increase in the tensile strength and tensile modulus of the resultant composite.

Table 2.4: Tensile properties of compression moulded composite samples fabricated by Zhang et al. (1999)

Composite Sample	Tensile strength [MPa]	Tensile modulus [GPa]
Pure carpet waste without glass mat	25.5	1.72
Carpet waste + 20 wt. % glass	40.7	2.12
Carpet waste + 30 wt. % glass	55.2	2.76
Carpet waste + 40 wt. % glass	84.1	5.90

Muzzy (2006) also fabricated composite samples from nylon and polypropylene face fibre post-consumer carpet waste by injection moulding and compression moulding. The flexural strength of the injection and compression moulded composite samples without fibre glass ranged from 31 – 70 MPa and their flexural modulus ranged from 0.8 – 2.7 GPa. On the other hand, the compression moulded samples with 30 wt. % glass fibre showed a flexural modulus ranging from 2 – 6 GPa and a flexural strength ranging from 54 – 147 MPa. The study carried out by Muzzy (2006) showed that the addition of 30 wt. % glass fibre increased the flexural strength by about 100 % and the flexural modulus by about 130 %. Therefore, it is evident from studies of Zhang et al. (1999) and Muzzy (2006) that the addition of glass

fibre significantly improves the mechanical properties of waste carpet structural composites (see Figure 2.5 - Figure 2.8). This is as a result of the relatively higher mechanical properties of glass fibres compared to other common polymers (i.e. nylon, polypropylene). However, a major drawback with the addition of glass fibre is its high cost. Additionally, cleaning, separation (according to their face fibre) and shredding of the carpet waste can also be costly, energy intensive and time consuming (Muzzy, 2006, Wang, 2010).

2.5. An Overview of Wood

Historically, wood has been and remains a widely used structural material. It is commonly used in structural load-bearing applications such as fencing, furniture, flooring, framing, panelling, scaffolding and many other building components, because of its good mechanical properties. Wood has high specific strength and is relatively cheap (Da Silva and Kyriakides, 2007). However, the mechanical properties of wood vary widely due to its natural origin. These variations are, in part, as a result of the growth conditions of timber which are influenced by various environmental factors such as soil type, water supply, and nutrients (Kretschmann, 2010, Porteous and Kermani, 2007).

Trees are divided into softwoods (coniferous) and hardwoods (deciduous) (Smith et al., 2013). Softwoods are generally needle-leaved evergreen trees such as pine and spruce, whereas hardwoods are typically broadleaf deciduous trees such as oak and Balsa (Wiedenhoeft, 2010). Softwoods are more commonly used in the UK compared to hardwood because they are readily available and typically have lower densities (TRADA, 2012b). The definition of softwood and hardwood bears little relation to its mechanical properties, as softwood (pine) is much stiffer than hardwood (balsa) (Porteous and Kermani, 2007). This is mainly due to the very low density of balsa, as the strength and stiffness properties of wood correlate with its density (Ashby and Jones, 2006).

2.5.1. Basic Microstructure of Wood

Since this study deals with the mechanical properties of wood, it is important to gain an understanding of the basic structure of wood. The microstructure of wood consists of long hollow cells aligned along the grain direction (parallel to the axis of the tree trunk) providing its strength and stiffness (Ashby and Jones, 2006). The longitudinal cells have hexagonal cross-sections and subdivided by transverse walls (see Figure 2.9). Also, relatively smaller

cells (rays) radially run through groups of the longitudinal cells as shown in Figure 2.9 (Easterling et al., 1982). This explains why wood is highly anisotropic; it is relatively weaker in the transverse direction compared to the longitudinal direction. The chemical composition of the cell wall of wood is given in Table 2.5.

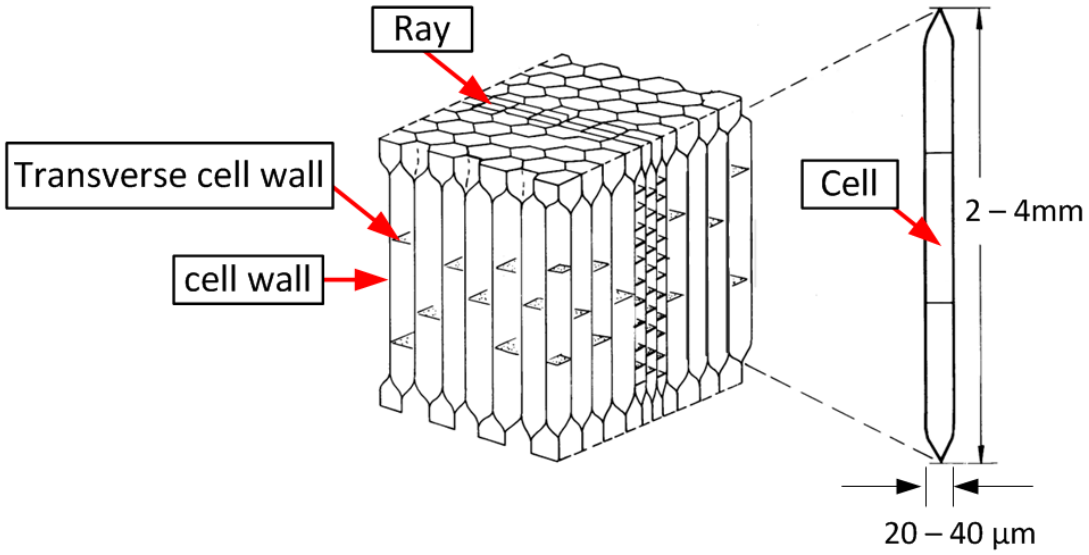

Figure 2.9: Microstructure of wood (Ashby and Jones, 2006)

Table 2.5: Chemical composition of the cell wall of wood (Ashby and Jones, 2006)

Material	Approximate weight [%]
Cellulose $(C_6H_{10}O_5)_n$	45
Lignin	20
Hemicellulose	20
Water	10
Extractives	5

The cell walls have a fibre-reinforced composite structure (cellulose fibres in a matrix of hemicellulose and lignin). The cellulose ($C_6H_{10}O_5$) fibres which account for about 45 wt. % of the cell wall are made by the tree from glucose. Lignin and hemicellulose can be viewed as the matrix which accounts for about 40 wt. % of the cell wall. The remaining 15 wt. % are water and extractives such as oil and salts which give wood its colour, smell and in some cases resistance to insects (Ashby and Jones, 2006, Asif, 2009). It should be noted that this is a simplified explanation as there are uncertainties such as different natural growth

conditions and the development of knots and branches (Kretschmann, 2010). Also, Matuana (2015) stated that the chemical composition of wood varies between its different species.

2.5.2. Wood as a Structural Material

Wood is an anisotropic material which means that its strength and stiffness are direction dependent. It has three principal axes: longitudinal, radial and tangential (see Figure 2.10). The longitudinal axis is parallel to the fibre direction, the radial axis is perpendicular to the fibre direction and normal to the growth rings, and the tangential axis is perpendicular to the fibre direction and tangential to the growth rings. However, according to Isopescu et al. (2012), although the mechanical properties are direction dependent, the difference between the mechanical properties in the radial and tangential directions is small compared to the difference between the longitudinal and the radial/tangential directions. In general structural design, the mechanical properties are classified into two groups; properties parallel-to-the-grain (longitudinal) and perpendicular-to-the-grain (tangential and radial). Wood is stiff and strong parallel-to-the-grain and relatively weak perpendicular-to-the-grain with the modes of deformation and failure in these directions being different.

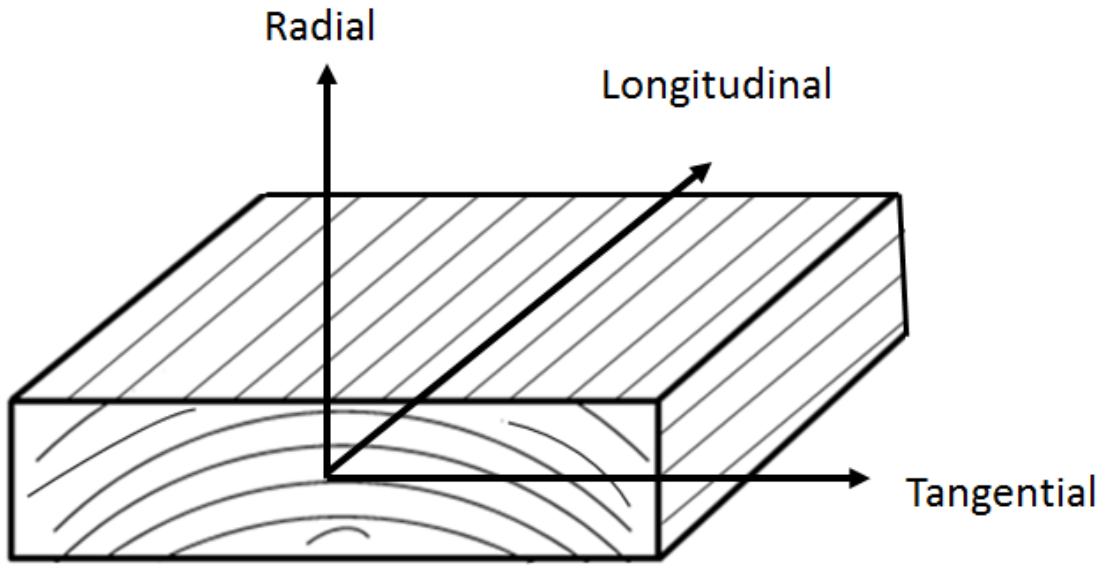

Figure 2.10: Three principal axes of timber with respect to fibre direction and growth rings

British Standard (BS EN 338, 2009) provides a strength classification system for structural timber (see Table 2.6). The characteristic stiffness and density are also included in the classification system. The mechanical properties given in Table 2.6 were obtained from tests carried out in accordance with BS EN 408 (2010). The strength classification system is

divided into two groups: (a) Poplar and softwood species and (b) Hardwood species. The letter 'C' of the poplar and softwood species denotes coniferous, whereas the letter 'D' denotes deciduous. The classification system ranges from C14 – D70. The number denotes the characteristic value of the bending strength for that particular species within the class. For example, C14 means that the timber class has a characteristic bending strength of 14 MPa. Three characteristic mechanical properties – bending strength (parallel-to-the-grain), modulus of elasticity (parallel-to-the-grain) and density are needed to assign a grade or species of wood to a strength class. The other mechanical properties may then be obtained from the values given for that class. These properties are needed in structural design and are independent of the wood species (Smith 2013).

The classification system according to BS EN 338 (2009) shows that the elastic moduli of timber parallel-to-the-grain and perpendicular-to-the-grain range from 7 – 20 GPa and 0.23 – 1.33 GPa, respectively. These values show that timber is significantly stiffer parallel-to-the-grain compared to perpendicular-to-the-grain. Hence, in structural load-bearing applications, timber is typically loaded parallel-to-the-grain. Furthermore, Smith (2013) explains that there is a correlation between the density and strength of timber. According to Porteous and Kermani (2007), the density of wood is a good indicator of its mechanical properties, provided that the wood section is straight grained (fibres parallel to the longitudinal axis) and free from knots and other defects. This trend is illustrated in Table 2.6; an increase in density shows an increase in the strength and stiffness properties.

Table 2.6: Characteristic strength, stiffness and density values of structural timber (Data extracted from BS EN 338 (2009))

Property	Poplar and softwood species												Hardwood species							
	C14	C16	C18	C20	C22	C24	C27	C30	C35	C40	C45	C50	D18	D24	D30	D35	D40	D50	D60	D70
	Characteristic strength properties [MPa]																			
Bending	14	16	18	20	22	24	27	30	35	40	45	50	18	24	30	35	40	50	60	70
Tension (parallel-to-the-grain)	8	10	11	12	13	14	16	18	21	24	27	30	11	14	18	21	24	30	36	42
Tension (perpendicular-to-the-grain)	0.4	0.4	0.4	0.4	0.4	0.4	0.4	0.4	0.4	0.4	0.4	0.4	0.6	0.6	0.6	0.6	0.6	0.6	0.6	0.6
Compression (parallel-to-the-grain)	16	17	18	19	20	21	22	23	25	26	27	29	18	21	23	25	26	29	32	34
Compression (perpendicular-to-the-grain)	2.0	2.2	2.2	2.3	2.4	2.5	2.6	2.7	2.8	2.9	3.1	3.2	7.5	7.8	8.0	8.4	8.8	9.7	10.5	13.5
Shear	3.0	3.2	3.4	3.6	3.8	4.0	4.0	4.0	4.0	4.0	4.0	4.0	3.4	4.0	4.0	4.0	4.0	4.0	4.5	5.0
	Characteristic stiffness properties [GPa]																			
Mean modulus of elasticity (parallel-to-the-grain)	7	8	9	9.5	10	11	11.5	12	13	14	15	16	9.5	10	11	12	13	14	17	20
5 % modulus of elasticity (parallel-to-the-grain)	4.7	5.4	6.0	6.4	6.7	7.4	7.7	8.0	8.7	9.4	10.0	10.7	8.0	8.5	9.2	10.1	10.9	11.8	14.3	16.8
Mean modulus of elasticity (perpendicular-to-the-grain)	0.23	0.27	0.30	0.32	0.33	0.37	0.38	0.40	0.43	0.47	0.50	0.53	0.63	0.67	0.73	0.80	0.86	0.93	1.13	1.33
Mean shear modulus	0.44	0.50	0.56	0.59	0.63	0.69	0.72	0.75	0.81	0.88	0.94	1.00	0.59	0.62	0.69	0.75	0.81	0.88	1.06	1.25
	Characteristic density [kg/m^3]																			
Mean density	350	370	380	390	410	420	450	460	480	500	520	550	570	580	640	650	660	750	840	1080

2.5.3. Some Factors Affecting the Properties of Wood

Wood is a variable structural material, and its properties can be affected by several factors such as its growth conditions, species type and its processing options (Asif, 2009). Natural defects in wood such as the presence of knots and the slope of the grain (with respect to its longitudinal axis) also affect its mechanical properties.

The slope of grain of wood refers to the fibre direction in reference to the longitudinal axis (Kretschmann, 2010). The slope of grain occurs when the fibres are at an angle to the longitudinal axis of the wood section, and can be attributed to irregularity during tree growth or when a wood section is not cut precisely parallel-to-the-grain. Excessive deviation of the fibres with respect to the longitudinal axis affects the mechanical properties of wood. More specifically, the strength properties of wood are significantly reduced because the fibres are not parallel to the longitudinal axis (Porteous and Kermani, 2007).

Knots are very common features in wood; they appear as round and relatively darker spots on wood sections (see Figure 2.11). They occur as a result of a portion of a branch intersected and enclosed in a tree trunk during the growth of a tree (Porteous and Kermani, 2007). The influence of knots depends on their size, shape and location in the wood section. According to Kretschmann (2010), large knots cause a reduction in the strength of wood. Porteous and Kermani (2007) also explained that the effect of knots on the mechanical properties of wood is due to the distortion of fibres, causing fibre discontinuity and non-uniform stress distributions.

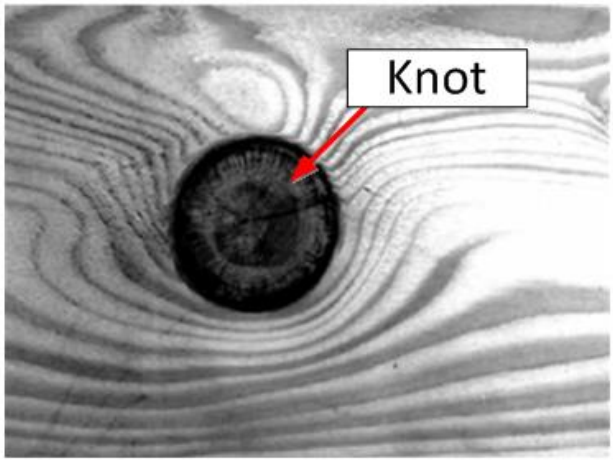

Figure 2.11: An image of a knot on a timber section (Kretschmann, 2010)

Furthermore, wood is hygroscopic; i.e. it absorbs moisture from the environment, which affects its mechanical properties (Glass and Zelinka, 2010). The dimensions of wood vary as it absorbs or loses moisture; moisture absorption makes wood swell, whereas, wood shrinks as it loses moisture. These dimensional changes result in warping and splitting of wood, which reduces the utility of wood products, e.g. loosening of tool handles or gaps in flooring. Moisture content affects the strength of timber; strength decreases with increase in moisture content (Kretschmann, 2010).

Wood is susceptible to decay and fungal attacks when its moisture content is higher than 20 % (Taylor, 1994). This leads to a high level of maintenance by means of preservative treatments containing biocides (fungicides and/or insecticides) to protect it against biological attacks to prevent degradation (Smith 2013). Additionally, preservative treatments help to prolong the lifespan of wood, thereby, allowing a more effective use of forest resources and eliminating replacement costs (Lebow, 2010).

2.5.4. End-of-Life of Wood

About 4.1 million tonnes of wood waste was generated in the UK in 2010 (Waste and Resources Action Programme, 2011). About 2.3 million tonnes of wood waste was recovered for bio-energy and recycling in the UK in 2010, which represents just over half of the total wood waste, with most of the remainder believed to have been sent to landfill. The panel board industry represented the largest end market for wood, consuming 1.1 million tonnes and representing about 50 % of wood recovered in 2010. The use of wood for bioenergy was the second highest waste wood outlet consuming 551,000 tonnes and representing about 24 % of the total wood recovered in 2010. Other recovered wood uses include animal/poultry bedding, pathways and coverings, and horticulture applications such as soil conditioners and composts combined represented a total of 580,000 tonnes which was about 26 % of the total wood recovered in 2010.

Wood re-use is the best option for wood's end-of-life waste stream (TRADA, 2011). This is because the carbon stored in the wood remains stored for another service life, and constitutes a reduction in waste generated. However, the quantity of wood re-used in the UK in 2010 was not reported.

The re-use of wood depends mainly on its physical condition whilst in-service. Wood waste that has been previously treated with preservatives such as Chromated Copper Arsenate (CCA) or creosote whilst in use (such as in fencing applications) is considered as a hazardous waste (Smith 2013). These hazardous wastes are therefore prohibited from re-use and energy recovery (TRADA, 2011). These hazardous wood wastes are likely to end up in landfill, and their decay releases CO_2 and methane into the environment which is a major concern.

2.6. An Overview of Polyvinyl Chloride (PVC)

Polyvinyl Chloride (PVC) is a highly versatile thermoplastic material and is used in a wide range of applications, such as fencing, flooring, pipes and fittings, cables and window profiles etc. According to Woolley and Kimmins (2000), salt (57 %) and crude oil (43 %) are the primary raw materials used for the production of PVC. The electrolysis of salt water produces chlorine, which is combined with ethylene (obtained from petroleum), and used for the formation of Vinyl Chloride Monomer (VCM) (British Plastics Federation, 2015). PVC is then produced by polymerising (or joining) molecules of VCM to form long molecular chains. Figure 2.12 shows a description of the formation VCM and PVC.

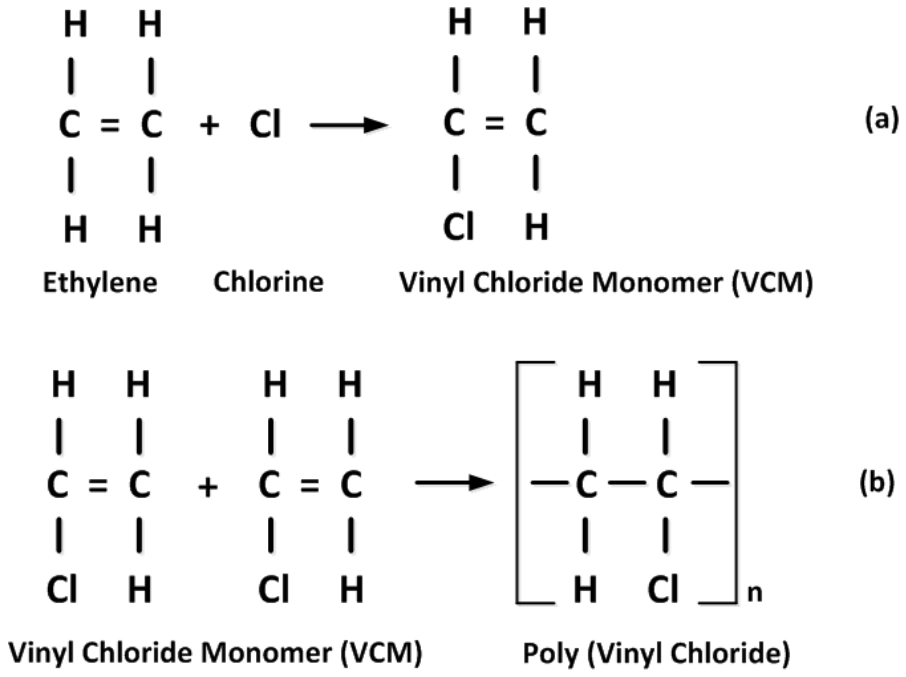

Figure 2.12: Chemical structure showing the formation of: (a) Vinyl Chloride Monomer (VCM) and (b) Polyvinyl Chloride (PVC)

PVC is one of the most commonly used plastics in the world; about 39.3 million tonnes of PVC was consumed worldwide in 2013 (Ceresana Research, 2014). About 5 million tonnes of PVC were consumed in Europe in 2014, with 3.5 million tonnes used in the building and construction sector (British Plastics Federation, 2015, European Council of Vinyl Manufacturers, 2014). According to British Plastics Federation (2015), about 500,000 tonnes of PVC are produced in the UK annually, and 370,000 tonnes of PVC were used in the building and construction sector in 2014. This shows that approximately 70 % of PVC consumption is used in the building and construction sector annually in the UK and Europe. Some of the specific applications in this sector include window and door frames, fencing, cable ducts and conduits, roller shutters and pipes. The building and construction sector represents about 20 % of the overall European plastics consumption (approximately 10.5 million tonnes), and PVC is the most commonly used plastic material in this sector (PlasticsEurope, 2015). The high consumption rate of PVC in the construction sector can be attributed to its good mechanical properties, cosmetic appearance, ability to be formed into complex shapes/geometry, chemical and water resistance and long service life (Agarwal and Gupta, 2011, Yu et al., 2016). The mechanical properties of rigid PVC are given in Table 2.7.

Table 2.7: Properties of Rigid PVC (Cambridge Engineering Selector 3.1, 2000)

Property	Value
Density	1350 – 1550 kg/m^3
Young's modulus	2.2 – 3.5 GPa
Tensile strength	30 - 70 MPa
Compressive strength	55 – 60 MPa

2.6.1. Manufacturing Process of Rigid PVC

Fillers, lubricants, pigments and other additives are typically added to PVC to produce various PVC compounds for different end-uses (British Plastics Federation, 2015). The addition of these additives helps to improve processing techniques (i.e. melt flow) and is also used to modify several properties such as the colour, stiffness, strength, flammability and chemical resistance of PVC (Kalpakjian, 1984, Patrick, 2005). According to the American Chemistry Council (2008), rigid PVC typically contains about 10 – 20 wt.% of these additives and fillers; however, the actual composition of a PVC compound for the production of rigid

profiles varies according to the manufacturer. Table 2.8 gives a representative formulation of a PVC compound used for the production of rigid profiles.

Table 2.8: Typical PVC formulation used for the manufacture of rigid PVC profiles (Data extracted from (WWF, 2005))

Material	Approximate Weight [wt. %]
PVC	81.5
Impact modifier (i.e. Acrylate rubber)	6.0
Pigment (i.e. TiO_2)	3.5
Heat stabilisers (i.e. Lead sulphate)	2.5
Fillers (i.e. $CaCO_3$)	5.0
Lubricant (i.e. Petroleum wax)	1.5

Heat stabilisers are used for the reduction and/or prevention of decomposition during the processing of PVC (WWF, 2005). Heat stabilisers also provide enhanced resistance to weathering; examples include lead sulphate and phosphate (Muralisrinivasan, 2011). Titanium oxide (TiO_2) is a very common pigment added to a rigid PVC compound that gives a white colour to the final product, and also improves its ultraviolet ray and chemical resistance (Abate, 2007, Yang et al., 2014). Impact modifiers (i.e. rubber) are additives added to PVC to improve its toughness, impact strength and durability (Patrick, 2005). Fillers are added to PVC to reduce cost and improve the mechanical properties of the final product. Lubricants (such as stearic acid and petroleum wax) are used to prevent the PVC compound from 'sticking' to the processing equipment and also help to improve processing (i.e. melt flow) during extrusion (Muralisrinivasan, 2011).

PVC posts and rails used for fencing applications are typically extruded (Markarian, 2008). The extrusion process is a continuous process suitable for the manufacture of long profiles. Figure 2.13 illustrates the extrusion process. The PVC compound is fed through a hopper into a barrel, and a rotating mechanical screw pushes the resin forward through the barrel. The PVC compound is heated through the friction of the rotating screw and/or externally through the heat of the barrel heating system, and is subsequently extruded through an outlet steel die (Kalpakjian, 1984, Callister and Rethwisch, 2008). The temperature in the barrel may vary between 135 ^{o}C and 370 ^{o}C. The outlet die is in the shape of the cross-

section of the extruded PVC section. The extruded PVC section is then cooled by passing it through a water bath (or cooling tank).

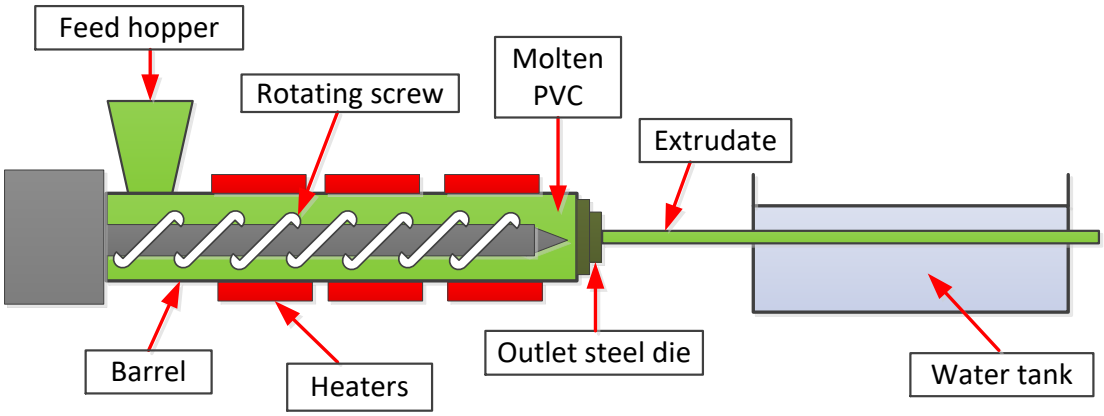

Figure 2.13: Illustrative diagram of a PVC extrusion process

2.6.2. End-of-Life of PVC

Over the years, there has been a rise in the production and consumption of plastic materials, and this has led to an increase in the plastic waste generated annually. Approximately 25.8 million tonnes of plastic waste was generated in Europe in 2014, with 30 % of waste recycled, 40 % incinerated for energy recovery and the remainder sent to landfill (PlasticsEurope, 2015). According to the Department for Environment, Food and Rural Affairs (2015), 3.2 million tonnes of plastic waste was generated in the UK. About 30 % of plastic waste was recycled, 30 % incinerated for energy recovery and the remaining 40 % sent to landfill in the UK in 2014 (PlasticsEurope, 2015). It is, therefore, evident that a large volume of plastic waste is sent to landfill in the UK and Europe.

According to Braun (2002), PVC waste accounts for about 10 % of total plastic waste in Europe; hence, the total amount of PVC waste in Europe in 2014 can thus be estimated at 2.58 million tonnes. There are three main end-of-life options for PVC waste; they include: (a) recycling (b) waste to energy through incineration, and (c) landfill disposal (VinylPlus, 2015). According to Recycling International (2015), a total of 95,525 and 474,411 tonnes of PVC waste were recycled in the UK and Europe, respectively in 2014. About 50 % of the recycled PVC waste in the UK was rigid profiles with the remainder being PVC films, cables and pipes. The recycling option includes the shredding and granulation of waste PVC, which is then

reprocessed for the production of new plastic products. A major factor with PVC recycling is that PVC waste is commonly mixed with different plastics, hence separation of this waste (by plastic type) is a vital preliminary and challenging step (Bajracharya et al., 2016). Furthermore, some PVC sections have metal reinforcements which make their recycling more difficult.

Another end-of-life option for PVC is incineration for energy recovery. PVC has a calorific value of about 20 MJ/kg; hence it is used as a fuel for power generation through incineration. This option, however, leads to the release of environmental pollutants such as dioxins and hydrocarbons into the environment (Akovali, 2012). PVC waste that is neither recycled nor incinerated is disposed of to landfill. Although PVC decomposes slowly, the presence of additives (such as lead based stabilisers) in PVC products can result in the formation of leachate, which is environmentally hazardous (European Commission, 2010). Furthermore, the disposal of plastic waste to landfill is becoming more costly, and regulatory policies are increasingly limiting the disposal of waste to landfill.

2.7. Comparison of the Environmental Assessment for Wood and PVC

Trees absorb and store significant amounts of carbon from the atmosphere through photosynthesis (Berenguer et al., 2014). Carbon River (2010) states that a tree absorbs 1747 kg of CO_2 per tonne over its lifecycle. However, global forest loss is occurring at a rate of 13.7 million hectares (137,000 km^2) per year with the timber trade being one of the main causes of this loss (Smith 2013). Furthermore, deforestation is responsible for the release of stored carbon and accounts for about 12 % of global CO_2 emissions (Van der Werf et al., 2009). A study carried out by Read et al. (2009) showed that a combination of decreased deforestation, effective forest management and afforestation can provide a significant reduction in CO_2 emissions. Hence, reduction in deforestation plays an important role in efforts to mitigate climate change.

Hammond and Jones (2011) developed a database (Inventory of Carbon and Energy), which contains the embodied energy and embodied carbon of structural materials. The system boundary utilised by the database was ‘cradle-to-gate’; this includes the extraction, refining, transportation and processing of the materials until the material is ready for use. According

to Giesekam et al. (2014), embodied emissions are emissions related to the production of a material, which are predominantly the extraction and processing of the materials. Hence, materials which undergo many stages during their production typically possess higher embodied energy. Embodied energy can be expressed in MegaJoules per kilogramme (MJ/kg) or MegaJoules per cubic metre (MJ/m^3). Embodied carbon is the amount of carbon dioxide emitted during the production of a material, and depends on the method of energy generation.

The database explains that the 'embodied carbon' given is typically based on the emissions from fossil fuel combustion. The database also explains that the embodied carbon for wood excludes the carbon sequestered by a tree during its growth. The carbon dioxide emissions for wood are divided into two: (a) those derived from fossil fuel combustion and (b) burning biomass fuel (i.e. wood offcuts and waste) (see Table 2.9). The addition of the two emission sources gives the total embodied carbon for wood. Therefore, the embodied energy and embodied carbon for wood are 10 MJ/kg and 0.71 kgCO_2/kg, respectively (see Table 2.9). Hammond and Jones (2011) also stated that the embodied carbon for wood obtained from a sustainably managed forest may be taken as the carbon emitted only from fossil fuel combustion (i.e. the first embodied carbon coefficient). The embodied energy and embodied carbon for PVC are 77.2 MJ/kg and 2.61 kgCO_2/kg, respectively (see Table 2.9). This shows that the embodied energy for PVC is about a factor of 8 greater than that of wood.

Table 2.9: Embodied energy and embodied carbon of wood and PVC (Data extracted from Hammond and Jones (2011))

Material	Embodied energy [MJ/kg]	Embodied Carbon [kgCO_2/kg]
Wood	10	0.71 (0.30_{fos} + 0.41_{bio})
PVC	77.2	2.61

The reason for the lower embodied energy and embodied carbon of wood compared to PVC can be attributed to the significantly lower energy intensive processes required to process a tree trunk into a useful structural material. Processing of timber predominantly includes cutting and drying (or seasoning) the wood section to prevent shrinkage and dimensional changes during its use. Asif (2009) also highlighted that the production of wood does not

include the melting stage, which can be energy intensive. On the other hand, the production of PVC is energy intensive. The carbon dioxide emitted per kilogram during the production of PVC is about four times greater than that of wood. This can be attributed to the greater quantity of carbon dioxide emitted during the extraction and processing of its raw materials (i.e. production of ethylene and chlorine). Asif et al. (2002) also stated that the production of PVC results in the release of toxic pollutants such as hydrocarbons and dioxins.

2.8. Timber and PVC Fencing

2.8.1. Fencing – An Overview

Fencing can be defined as physical barriers to control the movement of pedestrians and animals or to demarcate boundaries (Freedonia, 2012). There are different choices of fences available for equestrian fencing applications; they include timber, PVC and wire (plain, barbed and electric) fencing (Berto, 2003). In a guideline published by the British Horse Society (BHS) (2014), wire fencing is dangerous and less desirable. This is mainly due to the low visibility of wire fencing. Also, the use of electric wires is hazardous and may result in serious injury or death to both humans and animals (USDA, 2011, Gay, 2011). Furthermore, a common problem with the use of wire in equestrian fencing is 'sagging', slacking and stretching. The British Horse Society (BHS, 2014, Department for Environment Food and Rural Affairs, 2009) provides a guideline for equestrian fencing; noteworthy factors include:

- Uprights (posts) should be located every 1.5 m to 3 m apart, depending on the type of fencing, with at least two rails running between them.
- Lower rails should be placed at 0.5 m above ground level.
- Fence height requirements are listed below
    - Horses – 1.08 m to 1.38 m
    - Ponies – 1.0 m to 1.3 m
    - Stallions – 1.25 m to 2.0 m

The guidance given in BHS (2014) also states that an equestrian fencing system should have good transverse stiffness and strength, good aesthetics, high visibility, low cost and require low maintenance.

Structurally, an equestrian fencing system should act as a barrier to restrain horses (BHS, 2014). Equestrian fencing structures typically experience different types of combined loadings (i.e. bending, torsion, shear, impact) whilst in service. Therefore, it is essential to understand and quantify the properties of fencing structures. The quantification of these properties also requires the knowledge of the mechanical and geometric properties of the joints and structural members (i.e. posts and rails). However, no legislative requirement has yet been found for the load-bearing characteristics for equestrian fencing. Therefore, an aspect of this work focuses on the investigation of the load-deformation responses of equestrian fencing structures. Such knowledge also underpins appropriate material selection for the design of an equestrian fencing system.

Furthermore, moisture absorption and water uptake are important factors to consider in evaluating the suitability of novel composite materials for fencing structures. This is because these aforementioned factors can lead to the formation of cracks and voids at the fibre-matrix interface and can cause a reduction of the mechanical properties and dimensional instability of composites (Alomayri et al., 2014). According to Strong (2008), composites absorb moisture through the matrix, fibre, fibre-matrix interface, and porous regions or areas where micro-cracking or delamination have occurred. Whilst the aforementioned properties are important; it is also essential to take other noteworthy factors such as environmental degradation, cost and sustainability of the fencing materials, into consideration for the design of an equestrian fencing system.

Timber and PVC are common materials used in equestrian fencing, but timber predominates (Freedonia, 2012, Martin, 2006, Kline, 2014). Its major advantages include good mechanical properties (i.e. high flexural strength and flexural modulus), low cost and high visibility. However, timber fences require high maintenance as their service life is mainly determined by their resistance to decay, this is because timber is hydrophilic (TRADA, 1993). On the other hand, PVC is water resistant, thereby leading to and long service life (Agarwal and Gupta, 2011, Yu et al., 2016). Therefore, the use of suitable compatibilizing agents for good interfacial adhesion and the elimination of voids can reduce and limit the water absorption capabilities of novel waste carpet structural composites, making them suitable for outdoor applications (Yang et al., 2006). Furthermore, a reduction in the water absorption

capabilities leads to an improvement in dimensional stability and durability of composite materials. Figure 2.14 shows a typical equestrian timber post and rail fencing system.

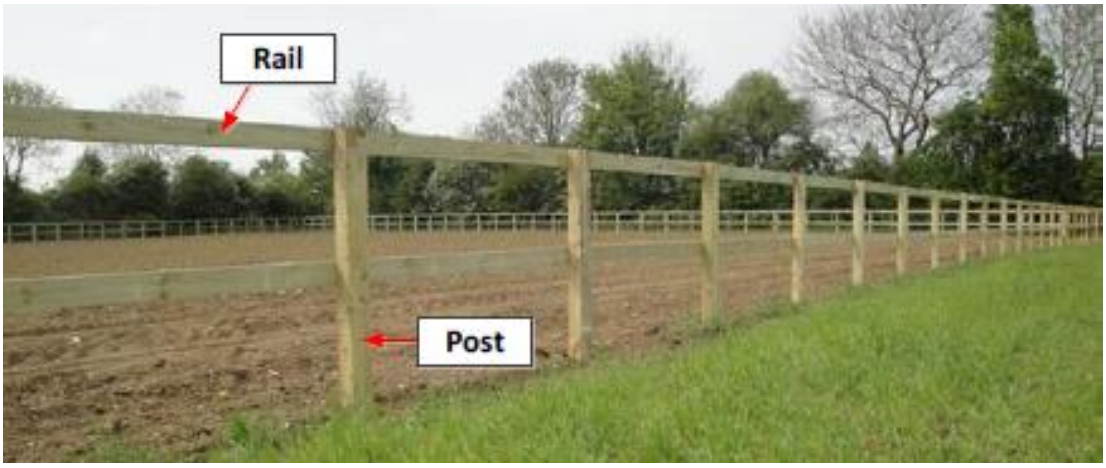

Figure 2.14: Image of a typical equestrian timber post and rail fencing system

2.8.2. Timber Fencing

Timber fencing is dominated by the use of sawn softwood and largely used in the agricultural and residential sector (Moore, 2015). The total sawn softwood consumption in the UK in 2014 was about 9,490,000 m^3. Figure 2.15 shows the quantity of sawn softwood utilised for fencing and outdoor applications in the UK from 2002 – 2014. 1,630,000 m^3 of softwood was used for fencing and outdoor (i.e. decking, sheds and barriers) applications in 2014. As shown in Figure 2.15, it appears that there has been a gradual increase in the demand for timber fencing materials in the UK, and this has led to the rise in the consumption of softwood over the years. Moore (2015) relates this increase to the rise in demand for relatively cheap repairs and improvements in fencing and barrier-type structures.

BS 1722-7 (2006) provides a specification for wooden rail and post fences. This specification includes information regarding component sizes, fastening types, concrete surrounding the bases of the posts and general installation instructions for a serviceable fence. It is worth noting that BS1722-7 (2006) is predominantly used for fencing installations on highways, and not typically used for equestrian fencing arenas and other types of fencing.

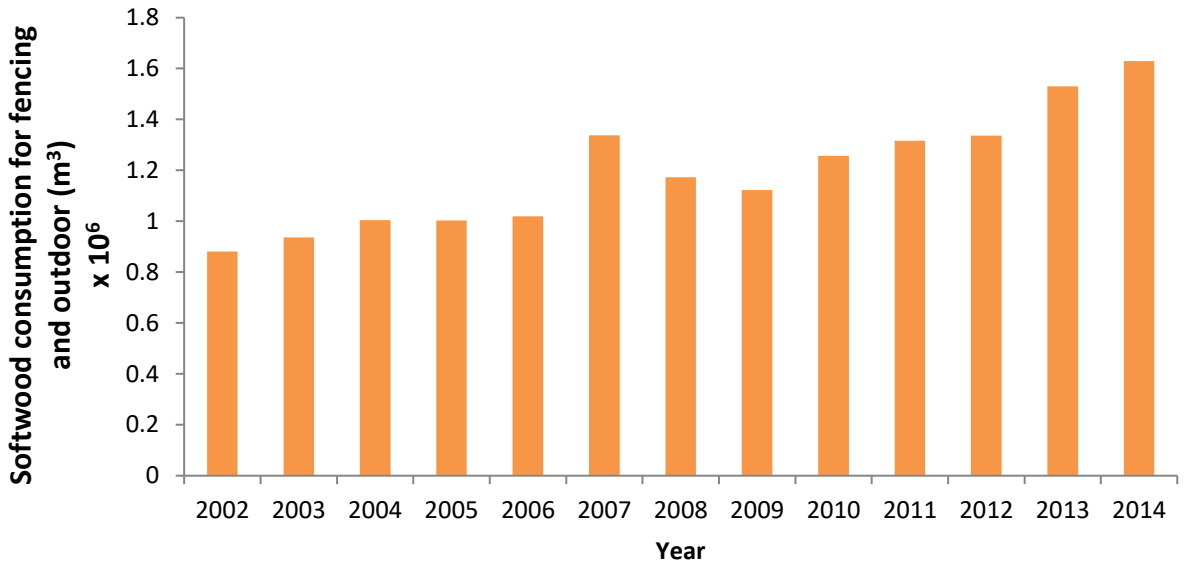

Figure 2.15: Sawn softwood consumption for fencing and outdoor applications in the UK from 2002 - 2014

Figure 2.16 shows the overall geometry of a typical equestrian timber post and rail fence based on guidance obtained from prior communications with Equestrian Surfaces Ltd. The posts are concreted into the ground to serve as supports for the rails.

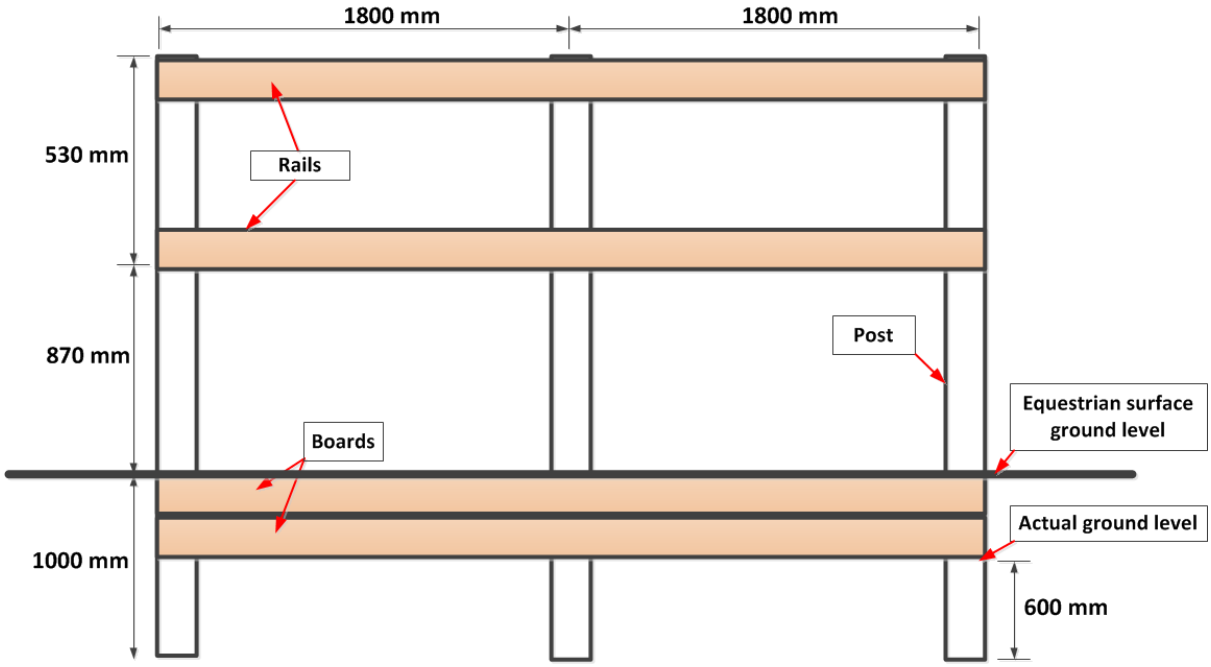

Figure 2.16: Overall geometry of a typical equestrian timber post and rail fence

TRADA (1993) suggests a 0.6 - 0.75 m depth of hole for the base of the timber posts. A mixture of silica sand and granulated synthetic carpet fibres or rubber crumbs is laid across the equestrian arena to the top of the timber boards. The timber boards are nailed to the

bottom of the posts and act as barriers for the equestrian surface compound. Typical equestrian timber fencing systems with two and three rail configurations are shown in Figure 2.17 and Figure 2.18, respectively. Table 2.10 shows the timber section type, size and quantity needed for a typical equestrian arena.

Figure 2.17: Image of a typical equestrian timber post and 2-rail fencing system

Figure 2.18: Image of a typical equestrian timber post and 3-rail fencing system

Table 2.10: Timber section type, size and corresponding quantity used for a typical equestrian fencing arena

Timber section	Dimension [width x depth x length] [mm]	Quantity used for typical equestrian fencing
Post	125 x 75 x 2400	75
Rail	100 x 47 x 3600	105
Board	150 x 38 x 3600	105

The dimensions may vary by ±5 mm

Wood preservative (such as creosote or CCA) is typically applied to the sides of the timber post in contact with the ground (BS 1722-7, 2006). BS EN 12620 (2002) specifies the mixture and aggregate properties used in the concrete surrounding the bases of the timber posts. Mechanical fasteners are commonly used in timber structures; this includes nails, staples,

screws, bolts and dowels (TRADA, 2012a). Nails are the most common type of fasteners used in timber constructions. They are manufactured from wires which have a tensile strength of 600 MPa, and their standard sizes in the UK typically range from 2.65 to 8 mm in diameter (Porteous and Kermani, 2007). Electroplated, galvanised or polymer coatings are applied to the nails for corrosion resistance and good surface finish. There is a minimum spacing requirement between each fastener, and the distance from each fastener to an end or edge of a structural member to prevent splitting failure when a joint is formed. Eurocode 5 (BS EN 1995, 2004) specifies a minimum of 7d spacing parallel-to-the-grain where d is the diameter of the nail; however, 4d spacing is conventionally used in England (TRADA, 2003). Furthermore, TRADA (2012a) recommends a minimum nail penetration of 35 mm into the post sections. According to USDA (2011), rails should be attached to the side of the posts facing the horses for safety purposes.

2.8.3. PVC Fencing

Plastic materials such as PVC are increasingly replacing traditional materials such as timber for equestrian fencing (Berto, 2003, Freedonia, 2012). In 2014, about 200,000 and 1.3 million tonnes of PVC were used for the production of rigid PVC profiles in the UK and Europe, respectively. These rigid profiles predominantly include window and door profiles, roller shutters and post/rail fencing sections (European Council of Vinyl Manufacturers, 2014). However, the actual quantity of rigid PVC used for fencing in the UK or Europe was not reported. The advantages of PVC over timber include the ability to be formed into complex shapes and its hydrophobic property (Agarwal and Gupta, 2011). However, PVC is more costly than timber, but requires relatively low maintenance and provides good aesthetics. The low maintenance required for PVC is due to its impermeability to moisture ingress and its resistance to temperature extremes and ultraviolet exposure (German, 1992). However, PVC has a lower flexural modulus than timber. It is worth noting that PVC fencing structures may utilise steel reinforcement to increase the overall stiffness and strength of the fencing structure.

ASTM F964 (2013) provides the specification for rigid PVC profiles used for agricultural, residential and commercial fencing and ASTM F1999 (2006) provides the installation specification for rigid PVC post and rail fencing. The structural load-bearing characteristics for the PVC structural members and/or the fence assembly are not addressed in these

standards. However, the geometric and mechanical properties of PVC posts and rails typically used for equestrian fencing are given in Table 2.11 (also see Appendix 1). The PVC post is a two-cell hollow section – one for the steel support and the other for the rail (see Figure 2.19). In addition, the post has openings on opposite faces of the rail cell.

Table 2.11: Section size, tensile strength, flexural modulus and quantity of PVC posts and rails used for a typical equestrian fencing arena (Duralock Performance Fencing, 2014)

Section type	Quantity	Dimension [width x depth x length] [mm]	Tensile strength [MPa]	Flexural modulus [GPa]
Post	60	150 x 100 x 1300	45 - 50	2.4 – 2.5
Rail	90	108 x 50 x 4000		
Board	60	108 x 50 x 4000		

Figure 2.20 shows a schematic diagram of a PVC fence assembly with two rails. An alternative assembly configuration with three rails without steel reinforcement is shown in Figure 2.21. As for the assembly of timber fencing, a hole is initially dug for the insertion of the PVC posts (Duralock Performance Fencing, 2014). The hole is then pre-filled with concrete to provide a rigid support for the posts. A 1500 mm long steel angle is driven into the wet concrete before fitting the posts. Afterwards, more concrete is applied inside the steel cell of the post until it covers the steel angle. The PVC rails are then slotted through the holes of the posts.

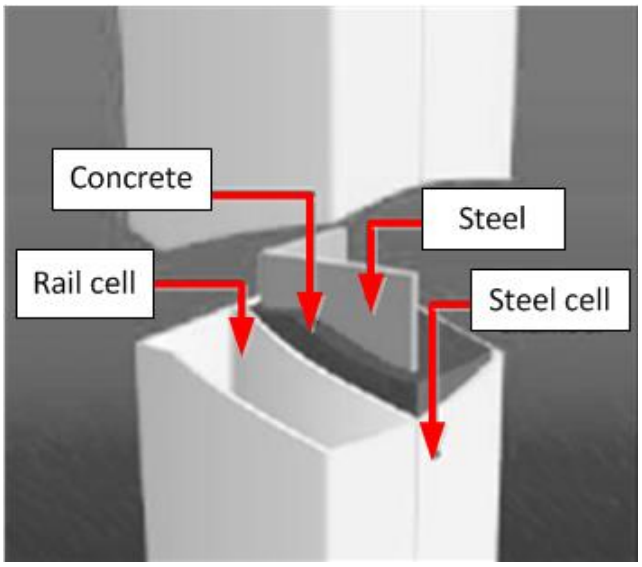

Figure 2.19: An image of a PVC post showing its two-cell hollow section (Duralock Performance Fencing, 2014)

The PVC fence can also be assembled with a flat steel plate that has two steel angles, and circular steel studs welded to it (see Figure 2.22). This assembly method does not require a pre-dug hole for the posts. Interlocking plastic grids are slotted over the circular steel studs welded to the steel plate (see Figure 2.23) before the insertion of the PVC posts over the welded steel angles. The rails (and kick boards) are then slotted through the holes of the posts. Figure 2.24 shows a representative equestrian PVC post and rail fencing system.

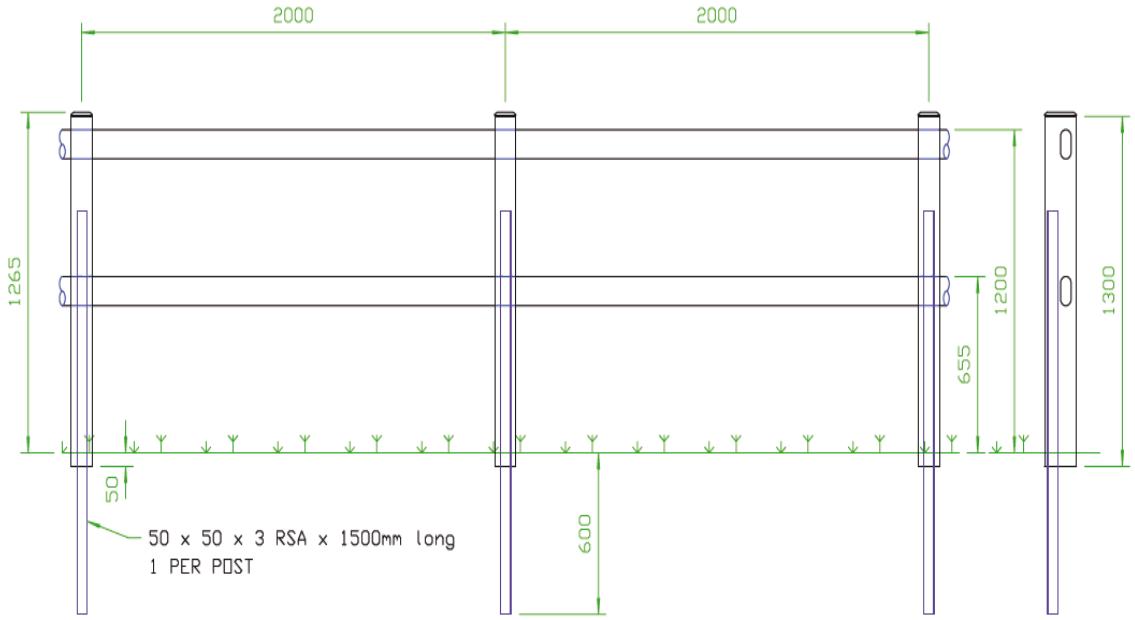

(a) (b)

Figure 2.20: Schematic diagram of an equestrian PVC fence assembly with two rails and steel reinforcement: (a) Front-view (b) Edge-view [all dimensions are in mm] (Duralock Performance Fencing, 2014)

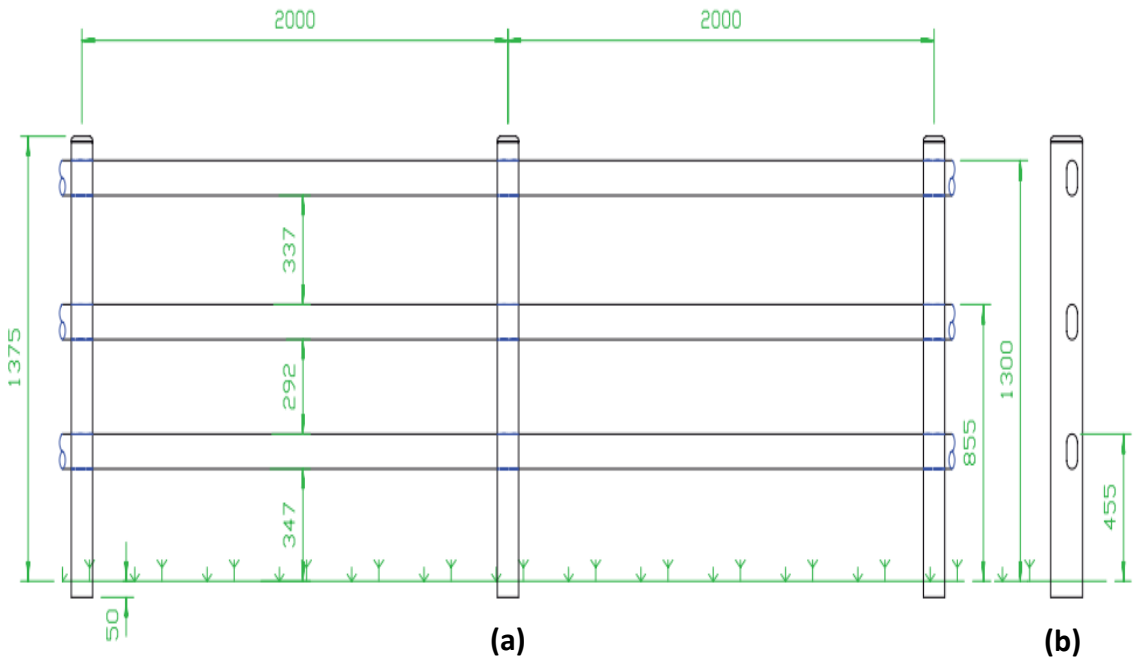

Figure 2.21: Schematic diagram of an equestrian PVC fence assembly with three rails and without steel reinforcement: (a) Front-view (b) Edge-view [all dimensions are in mm] (Duralock Performance Fencing, 2014)

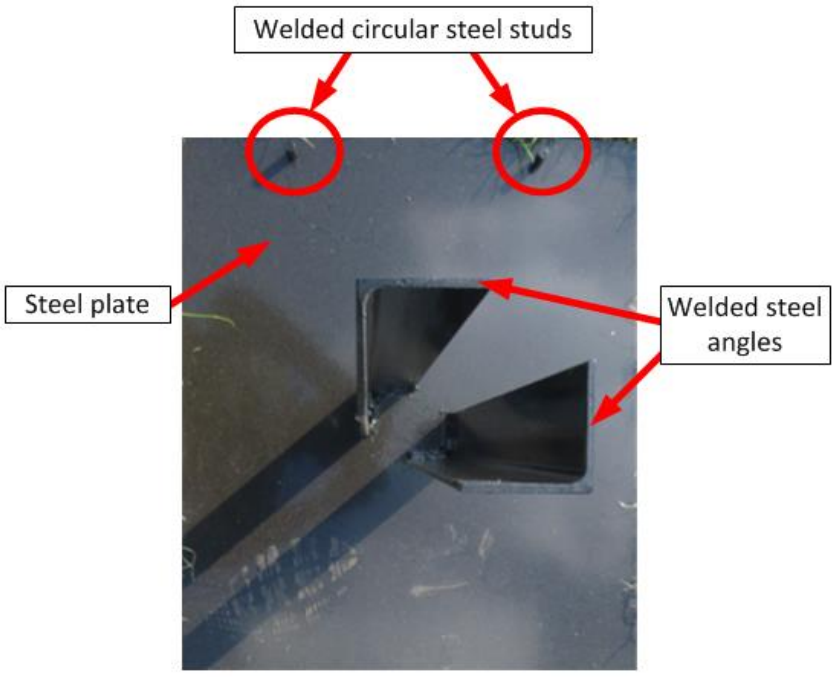

Figure 2.22: Photographic image of a top-down view of a steel plate with welded steel angles and circular steel studs

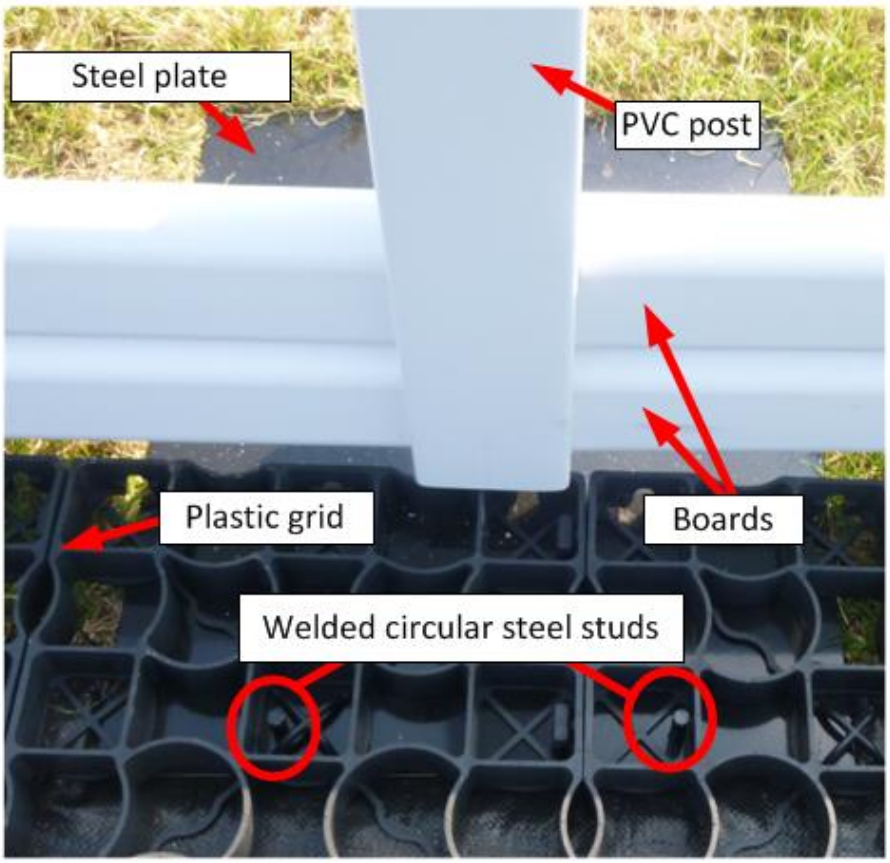

Figure 2.23: Details of the PVC base joint assembly

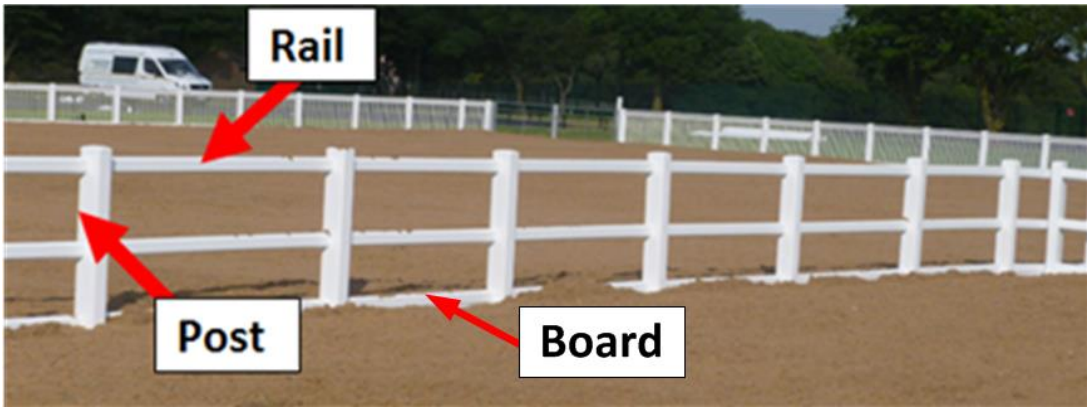

Figure 2.24: Image of a typical equestrian PVC post and rail fencing system

2.9. Chapter Summary

The issue of waste has become a major concern in the global economy. Increasing recycling remains a key priority of the European Union. Annually, 400,000 tonnes of carpet waste are sent for disposal to UK landfill sites, mainly because of the difficulty associated with processing it into viable alternative commodities. However, disposal of carpets to landfill is

becoming increasingly impractical due to rising landfill costs and reduced availability, both reflecting the environmental concerns surrounding disposal to landfill.

This chapter has reviewed the currently available end-of-use processing options for carpet waste. Options including the incineration of carpet for energy recovery, re-use, equestrian surface applications, fibre reprocessing and plastics reprocessing have been discussed. Energy from waste via incineration presently accounts for the largest volume of carpet waste disposal in the UK. Whilst this option has appeal as it is insensitive to the type/form of carpet waste, the greenhouse gas emissions arising are high. Nevertheless, from an environmental impact perspective, energy from carpet waste is preferred to the landfill option. Re-use of carpets can be the most cost-effective and environmentally neutral approach, as it is associated with significant savings in both raw materials and energy consumption; however, it is only viable for certain types of carpet waste and requires the availability of suitable processing centres. Recycling via fibre reprocessing and/or use in equestrian surface applications, whilst available, are not currently economically attractive as they incur additional labour costs stemming from the need to sort the carpets according to their face fibres.

Plastics reprocessing is a recycling option for carpet waste that offers both economic and environmental appeal, with estimates indicating that each tonne of recycled carpet saves 4.2 tonnes of CO_2 emissions. A number of studies have investigated the feasibility of using carpet waste within structural composites and thereby diverting waste from the landfill and incineration disposal options. The mechanical properties of several carpet based structural composites reported in the literature have been presented and discussed in this chapter. Variations in the mechanical properties of these composites have been reported, reflecting differences in polymer chemistry, processing conditions, and volume fraction of the constituent phases, arising in part from the type of carpet waste used. Literature studies have focused mainly on carpets having synthetic/man-made face fibres but the isolation of these waste streams requires an input of labour in the sorting stage of carpet waste processing. Furthermore, some of the reported manufacturing processes comprise of energy intensive stages, which reduces the environmental advantage of the recycling approach on account of increased greenhouse gas emissions. The addition of glass fibres to these recycled waste carpet composites offers improvements in mechanical properties for

load-bearing applications. However, glass fibre addition increases raw material costs and adds a further processing step in their manufacture.

This chapter also highlights that wood and rigid PVC are common structural materials used for equestrian fencing. Wood is anisotropic and its mechanical properties vary widely and are affected by several factors i.e. presence of knots, moisture content, species type etc. Wood is also susceptible to degradation due to biological attack and its hydrophilic nature results in its decay and dimensional instability. On the other hand, rigid PVC posts and rails used for fencing are typically extruded. Approximately 10 – 20 wt. % of additives are added to the PVC compound during the extrusion process to improve its mechanical properties. This chapter also gave details of common assembly methods, geometry and structural connections for equestrian wood and PVC fencing. It is, however, worth highlighting that there are no structural load-bearing standards for equestrian fencing.

The end-of-life options of wood and PVC were also presented and discussed; they include incineration for energy recovery, recycling and landfill disposal. The environmental assessments for wood and rigid PVC show that the embodied energy and carbon of the former are significantly lower than those of the latter. This reflects that wood possesses higher environmental benefits compared to PVC. However, global forest loss is occurring at a high rate of 13.7 million hectares (137,000 km^2) per year and deforestation accounts for about 12 % of global CO_2 emissions.

From the review, it can be concluded that there is a need for alternative structural materials with lower carbon footprints, in efforts to mitigate global climate change. Furthermore, there are significant environmental concerns with the issue of carpet waste and a number of technological challenges have prevented the manufacture and uptake of novel structural composites containing significant volumes of carpet waste. Hence, there is a need for further research to develop structural composites containing carpet waste using manufacturing processes that account for all types of carpets, are low cost, eliminate mechanical separation stages, are environmentally neutral and produce composites with well characterised mechanical properties suitable for equestrian fencing. It is also essential to address the need for an improved scientific understanding of the load-deformation response of equestrian timber and PVC fencing. This knowledge can then be transformed

into useful structural design guidance for the replacement of timber and PVC posts and rails with alternative novel and lower carbon footprint recycled waste carpet structural composite materials.

3. Chapter Three - Materials and Manufacturing Methods

3.1. Introduction

Given the challenges associated with carpet recycling reported in the literature (see Chapter 2), this chapter explores the possibility of recycling carpet waste through the development of novel waste carpet structural composites, which can be used as alternatives to timber and PVC in equestrian fencing. This chapter also describes the processing conditions with a view to understanding and optimising the feasibility of using carpet waste in the fabrication of novel composites. Furthermore, the input materials and manufacturing methods for three different prototype waste carpet structural composites are described. These prototype composites were manufactured in conjunction with the local industrial partner (ECO2 Enterprises), which was located in Burnley, Lancashire. A description of timber and PVC post and rail sections typically used for equestrian fencing is also given. The posts and rails were received from Equestrian Surfaces, Burnley.

3.2. Manufacturing Process for Novel Waste Carpet Structural Composites

The manufacturing of the composites were carried out at ECO2 Enterprises in Burnley Lancashire, and the choice of the materials and manufacturing processes were restricted to the infrastructure available at ECO2 Enterprises. The main processing equipment available at ECO2 Enterprises included a carpet waste granulator, Banbury mixer and a hydraulic press. As a result of these limited infrastructures and cost restraints, three different types of prototype waste carpet structural composites were fabricated, and are referred to as Composites A, B and C. Composites A and B consist of a polymer matrix enclosing a bonded carpet strip core. Polyurethane was chosen as the polymer matrix to enclose the bonded carpet strip core and also give good aesthetics. Furthermore, as the waste carpet structural composites are intended to be used in an outdoor environment, polyurethane also provides good resistance to degradation. Studies have also shown that the mechanical properties of polyurethane can be improved with the addition of fillers (Zhou et al., 2007, Uddin et al., 2005, Cao et al., 2005). On the other hand, the fabrication process for Composite C was different from that of Composites A and B. The manufacturing process for Composite C

involved shredding, granulation and extrusion of strips of carpet waste, before being moulded with no second phase polymer addition. Due to the prototype nature of this study, there were limitations in the number of manufactured samples, which also led to constraints in the evaluation of their repeatability.

Although other manufacturing processes could have been explored, the aforementioned manufacturing processes were chosen as a result of their viability based on the limited infrastructure available at ECO2 Enterprises. In addition, the chosen manufacturing processing options for Composites A – C may be used for different types of carpet waste (i.e. synthetic/man-made and natural face fibres), and potentially lead to the manufacture of structural composites containing large volumes of carpet waste. Furthermore, neither of the processes involved mechanical separation of the carpet fibres which may have been energy intensive. The details of the manufacturing processes for Composites A – C are given in Sections 3.2.1 and 3.2.2.

3.2.1. Manufacturing Processes for Composites A and B

Post-consumer wool carpet strips were bonded tuft-to-tuft with an adhesive (with a trade name of V4921) and subjected to a pressure of 14 MPa in a hydraulic press. Figure 3.1 shows diagrams of the formation of two pairs of the bonded tuft-to-tuft carpet strips. An overview of the manufacturing process which progresses sequentially through Images 1 – 7 is given in Figure 3.2. The size of the steel mould used for the fabrication of Composite A was 1000 mm x 110 mm x 65 mm. The base and sides of the steel mould were initially sprayed with polyurethane; the machine used to deliver the spray had an output of 20 g/sec. Thereafter, two pairs of bonded wool carpet strips described in Figure 3.1 were placed in the mould. Polyurethane was then sprayed on the aforementioned two pairs of bonded carpet strips before an additional three pairs of bonded wool carpet strips were placed on top of the polyurethane layer (see Image 5 of Figure 3.2). Additional polyurethane was sprayed to form the top layer of Composite A.

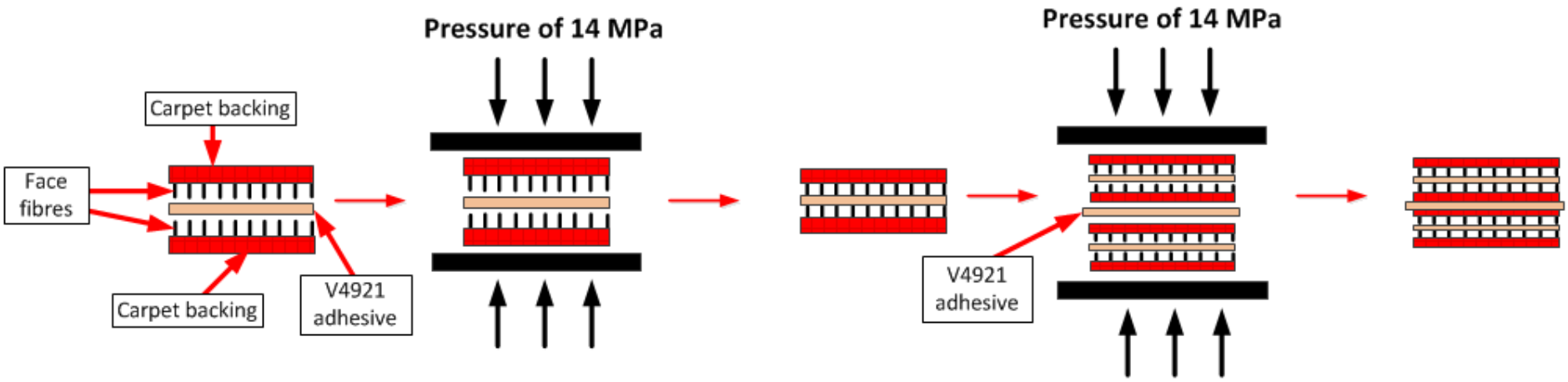

Figure 3.1: Formation of two pairs of the bonded tuft-to-tuft carpet strips enclosed in Composites A and B

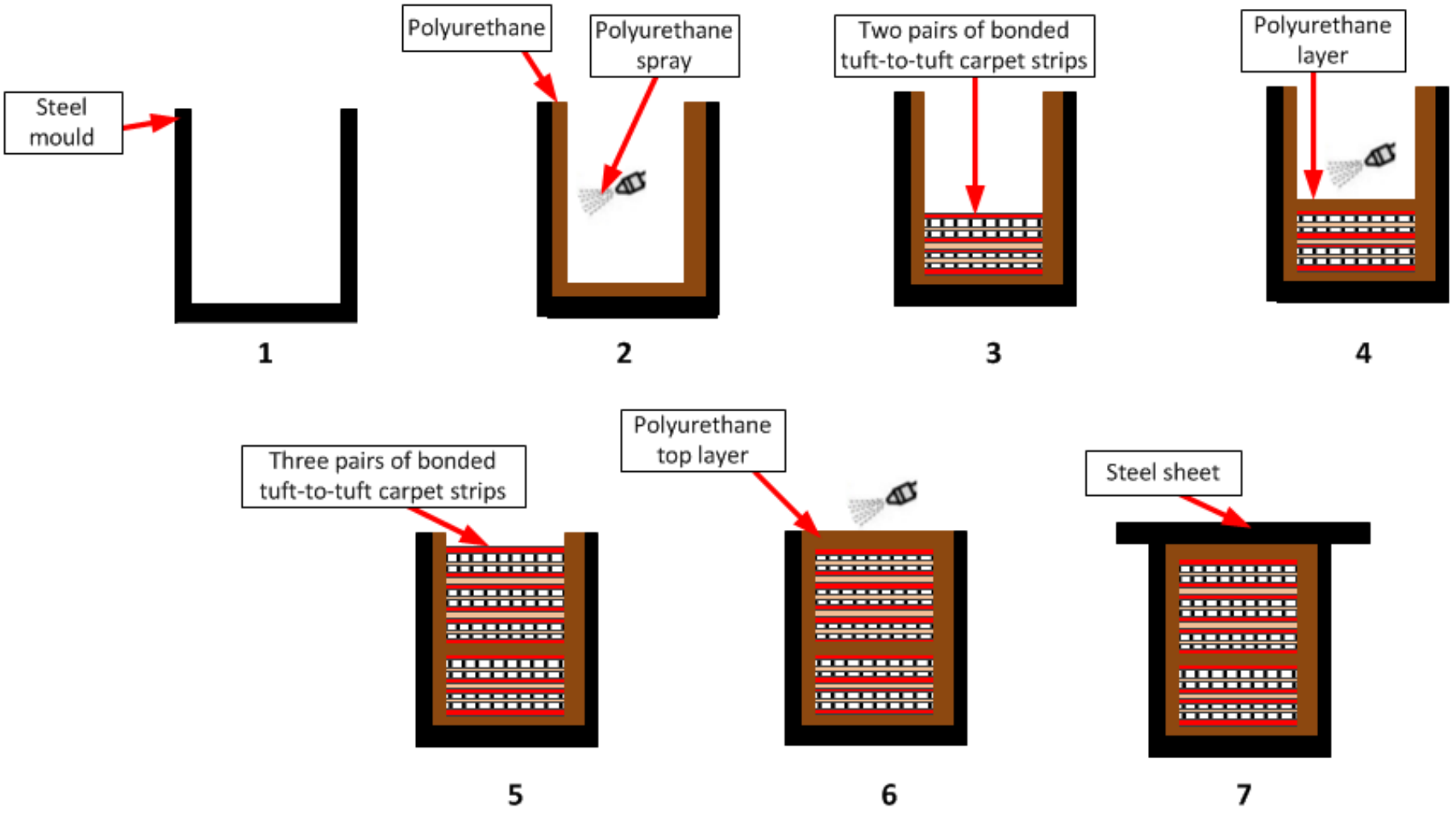

Figure 3.2: Diagrams showing the processes involved in the fabrication of Composites A and B

The mould was covered with a steel sheet and placed in a hydraulic press to enclose and prevent the release of the polyurethane matrix during the polymerisation process. It was left to cure for 40 minutes before it was de-moulded. The cross-section of Composite A is shown in Figure 3.3. The mass density of Composite A was 354 kg/m^3.

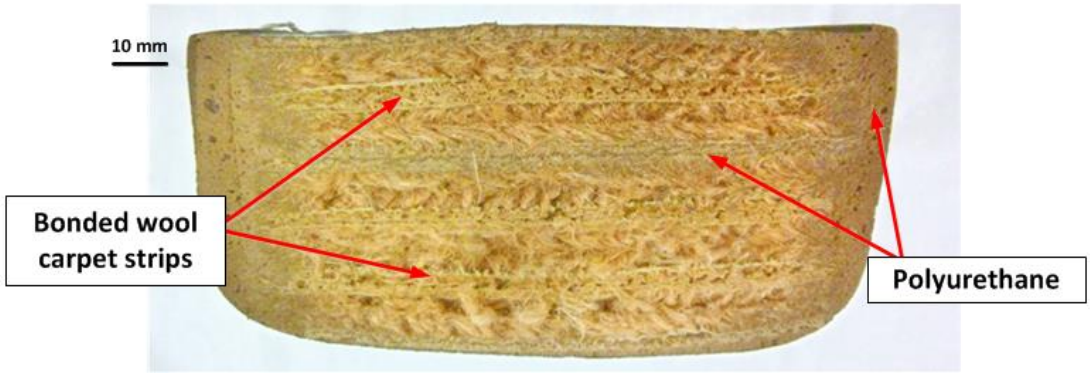

Figure 3.3: An image of the cross-section of Composite A

Composite B was manufactured using the same process as Composite A (see Figure 3.2). However, the polyurethane matrix used in the formulation of Composite B included 2 wt. % CoatForce10 (CF10) fibre filler to enhance its flexural stiffness. The addition of the CF10 fibre to the polyurethane was based on a recommendation from a polymer consultant as an approach worth exploring for the purpose of improving its flexural properties. The length and diameter of the CF10 fibre are 125 µm and 5 µm, respectively (Huynen, 2008). The CF10 fibre has a tensile strength of 850 MPa and a Young's modulus of 100 GPa. A more detailed chemical composition of CF10 is given in Appendix 2. Furthermore, two separate beams made of the matrix material (polyurethane) used to fabricate Composites A and B were manufactured to investigate their flexural properties. The first polyurethane beam, made without the use of filler, had a mass density of 227 kg/m^3. The second polyurethane beam with 9 wt. % CoatForce10 (CF10) fibre filler had a mass density of 245 kg/m^3. The quantity of the CF10 fibre (9 wt. %) added to the polyurethane was based on its availability, cost restraints and recommendation from a polymer consultant. The flexural properties of the beams help to define the optimum formulation and suitability of polyurethane as the matrix of the recycled waste carpet composites.

The dimensions of Composite B are larger than those of Composite A. The size of the mould used for the fabrication of Composite B was 2000 mm x 110 mm x 100 mm. The cross-section of Composite B is shown in Figure 3.4. As a result of limitations with the mould size

available, Composite B had two sets of three pairs of bonded carpet strips compared to the two and three pairs in Composite A (cf. Figure 3.3 and Figure 3.4). The mass density of Composite B was 382 kg/m^3.

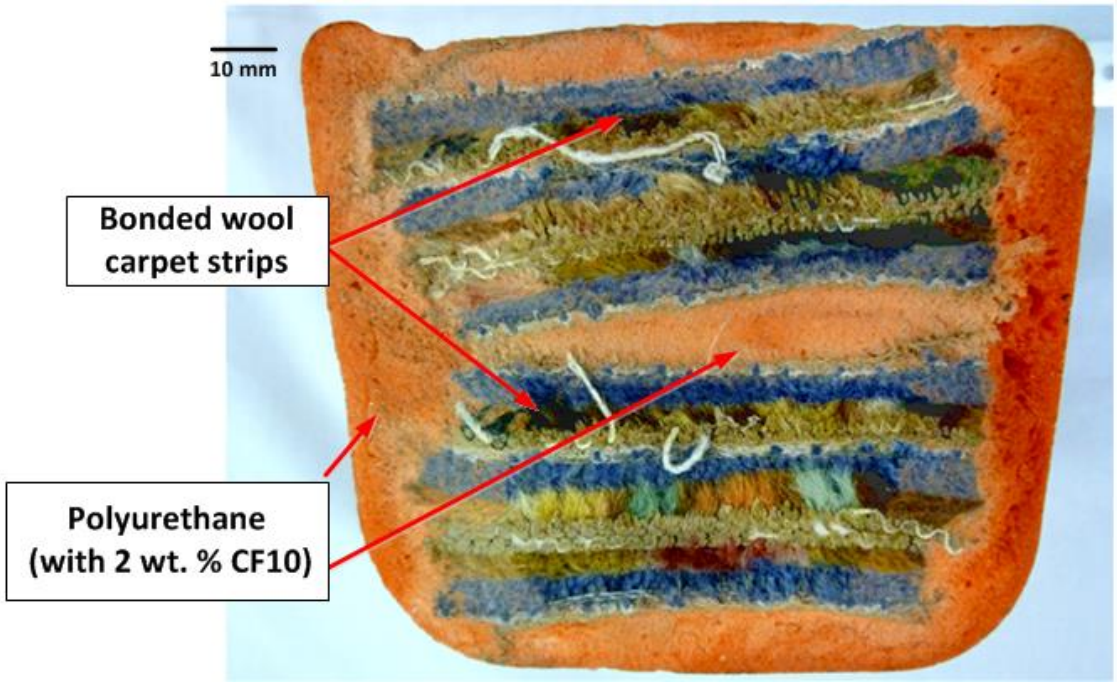

Figure 3.4: An image of the cross-section of Composite B

The geometric imperfections of the cross-sections of Composites A and B (see Figure 3.3 and Figure 3.4) were partly due to the pressure from the expansion (or foaming) of the polyurethane matrix causing rotation of the walls of the steel mould during the polymerisation process. Furthermore, the carpet strips embedded in the core of Composites A and B were manually stacked by hand lay-up, and thus contributed to the inhomogeneity of the composite beams. The hand lay-up technique and limited infrastructure available also led to variations in the thickness of the polyurethane matrix (cf. Image 7 in Figure 3.2 with Figure 3.3 and Figure 3.4). Hence, the imperfections and other defects such as voids and cavities shown in Figure 3.3 and Figure 3.4 can be attributed to the processing conditions of the novel composites, and may also affect their mechanical properties. Therefore, these processing conditions need to be controlled to give a reduction in the defects and flaws of the composites. These factors may also be mitigated by the use of modern automated equipment for large scale production.

The volume fractions of the constituents of Composites A and B were calculated from the measurements of their cross-sectional areas with the use of image processing software, ImageJ (Abramoff et al., 2004). Using this method, the polyurethane matrix and bonded carpet strips' volume fractions of Composites A and B were found to be 0.4 and 0.6, respectively. Furthermore, as a result of the dimensional instability of the prototype composites, four measurements of the width and depth of the cross-sections of Composites A and B along the length of the beams were taken (see Appendix 3), and give a standard deviation of up to 6 mm. As these prototype composites were fabricated as part of a trial study, the average dimensions (see Appendix 3) were used for the subsequent experimental analyses of the novel composites. Although there are limitations which affect the precision of the measurements, the subsequent experimental analyses carried out in this study, give an understanding of some fundamental mechanical properties of the novel composites.

It was also deemed appropriate to investigate the mechanical properties of the bonded waste wool carpet strips enclosed in Composites A and B, to determine the optimum configuration for the recycled waste carpet structural composite. Hence, pairs of identical waste wool carpet strips were bonded together in three different orientations (Tuft-to-Tuft, Tuft-to-Back, Back-to-Back) with an adhesive (with a trade name of V4921). All the bonded carpet strips were subjected to a through-thickness pressure of 14 MPa using a hydraulic press and left for five minutes whilst the adhesive cured at ambient temperature. Figure 3.5 shows illustrative diagrams of the three different orientations of the bonded waste wool carpet strips.

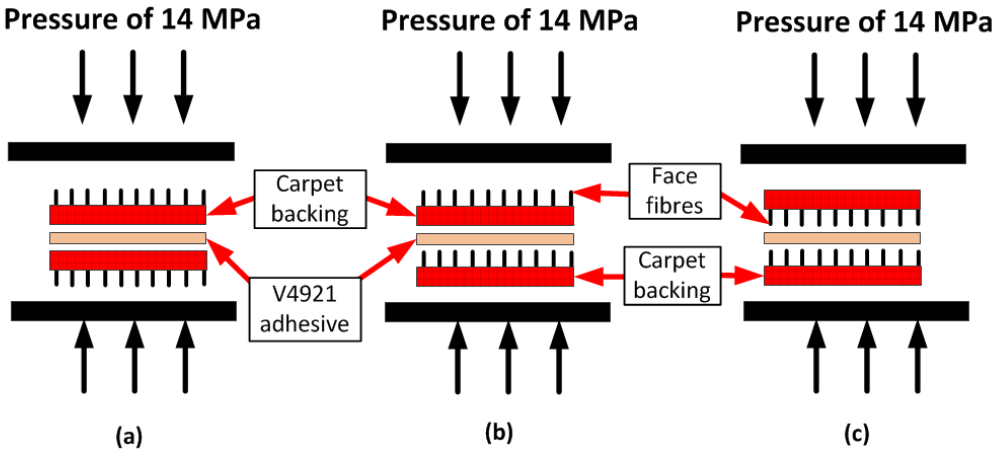

Figure 3.5: Diagrams of the three different orientations of the bonded waste wool carpet strips: (a) Back-to-Back (b) Tuft-to-Back and (c) Tuft-to-Tuft

As this type of investigation had not been reported in the open literature, uniaxial tensile tests were carried out to determine the maximum force required to separate the bonded strips. The details of these tests are given in Chapter 4, and the actual images of the bonded waste wool carpet strips are shown in Figure 3.6.

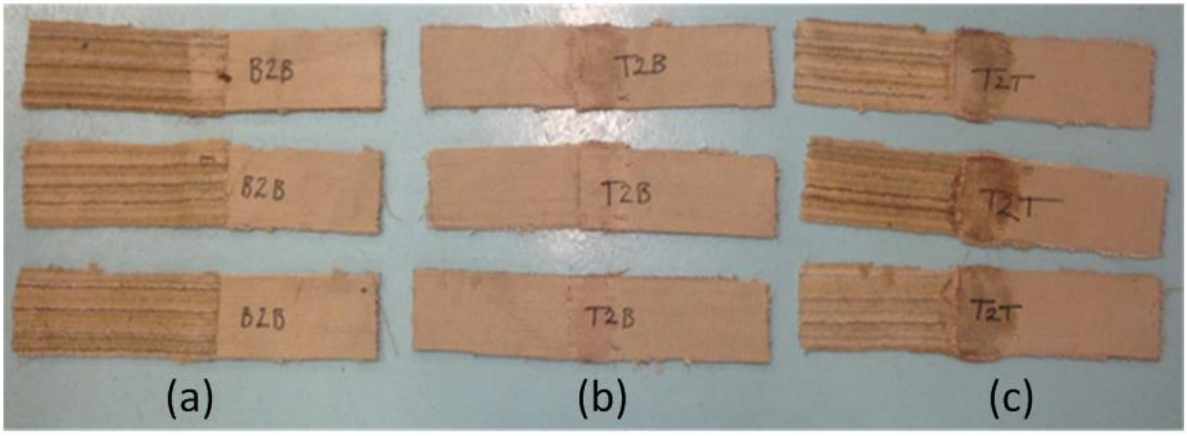

Figure 3.6: Images of the bonded waste wool carpet strips: (a) Back-to-Back (b) Tuft-to-Back and (c) Tuft-to-Tuft

There were some variations across the width of the bonded waste wool carpet strips (see Figure 3.6); this was because the carpet strips were manually cut by hand. As a result of these dimensional variations, four width measurements were taken and are given in Appendix 8; their averages were used to compute their shear strengths. The average width and bond length of the bonded waste wool carpet strips shown in Figure 3.6 were 100 mm and 60 mm, respectively. These aforementioned dimensions were based on constraints imposed by the grips of the universal testing machine. Additional details of the experimental test setup are given in Chapter 4.

3.2.2. Manufacturing Process for Composite C

The manufacturing process for Composite C was different from that of Composites A and B. Post-consumer waste carpets were initially sorted according to their face fibres using a Thermo Scientific microPHAZIR PC handheld Near-Infrared (NIR) analyzer (Thermo Scientific, 2010) into three different categories: Waste carpets with (a) Polypropylene face fibres (b) Synthetic face fibres; polypropylene, PET and nylon (c) Wool face fibres. The waste carpets were then separately shredded in a UNTHA VR140 granulator with a 40 mm screen. Four different formulations for Composite C were fabricated and are referred to as Composite C_PP, C_PPW, C_SF and C_SFW; their respective compositions are given in Table 3.1.

Table 3.1: Description of the four formulations for Composite C

Label	Composition
Composite C_PP	100 wt.% waste carpets with polypropylene face fibres
Composite C_PPW	50 wt. % waste carpets with polypropylene face fibres and 50 wt. % waste carpets with wool face fibres
Composite C_SF	100 wt. % waste carpets with synthetic face fibres
Composite C_SFW	50 wt. % waste carpets with synthetic face fibres and 50 wt. % waste carpets with wool face fibres

1kg of shredded carpet waste was mixed in a Banbury mixer until the temperature in the barrel reached 150 ^{o}C. The blended mixture was then placed in a steel mould of size 300 mm x 150 mm x 10 mm, and the mould was subjected to a pressure of 14 MPa in a hydraulic press for five minutes at ambient temperature. Afterwards, the sample was removed from the mould. Three samples were produced for each formulation. Figure 3.7 shows a flow diagram of the processes used in the fabrication of Composite C.

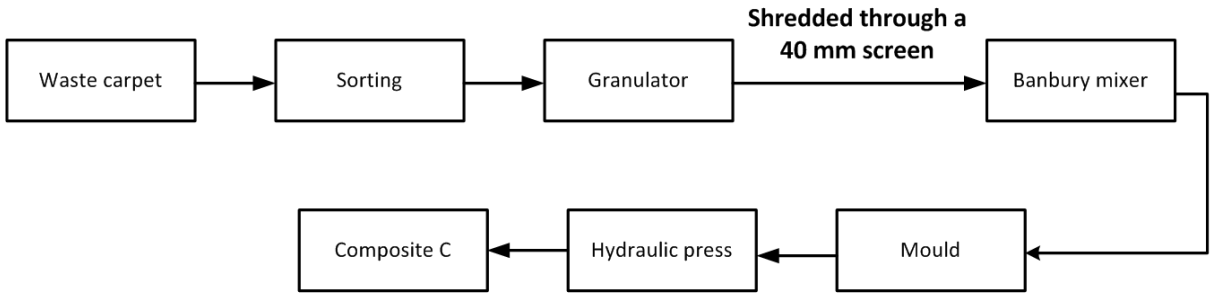

Figure 3.7: Flow diagram showing the processes involved in the manufacture of Composite C

Figure 3.8 shows images of the Composite C beams. A further examination of the Composite C beams revealed that Composite C_SFW had a large quantity of '*un-melted*' fibres due to the presence of significant amounts of elastomeric adhesive (SBR) (which typically contains inorganic fillers such as $CaCO_3$ and $BaSO_4$) and wool fibres, and therefore led to increased inhomogeneity. This is because wool fibres do not melt, and the elastomeric adhesive (SBR) which holds the carpet fibres together is a thermoset resin and does not also melt at high temperature. Therefore, in view of the points given above, the elastomeric adhesive, inorganic fillers ($CaCO_3$ and $BaSO_4$), dirt particles and the other carpet fibres (nylon, PET, wool) act as reinforcements in a polypropylene matrix. It is also worth highlighting that the melting point of the polypropylene fibres is about 160 ^{o}C which is significantly lower than

those of the other synthetic fibres; nylon and PET fibres have melting points which range from 215 – 265 ^{o}C and 256 – 268 ^{o}C, respectively (Palenik, 1999).

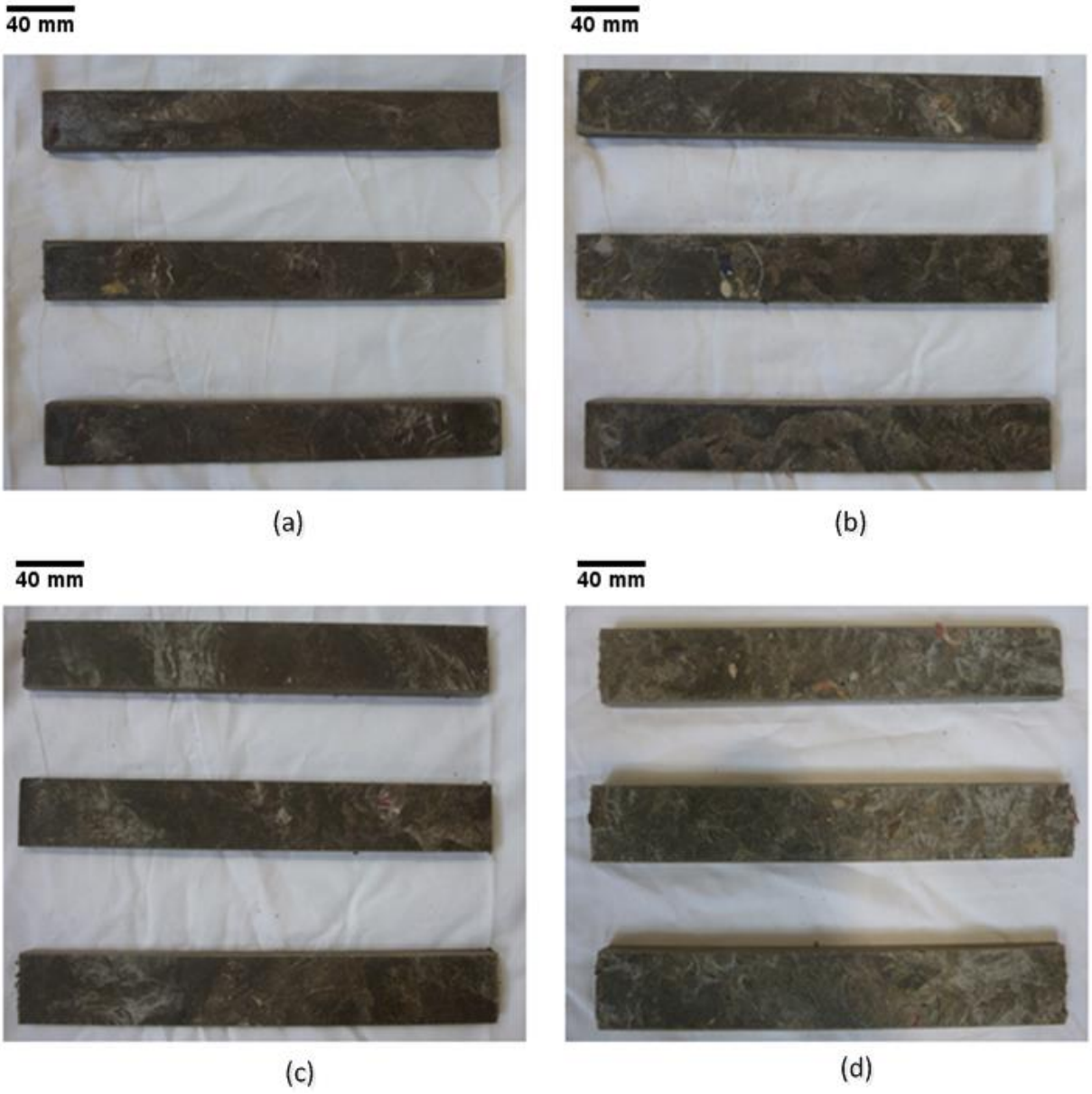

Figure 3.8: Images of Composite C beams: (a) C_PP (b) C_PPW (c) C_SF (d) C_SFW

The manufacturing process for Composite C introduced some surface roughness on the prototype samples, and the cross-section dimensions showed variations of about 3 mm (see Appendix 3). These variations reflect the differences in the type and volume fractions of the carpet waste used. These factors can also be attributed to the processing conditions of the Banbury mixer and the limited infrastructure available for the research study. In addition, Singh et al. (2016) stated that dimensional instability is a common factor in the fabrication of materials from recycled waste. Therefore, further study would be required to optimise

the dimensional stability and reproducibility of the novel composite samples. It should be highlighted that the manufacturing processes for the three different prototype composites (Composites A – C) all included a hydraulic press processing stage which has an energy intensity of about 12 MJ/kg (Song et al., 2009). Furthermore, compared to Composites A and B, the manufacturing process for Composite C involved additional energy intensive processing stages which include shredding of the carpet waste in a granulator and a high temperature extrusion process which has an energy intensity of about 19 MJ/kg (Song et al., 2009).

The average densities of the four formulations of Composite C are given in Table 3.2. The density of the materials is an important physical property and was subsequently used to estimate the unit size (in kg) of a typical equestrian fencing system comprised of the novel waste carpet structural composite posts and rails. The density may also be used to quantify the embodied energy and carbon of the novel composites and compared with those of other equestrian fencing materials.

Table 3.2: Average densities for the four formulations of Composite C beams

Composite C formulation	Density [kg/m^3]
100 wt.% waste carpets with polypropylene face fibres **(Composite C_PP)**	1135
50 wt. % waste carpets with polypropylene face fibres and 50 wt. % waste carpets with wool face fibres **(Composite C_PPW)**	1266
100 wt. % waste carpets with synthetic face fibres **(Composite C_SF)**	1297
50 wt. % waste carpets with synthetic face fibres and 50 wt. % waste carpets with wool face fibres **(Composite C_SFW)**	1403

Based on the compositions and densities of Composites C_PP and C_PPW, the addition of 50 wt. % waste carpets with wool face fibres to the former gave an increase in density of about 12 %. Similarly, the addition of 50 wt. % waste carpets with wool face fibres to C_SF gave an increase in density of about 8 %. It is, therefore, evident that the addition of waste carpets with wool face fibres resulted in an increase in the average densities of the resultant composites (see Table 3.2).

3.3. Description of Timber and PVC Posts and Rails Used for Equestrian Fencing

Timber and PVC posts and rails used for equestrian fencing were received from Equestrian Surfaces, Burnley. The timber posts and rails were ungraded and are believed to be the softwood species spruce. The moisture content of the posts and rails was measured with an ST-125 model moisture meter, and the average moisture content was 12 (± 2) %. The timber posts and rails were weighed, and their mass densities are given in Table 3.3. The average mass density of the timber posts and rails were 521 kg/m^3 and 465 kg/m^3, respectively and falls within the range of mean densities (350 – 550 kg/m^3) for softwood species given in BS EN 338 (2009). It is also worth noting that the classification system for structural timber given in BS EN 338 (2009) is based on samples with approximately 12 % moisture content.

Table 3.3: Mass, volume and density measurements of the timber posts and rails

Timber section	Mass [kg]	Volume [x 10^{-2}] [m^3]	Density [kg/m^3]	Average density [kg/m^3]
Timber Rail 1	5.3	1.24	425	465
Timber Rail 2	6.2		504	
Timber Post 1	6.9	1.37	507	521
Timber Post 2	8.0		586	
Timber Post 3	6.4		469	

Extruded rigid hollow PVC posts and rails which are also used for equestrian fencing were received from Equestrian Surfaces, Burnley. A material specification sheet listing the mechanical properties of the rigid PVC was provided by the manufacturer, Duralock Performance Fencing (see Appendix 1); the flexural modulus ranges from 2373 MPa to 2510 MPa, and the tensile strength from 45 MPa to 50 MPa. The measured mass densities of the PVC posts and rails are given in Table 3.4. The average density of the PVC posts and rails were 1484 kg/m^3 and 1175 kg/m^3, respectively, which falls very close to the range (1300 – 1580 kg/m^3) given in Callister and Rethwisch (2008) for rigid PVC. Sketches of the cross-sections of the PVC posts and rails are shown in Figure 3.9 and Figure 3.10, respectively. The geometry of the PVC post showing details of the cut-outs for the rails is given in Figure 3.11.

Table 3.4: Mass, volume and density measurements of the PVC posts and rails

PVC section	Mass [kg]	Volume [x 10^{-3}] [m^3]	Density [kg/m^3]	Average density [kg/m^3]
PVC Rail 1	5.0	4.17	1209	1175
PVC Rail 2	4.8		1156	
PVC Rail 3	4.8		1159	
PVC Post 1	3.3	2.20	1494	1484
PVC Post 2	3.3		1500	
PVC Post 3	3.2		1458	

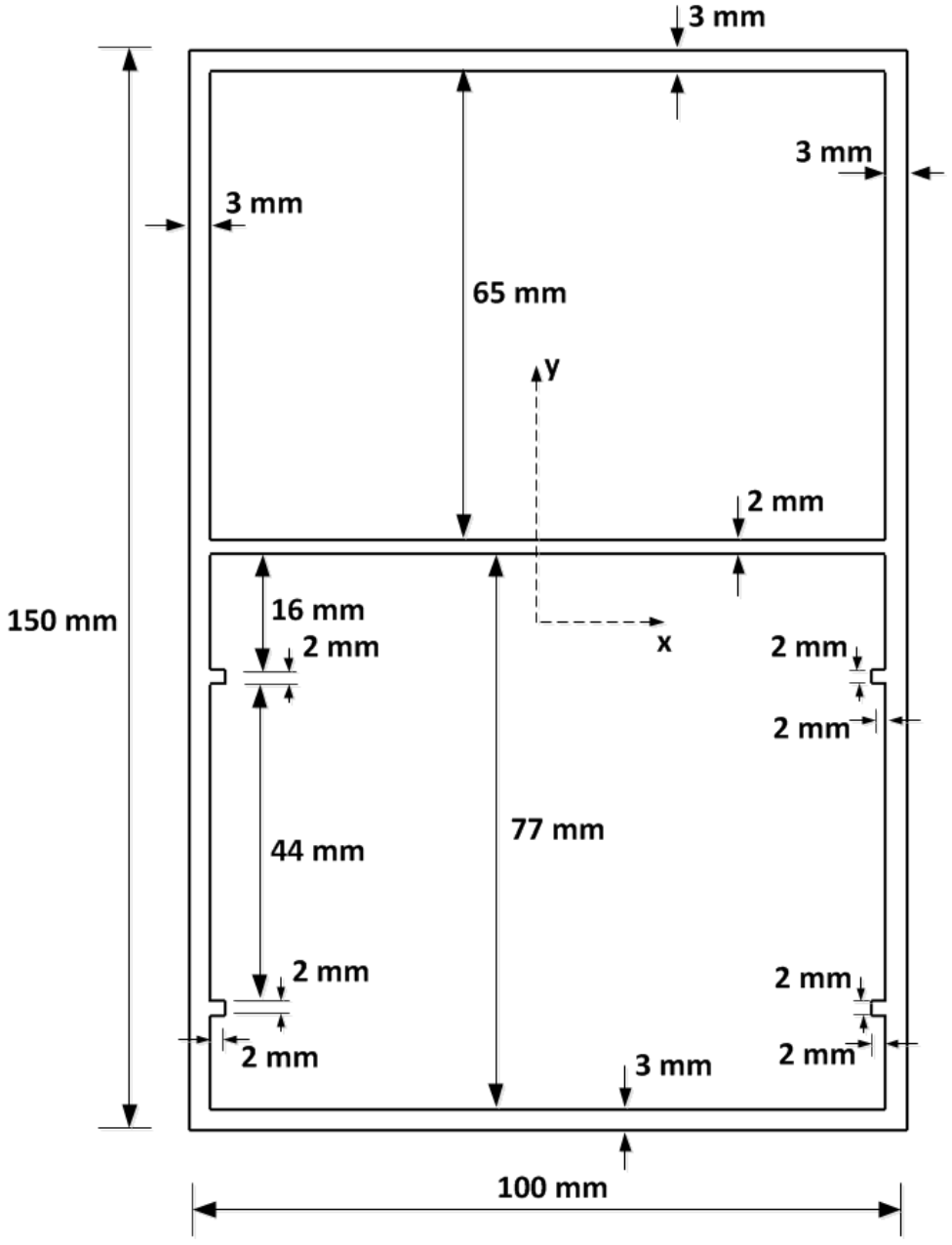

Figure 3.9: Sketch of the cross-section of a PVC post

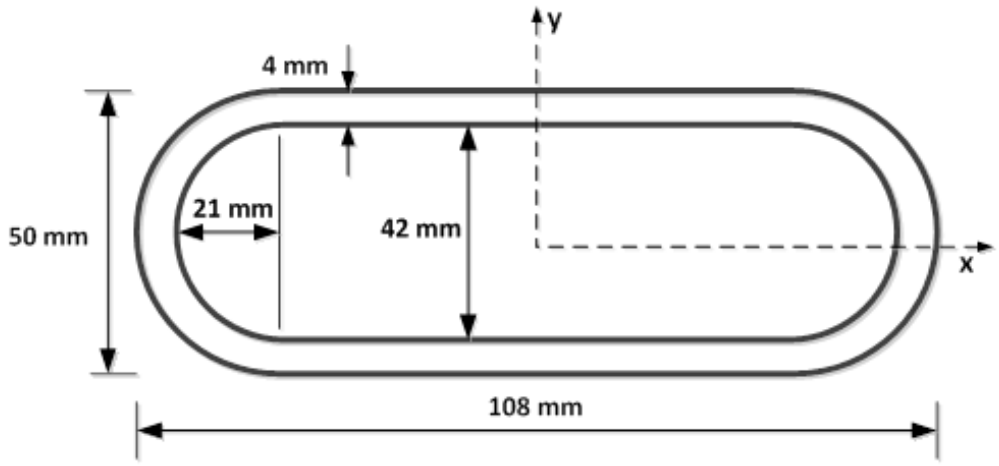

Figure 3.10: Sketch of the cross-section of a PVC rail

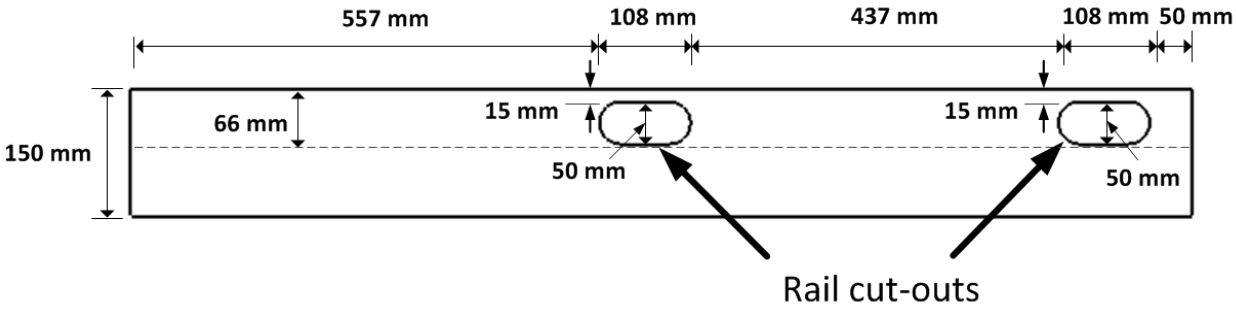

Figure 3.11: A sketch showing the side-view of the PVC post

3.4. Chapter Summary

Prototype novel structural composites have been fabricated from carpet waste as an alternative recycling option to replace the landfill and incineration options. The benefits of this approach also include the replacement of timber and PVC posts and rails in equestrian fencing and other structural applications. Timber and PVC posts and rails typically used for equestrian fencing have been described. Sketches of the PVC posts and rails have also been presented. Furthermore, the timber and PVC posts and rails were weighed, and their mass densities have been reported. These densities are important physical properties and may be used to estimate and compare the unit size of posts and rails in the design of an equestrian fencing system.

As this prototype study was carried out in collaboration with a small local industry (ECO2 Enterprises) in Burnley, Lancashire, there were limitations to the infrastructures available for the research work. Nevertheless, this chapter has explored options for recycling carpet

waste through the development of three different prototype novel waste carpet structural composites (Composites A – C), and their manufacturing processes have been described.

Composites A and B consisted of a polyurethane polymer matrix enclosing a bonded carpet strip core. This manufacturing process for Composites A and B does not require the need for mechanical separation of the carpet fibres, shredding or any fibre reprocessing procedure. The manufacturing process for Composite C differs from that of Composites A and B, and involved granulation and extrusion of strips of carpet waste at high temperature, before being moulded. It is also worth noting that there was no second phase polymer addition or reinforcement during the fabrication of Composite C. The manufacturing process for Composite C involved additional processing stages (i.e. shredding of the carpet waste and high temperature extrusion) compared to that of Composites A and B. Nevertheless, the study has demonstrated that the aforementioned manufacturing processes for the prototype novel composites may be used for carpet waste with synthetic/man-made (i.e. polypropylene, nylon, PET) and/or natural (i.e. wool) face fibres, and therefore, offers the potential to recycle significant amount of carpet waste.

Furthermore, variations in the physical properties (i.e. geometric imperfections, dimensional instability) and flaws of the novel prototype composites have been discussed, and are as a result of the processing techniques (i.e. hand lay-up) and limited equipment and infrastructure available for this research study. Therefore, these processing factors need to be controlled and could also be mitigated by the use of modern automated equipment for large scale production.

4. Chapter Four - Experimental Characterisation of Fencing Materials

4.1. Introduction

This chapter gives details of experimental tests (three-point bending, uniaxial tensile and compression) carried out on common fencing materials (specifically ungraded timber and rigid PVC posts and rails) and novel waste carpet structural composite materials (Composites A – C) to determine their mechanical properties. The details of these materials are given in Chapter 3. The results of these mechanical tests give an understanding of the mechanical properties of the novel waste carpet structural composite materials, and their suitability for use as alternative equestrian fencing materials to timber and PVC. In addition, statistical analyses and failure mode classifications were carried out. The chapter is concluded with a summary of the analyses and results of the experimental tests.

Furthermore, as polyurethane was used as the matrix of Composites A and B, an experimental investigation was carried out to quantify the effect of 9 wt. % CoatForce10 (CF10) fibre addition as filler reinforcement in polyurethane beams. As reported earlier in Chapter 3, the addition of the CF10 fibre to the polyurethane beam was based on a recommendation from a polymer consultant as well as its availability and cost limitations. This approach was also worth exploring as an option of enhancing the stiffness of the polyurethane matrix. Three-point bending tests were carried out to determine the relative flexural properties of unfilled polyurethane and 9 wt. % CF10 fibre filled polyurethane beams. Tensile tests were also carried on bonded single-lap joints of waste wool carpet strips at different orientations to determine their ultimate shear strengths. The knowledge of the shear strength of the carpet strips helps to define the suitability of the orientation of the bonded carpets strips to be used in the novel waste carpet structural composite.

4.2. Three-Point Bending Tests

4.2.1. Experimental Setup, Instrumentation and Test Procedure for the Three-Point Bending Tests

The three-point bending test records the applied load and centre deflection of the beam, from which the elastic flexural modulus may be determined. The flexural modulus is part of the information required to determine the flexural stiffness of beams. Three-point bending tests were carried out on timber and PVC post and rail sections, polyurethane beams and novel waste carpet structural composites (Composites A – C). Figure 4.1a shows a sketch of the three-point bending test setup. Figure 4.1b shows a sketch of the cross-section of the timber sections, novel waste carpet structural composites (Composites A – C) and polyurethane beams (unfilled and filled). Details of the cross-sections of the PVC posts and rails have been given in Section 3.3; however, their overall length, test span and second moment of area with respect to the plane of flexure are given in Table 4.1. There were variations along the length of the novel waste carpet structural composites (Composites A – C); hence, four measurements of the width and depth of their cross-sections along the length of the beams were taken (see Appendix 3). Table 4.1 gives the average dimensions of the beams tested in three-point bending.

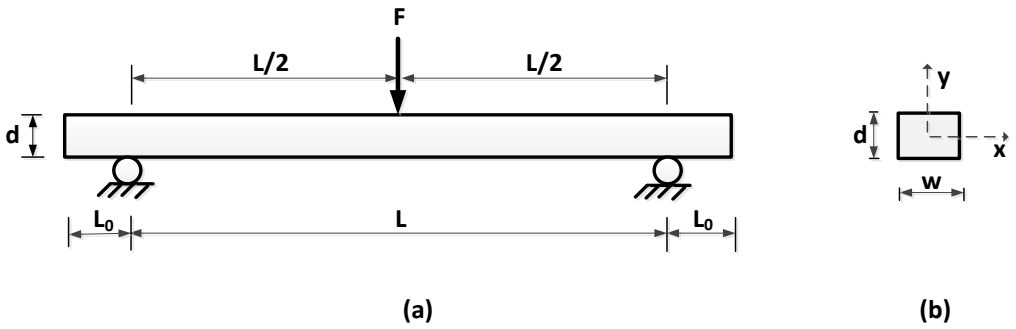

Figure 4.1: Sketch of the three-point bending test setup: (a) Side-view and (b) Cross-section view

One sample of each of Composites A and B was tested in three-point bending, and the tests were carried out three times. Based on the limitations on the number of samples fabricated, each Composite C sample was cut into three beams; hence, nine beams of each Composite C formulation (C_PP, C_PPW, C_SF and C_SFW) were tested to determine their elastic flexural moduli. Furthermore, to optimise material usage, five of the nine beams were then

loaded until failure occurred in three-point bending and the remaining four beams were failed in uniaxial tension.

Table 4.1: Details of beams tested in three-point bending

Beam	Overall length [$L + 2L_0$] [mm]	Span [L] [mm]	Average width [w] [mm]	Average depth [d] [mm]	Support overhang [L_0] [mm]	Second moment of area about x-axis [mm^4]
Composite A	995	800	108	50	97.5	1,125,000
Composite B	2,000	1,650	113	103	175	10,289,846
Composite C	293	240	39	11	26.5	4,326
Unfilled polyurethane (U1 – U5)	228	195	41	12	16.5	5,904
Filled polyurethane (F1 – F5)	220	192	41	12	14	5,904
Timber post (1 – 3)	1,580	1,400	122	71	90	3,638,762
Timber Post (4)	1,600	1,500	115	70	50	3,287,083
	1,073	973				
	874	774				
	762	662				
Timber rail (1 – 2)	3,600	2,800	93	37	400	392,561
PVC post (1 – 3)	1,260	1,060	N/A		100	4,769,499
PVC rail (1 – 3)	4,000	3,400	N/A		300	400,126

Five unfilled polyurethane beams (U1 – U5) and five 9 wt. % CoatForce 10 (CF10) fibre filled polyurethane beams (F1 – F5) were loaded in three-point bending until failure occurred. Three repeat tests were carried out on three timber posts (1 – 3), two timber rails (1 – 2), three PVC posts (1 – 3) and three PVC rails (1 – 3). A separate timber post (labelled Timber Post 4 in Table 4.1) was tested at four different spans so that the elastic shear and flexural moduli could be determined. The same timber post (Timber Post 4) was tested throughout, the longest span was tested first, and the shorter spans were tested after shortening the beam (see Table 4.1). The load-centre deflection data for the beams is given in Appendix 5.

The three-point bending tests on the timber, PVC and Composites A and B beams were carried out using a test rig in which the beams were simply supported on steel rollers and loaded by means of dead weights added to a hanger located at mid-span. An image of the test rig showing Composite A loaded in three-point bending is given in Appendix 4. The centre deflection corresponding to each increment of load was recorded. The dial gauge used to record the centre deflection of the beam had a 50 mm travel and a displacement resolution of 0.01 mm.

As the Composite C (C_PP, C_PPW, C_SF and C_SFW) and polyurethane beams were able to fit into the universal testing machine (Zwick Z020), three-point bending tests were carried out on the aforementioned beams at a crosshead displacement rate of 2 mm/min. Figure 4.2 shows an image of the Composite C_PP set up on the testing machine. The load and deflection data were recorded by a computer controlled data acquisition system. The Composite C beams were nominally identical, and the average dimensions are given in Table 4.1.

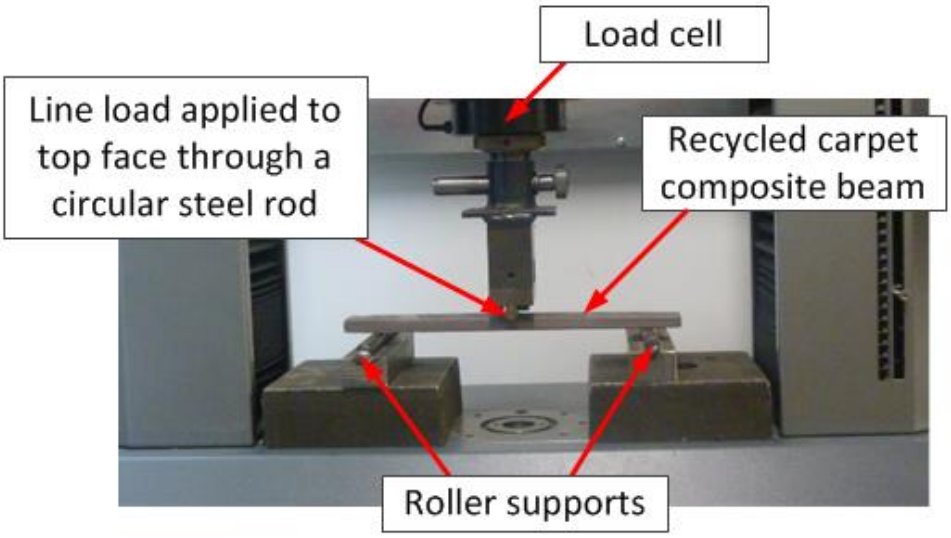

Figure 4.2: Image of Composite C_PP beam setup for three-point bending in a Zwick Z020 testing machine

The central deflection w_c of a simply supported beam subjected to three-point bending is given by Equation (1) (Sims et al., 1987). Equation (1) can be re-arranged in two ways, as shown by Equations (2) and (3). These two equations can represent straight lines. Regression lines fitted to load-centre deflection data may be used to determine their slopes (each equal to their transverse stiffnesses, m) at different spans. Using these transverse

stiffnesses, m, a plot of 1/mL against L^2 yields a straight line with a gradient of 1/48D and an intercept of 1/4kQ. Alternatively, a plot of $1/mL^3$ against $1/L^2$ yields a straight line with a gradient of 1/4kQ and an intercept of 1/48D.

$$w_c = \frac{FL^3}{48D} + \frac{FL}{4kQ} \tag{1}$$

$$\frac{w_c}{FL} = \frac{L^2}{48D} + \frac{1}{4kQ} \rightarrow \frac{1}{mL} = \frac{L^2}{48D} + \frac{1}{4kQ} \tag{2}$$

$$\frac{w_c}{FL^3} = \frac{1}{L^2k4Q} + \frac{1}{48D} \rightarrow \frac{1}{mL^3} = \frac{1}{L^2k4Q} + \frac{1}{48D} \tag{3}$$

$$\text{where } m = F / w_c$$

In Equations (1) – (3), w_c is the central deflection, Q is the shear stiffness, D is the flexural rigidity, F is the centrally applied load, k is the shear correction factor (5/6 for rectangular cross-section beams (Dong et al., 2010)), and L is the test span. $D = EI$ and $Q = GA$ where E is the flexural modulus, I is the second moment of area with respect to the plane of flexure, G is the shear modulus, A is the cross-sectional area of the beam and m is the slope of the load-centre deflection curve. Equation (4) gives the central deflection w_c of a simply supported beam subjected to three-point bending when shear deformation is neglected (cf. Equation (1)). Equation (5) gives the formula for the flexural strength of a beam in three-point bending (BS EN 178, 2013)

$$w_c = \frac{FL^3}{48D} = \frac{FL^3}{48EI} \tag{4}$$

$$\sigma_f = \frac{3F_{max}L}{2wd^2} \tag{5}$$

L is the span, w is the width of the beam, d is the depth of beam, F_{max} is the maximum load on the load-centre deflection curve and σ_f is the flexural strength. Equations (1) – (3) were used to analyse the load-centre deflection data for Timber Post 4 to determine its shear and flexural moduli. Equation (4) was used to determine the flexural modulus of the other beams tested in three-point bending. Equation (5) was used to determine the flexural strengths of the materials (BS EN 178, 2013).

In addition, the absorbed energy in bending by the Composite C beams was determined using the trapezoidal rule to calculate the area under the load-centre deflection curve. This

property gives an indication of the ability of the Composite C beams to absorb energy and plastically deform before fracture. Furthermore, understanding the energy absorption capabilities is vital in the design of composites for impact loadings.

4.2.2. Results and Discussion of the Three-Point Bending Tests

The load-centre deflection responses for Composites A and B are shown in Figure 4.3 and Figure 4.4, respectively. Three tests (1 – 3) were carried out, and regression lines were fitted to the data to determine the slopes (transverse stiffnesses), m of the lines. These slopes were used to determine their flexural moduli using Equation (4).

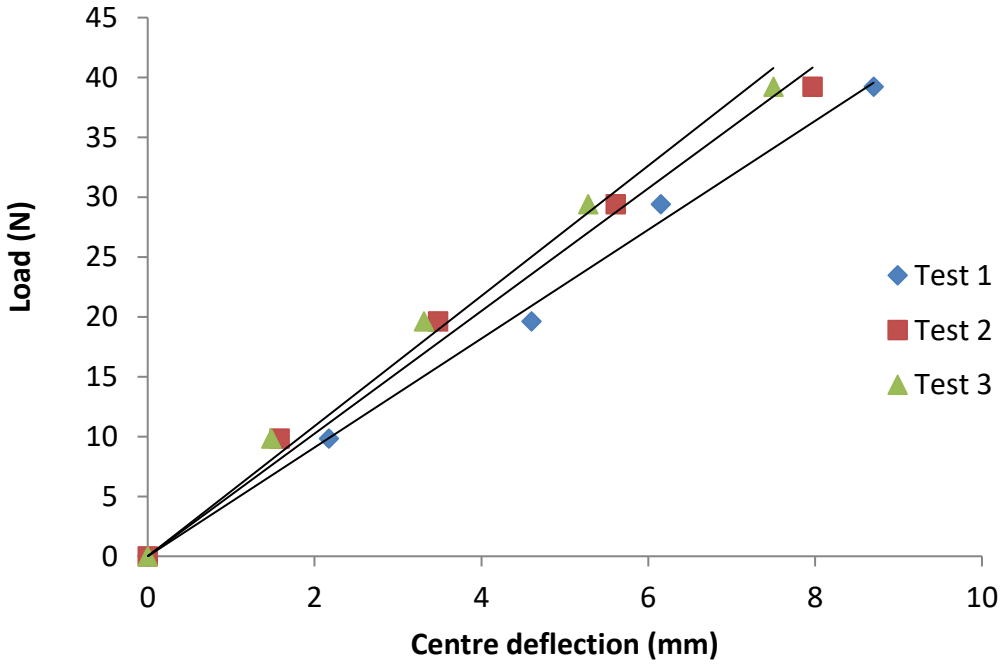

Figure 4.3: Load versus centre deflection plots for Composite A (span = 800 mm)

The average flexural moduli for Composites A and B were 0.047 GPa and 0.185 GPa, respectively (see Table 4.2). The average flexural modulus of Composite B is about four times greater than that of Composite A. This difference may be attributed to the 2 wt. % CoatForce10 (CF10) fibre filler added to the polyurethane matrix of Composite B. However, there were limitations in the number of samples tested, and therefore limited repeatability in this prototype study.

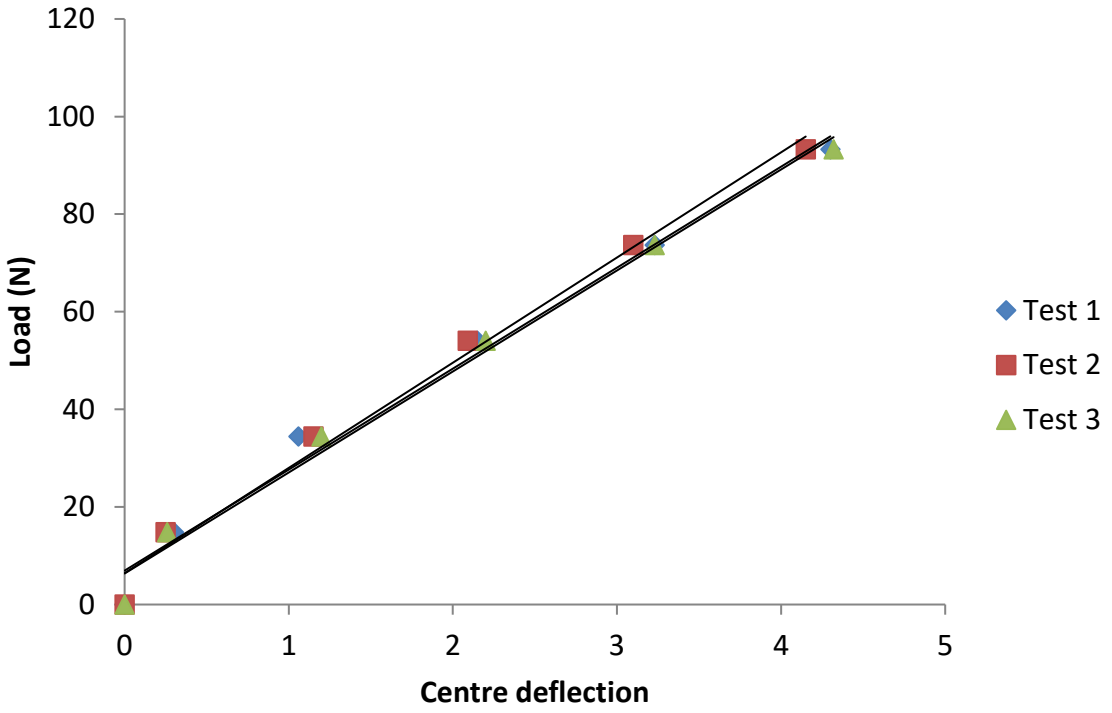

Figure 4.4: Load versus centre deflection plots for Composite B (span = 1650 mm)

Table 4.2: Transverse stiffnesses and flexural moduli for Composites A and B

Beam	Transverse stiffness [N/mm]				Flexural modulus [GPa]			
	Test 1	Test 2	Test 3	Test Average	Test 1	Test 2	Test 3	Test Average
Composite A	5.2	4.9	4.6	4.9	0.049	0.047	0.044	0.047
Composite B	20.1	20.9	20.1	20.4	0.183	0.190	0.183	0.185

36 Composite C beams were tested in three-point bending to determine their flexural moduli. Figure 4.5, Figure 4.6, Figure 4.7 and Figure 4.8 show the average load-centre deflection responses for nine beams of each Composite C formulation (C_PP, C_PPW, C_SF and C_SFW), respectively. The upper and lower bound values are also shown in the figures. It is evident that the aforementioned load-centre deflection responses are linear.

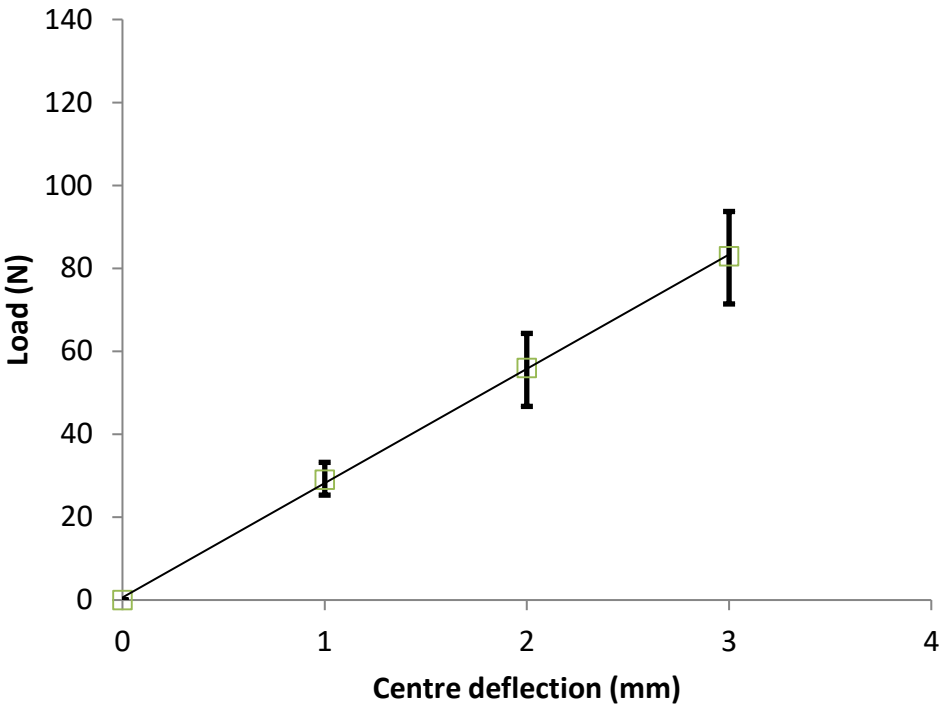

Figure 4.5: Average load versus centre deflection plots for nine Composite C_PP beams (span = 240 mm)

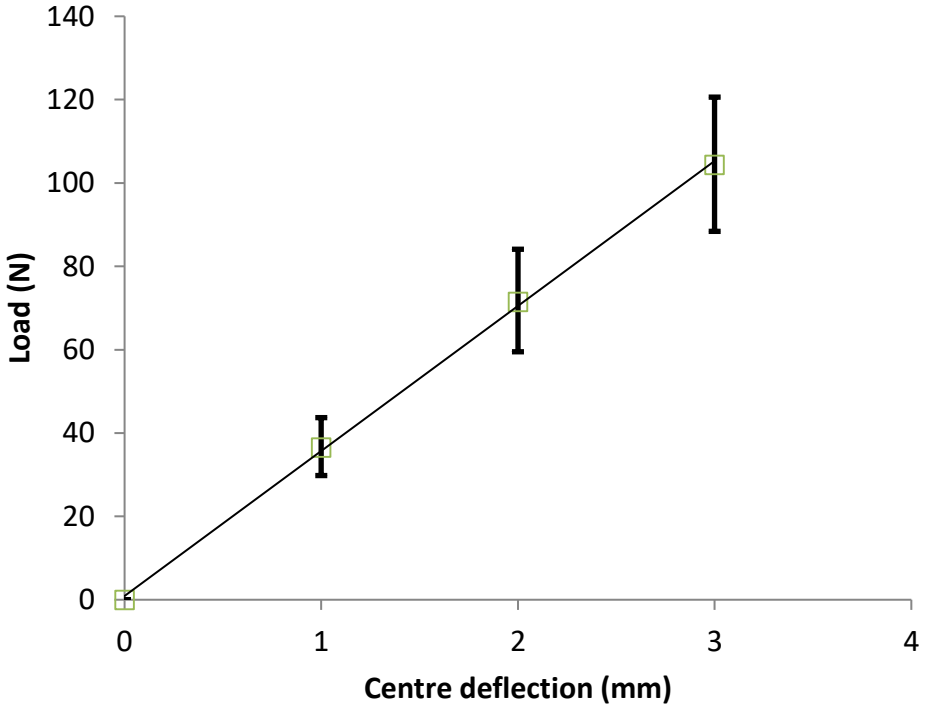

Figure 4.6: Average load versus centre deflection plots for nine Composite C_PPW beams (span = 240 mm)

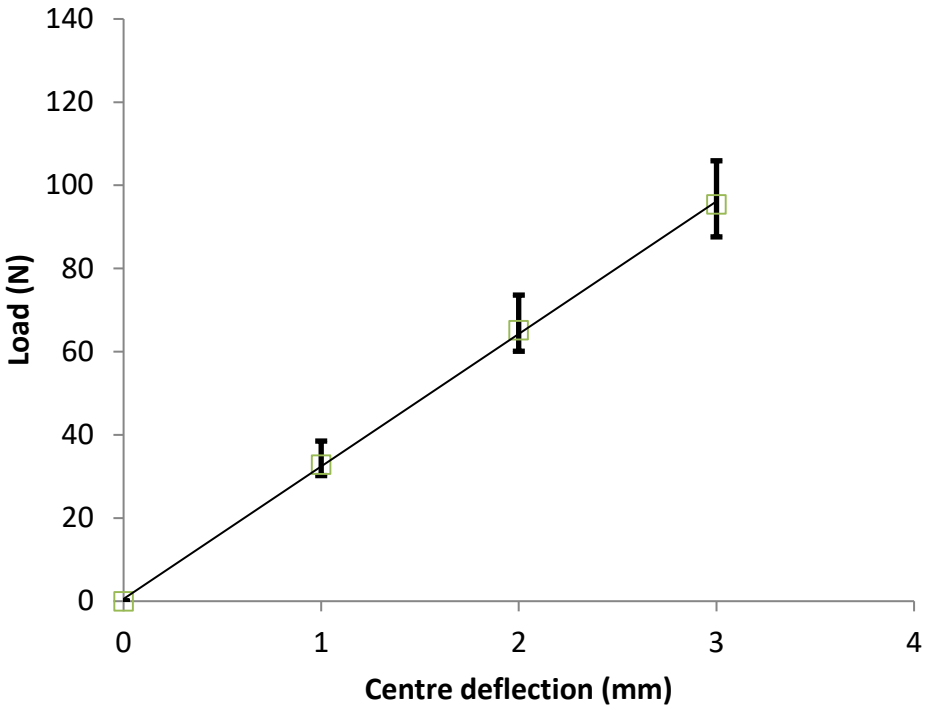

Figure 4.7: Average load versus centre deflection plots for nine Composite C_SF beams (span = 240 mm)

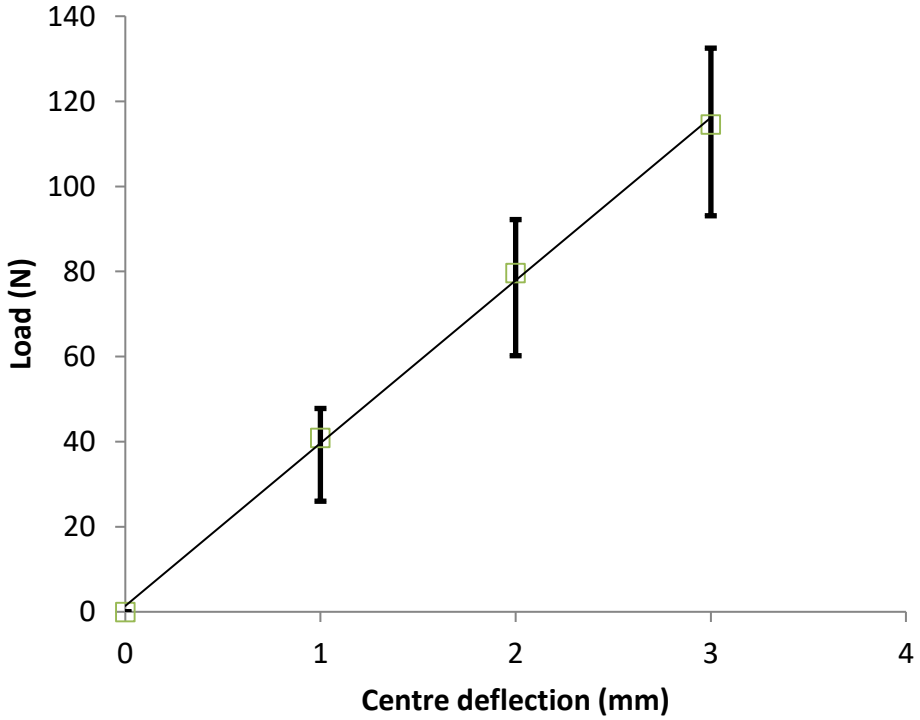

Figure 4.8: Average load versus centre deflection plots for nine Composite C_SFW beams (span = 240 mm)

The transverse stiffness and flexural modulus of each of the Composite C beams are given in Appendix 5. The flexural moduli of the Composite C beams are compared in Figure 4.9. The average flexural modulus for Composite C_PP and C_PPW were 2.3 GPa and 2.6 GPa, respectively. These values show that the addition of 50 wt. % waste carpets with wool face fibres to 50 wt. % waste carpets with polypropylene face fibres gave a 13 % increase in the average flexural modulus. The average flexural modulus for C_SF was also 2.3 GPa (the same value as C_PP). The addition of 50 wt. % waste carpets with wool face fibres to 50 wt. % waste carpets with synthetic face fibres also gave a 35 % increase in the average flexural modulus i.e. from 2.3 GPa to 3.1 GPa. These results show that the addition of waste carpets with wool face fibres to waste carpets with polypropylene face fibres or synthetic face fibres (i.e. polypropylene, nylon, PET) resulted in an increase in the flexural modulus.

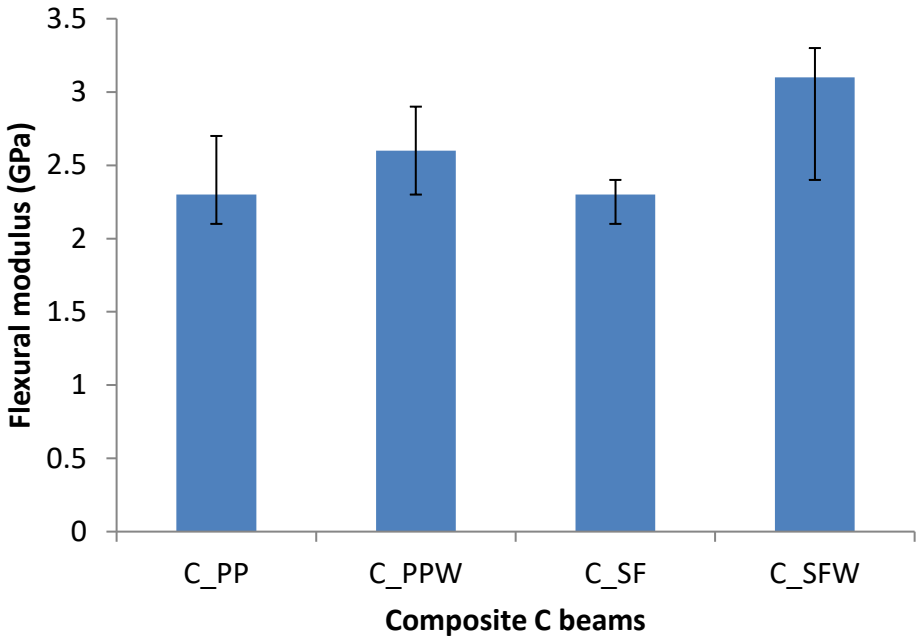

Figure 4.9: Comparison of the flexural modulus of Composite C beams

The average flexural moduli, standard deviations and coefficients of variation of the Composite C beams tested in three-point bending are given in Table 4.3. Of the four formulations of Composite C, Composite C_SFW had the highest standard deviation and coefficient of variation of 0.3 GPa and 10.4 %, respectively. Composite C_SF had the lowest standard deviation and coefficient of variation of 0.1 GPa and 5.5 %, respectively. Composite

C_PP and C_PPW had approximately the same standard deviation of 0.2 GPa, and their coefficients of variation were 8.0 % and 6.6 %, respectively.

The overall average flexural modulus for the Composite C beams was 2.6 GPa. It is evident that the average flexural modulus for the Composite C beams (2.6 GPa) is significantly greater than those of Composite A (0.047 GPa) and B (0.185 GPa).

Table 4.3: Average flexural moduli, average flexural strengths, standard deviations and coefficients of variation for Composite C beams

Composite C beam	Flexural modulus			Flexural strength		
	Average [GPa]	Standard deviation (SD) [GPa]	Coefficient of variation [%]	Average [MPa]	Standard deviation (SD) [MPa]	Coefficient of variation [%]
C_PP	2.3	0.2	8.0	31.8	3.8	12.1
C_PPW	2.6	0.2	6.6	31.0	1.8	5.8
C_SF	2.3	0.1	5.5	25.9	2.0	7.8
C_SFW	3.1	0.3	10.4	28.1	3.9	14.0
Overall average flexural modulus					**2.6 GPa**	
Overall average flexural strength					**29.2 MPa**	

It is worth noting that based on the limitations on the number of samples fabricated; five of the nine beams from each formulation of Composite C were loaded until failure occurred (total of 20 beams), whereas, the remaining beams failed in uniaxial tension. The maximum load and flexural strength for each of the 20 beams are given in Appendix 5. The load-centre deflection plots for the beams tested in three-point bending until failure are shown in Figure 4.10, Figure 4.11, Figure 4.12 and Figure 4.13. The responses were initially linear which became nonlinear when the centrally applied load exceeded 200 N.

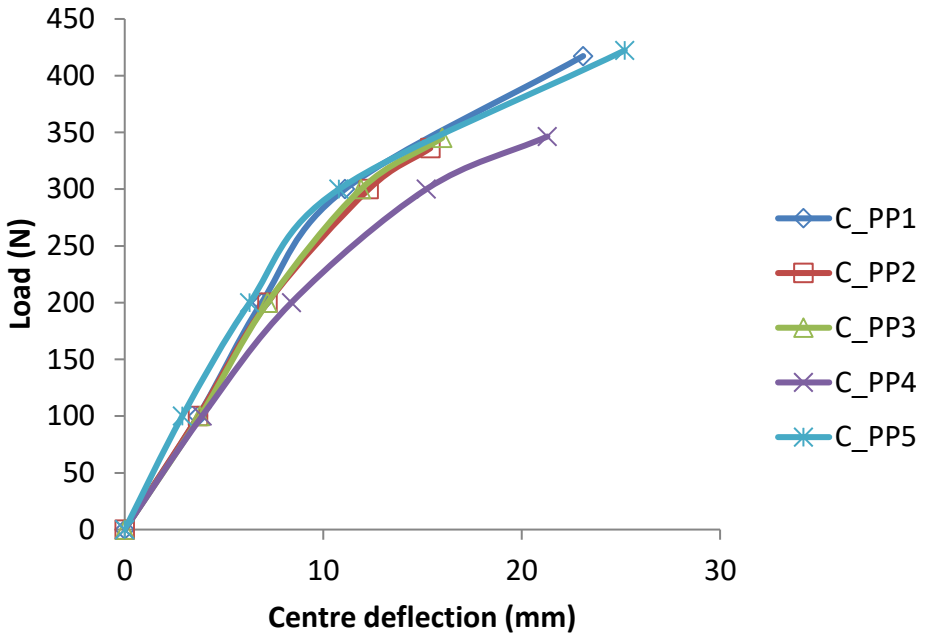

Figure 4.10: Load versus deflection plots for five Composite C_PP beams loaded in three-point bending until failure occurred (span = 240 mm)

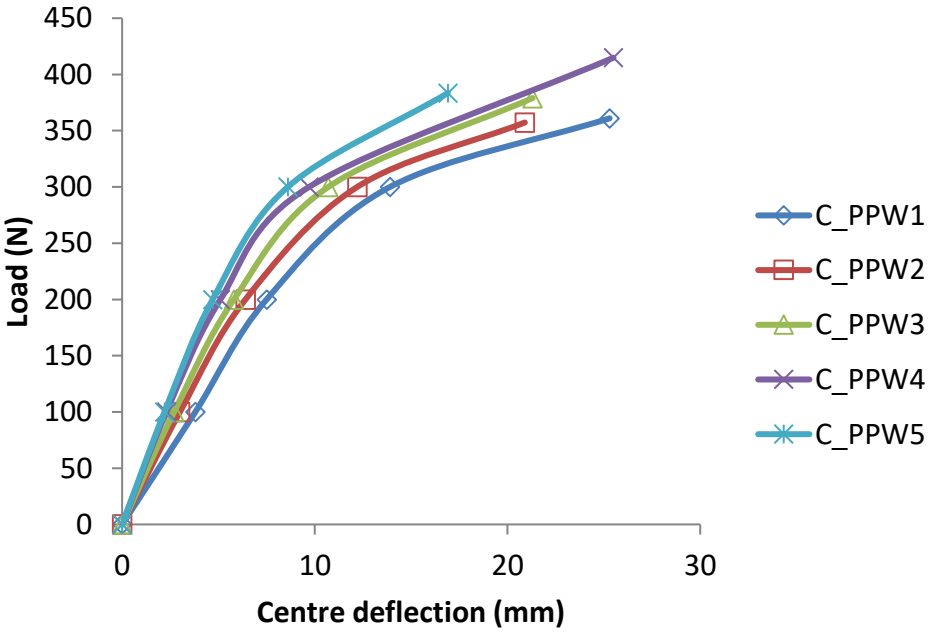

Figure 4.11: Load versus deflection plots for five Composite C_PPW beams loaded in three-point bending until failure occurred (span = 240 mm)

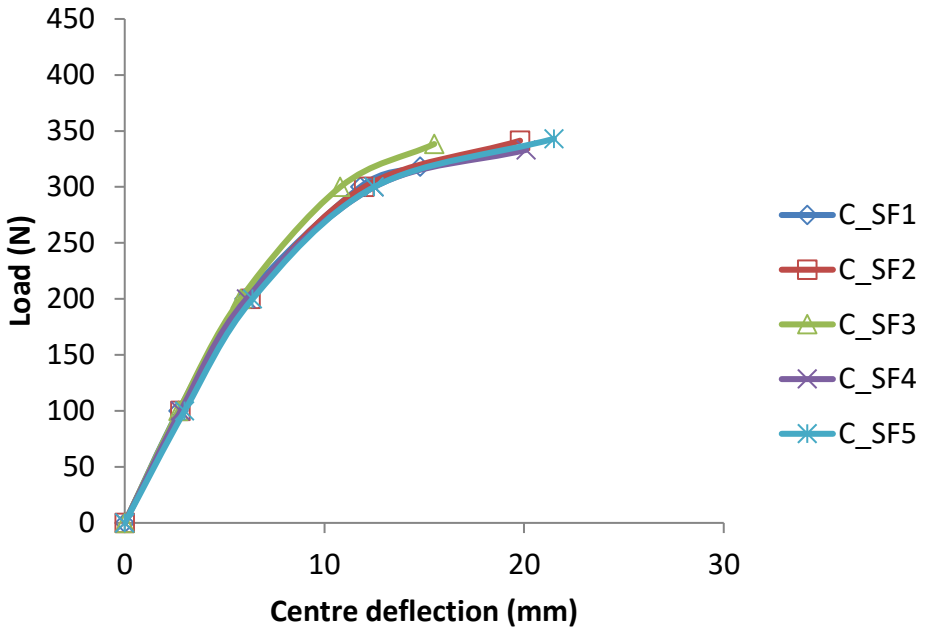

Figure 4.12: Load versus deflection plots for five Composite C_SF beams loaded in three-point bending until failure occurred (span = 240 mm)

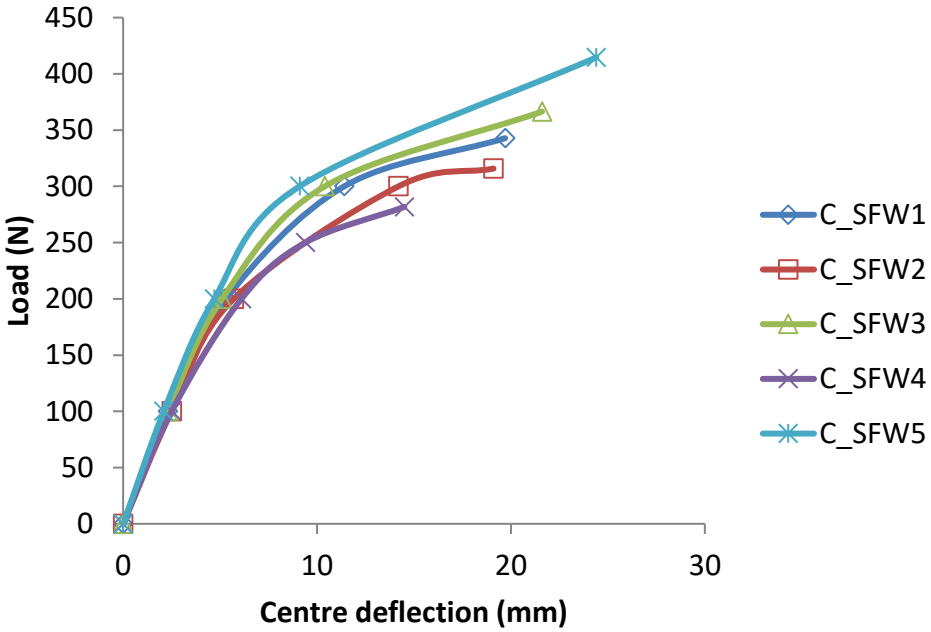

Figure 4.13: Load versus deflection plots for five Composite C_SFW beams loaded in three-point bending until failure occurred (span = 240 mm)

The average flexural strengths for the Composite C beams are compared in Figure 4.14. The average flexural strength for Composite C_PP was 31.8 MPa which was the highest of the four formulations of Composite C, whereas Composite C_SF had the lowest average flexural strength of 25.9 MPa. The average flexural strengths for Composite C_PP and C_PPW were 31.8 MPa and 31.0 MPa, respectively, which are almost equal. However, the coefficient of variation for the flexural strengths of Composite C_PPW beams was 5.8 % which is about half of that of Composite C_PP (12.1 %). The coefficient of variation for the flexural strengths of Composite C_SFW was 14 %, which is the highest value amongst the four types of Composite C beam. The overall average flexural strength for the 36 Composite C beams was 29.2 MPa.

The energy absorbed in three-point bending by the Composite C beams was determined using the trapezoidal rule to calculate the area under the load-centre deflection curve. The average energy absorbed, standard deviations and coefficients of variation for the respective Composite C beams are given in Table 4.4. Representative images of the fractured surfaces of the Composite C (C_PP, C_PPW, C_SF and C_SFW) beams and their respective Scanning Electron Microscopy (SEM) images are given in Figure 4.15 - Figure 4.18.

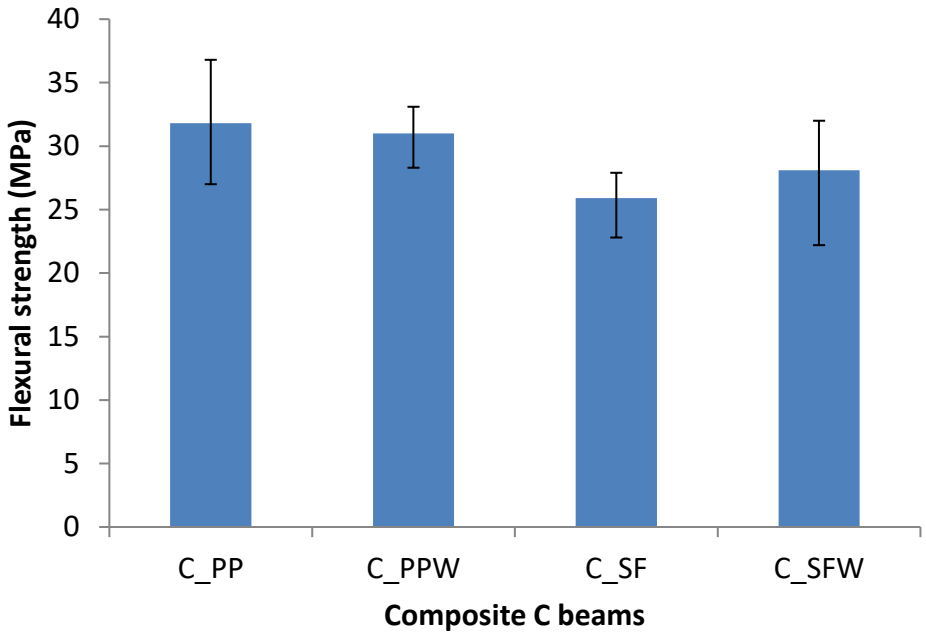

Figure 4.14: Comparison of the flexural strength of Composite C beams

Table 4.4: Average energy absorbed in three-point bending by the Composite C beams and their standard deviations and coefficients of variation

Composite C beam	Energy absorbed		
	Average [J]	Standard deviation (SD) [J]	Coefficient of variation [%]
C_PP	4.7	1.7	37
C_PPW	5.6	1.1	20
C_SF	4.1	0.9	22
C_SFW	4.9	1.6	33
Overall average energy absorbed in bending			**4.9 J**

The energy absorbed in bending by each Composite C beam is given in Appendix 5, and ranged from 2.8 J – 7.3 J, with an overall average of 4.9 J. The coefficients of variation for the Composite C beams ranged from 20 – 37 %, thus reflecting high differences (see Table 4.4). These large differences can be related to the microscopic imperfections and inhomogeneity of the beams (see Figure 4.15 - Figure 4.18). Furthermore, the melt blended mixture contained different immiscible polymers (i.e. nylon and polypropylene), dirt particles, fillers, chemicals and impurities (typical of post-consumer carpet waste) which may have contributed to the variations in the mechanical properties of the Composite C beams. The SEM images are shown in Figure 4.15 - Figure 4.18; they show evidence of fibre pull-out, voids and cavities. The presence of these defects indicates poor adhesion between the waste fibre blends and thus led to a non-uniform distribution of applied stresses on the beams' cross-sections.

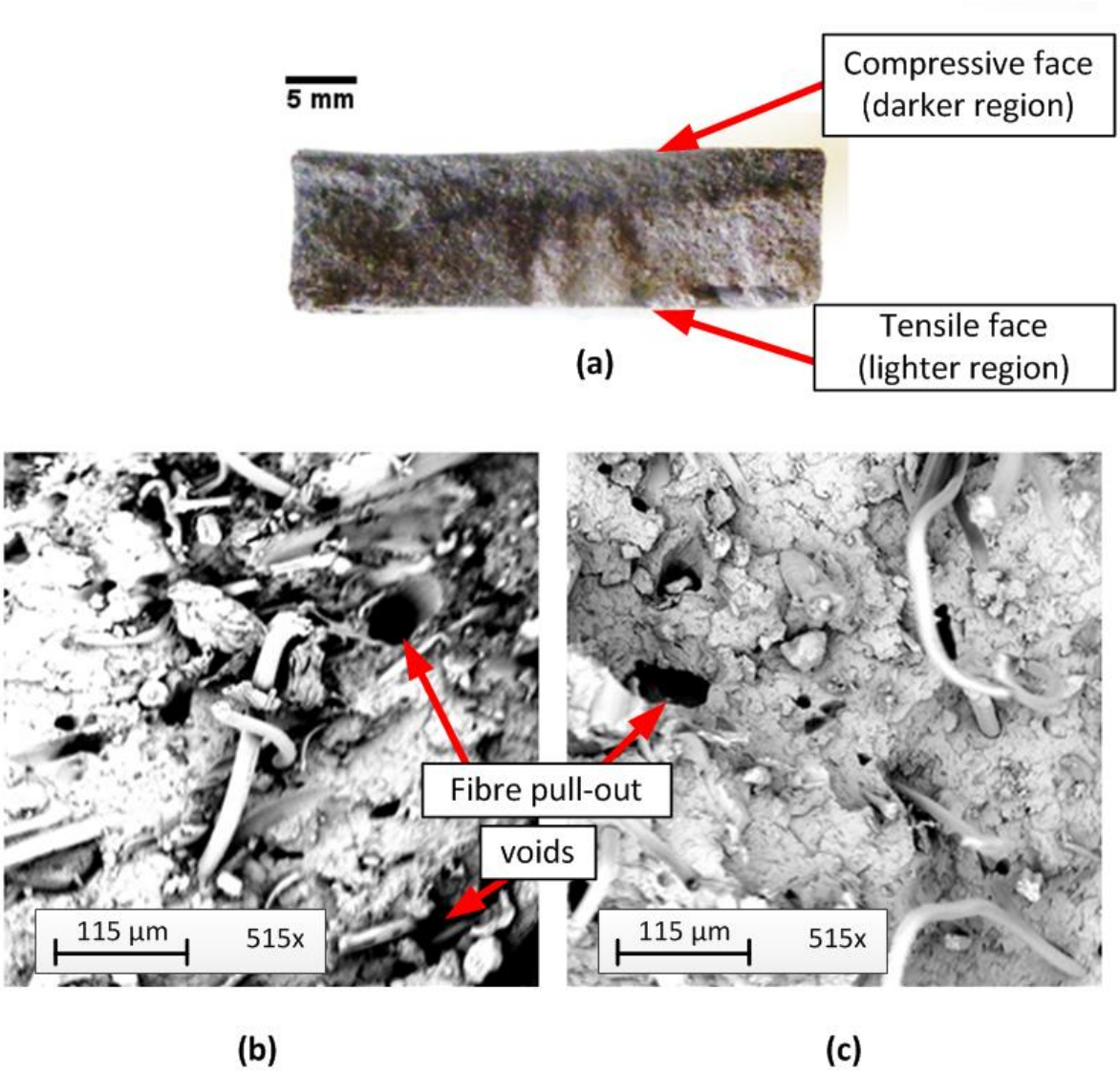

Figure 4.15: Composite C_PP beam loaded to failure in three-point bending: (a) Cross-section view of the fracture surface (b) SEM image of the fracture surface (darker region of the fracture surface) and (c) SEM image of the fracture surface (lighter region of the fracture surface)

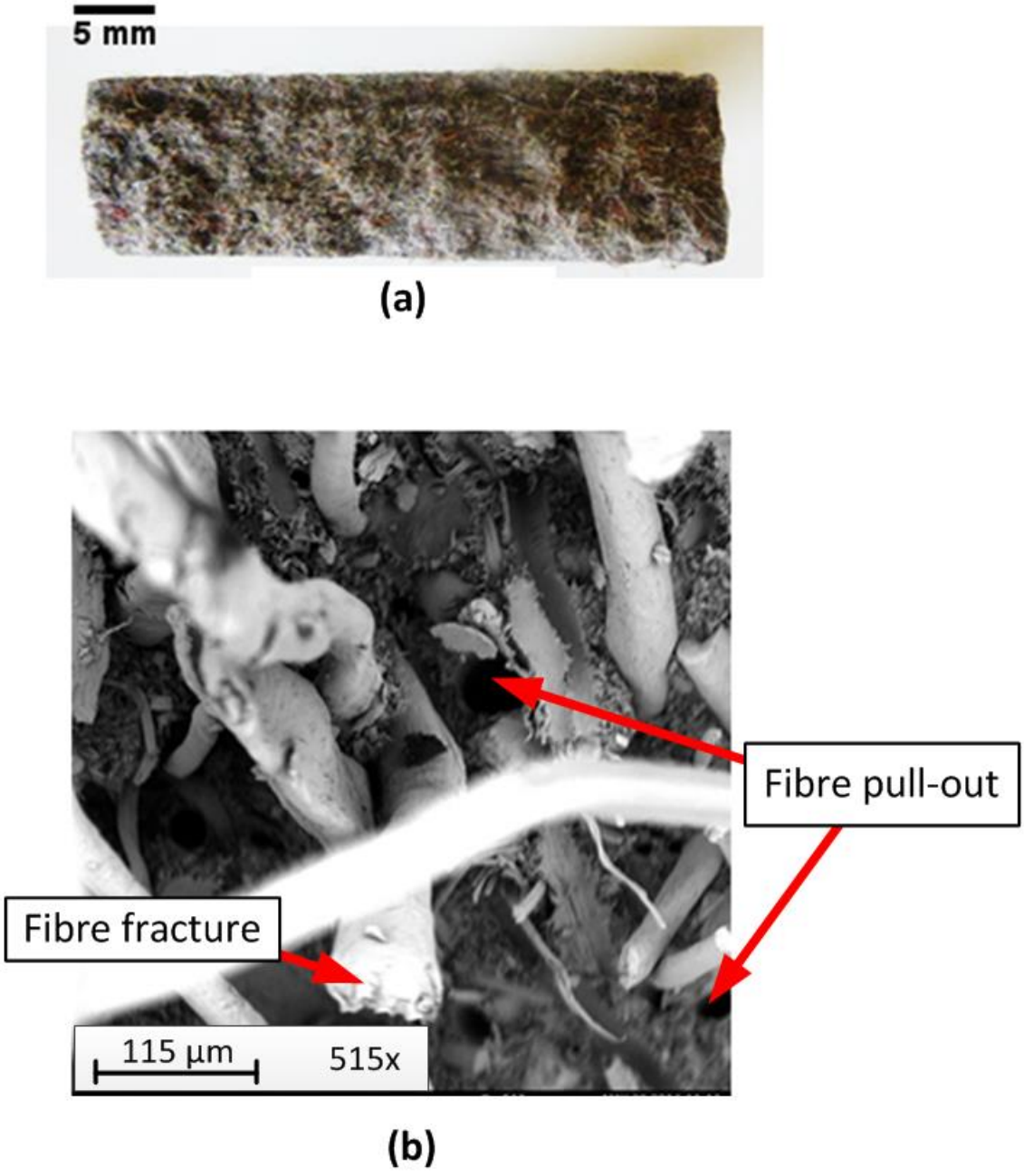

Figure 4.16: Composite C_PPW beam loaded to failure in three-point bending: (a) Cross-section view of the fracture surface and (b) SEM image of the fracture surface

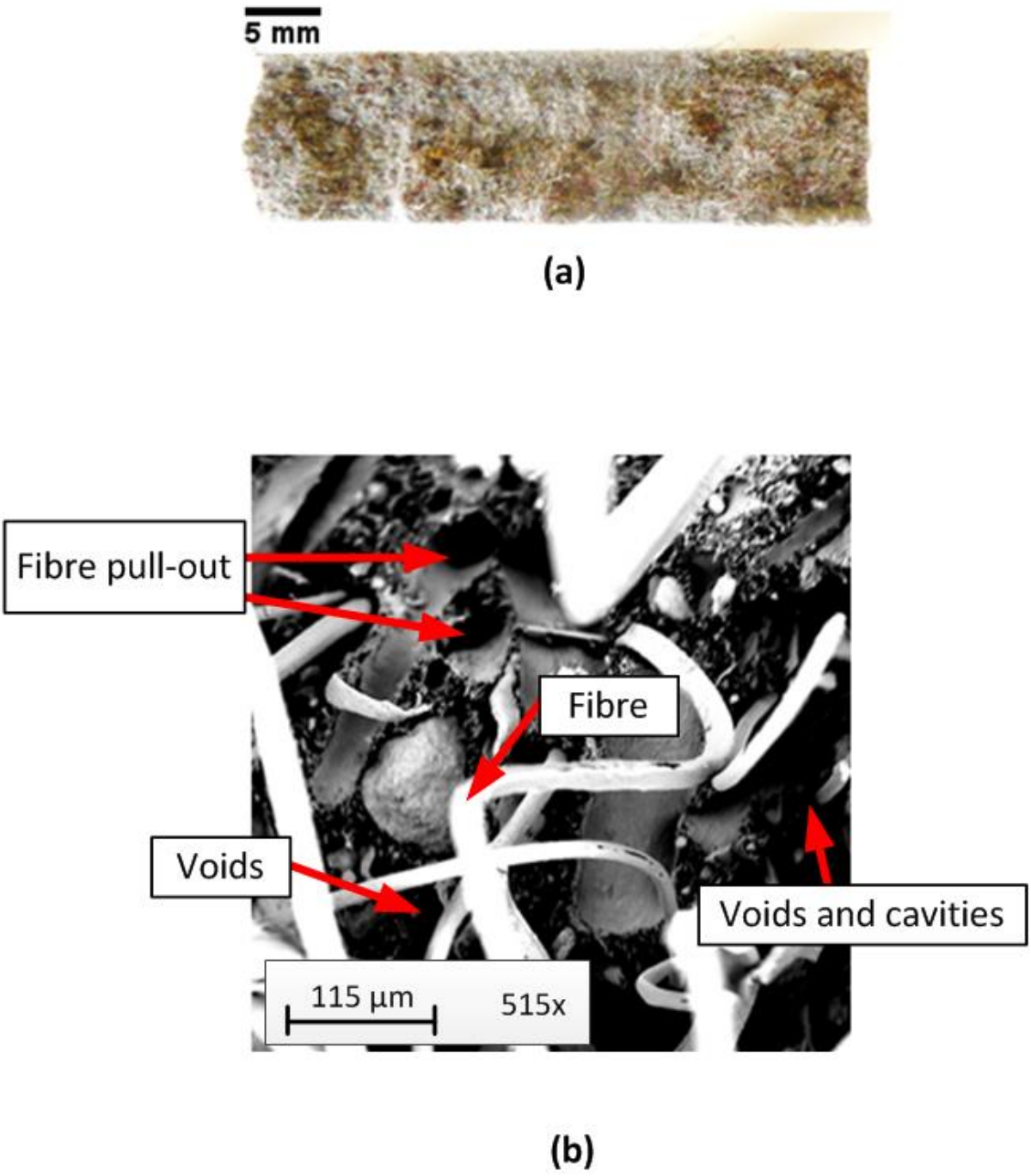

Figure 4.17: Composite C_SF beam loaded to failure in three-point bending: (a) Cross-section view of the fracture surface and (b) SEM image of the fracture surface

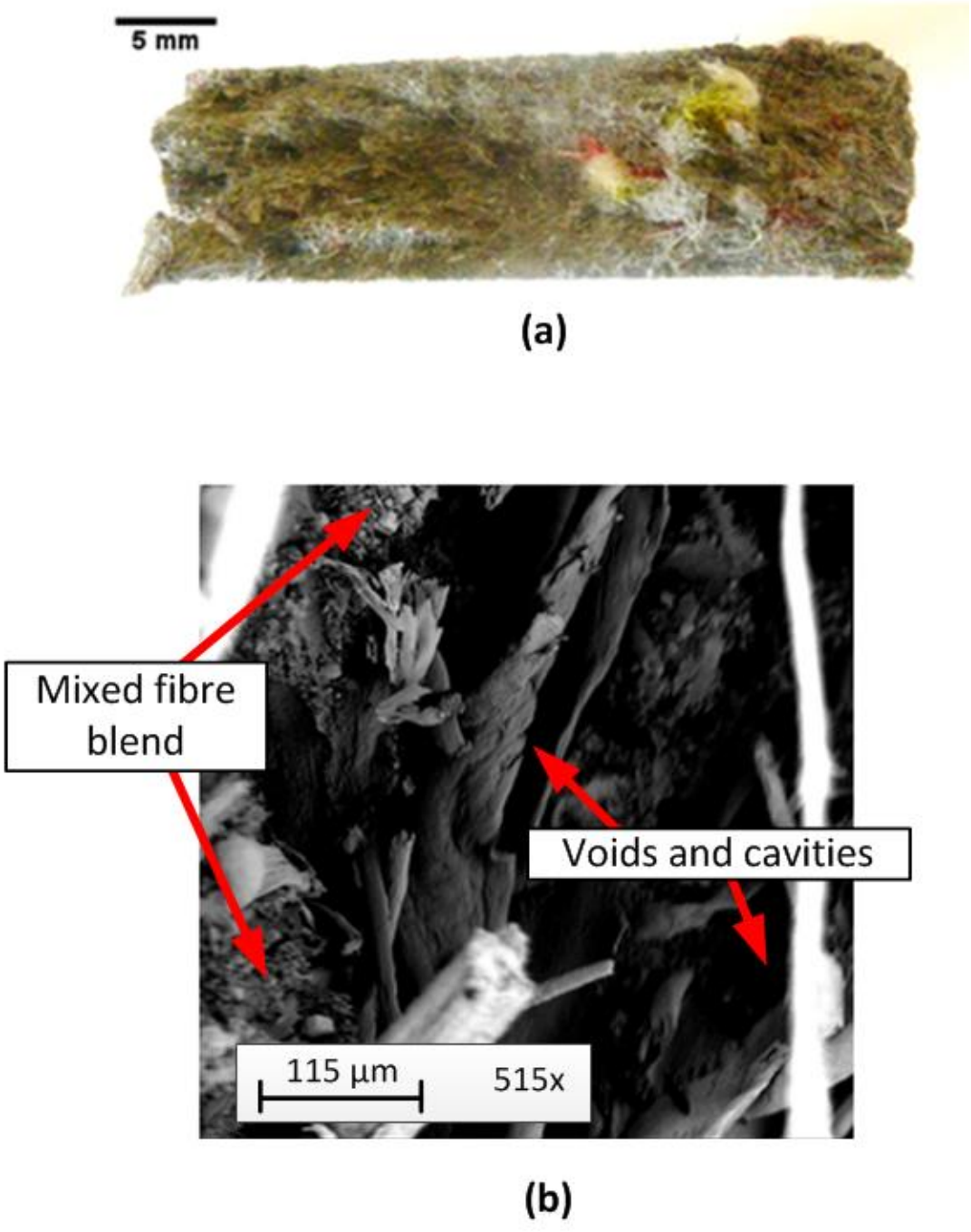

Figure 4.18: Composite C_SFW beam loaded to failure in three-point bending: (a) Cross-section view of the fracture surface and (b) SEM image of the fracture surface

More specifically, the fractured surface of Composite C_PP had two different regions – the darker and lighter regions highlighted in Figure 4.15b. The top face in Figure 4.15b (darker region) was in compression, while the bottom was in tension; SEM images of both regions are given in Figure 4.15c and Figure 4.15d, respectively. It appears that there was no significant microscopic difference between Figure 4.15c and Figure 4.15d, and the images showed evidence of fibre pull-out and voids. On the other hand, more exposed fibres, flaws and pores were found on the fractured surfaces of Composites C_PPW, C_SF and C_SFW compared to C_PP which may be attributed to the higher proportions of other synthetic and wool fibres in the former composites.

Three timber posts (1 – 3) and two timber rails (1 and 2) were tested three times in bending and their average deflections were used to plot their load-centre deflection responses shown in Figure 4.19 and Figure 4.20, respectively. Load versus centre deflection plots for three PVC posts (1 – 3) and three PVC rails (1 – 3) are shown in Figure 4.21 and Figure 4.22, respectively.

Table 4.5 gives the average transverse stiffnesses and flexural moduli of the timber and PVC posts and rails. It should be noted that the PVC posts were loaded in two orientations. Load was initially applied on the face with the two cut-outs (for rail insertions) in the PVC post closer to the loading point (referred to as Orientation A in Figure 4.21 and Table 4.5), and then with the post rotated 180 degrees (referred to as Orientation B in Figure 4.21 and Table 4.5) and the same loading applied. Images of the two different loading orientations (A and B) are given in Appendix 6. The response repeatability for the PVC posts and rails is good, especially for the latter. The load-centre deflection responses for the timber and PVC posts and rails are linear, and regression lines have been fitted to the data to determine their slopes (or transverse stiffnesses), m. These slopes were used to determine their flexural moduli using Equation (4).

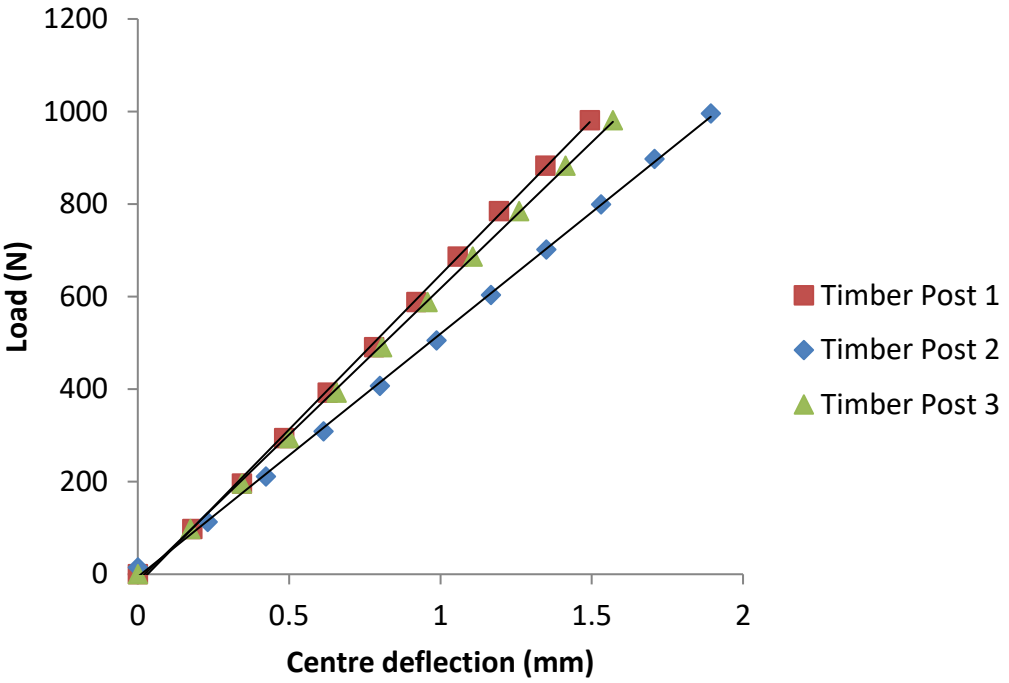

Figure 4.19: Load versus centre deflection plots for three timber posts (span = 1400 mm)

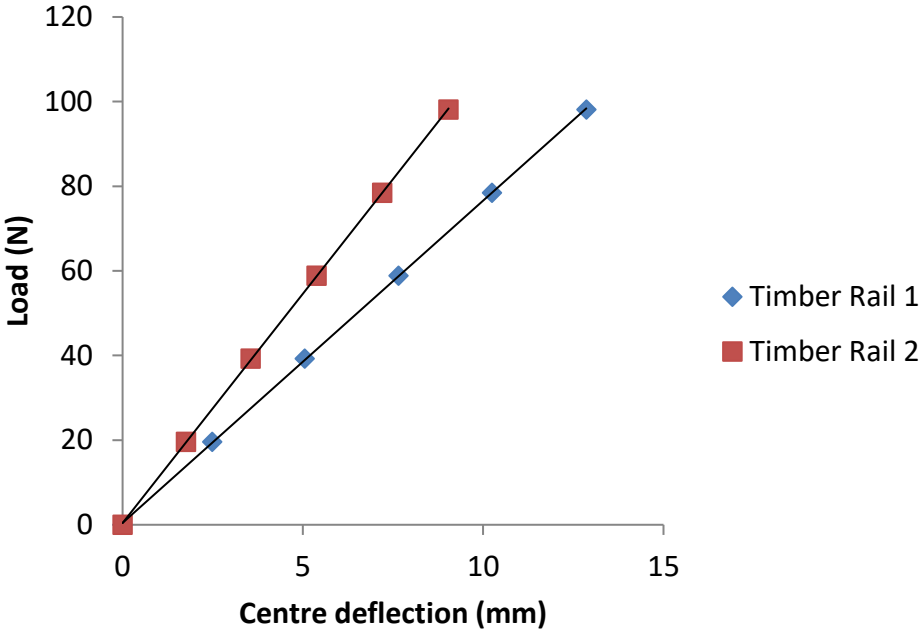

Figure 4.20: Load versus centre deflection plots for two timber rails (span = 2800 mm)

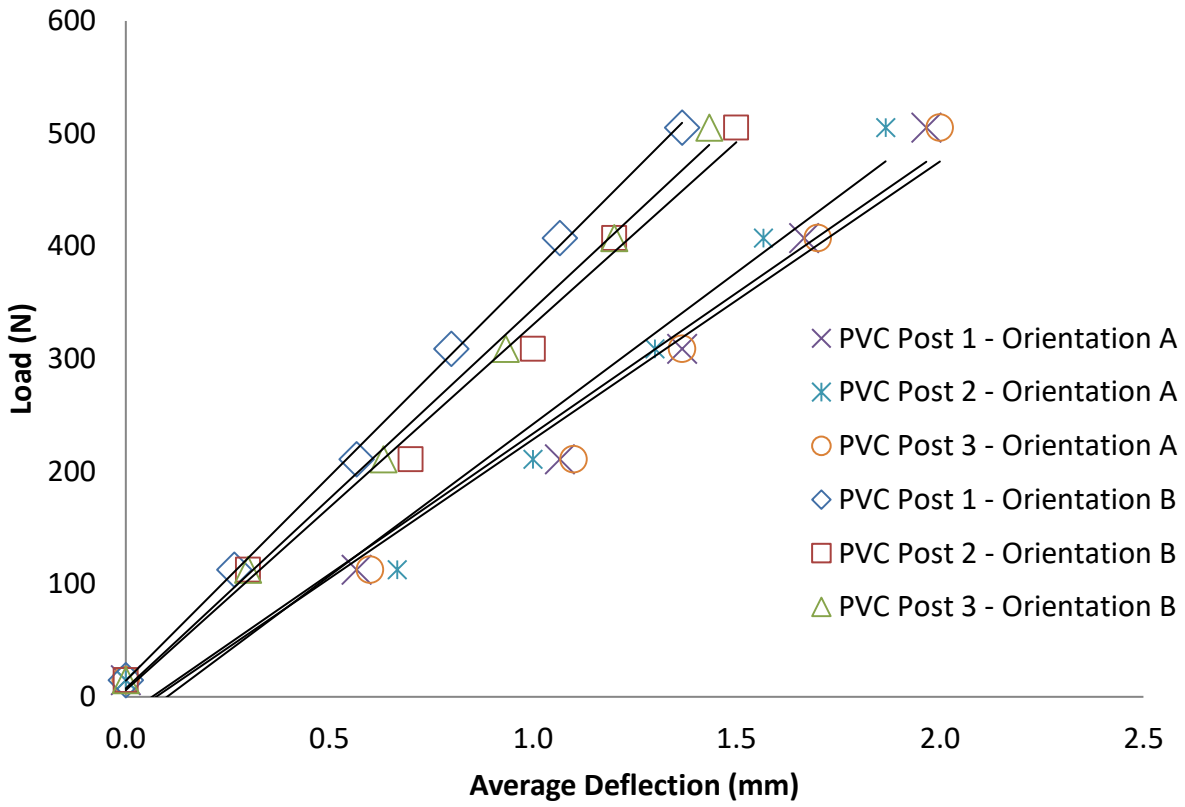

Figure 4.21: Load versus centre deflection plots for three PVC posts (span = 1060 mm)

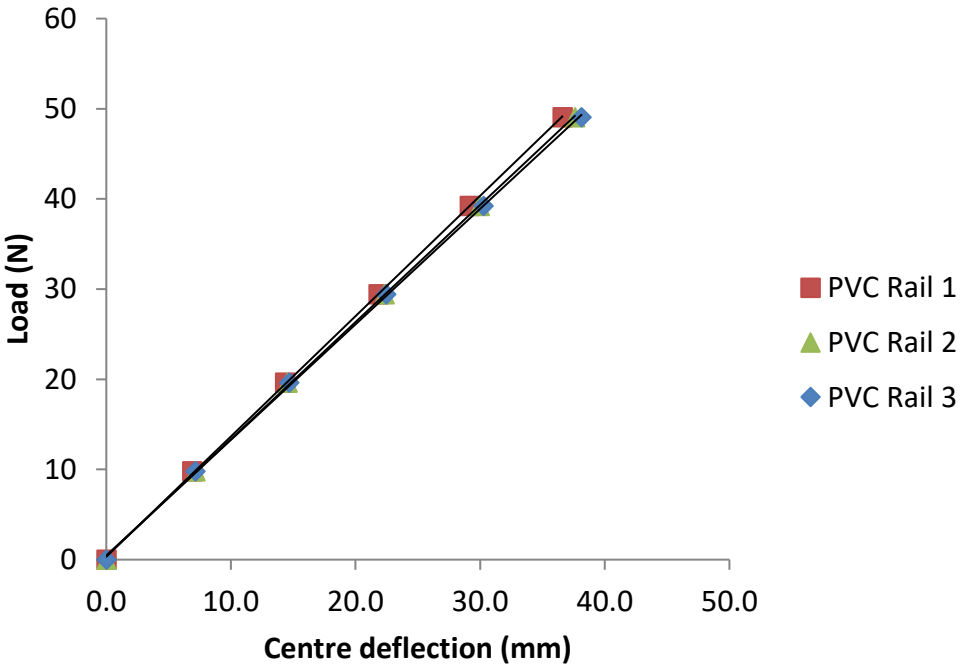

Figure 4.22: Load versus centre deflection plots for three PVC rails (span = 3400 mm)

The results of the three-point bending tests on the timber posts and rails showed that their flexural moduli varied from 8.1 GPa to 13.5 GPa. The large differences between the measured flexural moduli of the timber posts and rails illustrate the natural variability of timber and are typical of ungraded timber sections. The average flexural moduli for the timber posts and rails were 9.4 GPa and 11.3 GPa, respectively. The flexural moduli of the PVC rails ranged from 2.6 – 2.7 GPa; these values are close to the data provided by the manufacturers, Duralock Performance Fencing (2.4 – 2.5 GPa) (see Appendix 1).

Based on the two loading orientations (A and B), the average flexural modulus for the PVC post was 1.6 GPa, which is about 40 % lower than that of the PVC rail (see Table 4.5). The reasons for the lower flexural modulus of the PVC posts may be attributed to shear deformation effects, as the span to depth ratio for the PVC posts was only about 7:1 compared to that of the PVC rail which was 68:1. Furthermore, the PVC posts had two cut-outs (for rail insertions) on opposite faces, which may have also contributed to its lower flexural modulus. Images of a simply supported PVC post, with centrally applied load at the different orientations (A and B), are shown in Appendix 6. The aforementioned images show that the pair of the rail cut-outs of the PVC post was directly under the applied load and thus contributed to some local elastic deformation in the region. The analysis also shows that the average flexural modulus for loading orientation B was about 38 % larger than that for orientation A, possibly due to the pair of rail cut-outs being relatively further away from the loading point in the former case.

As described earlier, a fourth timber post (Timber Post 4) was tested at four different spans, so that the elastic shear and flexural moduli could be determined. Three tests were carried out at each span (load-centre deflection data is given in Appendix 5); however, only the results from the third test (Test 3) for each span were used to determine the flexural and shear moduli. The load-centre deflection responses for Timber Post 4 are shown in Figure 4.23. The plots all show linear responses, and regression lines have been fitted to the data to determine their slopes (each equal to the transverse stiffnesses, m) at different spans. As expected, as is evident from Figure 4.23, the transverse stiffness increases as the span decreases.

Table 4.5: Average transverse stiffnesses and flexural moduli of timber and PVC posts and rails

Beam	Average transverse stiffness [N/mm]	Average flexural modulus [GPa]
Timber Post 1	671	10.7
Timber Post 2	526	8.1
Timber Post 3	632	9.5
Average flexural modulus for timber posts		**9.4**
Timber Rail 1	8	9.1
Timber Rail 2	11	13.5
Average flexural modulus for timber rails		**11.3**
PVC Post 1	250	1.3
PVC Post 2	269	1.4
PVC Post 3	247	1.3
Average flexural modulus for PVC posts (Orientation A)		**1.3**
PVC Post 1 (R180)	362	1.9
PVC Post 2 (R180)	324	1.7
PVC Post 3 (R180)	337	1.8
Average flexural modulus for PVC posts (Orientation B)		**1.8**
PVC Rail 1	1.33	2.7
PVC Rail 2	1.30	2.7
PVC Rail 3	1.28	2.6
Average flexural modulus for PVC rails		**2.7**

Each of the regression lines fitted to the data points in Figure 4.23 had correlation coefficients of 0.99. Plots of 1/mL versus L^2 (based on Equation (2)) and $1/mL^3$ versus $1/L^2$ (based on Equation (3)) are shown in Figure 4.24 and Figure 4.25, respectively. The regression line fitted to the data points in Figure 4.24 had a correlation coefficient of 0.99, whereas the regression line fitted to the data points in Figure 4.25 had a significantly lower correlation coefficient of 0.75. In order to reduce the scatter of the data points in Figure 4.25, the load-centre deflection data for the 973 mm span beam was excluded from the regression analysis and a plot of $1/mL^3$ versus $1/L^2$ was plotted with only 3 data points (see Figure 4.26). The decision to exclude data was made because the data point was considered as an outlier, and by so doing, the value of the correlation coefficient increased from 0.75 to 0.93 (cf. Figure 4.25 and Figure 4.26). The substantial improvement in the correlation coefficient justified the exclusion of the data point.

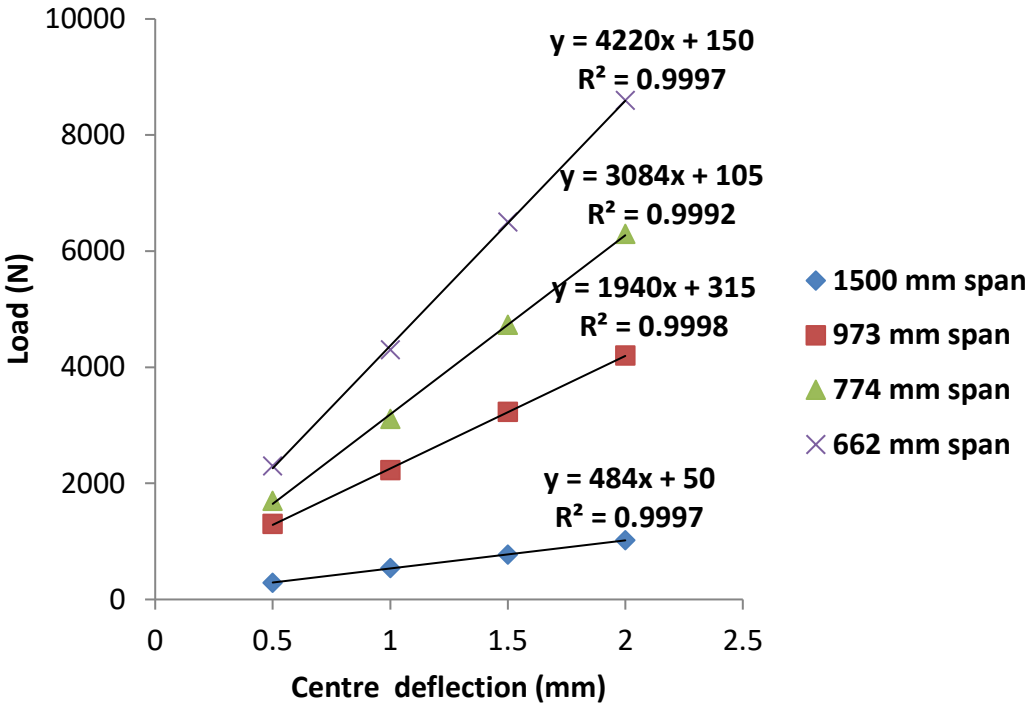

Figure 4.23: Load versus centre deflection plots for Timber Post 4

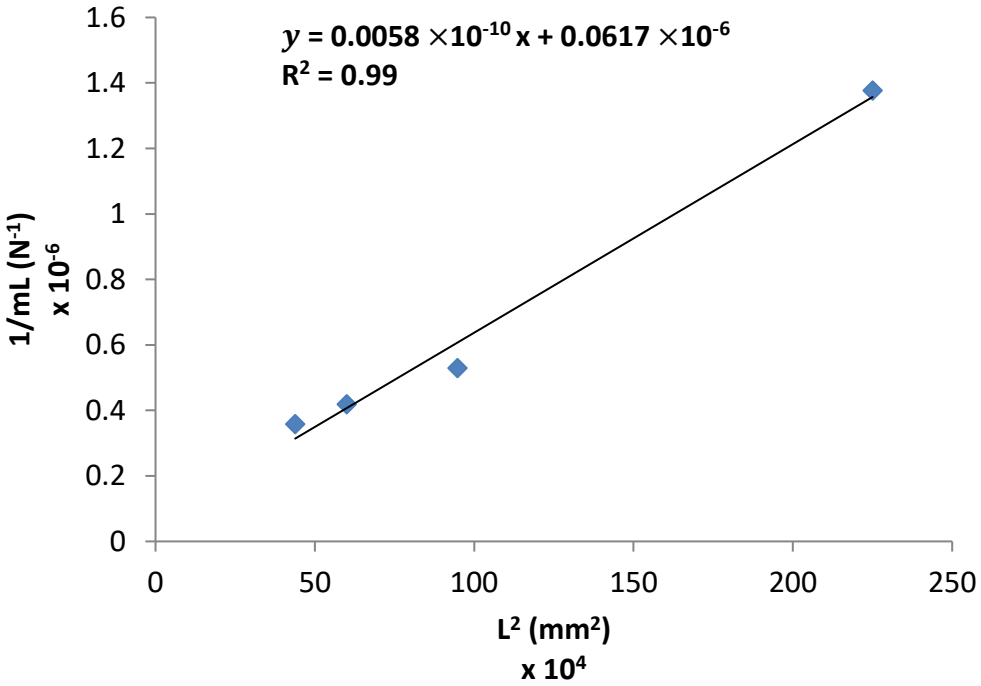

Figure 4.24: A plot of 1/mL versus L^2 for Timber Post 4

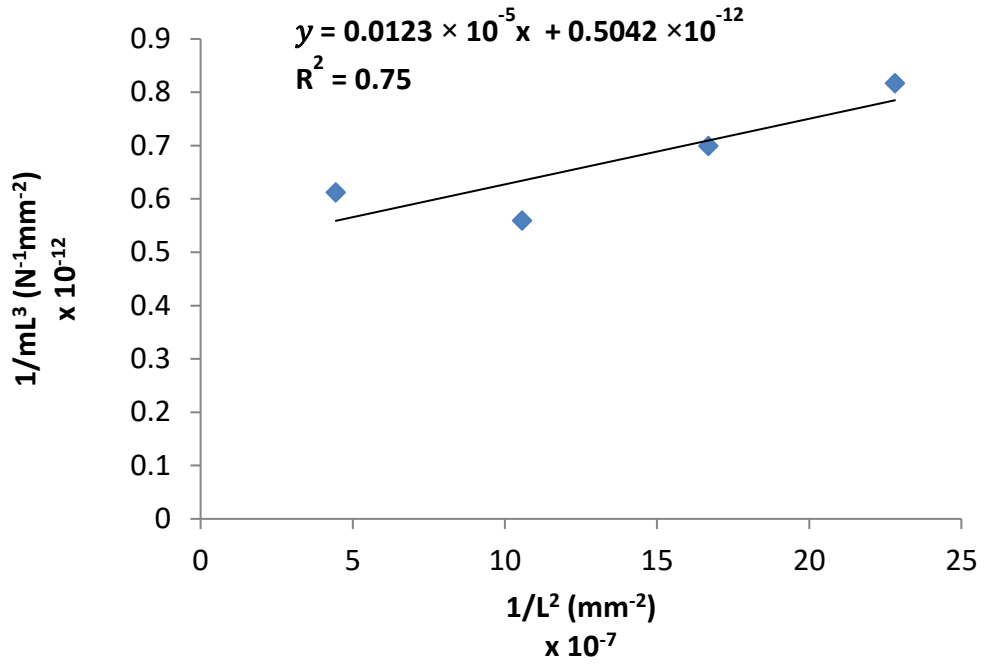

Figure 4.25: A plot of $1/mL^3$ versus $1/L^2$ for Timber Post 4 (4 data points)

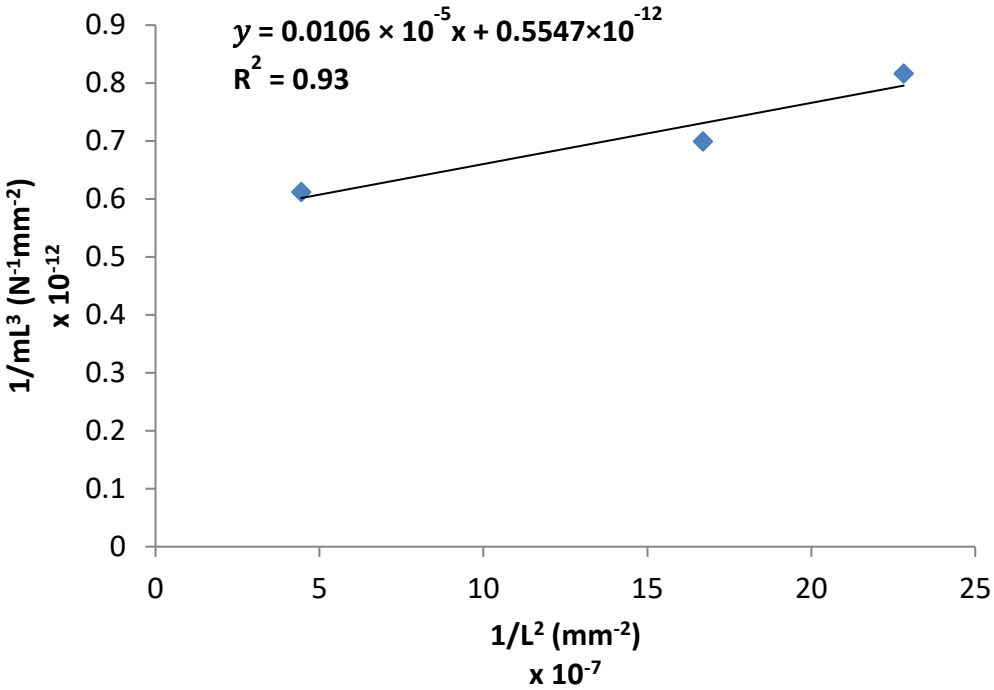

Figure 4.26: A plot of $1/mL^3$ versus $1/L^2$ for Timber Post 4 (3 data points)

The flexural and shear moduli of Timber Post, 4 determined using Equations (2) and (3), are given in Table 4.6. However, according to Sims et al. (1987), it is more accurate to use the gradient of the regression lines rather than the values of the intercepts. Following this method, the flexural and shear moduli were determined from the slope of the straight lines fitted to the data points in Figure 4.24 and Figure 4.26, respectively. Hence, the flexural and shear moduli of Timber Post 4 were determined to be 10.9 GPa and 0.4 GPa, respectively.

Table 4.6: Flexural and shear moduli for Timber Post 4 using Equations (2) and (3)

Equation	Flexural modulus [GPa]	Shear modulus [GPa]
(2)	10.9	0.6
(3)	11.4	0.4

Figure 4.27 and Figure 4.28 show the load versus centre deflection responses obtained from the three-point bending tests carried out on the unfilled polyurethane (U1 – U5) and 9 wt. % CF fibre filled polyurethane (F1 – F5) beams, respectively. The responses of the unfilled polyurethane beams showed an initial linear elastic response which becomes nonlinear when the central deflection exceeds 15 mm, whereas, the responses of the 9 wt. % CF10 fibre filled polyurethane beams become nonlinear when the centre deflection exceeds 10 mm. The responses also showed that the unfilled polyurethane beams exhibit a more ductile response compared to the 9 wt. % CF10 fibre filled polyurethane beams. The slope (transverse stiffness), m of each load-centre deflection response for each polyurethane beam was calculated between loads 10 N and 40 N (i.e. the linear portion of the graph). Table 4.7 shows the transverse stiffnesses, flexural moduli, flexural strengths and maximum deflections of the unfilled and 9 wt. % CF fibre filled polyurethane beams.

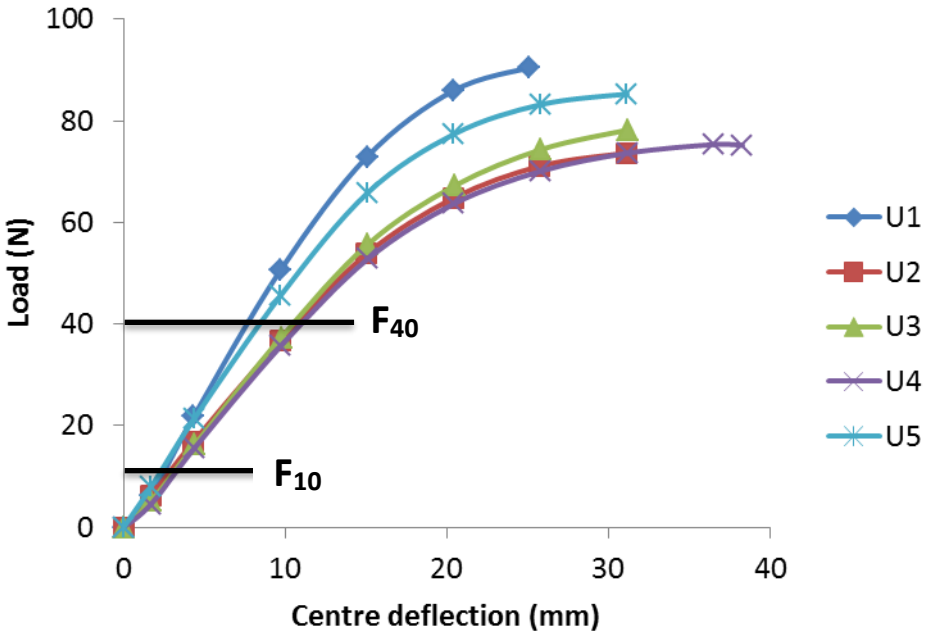

Figure 4.27: Load versus centre deflection plots for five unfilled polyurethane beams (U1 – U5) (span = 195 mm)

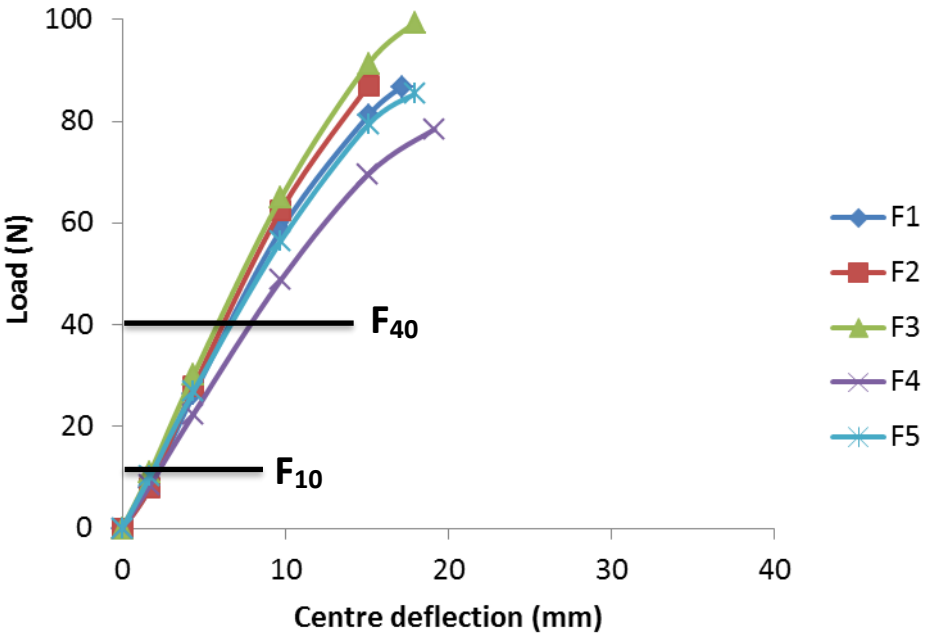

Figure 4.28: Load versus centre deflection plots for five 9 wt. % CF10 fibre filled polyurethane beams (F1 – F5) (span = 192 mm)

Table 4.7: Test Results for five Unfilled (U1 – U5) and five Filled (F1 – F5) polyurethane beams

Specimen name	Transverse stiffness [N/mm]	Flexural modulus [MPa]	Maximum load [N]	Flexural strength [MPa]
U1	5.7	136	90	4.3
U2	3.7	101	74	3.7
U3	4.0	110	79	4.0
U4	3.8	101	75	3.7
U5	4.8	124	85	4.2
Average	**4.4**	**114.4**	**80.6**	**4.0**
Standard deviation	**0.8**	**15.3**	**6.8**	**0.3**
Coefficient of variation (%)	**19.2**	**13.4**	**8.4**	**7.0**
F1	6.6	157	87	4.2
F2	7.2	155	98	4.5
F3	7.2	188	99	4.9
F4	5.1	131	77	3.8
F5	6.1	163	85	4.2
Average	**6.4**	**158.8**	**89.2**	**4.3**
Standard deviation	**0.9**	**20.4**	**9.3**	**0.4**
Coefficient of variation (%)	**13.7**	**12.8**	**10.4**	**9.5**

The average flexural modulus for the unfilled polyurethane beams was 114 MPa, whereas, the average flexural modulus for the 9 wt. % CF10 fibre filled polyurethane beams was 159 MPa. These results showed that there was an approximate 40 % increase in the average flexural modulus of the polyurethane beams with 9 wt. % CF10 fibre compared to the unfilled polyurethane beams. Furthermore, the coefficient of variation of both sets of polyurethane beams was approximately 13 %. The average flexural strength of the unfilled polyurethane beams was 4 MPa and the average flexural strength of the 9 wt. % CF10 fibre filled polyurethane was 4.3 MPa, reflecting a 7.5 % increase in average flexural strength. The coefficients of variation of the flexural strengths of the unfilled and filled polyurethane beams were 7 % and 9.5 %, respectively reflecting a reasonably small difference.

4.3. Compression Test

4.3.1. Experimental Setup, Instrumentation and Test Procedure for the Compression Tests

Compression tests were carried out on timber specimens in a 250 kN capacity universal testing machine (Instron 8802). Two sets of compression tests were carried out. In the first set, the specimens were loaded perpendicular–to-the-grain and in the second, they were loaded parallel-to-the-grain (see Figure 4.29). 20 specimens were tested in compression (10 specimens in each set); the specimens compressed perpendicular–to-the-grain and parallel-to-the-grain are labelled PR1 – PR10 and PL1 – PL10, respectively. The dimensions of the specimens are given in Table 4.8 (also see Figure 4.29). The test specimens were compressed between rigid platens under displacement control at a crosshead displacement rate of 0.6 mm/min. The geometry of the specimens and crosshead displacement rate were obtained from BS EN 408 (2010). The load and displacement were recorded by a computer controlled data acquisition system. In order to determine the failure modes in compression, the front face of each specimen was monitored by a video camera to determine the failure mode classification according to ASTM D143 (2009) (see Figure 4.30).

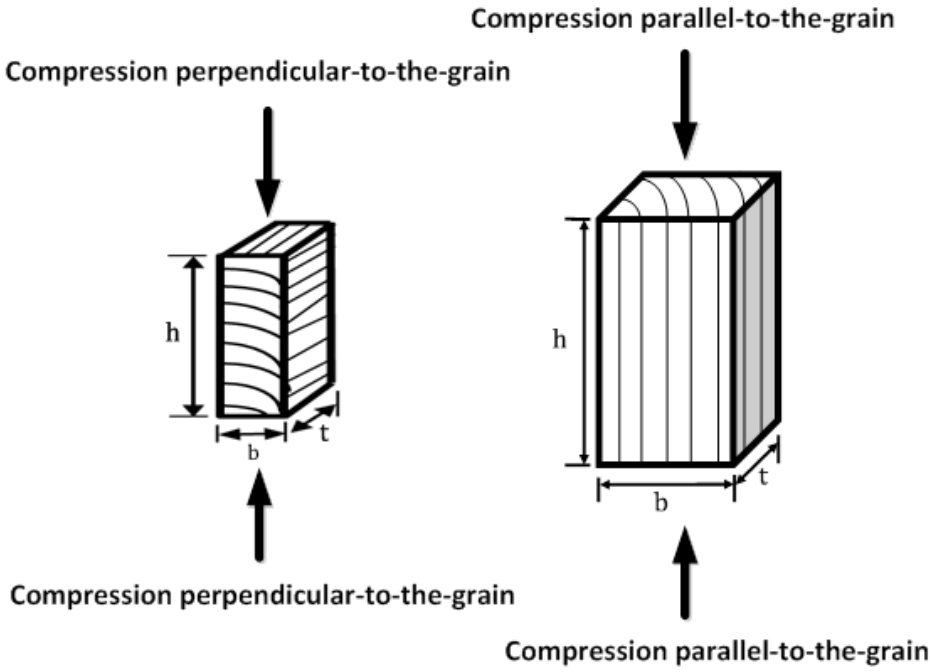

Figure 4.29: Schematic drawing of the compression test specimens [Note: the sketch is not drawn to scale]

Table 4.8: Details of the compression test specimens

Compression direction	Specimen dimensions [mm]		
	b	t	h
Parallel-to-the-grain (PL1 – PL10)	40	40	240
Perpendicular-to-the-grain (PR1 – PR10)	45	70	90

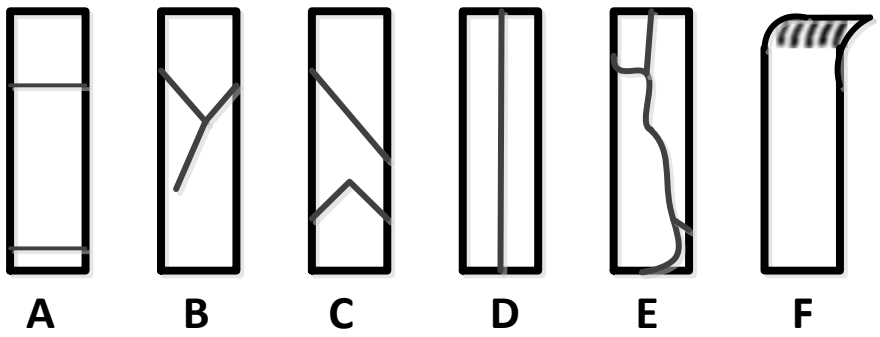

Figure 4.30: Uniaxial compression parallel-to-the-grain failure modes of timber samples according to ASTM D143 (2009): (A) Crushing (B) Wedge Split (C) Shearing (D) Splitting (E) Compression and Shearing parallel-to-the-grain (F) Brooming or End-Rolling

The compressive strength parallel-to-the-grain is the maximum compressive stress sustained by the specimen in that direction and was calculated using Equation (6). However, a compression test perpendicular-to-the-grain does not produce a clearly defined maximum stress. Instead, the load-deformation response shows a continuously increasing stress as the shortening of the specimen becomes very large. However, BS EN 408 (2010) defines the compressive strength perpendicular-to-the-grain as the stress corresponding to a predefined compressive strain (see Figure 4.31), which can then be calculated using Equation (7). The compressive strength perpendicular-to-the-grain was calculated using an iterative process; firstly, a maximum compressive load $\mathrm{F_{c,90,max,est}}$ was estimated. Using the load-deformation test data, the gradient of the load-deformation curve defined by $\mathrm{F_{10}}$ and $\mathrm{F_{40}}$ (10 % and 40 % of the estimated maximum load, $\mathrm{F_{c,90,max,est}}$, respectively) was calculated. A straight line (line 1 in Figure 4.31) passing through these two data points ($\mathrm{F_{10}}$ and $\mathrm{F_{40}}$) was drawn. Parallel to line 1, line 2 was drawn with its origin at load = 0 and deformation = 0.01 × h (where h is the initial height of the specimen) as shown in Figure 4.31. The load corresponding to the intersection of line 2 with the load-deformation curve is then regarded as the maximum load, with the condition that the value is within 5 % of the

estimated maximum load, $F_{c,90,max,est}$. Thereafter, the compressive strength perpendicular-to-the-grain $f_{c,90}$ was calculated using Equation (7).

$$f_{c,0} = \frac{F_{c,0,max}}{b \cdot t} \tag{6}$$

$$f_{c,90} = \frac{F_{c,90,max}}{b \cdot t} \tag{7}$$

In Equations (6) and (7) $f_{c,0}$ is the compressive strength parallel-to-the-grain, $F_{c,0,max}$ is the maximum load parallel-to-the-grain, $f_{c,90}$ is the compressive strength perpendicular-to-the-grain, $F_{c,90,max}$ is the maximum load perpendicular-to-the-grain, b is the width of the specimen and t is its thickness.

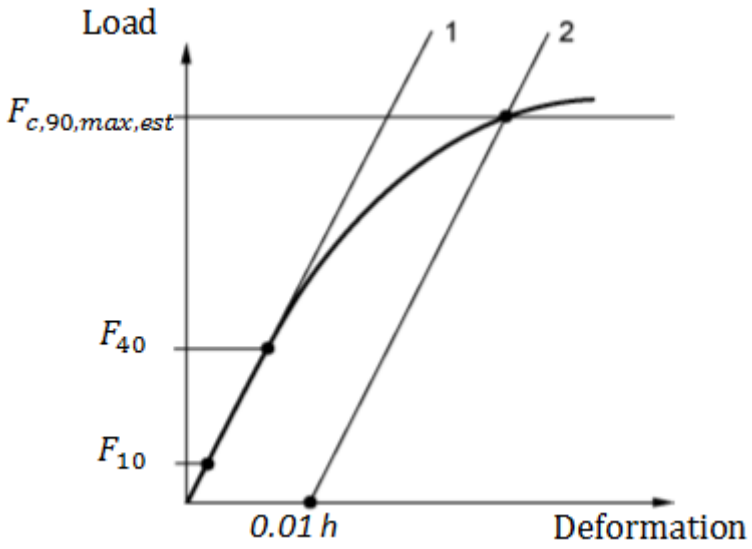

Figure 4.31: Typical load-deformation response for a compression test perpendicular-to-the-grain

4.3.2. Results and Discussion of the Compression Tests

Figure 4.32 and Figure 4.33 show the compression-deformation responses for 10 specimens (5 specimens in each Figure, PR1 – PR5 and PR6 - PR10) tested perpendicular-to-the-grain. The results of the compression tests perpendicular-to-the-grain show identical load-deformation curves for all the 10 specimens (PR1 – PR10); the compression-deformation responses showed an initial linear elastic response which becomes increasingly nonlinear after about 2 mm of compression (see Figure 4.32 and Figure 4.33).

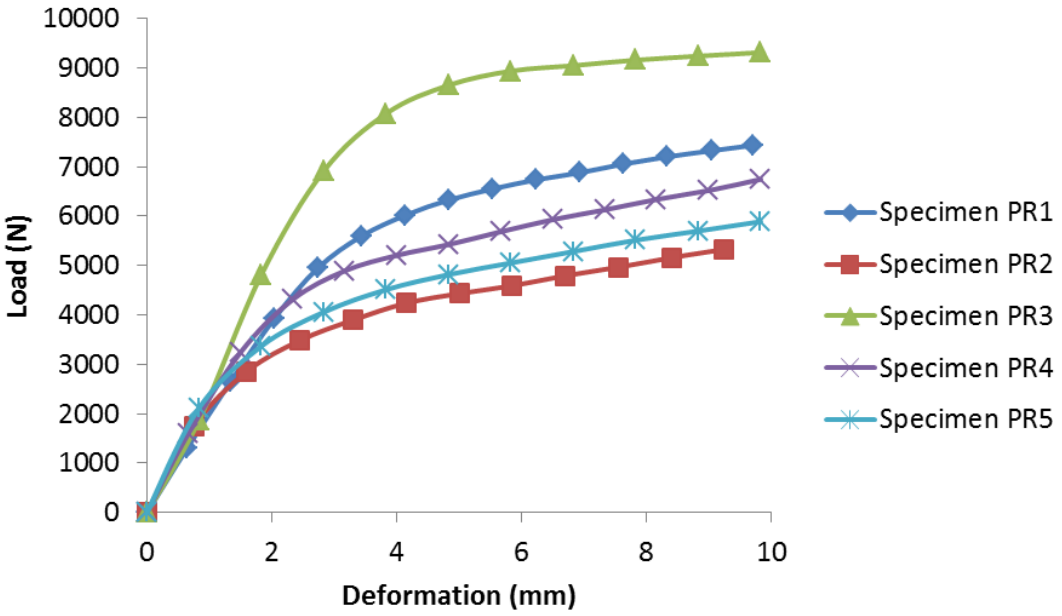

Figure 4.32: Load versus deformation responses of five timber specimens tested perpendicular-to-the-grain (PR1 - PR5)

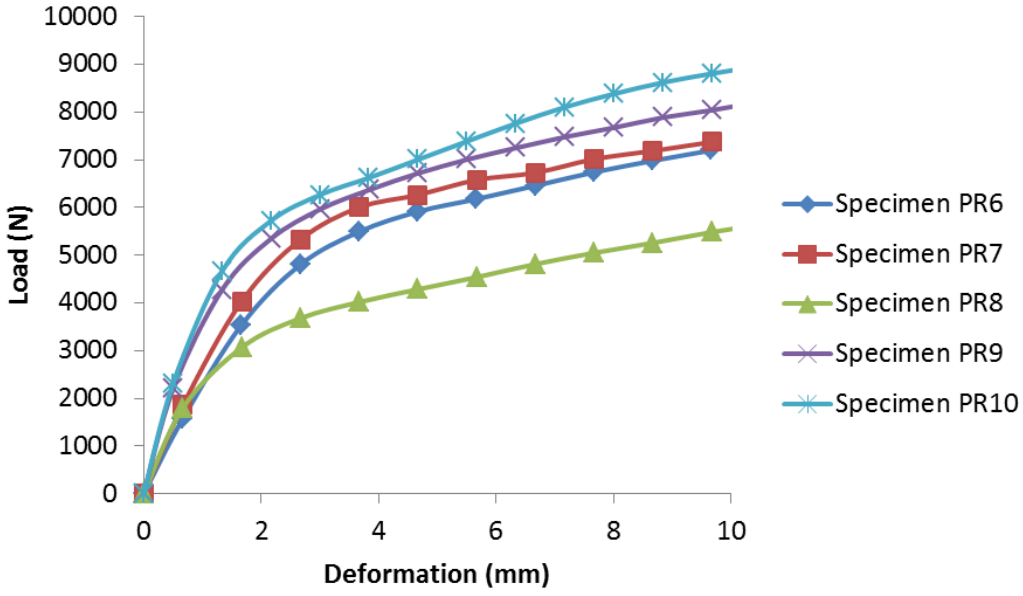

Figure 4.33: Load versus deformation responses of five timber specimens tested perpendicular-to-the-grain (PR6 – PR10)

Figure 4.34 shows the typical failure progression of the specimens tested perpendicular-to-the-grain; failure progresses from left to right (Images 1 – 4). All the specimens tested perpendicular-to-the-grain showed the same mode of deformation with no macroscopic crack development before the maximum load, $F_{c,90,max}$ was reached. This mode of deformation can be attributed to the progressive bending (linear elastic response) of the polygonal cell walls, and the subsequent buckling and collapse (nonlinear response) of the cell walls (see Figure 4.35) (Ashby and Jones, 2006).

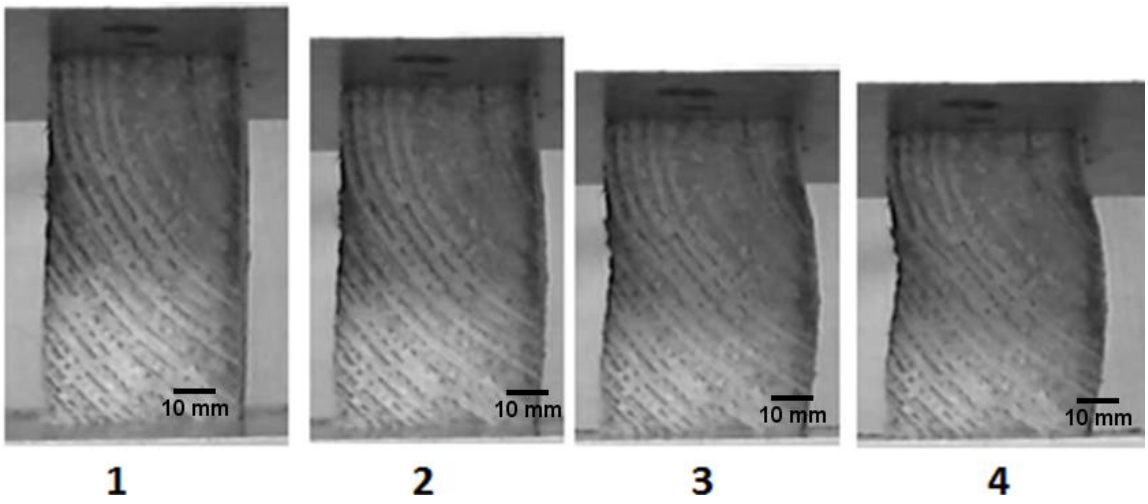

Figure 4.34: Failure progression of specimen PR1 compressed perpendicular-to-the-grain

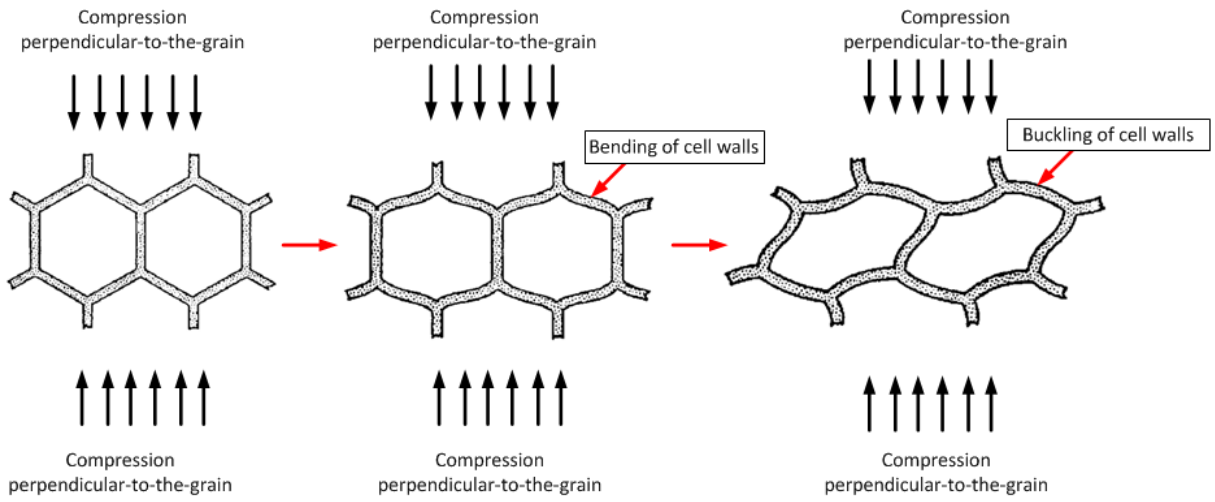

Figure 4.35: Progressive bending and buckling of the cell walls as wood is compressed perpendicular-to-the-grain (Easterling et al., 1982, Ashby and Jones, 2006)

An example calculation for the compressive strength perpendicular-to-the-grain, $F_{c,90,max}$ for specimen PR1 is explained. 6700 N was chosen as $F_{c,90,max,est}$, which gave the values F_{10}

and F_{40} as 670 N and 2680 N, respectively. For these two load values, the corresponding deformations were found from the load-deformation data. However, the load-deformation data did not have the exact values of 670 N and 2680 N; hence, linear interpolation was carried out between the two nearest consecutive data points as shown in Table 4.9. Hence, the interpolated corresponding deformation values for 670 N (F_{10}) and 2680 N (F_{40}) were 0.33 mm and 1.35 mm, respectively; a straight line (line 1) passing through these data points was drawn on the curve (see Figure 4.36). Parallel to line 1, a second line (line 2) was drawn from the deformation axis, with a value equal to 0.01 multiplied by the initial height, h of the specimen which for this case resulted in an offset of 0.9 mm (0.01 × 90 mm) on the deformation axis.

Table 4.9: Load-deformation data for 670 N and 2680 N of specimen PR1

Load [N]	Load [N]	Deformation [mm]	Deformation [mm]
F_{10} = 670	643.42	0.32	0.33
	693.98	0.34	
F_{40} = 2680	2651.76	1.34	1.35
	2695.08	1.36	

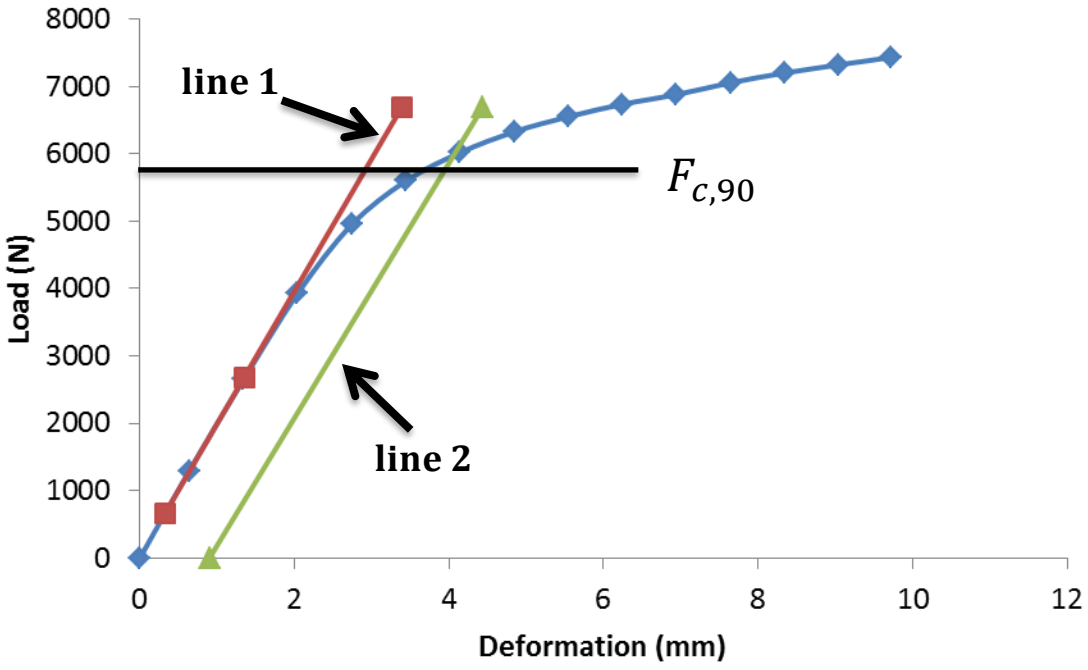

Figure 4.36: Load versus deformation response for specimen PR1 (1st iteration)

The point of intersection for line 2 and the load-deformation curve was 6000 N. In the first iteration; the value was outside the 5 % range of the estimated starting value (6700 N). Hence, a second iteration was carried out using 6000 N as the $F_{c,90,max,est}$; which gave the values F_{10} and F_{40} as 600 N and 2400 N, respectively. The load-deformation data did not also have the exact values of 600 N and 2400 N; hence, a linear interpolation was also carried out between the nearest consecutive data points as shown in Table 4.10. F_{10} and F_{40} gave corresponding deformation values of 0.30 mm and 1.22 mm, respectively.

Table 4.10: Load-deformation data for 600 N and 2400 N of specimen PR1

Load [N]	Load [N]	Deformation [mm]	Deformation [mm]
F_{10} = 600	566.02	0.28	0.30
	602.03	0.30	
F_{40} = 2400	2370.38	1.20	1.22
	2403.80	1.22	

Following the same process, the second line (line 2) intersected the curve at 5900 N (see Figure 4.37) which gave a deviation of 1.6 %; which is within the defined tolerance of 5 % that was specified in BS EN 408 (2010).

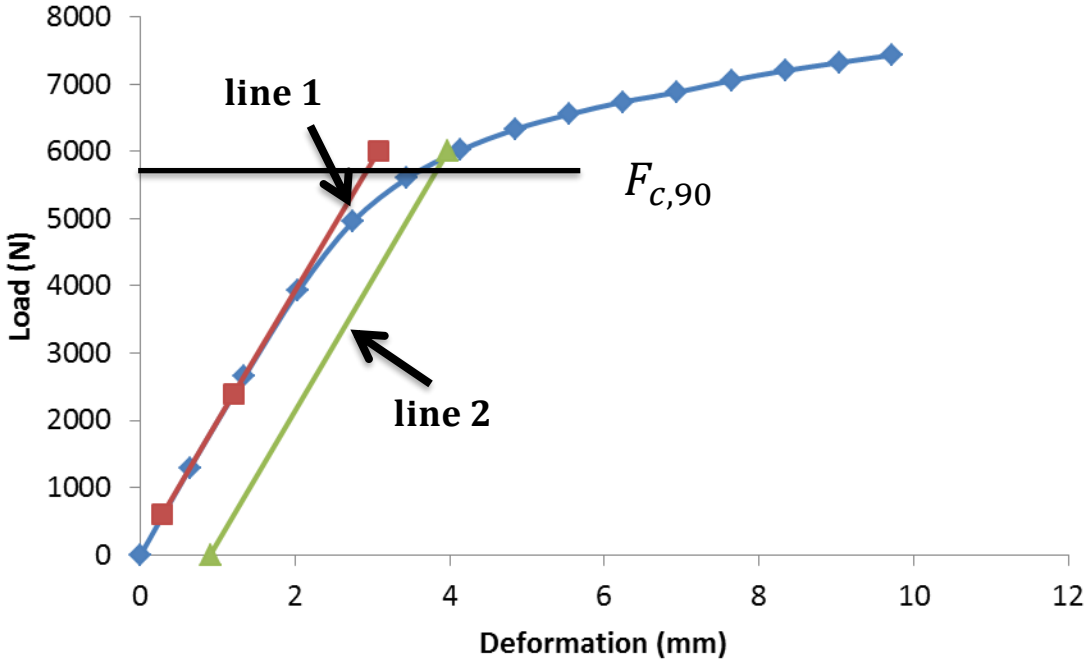

Figure 4.37: Load versus deformation response for specimen PR1 (2nd iteration)

This iterative method was carried out on the results for each perpendicular-to-the-grain compression test specimen to determine their maximum compressive loads $F_{c,90,max}$ and corresponding compressive strengths (see Table 4.11) using Equation (7). A maximum of eight iterations was carried out for the specimens. Table 4.11 also shows the average, standard deviation and coefficient of variation of the compressive strengths perpendicular-to-the-grain. The compressive strengths perpendicular-to-the-grain ranged from 1.1 – 2.6 MPa.

Table 4.11: Maximum compressive loads and compressive strengths perpendicular-to-the-grain for specimens PR1 – PR10

Specimen	Maximum compressive load perpendicular-to-the-grain [kN]	Compressive strength perpendicular-to-the-grain [MPa]
PR1	5.9	1.87
PR2	**3.5**	**1.10**
PR3	**8.1**	**2.57**
PR4	4.8	1.52
PR5	4.0	1.27
PR6	5.1	1.62
PR7	5.8	1.84
PR8	3.8	1.21
PR9	5.7	1.81
PR10	5.5	1.75
Average	**5.2**	**1.66**
Standard deviation (SD)	**1.3**	**0.42**
Coefficient of variation (%)	**26**	**26**

Figure 4.38 and Figure 4.39 show the compression-deformation responses for 10 specimens (5 specimens in each Figure, PL1 – PL5 and PL6 - PL10) tested parallel-to-the-grain. The figures show an initial elastic linear response that stops as failure initiates within the specimen. The maximum stress obtained corresponds to the compressive strength. The plots also showed that the compression strength parallel-to-the-grain is significantly higher than perpendicular-to-the-grain.

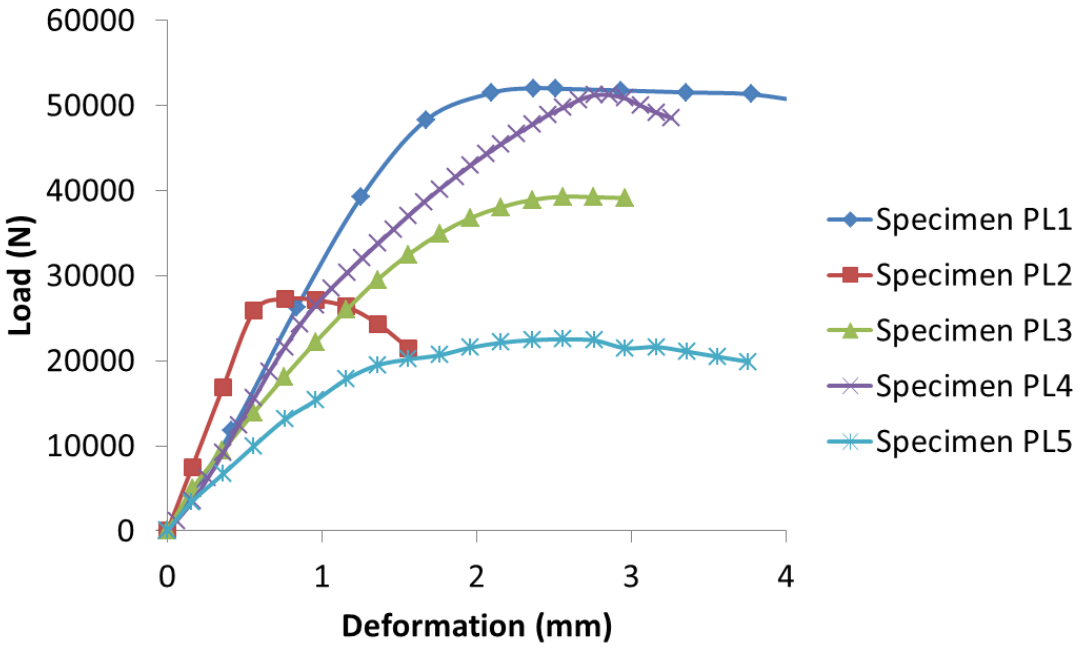

Figure 4.38: Load versus deformation responses for five timber specimens tested parallel-to-the-grain (PL1 - PL5)

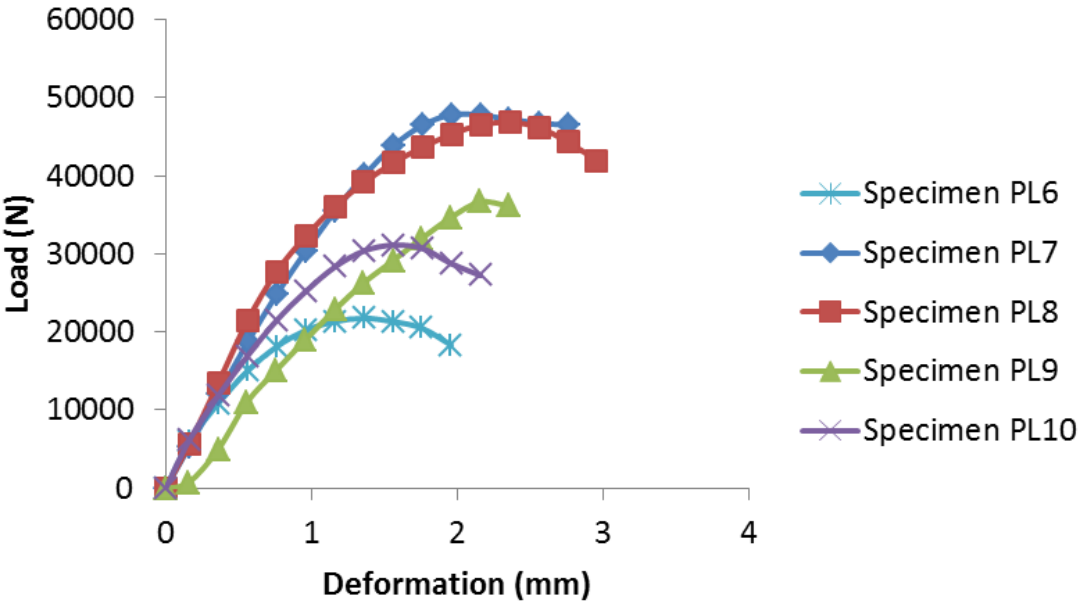

Figure 4.39: Load versus deformation responses for five timber specimens tested parallel-to-the-grain (PL6 – PL10)

In contrast to the compression perpendicular-to-the-grain, different failure modes occurred in the specimens compressed parallel-to-the-grain. Four specimens (PL1 – PL4) exhibited similar failure modes (mode E in Figure 4.30). This mode of failure can be attributed to the collapse of the internal longitudinal cells, and subsequent shearing of the fractured cells (see Figure 4.40). Easterling et al. (1982) also relate the collapse at the end of the cells, as the dominant compressive failure mode when wood is compressed parallel-to-the-grain. The failure progression for PL1 is shown in Figure 4.41 (failure progresses from left to right (Images 1 – 6)).

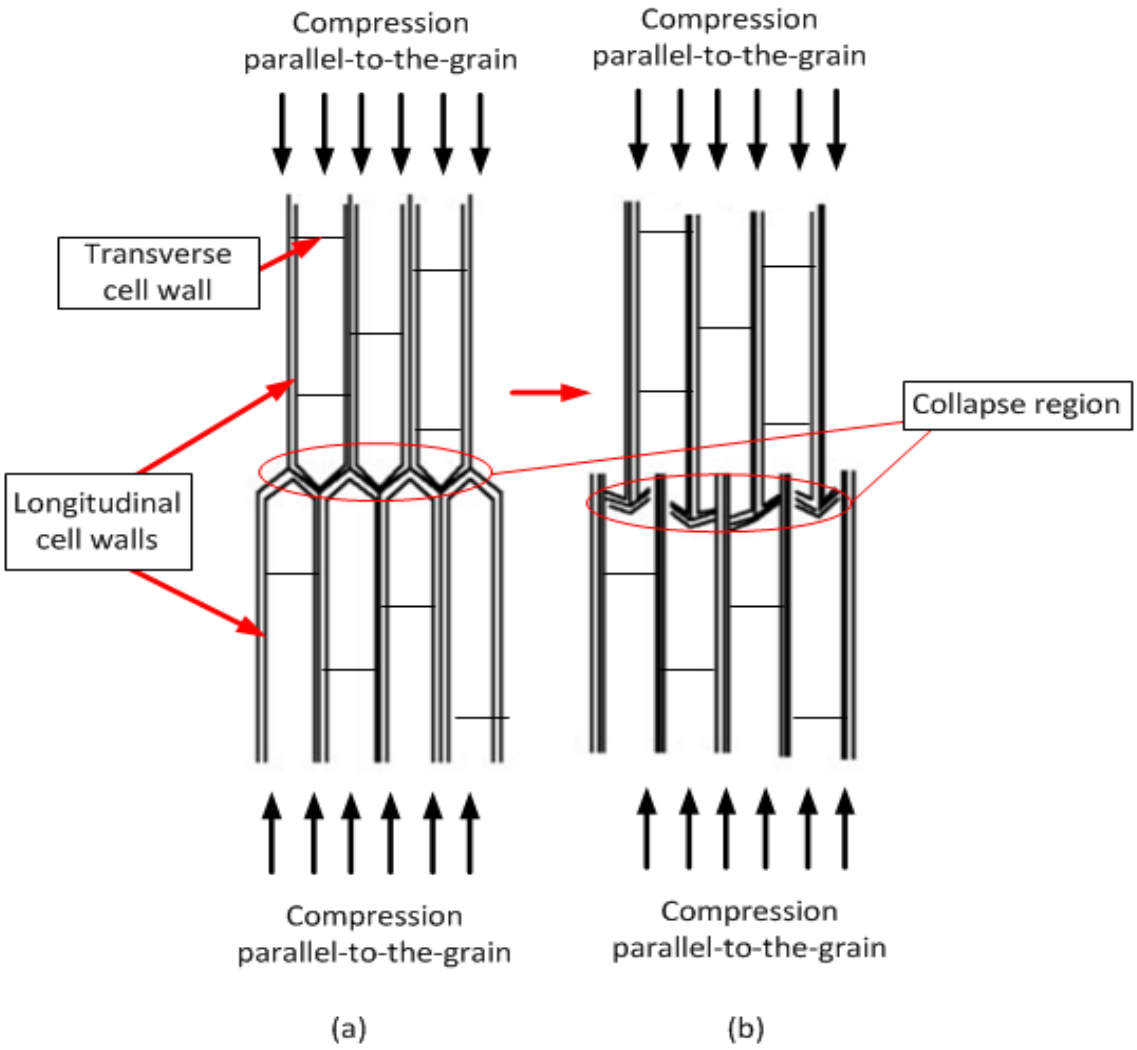

Figure 4.40: Compression parallel-to-the-grain: (a) Before and (b) After (Sandberg et al., 2013)

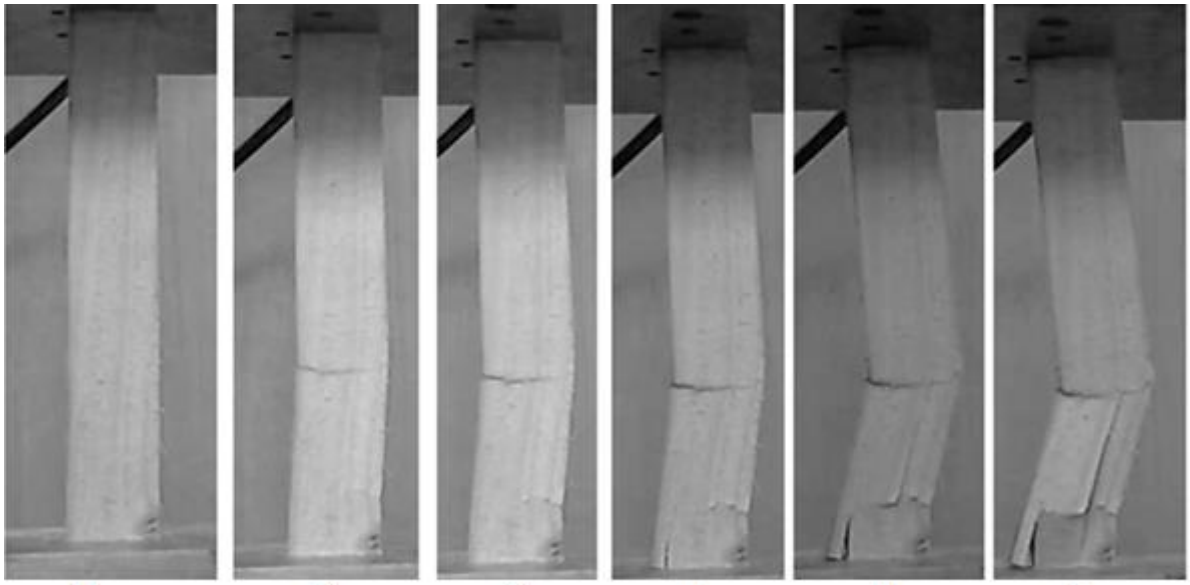

Figure 4.41: Compression and shearing parallel-to-the-grain failure progression (PL1)

Specimens PL5, PL8, PL9, and PL10 also showed similar modes of deformation (mode D). This splitting deformation mode (mode D) of the specimens is shown in Figure 4.42; failure progresses from left to right (Images 1 – 7). Splitting occurred as a result of an internal defect in the specimen i.e. the presence of a knot. According to Kretschmann (2010), the presence of knots and other natural defects reduces the strength properties of the timber.

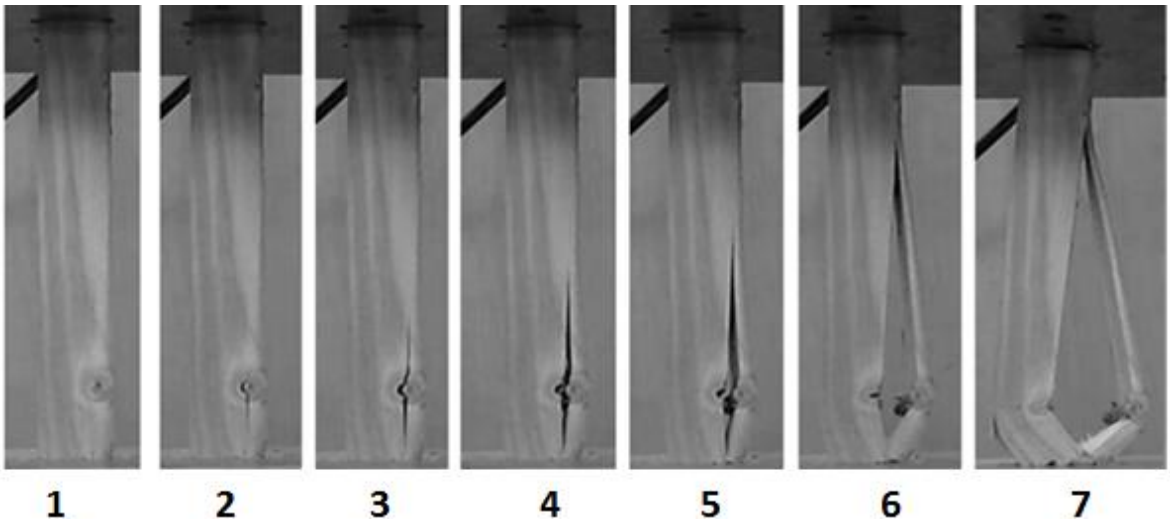

Figure 4.42: 'Splitting' failure progression (PL5)

The mode of failure which occurred in specimens PL6 and PL7 is called Brooming (or End-rolling, see Figure 4.43). ASTM D143 (2009) explains that this mode of deformation (mode F) can be associated with excess moisture content at the ends of the specimens.

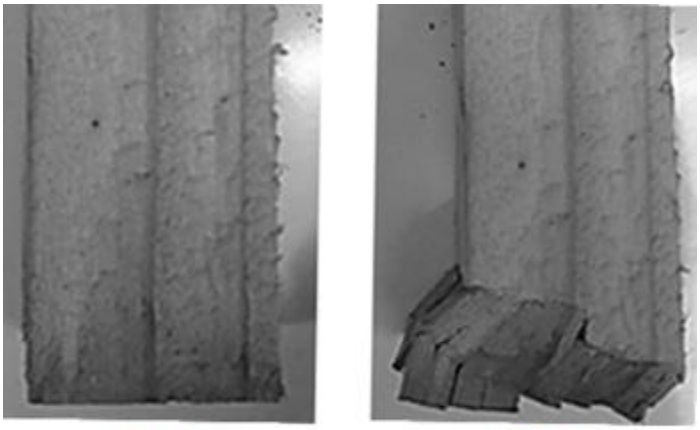

Figure 4.43: 'Brooming' or 'End-rolling' failure in compression (PL7): (a) Before and (b) After testing

The compressive strength parallel-to-the-grain for each specimen was determined using Equation (6) and is given in Table 4.12. Table 4.12 also gives the average, standard deviation and coefficient of variation of the compressive strengths parallel-to-the-grain. The compression strengths parallel-to-the-grain ranged from 13.6 – 32.5 MPa.

Table 4.12: Maximum compressive loads and compressive strengths parallel-to-the-grain for specimens PL1 – PL10

Specimen	Maximum compressive load parallel-to-the-grain [kN]	Compressive strength parallel-to-the-grain [MPa]
PL1	**52.0**	**32.5**
PL2	27.4	17.1
PL3	39.9	24.9
PL4	51.3	32.1
PL5	22.6	14.1
PL6	**21.8**	**13.6**
PL7	48.0	30.0
PL8	46.9	29.3
PL9	37.8	23.6
PL10	31.3	19.6
Average	**37.9**	**23.68**
Standard Deviation (SD)	**11.6**	**7.27**
Coefficient of Variation (%)	**31**	**31**

The average compressive strength perpendicular-to-the-grain was 1.7 MPa, whereas, the average compressive strength parallel-to-the-grain was 23.7 MPa. The ratio of the average

parallel-to- and perpendicular-to-the-grain compressive strengths was approximately 14:1. This is consistent with the highly orthotropic nature of timber. The corresponding coefficients of variation for the compressive strengths perpendicular-to and parallel-to-the-grain were 26 % and 31 %, respectively; these high values show the natural variability of timber even among specimens that were cut from the same timber section. Kretschmann (2010) also stated that the mechanical properties of timber vary considerably even in clear (no visible defect) specimens. The variation in the mechanical properties can be due to the fact that timber is a natural material and tree growth is affected by different environmental factors.

4.4. Uniaxial Tensile Test

4.4.1. Experimental Setup, Instrumentation and Test Procedure for the Uniaxial Tensile Tests

Uniaxial tensile tests were carried out on 16 nominally identical Composite C materials (four for each formulation – C_PP, C_PPW, C_SF and C_SFW) and five nominally identical PVC coupons (P1 – P5) using a universal testing machine (Zwick Z020) which had a load capacity of 20 kN. The grips of the machine were used to secure the ends of the specimens so that the tensile force was applied uniaxially to the specimens. Figure 4.44 shows sketches of the uniaxial test specimens, and the dimensions are given in Table 4.13.

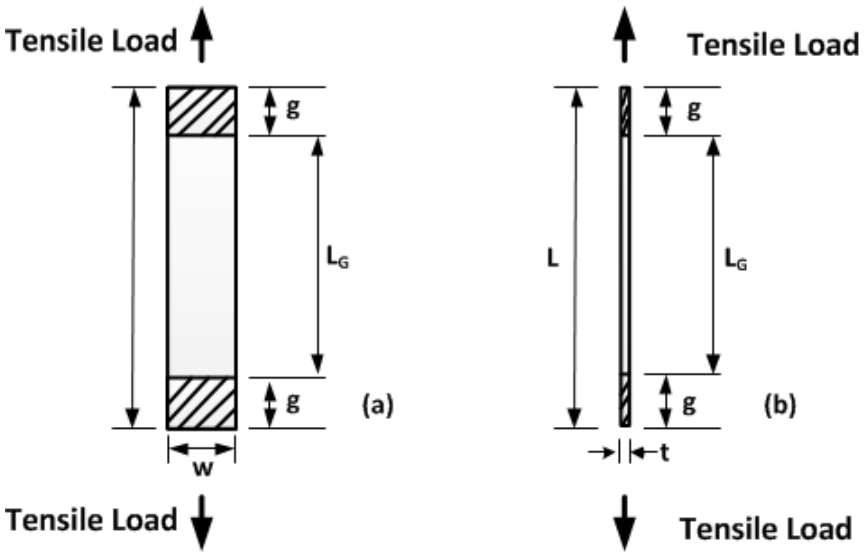

Figure 4.44: Sketches of a uniaxial tensile test specimen (a) Front-view (b) Side-view

Table 4.13: Dimensions of the uniaxial test specimens

Material	Width [w] [mm]	Thickness [t] [mm]	Overall length [L] [mm]	Gauge length [L_G] [mm]	Grip length [g] [mm]
Composite C	39	11	293	193	50
PVC	20	3	180	80	50

The loads applied to the Composite C materials were recorded by the data acquisition system of the testing machine, whereas the longitudinal strains were recorded with a digital image correlation system (Imetrum), with a gauge length of 50 mm. This advanced digital image correlation system (Imetrum) utilises a non-contact video extensometer with a high resolution to track the longitudinal strains until the material fractures. The experimental setup is shown in Figure 4.45. A speckle pattern made of randomly distributed white dots was marked on the Composite C tensile test coupons for the purpose of the digital image correlation analysis (see Figure 4.46).

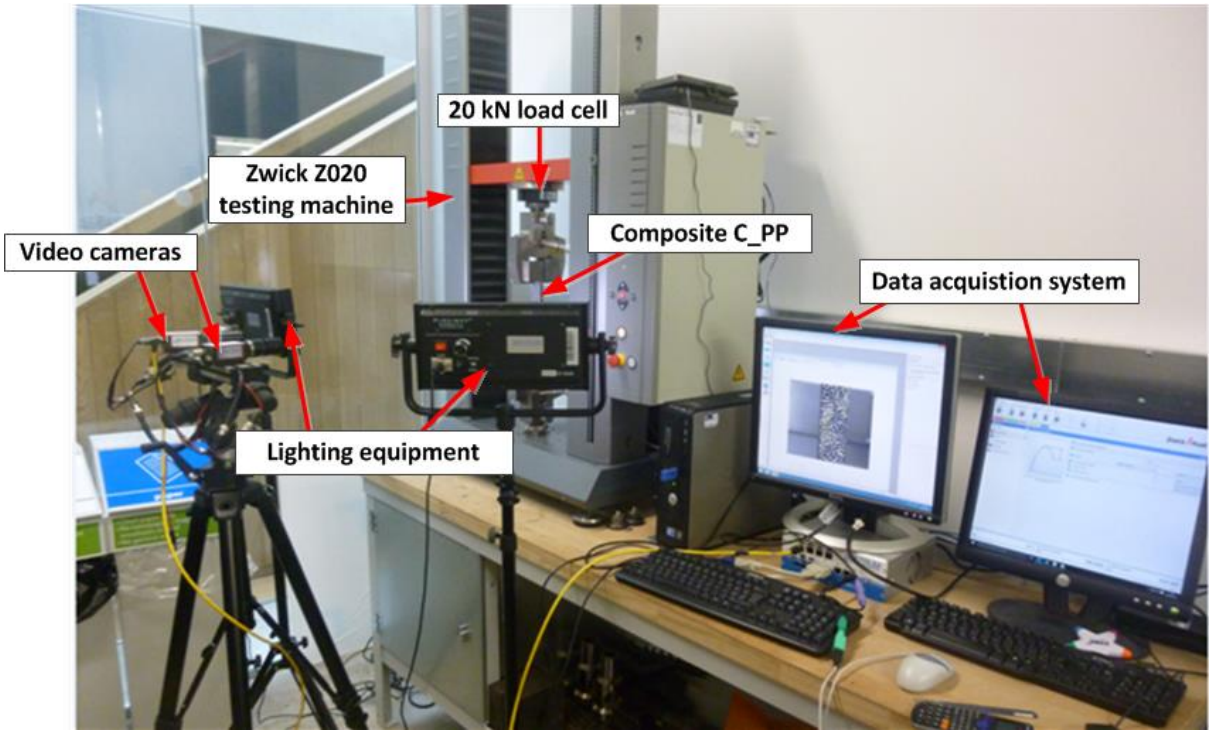

Figure 4.45: Image of the uniaxial tensile test setup on the Composite C_PP material

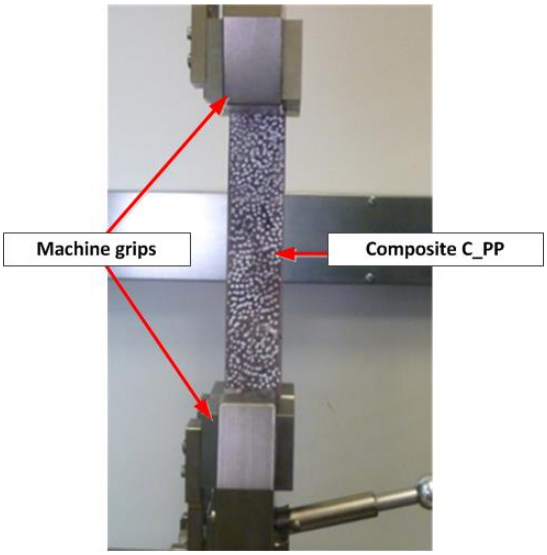

Figure 4.46: Close-up view of the uniaxial tensile test setup on the Composite C_PP material

The Composite C specimens were labelled C_PP6 – C_PP9, C_PPW6 – C_PPW9, C_SF6 – C_SF9 and C_SFW6 – C_SFW9 which corresponds to the formulations of Composite C_PP, C_PPW, C_SF and C_SFW, respectively (four samples for each formulation). It is worth noting that these specimens were initially tested elastically in three-point bending. The maximum loads for the specimens were obtained and used to determine their tensile strengths. The maximum tensile loads, strengths, moduli and absorbed energies (area under the curve) for the Composite C specimens were determined. However, the files containing the longitudinal strains for specimens C_PP6 and C_SF7 were lost as a result of computer errors; hence, the tensile moduli and absorbed energies for these specimens were not determined.

Five PVC tensile test coupons (P1 – P5) were cut longitudinally out of a PVC post. A mechanical extensometer which was connected to the universal testing machine (Zwick Z020) was attached to the PVC coupons to record their longitudinal extensions. The extensometer had a gauge length of 50 mm. The PVC coupons were initially loaded to 600 N at an extension rate of 2 mm/min and then unloaded. Thereafter, the coupons were loaded until the crosshead extensions recorded by the universal testing machine (Zwick Z020) reached 20 mm.

The tensile strength was calculated using Equation (8). The elastic tensile modulus for the Composite C and PVC coupons was calculated using Equations (9) and (10), respectively.

$$\text{Tensile strength} = \frac{F_{max}}{w \cdot t} \tag{8}$$

$$\text{Tensile modulus for Composite C} = \frac{(F_{4000} - F_{2000}) \cdot L_G}{(e_{4000} - e_{2000})\, w \cdot t} \tag{9}$$

$$\text{Tensile modulus for PVC} = \frac{(F_{400} - F_{100}) \cdot L_G}{(e_{400} - e_{100})\, w \cdot t} \tag{10}$$

In Equations (8) - (10), w is the width, t is the thickness and F_{max} is the ultimate tensile load. $F_{4000} - F_{2000}$ and $F_{400} - F_{100}$ are increments of load on the straight portion of the load-extension curve, in Newtons; $e_{4000} - e_{2000}$ and $e_{400} - e_{100}$ are their corresponding extensions. The gauge length, L_G for Composite C and PVC was 50 mm; this was the set gauge length on the digital image correlation system (Imetrum) and the extensometer for the Composite C and PVC coupons, respectively.

4.4.2. Results and Discussion for the Uniaxial Tensile Tests

Figure 4.47, Figure 4.48, Figure 4.49 and Figure 4.50 show the tensile load-extension plots for the Composite C_PP, C_PPW, C_SF and C_SFW specimens, respectively. The maximum tensile load, tensile strength, elastic tensile modulus and energy absorbed for each of the Composite C specimens tested in uniaxial tension are given in Appendix 7.

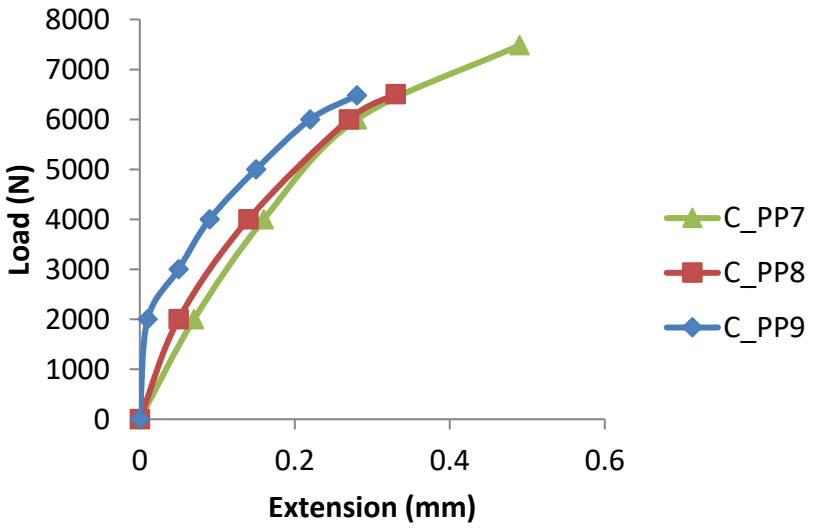

Figure 4.47: Tensile load versus extension plots for three Composite C_PP specimens

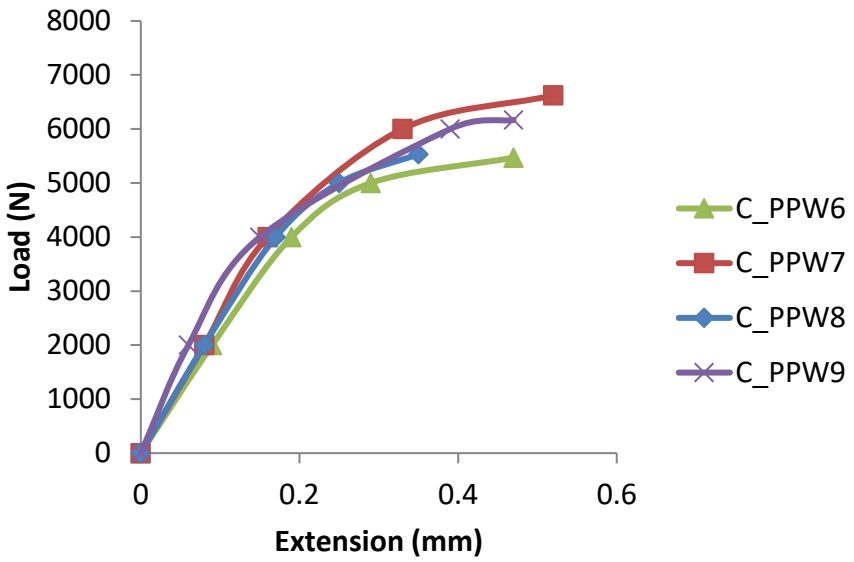

Figure 4.48: Tensile load versus extension plots for four Composite C_PPW specimens

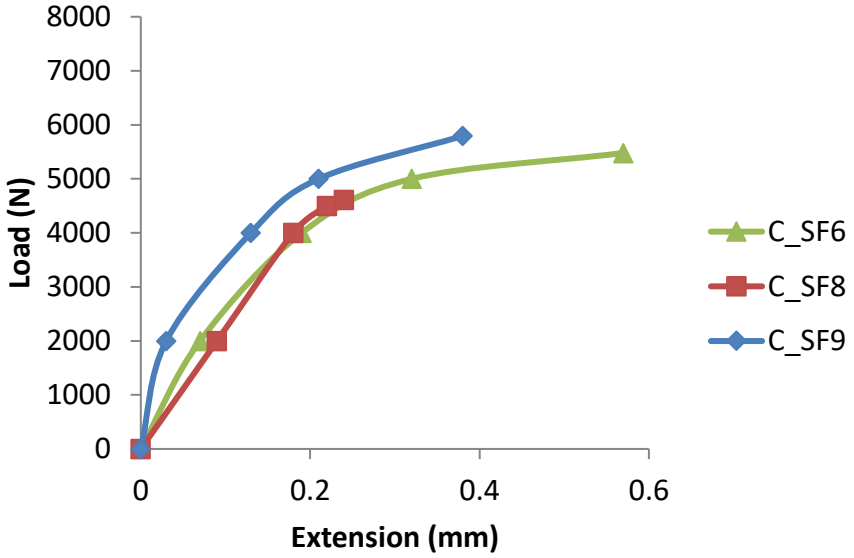

Figure 4.49: Tensile load versus extension plots for three Composite C_SF specimens

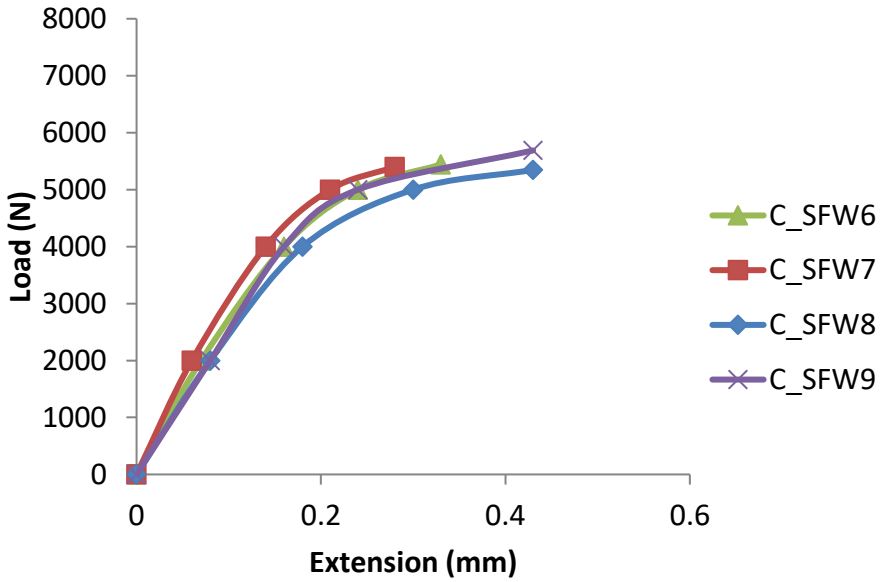

Figure 4.50: Tensile load versus extension plots for four Composite C_SFW specimens

Figure 4.51 shows an image of the failure mode for a Composite C_PP specimen in uniaxial tension. All the Composite C specimens failed in a brittle manner.

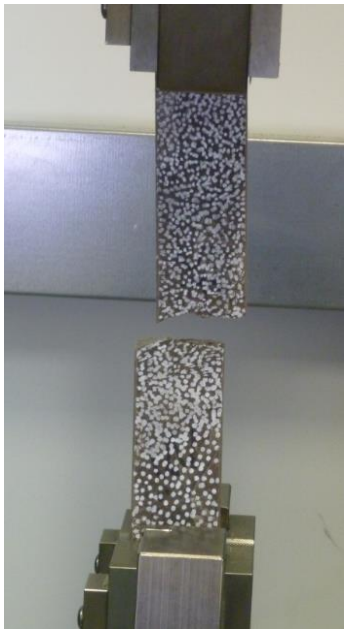

Figure 4.51: Failure mode of a Composite C specimen (C_PP) in uniaxial tension

Table 4.14 gives the average tensile strengths and moduli for the Composite C specimens. The standard deviations and coefficients of variation are also presented in Table 4.14. Furthermore, the tensile moduli of the Composite C specimens are compared in Figure 4.52, and their tensile strengths are compared in Figure 4.53; the upper and lower bounds are also indicated in the aforementioned Figures.

Table 4.14: Average tensile moduli, average tensile strengths, standard deviations and coefficients of variation for Composite C specimens

Composite C	Tensile modulus			Tensile strength		
	Average [GPa]	Standard deviation (SD) [GPa]	Coefficient of variation [%]	Average [MPa]	Standard deviation (SD) [MPa]	Coefficient of variation [%]
C_PP	2.9	0.2	8.4	17.8	1.5	8.7
C_PPW	2.7	0.3	10.2	14.2	1.4	9.9
C_SF	2.3	0.3	14.0	12.8	1.2	9.5
C_SFW	2.8	0.3	12.3	13.2	0.6	4.2
Overall average tensile modulus					**2.7 GPa**	
Overall average tensile strength					**14.5 MPa**	

The average tensile modulus for Composite C_PP and C_PPW was 2.9 GPa and 2.7 GPa, respectively. These values show that the addition of 50 wt. % waste carpets with wool face fibres to 50 wt. % waste carpets with polypropylene face fibres resulted in a 7 % reduction in the average tensile modulus. On the other hand, the average tensile modulus for Composite C_SF and C_SFW was 2.3 and 2.8 GPa, respectively, reflecting an approximate 22 % increase in tensile modulus. The overall average tensile modulus for the Composite C test coupons was 2.7 GPa, and the corresponding coefficient of variation ranged from 8.4 – 14.0 %.

Of the four formulations for Composite C material, Composite C_PP had the highest average tensile strength of 17.8 MPa, whereas Composite C_SF had the lowest average tensile strength of 12.8 MPa. The addition of 50 wt. % waste carpets with wool face fibres to 50 wt. % waste carpets with polypropylene face fibres resulted in an approximate 20 % reduction in the tensile strength (cf. Composite C_PP and C_PPW in Figure 4.53). The average tensile strength for Composite C_SFW was 3 % greater than that of Composite C_SF. The overall average tensile strength for the Composite C test coupons was 14.5 MPa, and the coefficient of variation ranged from 4.2 – 9.9 %. Table 4.15 gives the average energy absorbed, as well as standard deviations and coefficients of variation for the Composite C uniaxial tensile test specimens. The average energies absorbed by Composite C_PP, C_PPW, C_SF and C_SFW were 1.7 J, 1.9 J, 1.5 J and 1.4 J, respectively. These energy values are reasonably similar; however, the coefficients of variation for the different types of Composite C specimens

ranged from 24 – 57 % reflecting substantial differences. The overall average energy absorbed in tension by the Composite C specimens was 1.6 J.

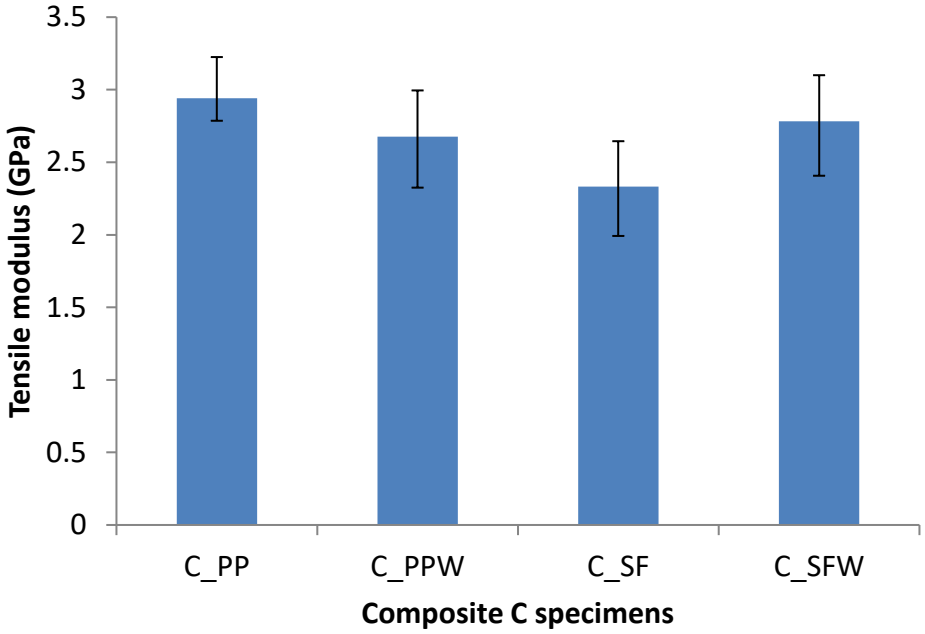

Figure 4.52: Comparison of the tensile modulus of Composite C specimens

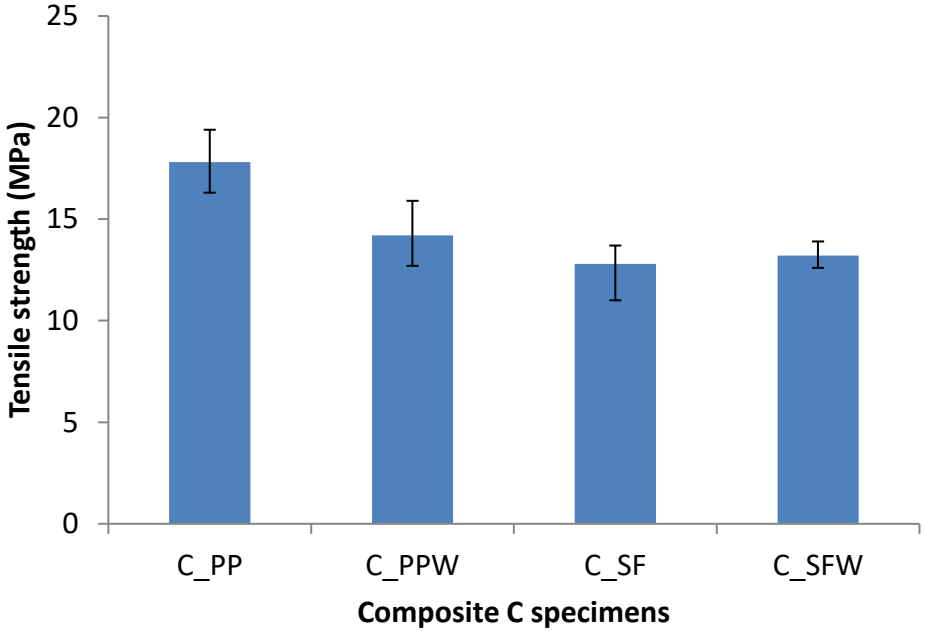

Figure 4.53: Comparison of the tensile strength of Composite C specimens

Table 4.15: Energy absorbed by the Composite C specimens in uniaxial tension and their standard deviations and coefficients of variation

Composite C beam	Energy absorbed		
	Average [J]	Standard deviation (SD) [J]	Coefficient of variation [%]
C_PP	1.7	0.6	37
C_PPW	1.9	0.5	26
C_SF	1.5	0.9	57
C_SFW	1.4	0.3	24
Overall average energy absorbed in tension			**1.6 J**

As mentioned earlier, the Composite C tensile test specimens failed in a brittle manner. Figure 4.54 - Figure 4.57 show images of their failure modes and SEM images of their respective fracture surfaces. It is also evident from the SEM images that Composites C_PPW and C_SFW (both with carpet waste with wool face fibres) had a greater quantity of exposed fibres compared to Composites C_PP and C_SF (without carpet waste with wool face fibres). All the SEM images of the Composite C tensile test specimens show evidence of voids, cavities, fibre pull-out and exposed fibres. These defects can be attributed to several factors which include the type/source of carpet waste, immiscibility of the polymers and fillers of the waste fibre blend and processing conditions.

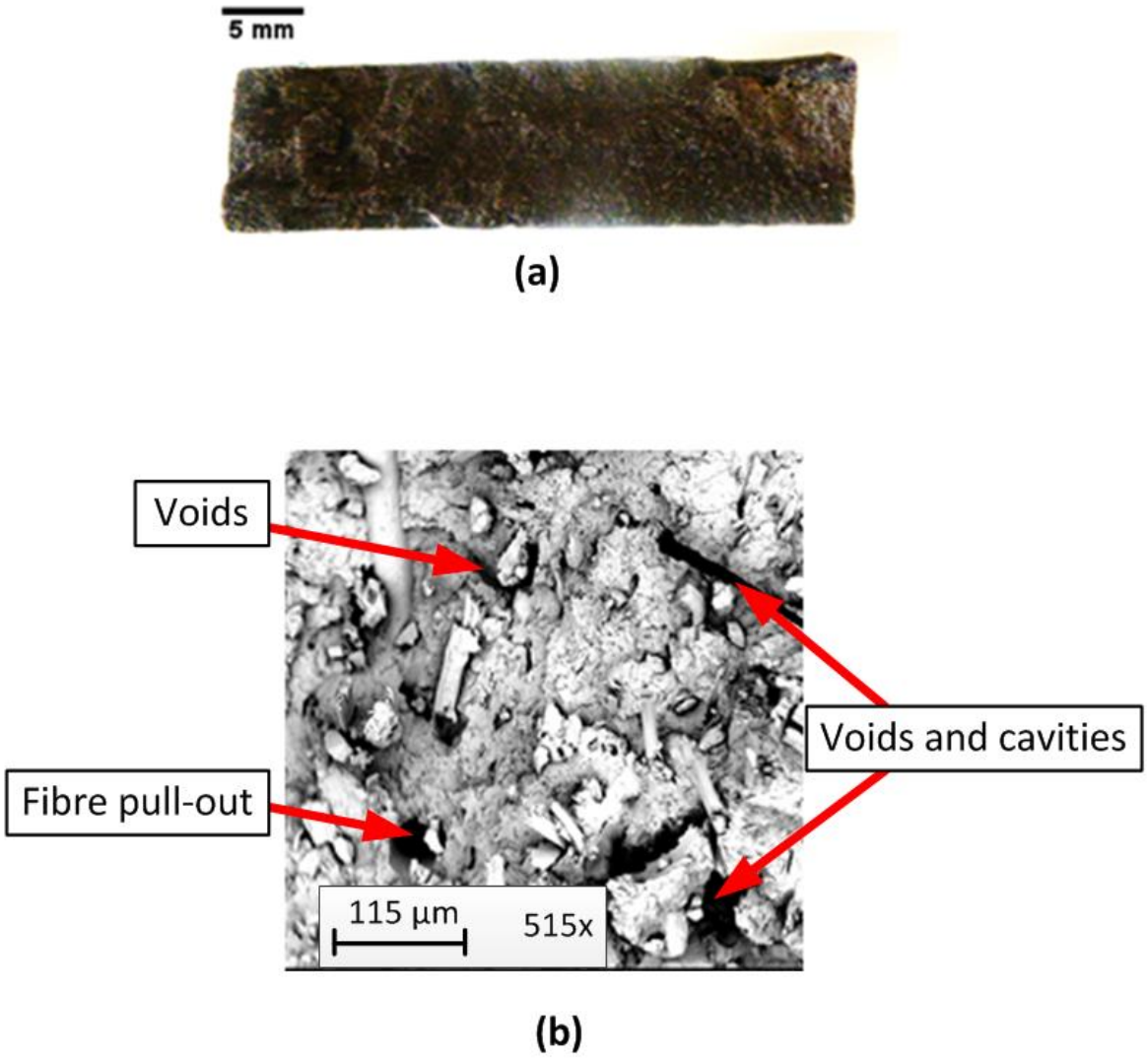

Figure 4.54: Composite C_PP specimen failed in uniaxial tension: (a) Cross-section view of the fracture surface (b) SEM image of the fracture surface

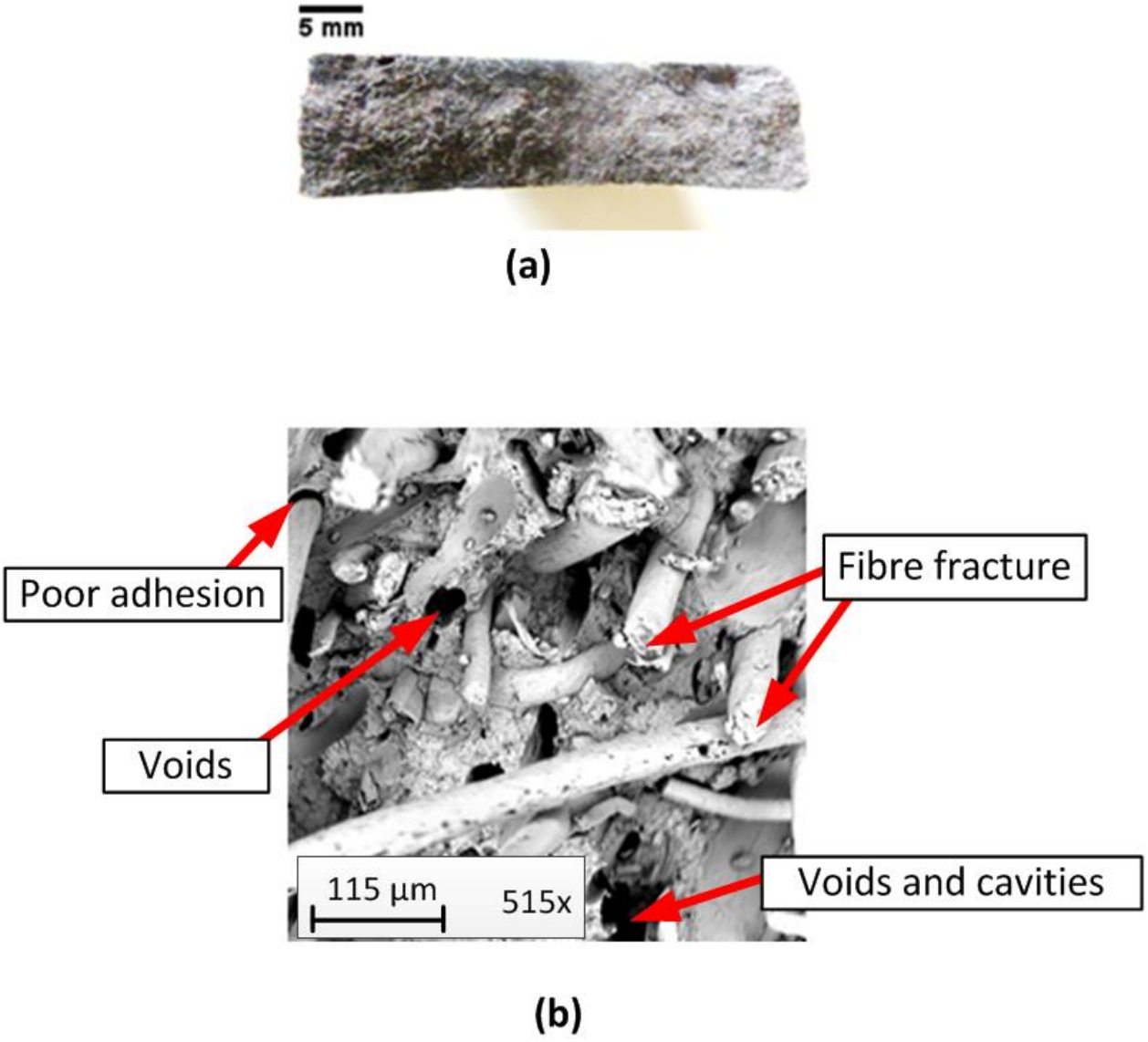

Figure 4.55: Composite C_PPW specimen failed in uniaxial tension: (a) Cross-section view of the fracture surface (b) SEM image of the fracture surface

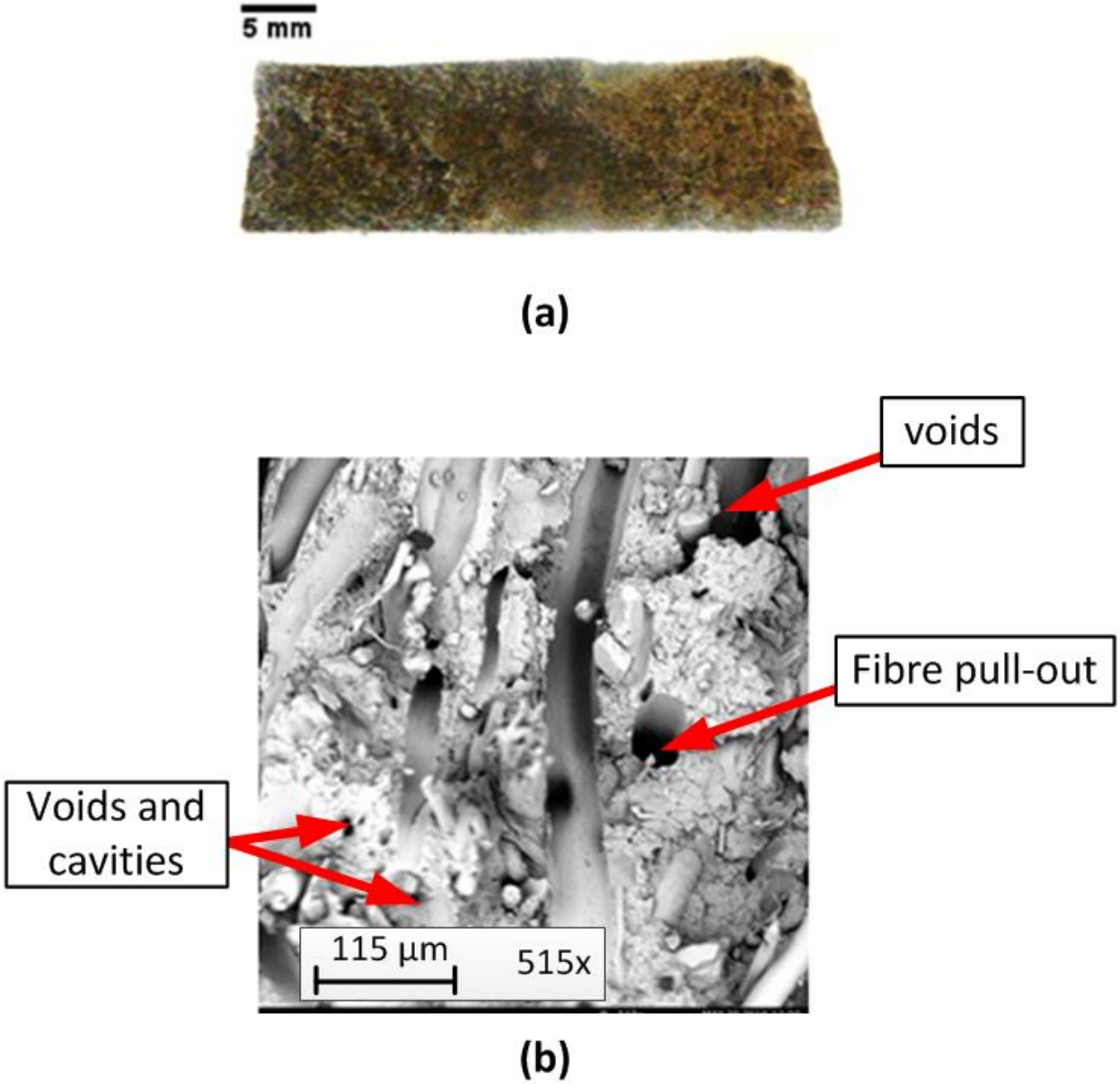

Figure 4.56: Composite C_SF specimen failed in uniaxial tension: (a) Cross-section view of the fracture surface (b) SEM image of the fracture surface

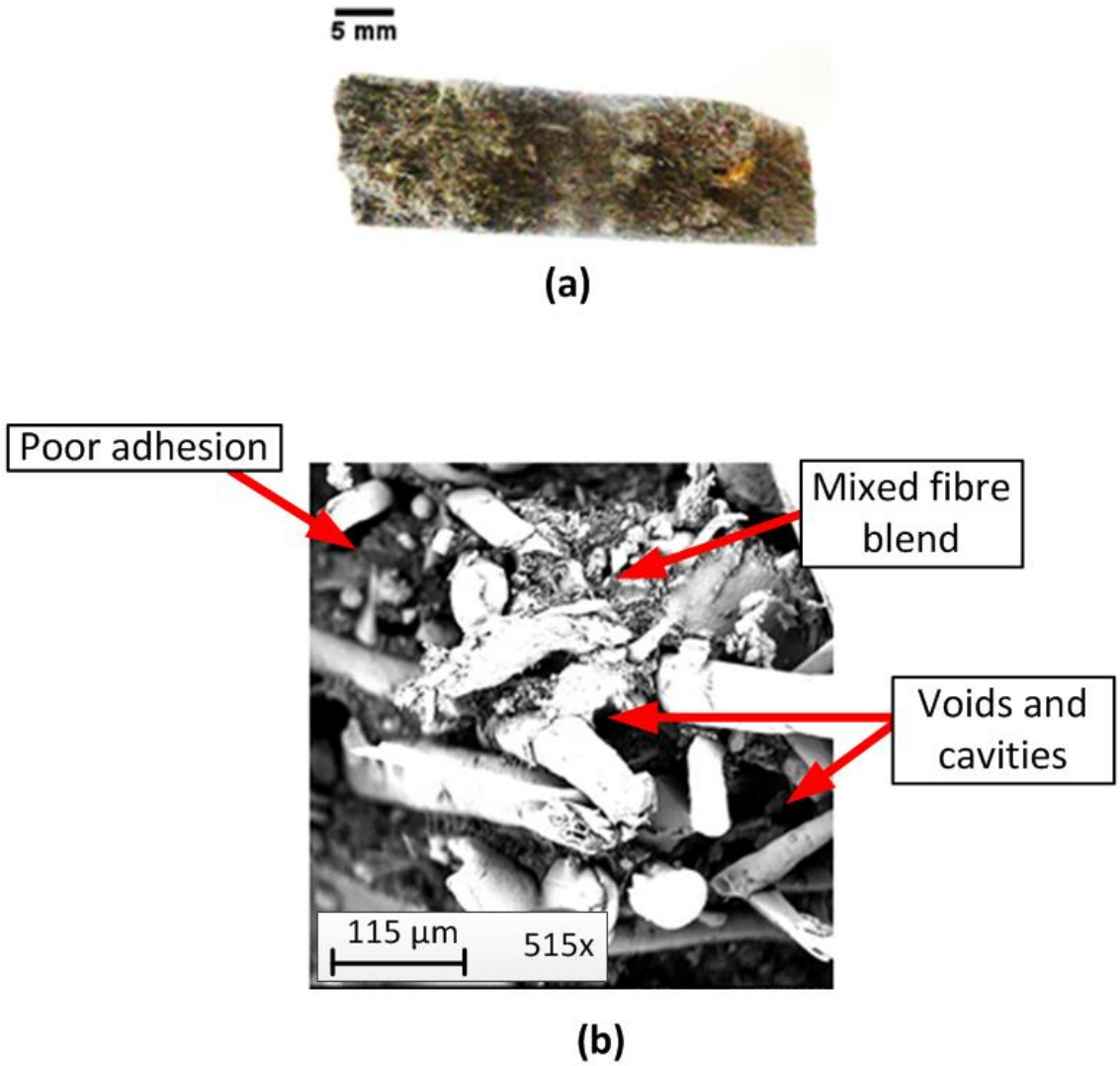

Figure 4.57: Composite C_SFW specimen failed in uniaxial tension: (a) Cross-section view of the fracture surface (b) SEM image of the fracture surface

Figure 4.58 shows the tensile load versus extension plots for five PVC coupons (P1 – P5) until the load applied reached 600 N. It is evident that the responses for all five coupons are linear and identical. The tensile load versus extension responses for the five PVC coupons until the crosshead extension of the universal testing machine (Zwick Z020) reached 20 mm are shown in Figure 4.59. Figure 4.60 shows a representative image of the uniaxial tensile PVC coupons when the crosshead extension of the universal testing machine reached 20 mm. The necking of the PVC coupon began at the maximum tensile load. The tensile moduli and strengths for the five PVC coupons are given in Table 4.16.

The average tensile modulus and average tensile strength of the five PVC coupons were 3.4 GPa and 44.6 MPa, respectively. The average tensile strength of the PVC coupons is reasonably close to the range of tensile strengths (45 – 50 MPa) given by the manufacturer – Duralock Performance Fencing (see Appendix 1). Furthermore, the coefficients of variation of the tensile moduli and strengths are 7.2 % and 3.4 %, respectively (see Table 4.16).

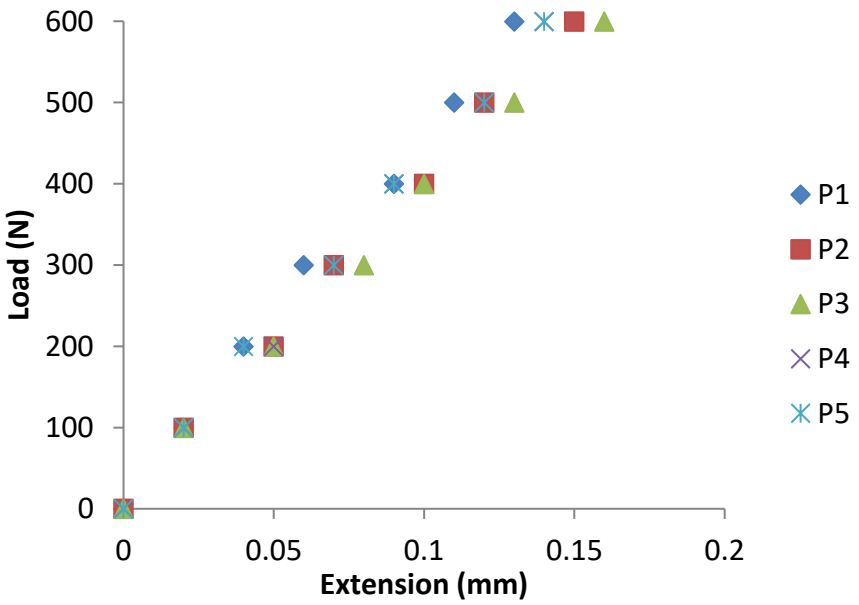

Figure 4.58: Tensile load versus extension plots for five PVC coupons until the load applied reached 600 N

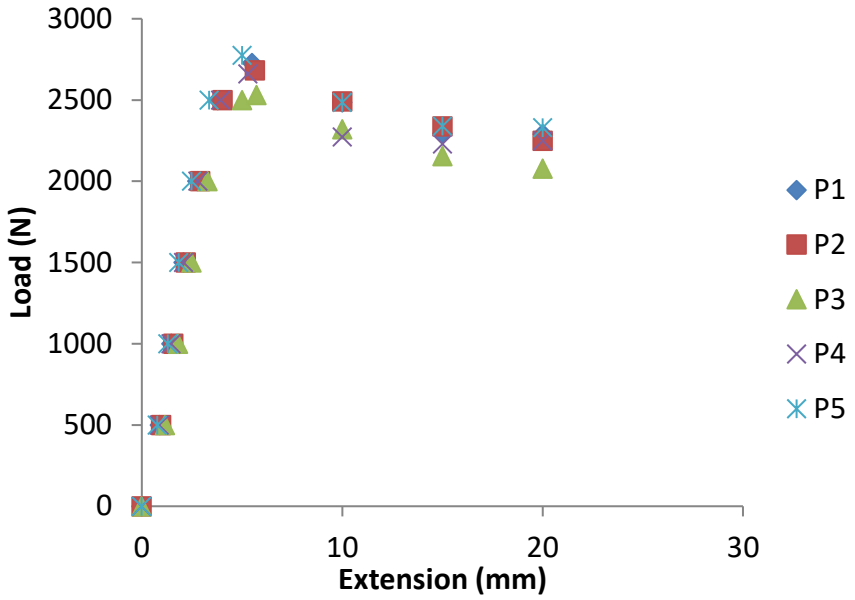

Figure 4.59: Tensile load versus extension plots for five PVC coupons up to a crosshead extension of 20 mm

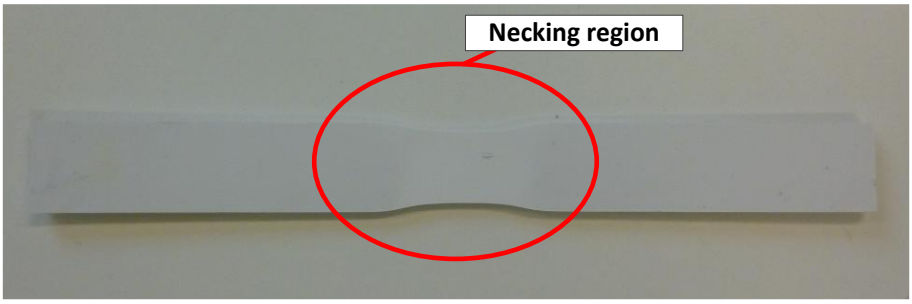

Figure 4.60: Image showing the necking region of a PVC coupon (P1) tested in uniaxial tension

Table 4.16: Tensile moduli and strengths for five PVC coupons

PVC coupon	Tensile modulus [GPa]	Tensile strength [MPa]
P1	3.6	45.5
P2	3.1	44.7
P3	3.1	42.2
P4	3.6	44.4
P5	3.6	46.3
Average	**3.4**	**44.6**
Standard deviation (SD)	**0.2**	**1.5**
Coeffecient of Variation (%)	**7.2**	**3.4**

4.5. Tensile Shear Tests on Bonded Wool Carpet Strips

4.5.1. Experimental Setup, Instrumentation and Test Procedure for the Tensile Shear Tests on Bonded Wool Carpet Strips

Figure 4.61 shows schematic diagrams of the bonded carpet joint specimens. Two series of tensile tests were carried out on the bonded carpet strips to determine the maximum force required to separate the bonded strips. The first series was carried out using a universal testing machine (Instron 8802) which had a maximum load capacity of 250 kN, whereas, the second series of tests was carried out on Zwick Z020 universal testing machine which had a maximum load capacity of 20 kN. 18 specimens were tested (9 specimens in each series).

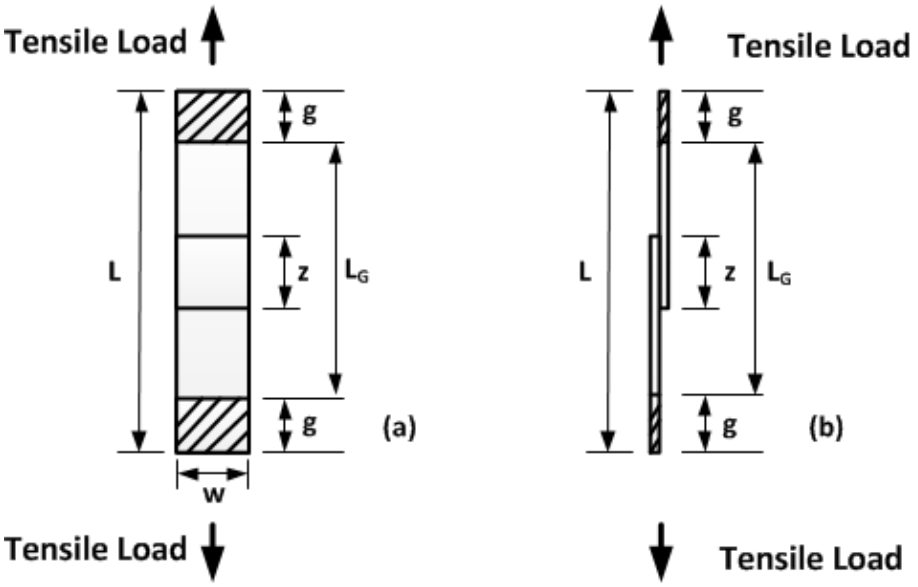

Figure 4.61: Sketch of the bonded carpet joint specimens: (a) Front-view and (b) Side-view

The specimens in each series had approximately the same nominal dimensions. There were some minor variations across the width of the carpet strips; hence, four width measurements were recorded (see Appendix 8). The average width measurements, as listed in Table 4.17, were used to compute the shear strength. The grips were used to secure the ends of the specimens so that they were subjected to uniform tension. The crosshead displacement was applied at a rate of 5 mm/min until rupture occurred. A digital camera was also placed in front of the first series of tests to monitor their failure modes. The load and overall extension of the specimens were recorded by a computer controlled data acquisition system. It is worth noting that the results of two specimens in the first series of

tests (two Back-to-Back bonded joint specimens) were discarded because of misalignment of the specimens in the testing machine.

Table 4.17: Dimensions of carpet joint specimens

Series	Average width [w] [mm]	Overall length [L] [mm]	Bond length [z] [mm]	Gauge length [L_G] [mm]	Average bond area [mm^2]	Grip length [g] [mm]
1	100	320	60	180	6000	70
2	55	260	55	180	3025	40

The ultimate shear strength of the bonded carpet joint specimens was calculated by dividing the maximum load by the bond area using Equation (11).

$$\tau_{max} = \frac{F_{max}}{z \cdot w} \tag{11}$$

In Equation (11), τ_{max} is the ultimate shear strength of the overlap region, F_{max} is the maximum load, z is the bond length and w is the width.

4.5.2. Results and Discussion of the Tensile Shear Tests on Bonded Wool Carpet Strips

Figure 4.62, Figure 4.63, and Figure 4.64 show the failure progressions for the Tuft-to-Tuft, Tuft-to-Back and Back-to-Back bonded joints, respectively; failure progresses from left to right in each figure. For both series of tests, all the specimens had a cohesive failure which is characterised by separation within the adhesive. The failure progression for the Tuft-to-Tuft and Back-to-Back bonded joints started at one edge of the bonded joints and propagated to the opposite edge (see Figure 4.62 and Figure 4.64). On the other hand, separation within the adhesive started in the middle of the Tuft-to-Back bonded joints and propagated outwards towards the edges of the joints (see Figure 4.63).

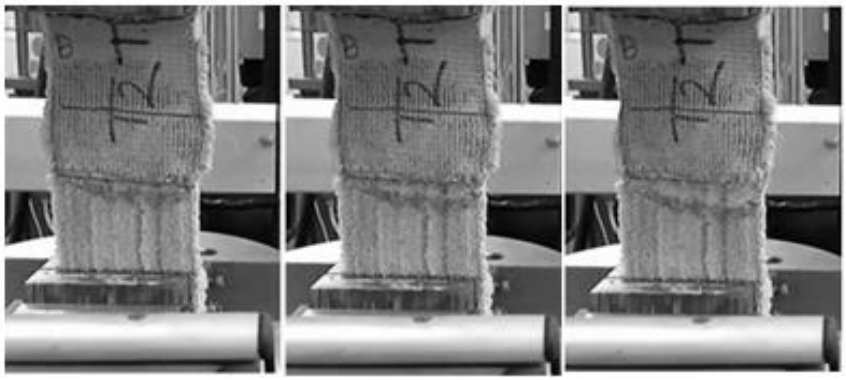

Figure 4.62: Failure progression for the Tuft-to-Tuft bonded joint

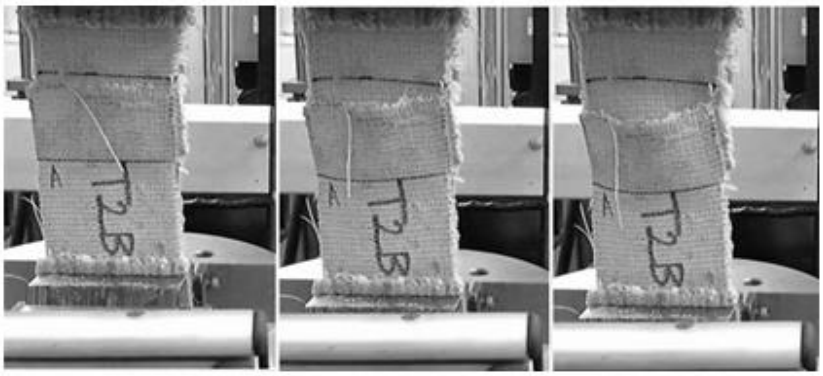

Figure 4.63: Failure progression for the Tuft-to-Back bonded joint

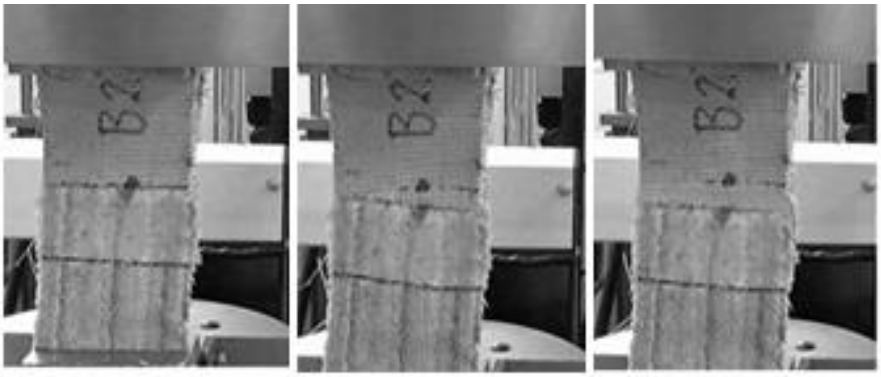

Figure 4.64: Failure progression for the Back-to-Back bonded joint

Table 4.18 lists the maximum load, and corresponding shear strengths of each specimen tested. In the first series of tests, the average ultimate shear strength for the Back-to-Back, Tuft-to-Back and Tuft-to-Tuft bonded joints was 67 kPa, 61 kPa and 20 kPa, respectively. The results showed that the Back-to-Back bonded joints had the highest shear strength.

The specimens in the second series of joint tests had different dimensions from the specimens in the first series (see Table 4.17). The average shear strengths for the second series of joint tests for Tuft-to-Tuft, Tuft-to-Back and Back-to-Back orientations were 39 kPa, 51 kPa and 84 kPa, respectively. The results from the second series of tests also showed that the Back-to-Back bonded joints had the highest average shear strength.

Table 4.18: Shear strengths obtained from tension tests on three orientations of bonded carpet joint specimens

Series	Single-lap joint configuration	Specimen label	Maximum load [N]	Average maximum load [N]	Ultimate shear strength [kPa]	Average ultimate shear strength [kPa]
1	Tuft-to-Tuft	1T2T_1	162	118	27.0	20
		1T2T_2	70		11.7	
		1T2T_3	123		20.5	
	Tuft-to-Back	1T2B_1	442	365	73.7	61
		1T2B_2	305		50.9	
		1T2B_3	346		57.7	
	Back-to-Back	1B2B_1	401	401	66.8	67
2	Tuft-to-Tuft	2T2T_1	131	117	43	39
		2T2T_2	79		26	
		2T2T_3	140		46	
	Tuft-to-Back	2T2B_1	215	154	71	51
		2T2B_2	141		47	
		2T2B_3	107		35	
	Back-to-Back	2B2B_1	229	255	76	84
		2B2B_2	322		106	
		2B2B_3	214		71	

Figure 4.65 shows a comparison between the two series of joint tests for each orientation; the results showed differences in the shear strengths for the two series of tests. The average shear strengths for the Tuft-to-Tuft and Back-to-Back bonded joints from the first series was lower than those from the second series, whereas the average shear strength for the Tuft-to-Back bonded joints in the first series of tests was greater than that of the second series of tests.

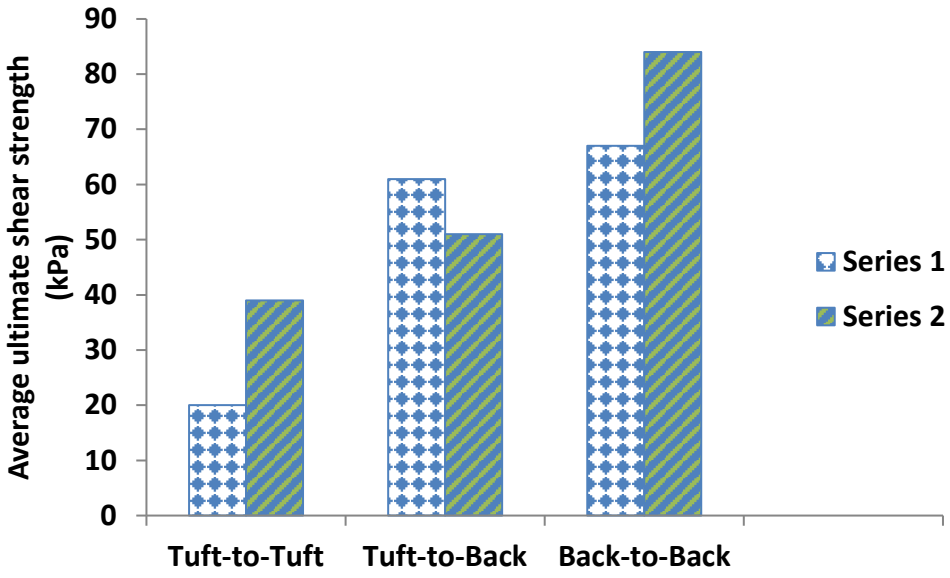

Figure 4.65: Comparison between the two series of single-lap joint tests for each orientation

The differences between the two series of test results may be due to differences in the waste carpet strips (the adherends) which may not have been identical. Although only waste carpet strips with wool face fibres were used, the carpet strips may have been exposed to different in-service conditions, thus contributing to differences in the quantity of flaws, impurities and dirt particles in the waste carpet strips. It is also worth noting that the load capacity of the test machines for the different series of tests was different; the first had a load capacity of 250 kN, and the second had a 20 kN load capacity. The maximum loads in the first sets of tests ranged from 70 – 442 N, thus reflecting very low loads compared to the load capacity of the test machine and may have contributed to the differences in results.

The first series of test results showed that the average ultimate shear strength for the Back-to-Back specimens is 235 % greater than that of the Tuft-to-Tuft specimens. Similarly, the second series of test results showed a 115 % greater ultimate shear strength for the Back-to-Back specimens compared to the Tuft-to-Tuft specimens. As the aim of the test was primarily comparative, it can be concluded that the Back-to-Back bonded joints had the highest average shear strength whereas the Tuft-to-Tuft had the lowest for both test series.

4.6. Chapter Summary

Experimental tests have been carried out to determine the mechanical properties of waste carpet structural composites (Composites A – C), timber and PVC posts and rails, polyurethane beams and bonded waste carpet strips. The instrumentation and analysis techniques have been described. Furthermore, repeat tests and statistical analyses have been carried out and reported. Average values of the moduli and strengths obtained from the experimental tests described in this chapter are given in Table 4.19. The test results give an understanding of the mechanical properties of the novel waste carpet structural composite materials, and their suitability for use as alternative equestrian fencing materials to timber and PVC.

Table 4.19: Average moduli and strengths of the materials tested

Material	**Property**	
Composite A	Flexural modulus	0.047 GPa
Composite B		0.185 GPa
Composite C	Flexural modulus	2.6 GPa
	Flexural strength	29.2 MPa
	Tensile modulus	2.7 GPa
	Tensile strength	14.5 MPa
Timber posts	Flexural modulus	9.4 GPa
	Shear modulus	0.4 GPa
Timber rails	Flexural modulus	11.3 GPa
Timber specimens	Compressive strength (parallel-to-the-grain)	26.7 MPa
	Compressive strength (perpendicular-to-the-grain)	1.7 MPa
PVC posts	Flexural modulus	1.6 GPa
PVC rails		2.7 GPa
PVC coupons	Tensile modulus	3.4 GPa
	Tensile strength	44.6 MPa
Unfilled polyurethane	Flexural modulus	114 MPa
	Flexural strength	4 MPa
filled polyurethane (9 wt. % CF10 fibre)	Flexural modulus	159 MPa
	Flexural strength	4.3 MPa

The results of the three-point bending tests showed that the average flexural moduli for the waste carpet structural composites (Composite A – C) were 0.047 GPa, 0.185 GPa and 2.6 GPa, respectively. The average flexural strength for Composite C was 29.2 MPa. Uniaxial tensile tests were also carried out on flat specimens of Composite C material; the elastic tensile modulus ranged from 2.0 – 3.2 GPa and the tensile strength ranged from 11 – 19 MPa. The overall average energy absorbed in bending and in tension by the Composite C materials were 4.9 J and 1.6 J, respectively. Digital camera and SEM images were taken to investigate the failure modes of the Composite C material; the failure modes and variations in their mechanical properties can be attributed to the presence of flaws (such as voids), impurities and dirt particles in the raw material (waste carpet), processing conditions, as well as the type and source of carpet waste used.

The average flexural moduli for the unfilled and filled (with 9 % CF10 fibre addition) polyurethane beams were 114 MPa and 159 MPa, respectively, reflecting a 40 % increase in flexural modulus due to the filler. The average flexural strengths for the unfilled and filled polyurethane beams were 4 MPa and 4.3 MPa, respectively reflecting a relatively small difference in their average flexural strengths. The results of the tensile shear tests on bonded single-lap joints of wool waste carpet strips at different orientations (Tuft-to-Tuft, Tuft-to-Back, Back-to-Back) have been reported. Additionally, photographs taken to monitor the failure progression of the specimens during the tests showed that all the specimens had a cohesive failure mode which is characterised by separation within the adhesive. The test results showed that the Back-to-Back bonded joints had the highest shear strength, whereas the Tuft-to-Tuft orientation had the lowest shear strength. Based on the limited study and small set of test results, the experimental analyses indicate that the Back-to-Back bonded joint orientation may be most suitable for inclusion in the fabrication of waste carpet structural composites.

Compression and three-point bending tests were carried out on timber sections. 20 specimens were tested in compression parallel-to- and perpendicular-to-the grain (10 in each set). The average compressive strengths parallel-to- and perpendicular-to-the-grain were 26.7 and 1.7 MPa, respectively; these results showed that timber is a highly orthotropic material and has significantly greater compressive strength parallel-to-the-grain compared to perpendicular-to-the-grain. Different failure modes which include shearing,

splitting and brooming (or end-rolling) were observed in the specimens compressed parallel-to-the-grain, whereas, progressive bending (linear elastic response) of the polygonal cell walls, and the subsequent buckling and collapse (nonlinear response) of the cell walls occurred when compressed perpendicular-to-the-grain. The results of the three-point bending tests showed that the average flexural modulus of the timber posts and rails varies from 8.1 - 13.5 GPa, not untypical of ungraded timber. Furthermore, three-point bending tests and analyses which included shear deformation effects on a separate timber post showed that the flexural and shear moduli are 10.9 GPa and 0.4 GPa, respectively.

The average flexural moduli for the PVC posts and rails were 1.6 GPa and 2.7 GPa, respectively. The lower flexural modulus of the PVC posts compared to the rails can be attributed to shear deformation effects and local elastic deformation at the locations of the cut-outs in the PVC posts. However, the average flexural modulus of the PVC rails is close to the data provided by the manufacturer (2.4 – 2.5 GPa). The results of the tensile tests carried out on PVC coupons showed an average tensile modulus and strength of 3.4 GPa and 44.6 MPa, respectively. The average tensile strength is also reasonably close to that provided by the manufacturer.

As the flexural modulus is a vital structural property and part of the information used to determine the transverse stiffness of equestrian fencing; the flexural moduli of timber and PVC are used to compare with those of the novel waste carpet structural composites. The results showed that the average flexural modulus for Composite C was significantly greater than those of Composites A and B. Also, the average flexural moduli for Composite C (2.6 GPa) and PVC (2.7 GPa) are reasonably close. Nevertheless, the overall average flexural modulus for Composite C is only about a quarter of that of timber.

5. Chapter Five – Experimental Characterisation of Fencing Structures

5.1. Introduction

This chapter describes the experimental setup, overall geometry and loading procedure adopted for load tests on representative two-bay timber and PVC post and rail fencing structures. The results from the load tests on the fences are also presented and discussed. It is worth highlighting that the overall geometry adopted for the load tests on the timber and PVC fences are the same as those typically used for equestrian fencing. Details of the joints used to secure the bases of the timber and PVC posts to their foundations are described. Furthermore, test details of tip-loaded cantilever bending tests on the timber and PVC posts are given, and their results are presented. There are currently no load tests reported on timber or PVC fencing in the open literature. Therefore, these test results provide useful experimental benchmark data on the timber and PVC fences for assessing the structural stiffness requirements of the novel waste carpet structural composites.

5.2. Details of the Base Joints for the Timber and PVC Fencing Structures

5.2.1. Details of the Base Joint for the Timber Fence

The bases of timber posts are typically concreted into the ground in practice, and their stiffnesses may vary and depend on several environmental factors i.e. moisture content, temperature etc. However, for this study, the timber posts were rigidly clamped in the laboratory with a thick steel plate, nuts and threaded steel rods fastened to a welded steel angle. Figure 5.1 shows the layout details of the bolted joint at the base of the posts.

A 15 mm thick steel plate was bolted on the front face of the timber post to a welded steel angle with triangular gusset plates on the back face. Eight nuts and four 150 mm long by 12 mm diameter threaded steel rods were used to bolt the steel plate to the steel angle. The four bolt holes in the steel plate, welded steel angle and timber post were also 12 mm in diameter. The nuts were torqued to 30 Nm. The horizontal leg of the welded steel angle was bolted to a rigid steel reaction frame.

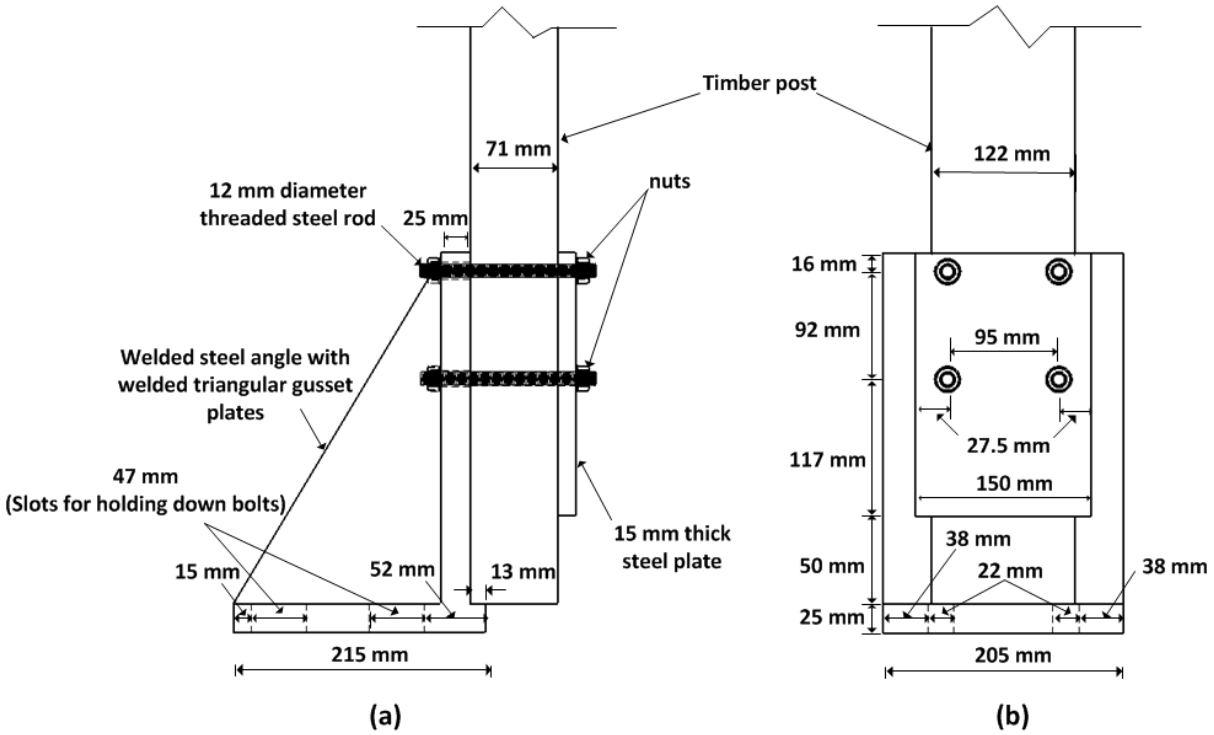

Figure 5.1: Details of the joint assembly at the base of the timber posts: (a) Side-view and (b) Front-view

5.2.2. Details of the Base Joint for the PVC Fence

To simulate the joint at the base of the PVC post, two 46 mm diameter nuts and threaded steel rods, which passed through the holes of a 4.5 mm thick steel plate (with welded steel angles and circular steel studs), were used to clamp it to the ground. The nuts were torqued to 30 Nm. Figure 5.2 gives details of a plan and front view of the 4.5 mm thick steel plate with welded steel angles and circular steel studs (for locating the interlocking plastic grids). Thereafter, a PVC post was inserted over the welded steel angles so that the steel angle contacted the inner faces of the PVC post, and the base of the PVC post contacted the top face of the 4.5 mm thick steel plate (see Figure 5.3).

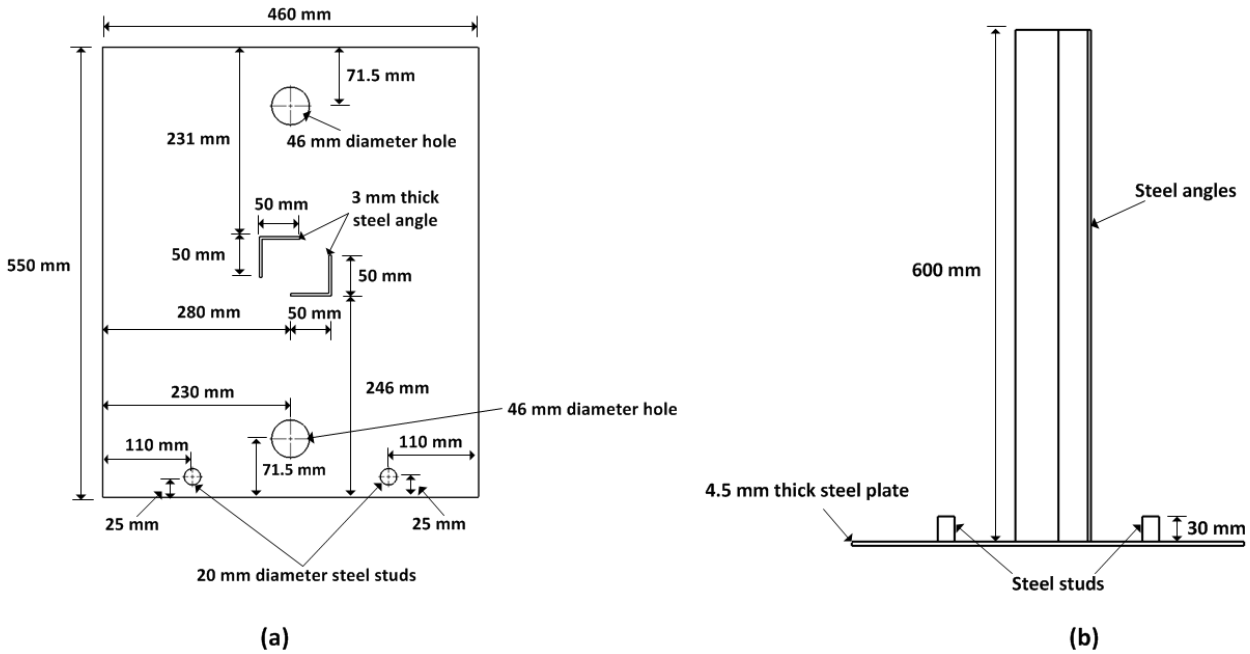

Figure 5.2: Details of the steel plate with welded steel angles and circular steel studs: (a) Plan-view and (b) Front-view

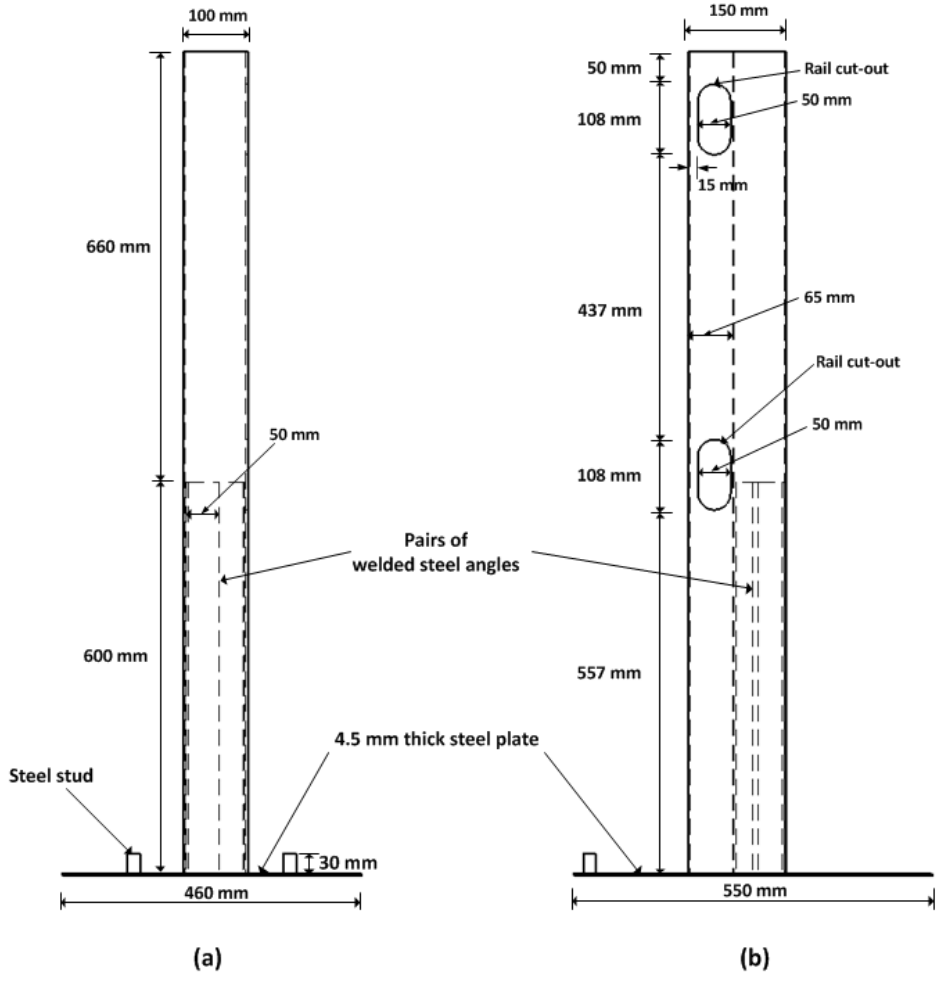

Figure 5.3: Details of the PVC post assembly: (a) Front-view and (b) Side-view

5.3. Tip-loaded Cantilever Bending Tests on Timber and PVC Posts

5.3.1. Cantilever Test on Timber Post

Tip-loaded cantilever bending tests were carried out to determine the rotational stiffness of the bolted joint used to secure the base of the timber post to the foundation. The behaviour of a semi-rigid joint is characterised by its moment-rotation curve. Obtaining the rotational stiffnesses of the bolted base joint also allows the development of a more accurate FE model (rather than assuming rigidly fixed base joints) for the two-bay timber fence. This is because there is always a quantifiable amount of rotational stiffness present in joints.

A sketch of the semi-rigid cantilever analysis model is shown in Figure 5.4. The beam, AB is assumed to be uniform, straight and of span, L. Point A is the semi-rigid bolted joint. Equation (12) gives the deflection at point B when shear deformation is neglected. Equation (13) gives the moment–rotation relationship of the joint at Point A.

$$w_B = \frac{FL^3}{3EI} + \frac{FL^2}{K} \tag{12}$$

$$M_A = K\emptyset_A \tag{13}$$

$$FL = K\left(\frac{w_B}{L} - \frac{FL^2}{3EI}\right) \tag{14}$$

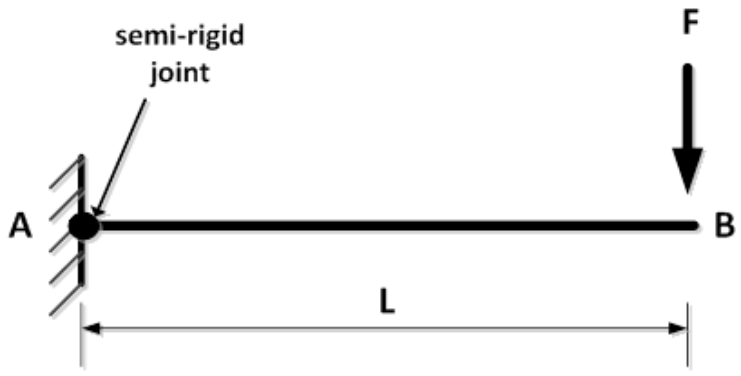

Figure 5.4: Semi-rigid beam analysis model

In Equations (12) - (14), w_B is the deflection at point B, F is the load applied at point B, L is the cantilever span, E is the elastic flexural modulus (obtained from the three-point bending tests), I is the second moment of area with respect to the plane of flexure, M_A is the

moment at the semi-rigid support (bolted joint), $\emptyset_A$ is the rotation at A, and K is the rotational stiffness of the bolted joint. The length, L of the cantilever beam was taken as the distance from the loading point to the top of the bolted steel plate. Re-arranging Equation (12) gives Equation (14). Equation (13) can be compared to Equation (14), in which, the FL term represents the moment at the semi-rigid support, M_A and the $\left(\frac{w_B}{L} - \frac{FL^2}{3EI}\right)$ term represents the semi-rigid joint rotation at A, namely $\emptyset_A$. Thus, a plot of FL against $\left(\frac{w_B}{L} - \frac{FL^2}{3EI}\right)$ yields a straight line with a gradient of K, which is the rotational stiffness at joint A.

The cantilever test was carried out using the test rig shown in Figure 5.5, in which load was applied in increments of 98.1 N up to 784.8 N.

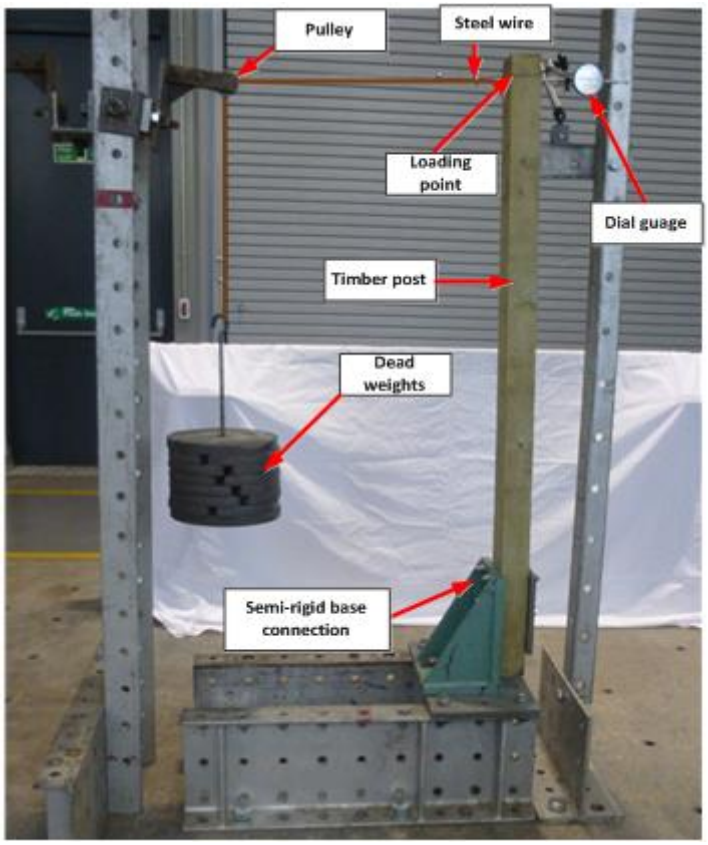

Figure 5.5: Image of cantilever test setup on timber post

The loading point was located 40 mm below the top of the post. A dial gauge, which had a 50 mm travel and a displacement resolution of 0.01 mm, was mounted at the back of the post to record the horizontal deflections corresponding to each load increment. The details

of the timber post used in the cantilever test are given in Table 5.1. Three repeat tests were carried out, and the average was used to determine the rotational stiffness of the bolted joint at the base of the post.

Table 5.1: Details of the timber post tested in tip-loaded cantilever bending

Span [L] [mm]	Width [w] [mm]	Depth [d] [mm]	Second moment of area [I] [mm^4]
1250	120	72	3,732,480

5.3.2. Cantilever Test on PVC post

Figure 5.6 shows an image of the cantilever test on the PVC post assembly. A line load was applied on the PVC post through a circular steel rod attached to a 2.5 kN load cell (see Figure 5.7 for a close-up view). The other end of the load cell was connected to the ram of the jack. The loading point was located 105 mm below the top of the PVC post. The load was applied in increments of 40 N up to 280 N. A dial gauge, which had a 50 mm travel and a displacement resolution of 0.01 mm was mounted at the back of the PVC post to record horizontal deflections corresponding to each load increment. Three repeat tests were carried out on the PVC post.

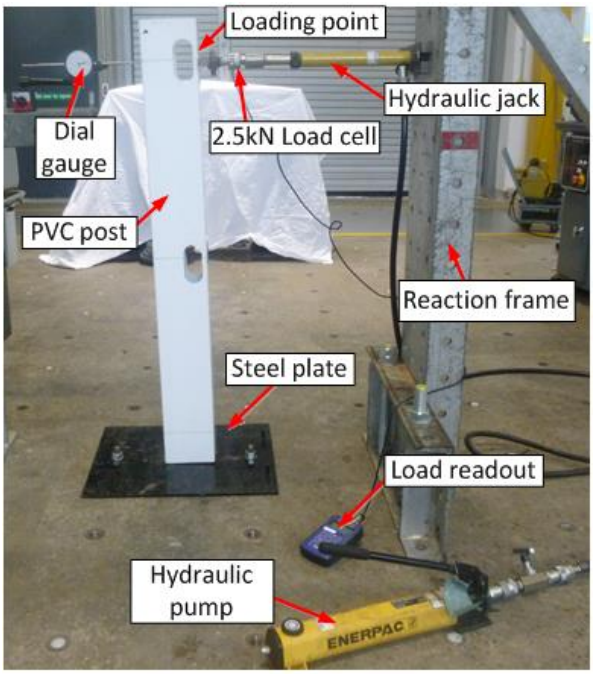

Figure 5.6: Image of cantilever test setup on PVC post

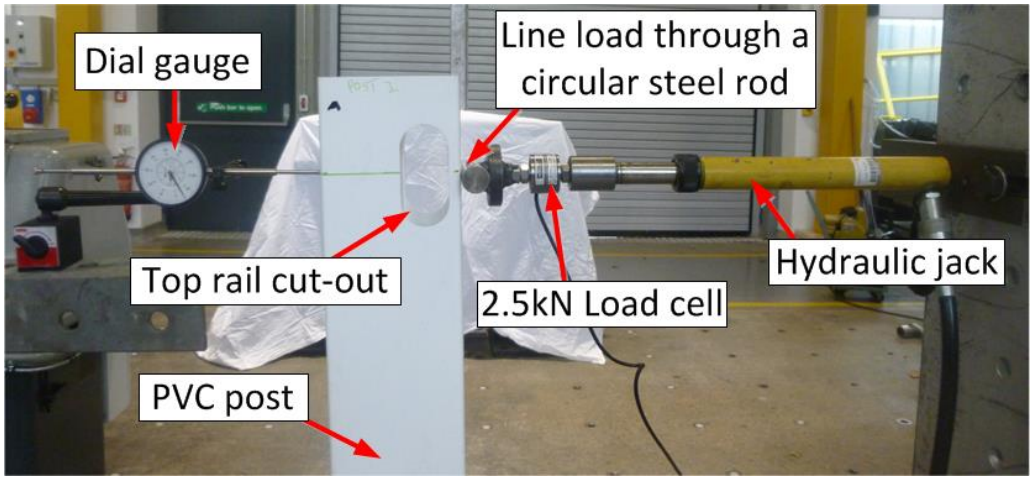

Figure 5.7: Close-up view of the loading arrangement on the PVC post

5.4. Load Tests on Timber and PVC Fencing Structures

Load tests were carried out on two-bay timber and PVC post and rail fences, which are representative of typical multi-bay fencing systems. It was decided to test a two-bay rather than a one-bay frame because the former is more representative of the practical scenario compared to the latter. Turvey (2015) also explained that load tests on multi-bay frames provide information about the stiffness benefits which may occur as a result of the structural continuity across bays. Furthermore, guard-rail and safety barrier testing (similar to fencing structures) is carried out by applying loads at the top of the centre post and mid-bay points of a two-bay frame (BS 14122-3, 2016). Hence, as there have been no load tests reported on timber or PVC fencing in the open literature, it was deemed reasonable to apply the loads at the top of the centre post and at the mid-bay points of the timber and PVC fencing structures.

The experimental load tests carried out on the timber and PVC fences were linear elastic. Although the nonlinear deformation, collapse testing and dynamic response of the fencing structures are also important, linear elastic analysis can predict the serviceability deformations of timber and PVC fencing reasonably accurately. Several authors (Bakis et al., 2002, Satasivam and Bai, 2014) have also highlighted that the serviceability design of structures is often more critical than the strength design. The timber and PVC fences were tested to maximum loads of 1400 N and 600 N, respectively. This was because a number of preliminary load tests were carried out on the fencing structures to ensure that the

deformations corresponding to the aforementioned respective maximum loads were linear elastic.

5.4.1. Test Setup, Instrumentation and Test Procedure for the Load Tests on a Two-Bay Timber Fence

Load tests were carried out on a two-bay timber post and rail fence that comprised of three posts and two rails, as shown in Figure 5.8. The rails were connected to the posts with two nails (see Figure 5.9), and the two-bay timber fence had a total of six rail-to-post nailed connections. The nails had a shank diameter of 4 mm and a length of 100 mm. The rail-to-post nailed connection configuration was based on the guidance given in TRADA (2003), and thus the distance between each nail and edge of the timber rail was at least 30 mm. The rail-to-post nailed connection configuration is also similar to that used in practice.

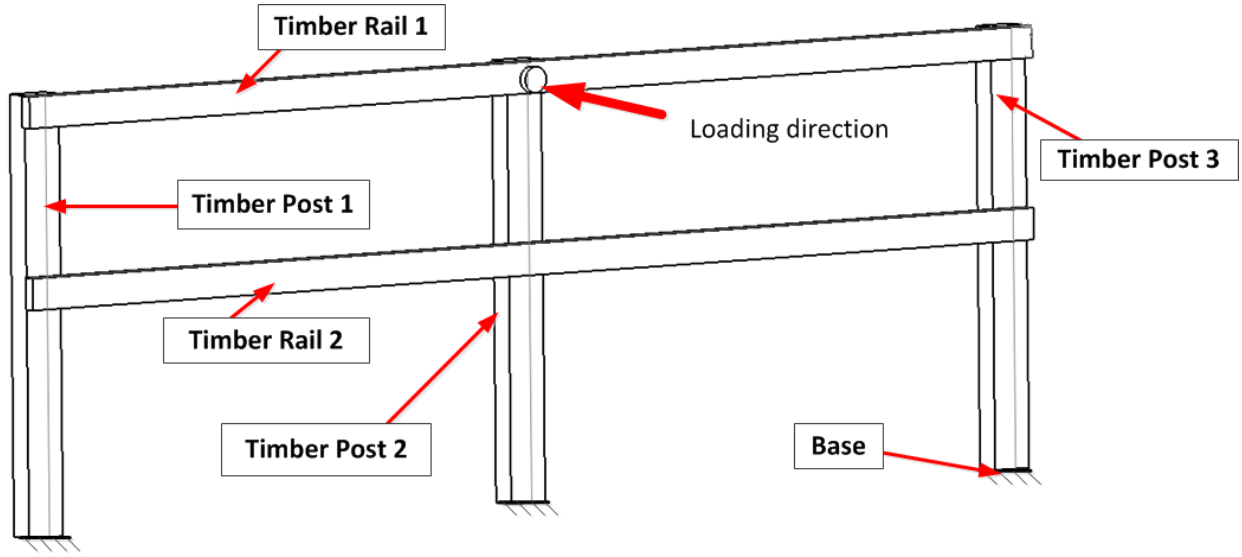

Figure 5.8: Illustrative diagram of the test setup for the two-bay timber post and rail fence

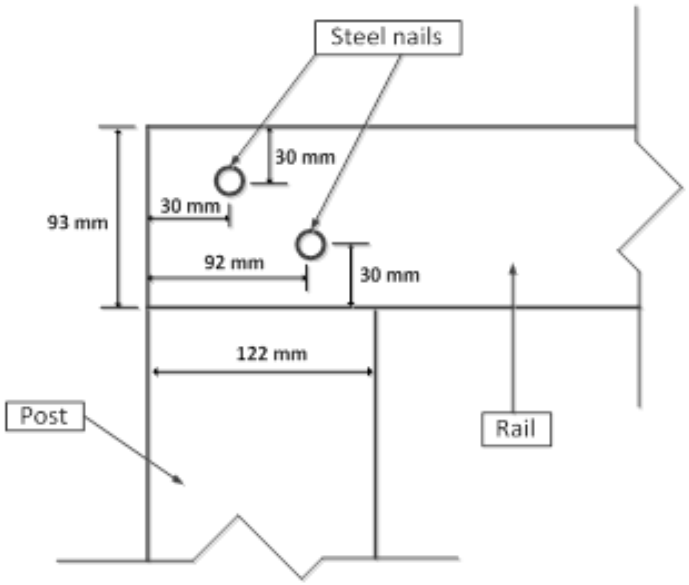

Figure 5.9: Details of the rail-to-post nailed connection

A schematic drawing showing the loading arrangement and overall geometry of the two-bay timber fence is shown in Figure 5.10. The two-bay timber fence was tested under incremental static loading applied at the mid-point on the top rail (at Node B in Figure 5.10). Loading was applied normal to the plane of the timber fence. A 100 N load was applied initially and then increased in 100 N increments. The timber fence was tested to a maximum load of 1400 N.

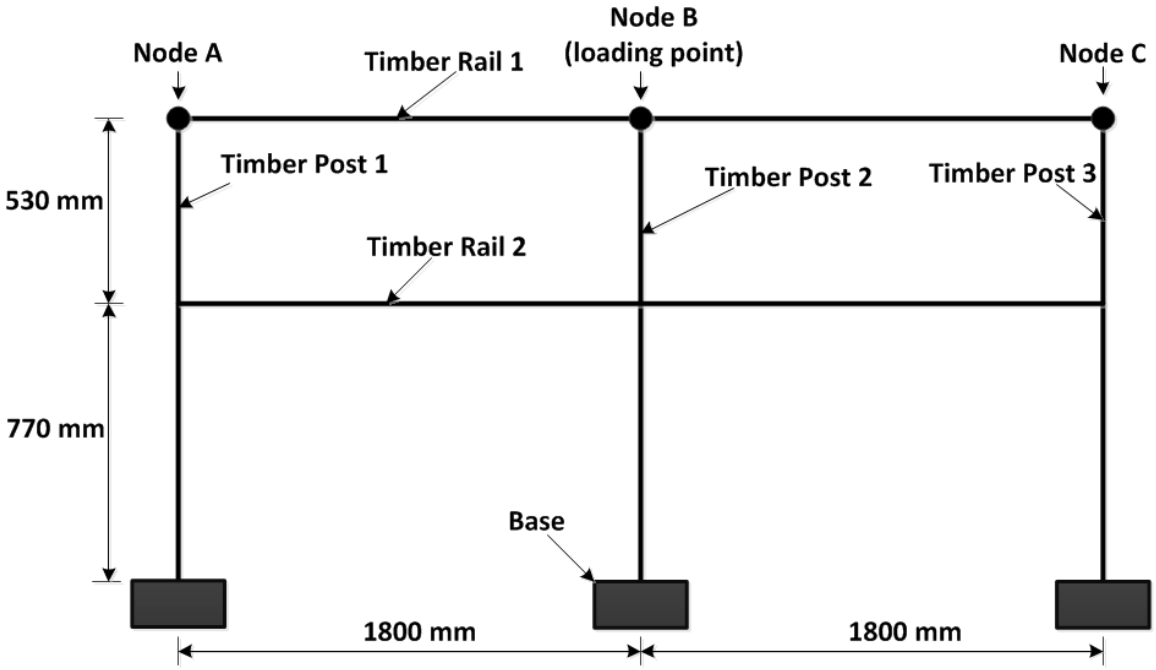

Figure 5.10: Overall geometry of the timber post and rail fence

The deflections corresponding to each load increment at the top of the three posts (at Nodes A - C in Figure 5.10) were measured with dial gauges. The load-unload test procedure was repeated three times. Figure 5.11 shows an image of the two-bay timber fence and the loading arrangement.

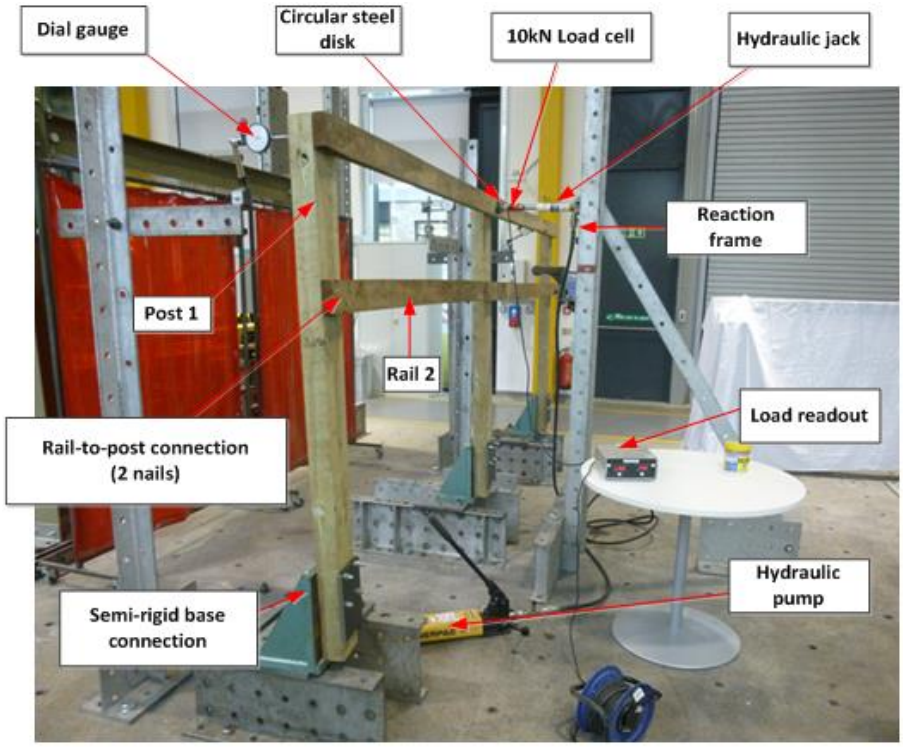

Figure 5.11: Load test on the two-bay timber fence

A steel disk, with a ball joint (see Figure 5.12) was bonded to the face of the top rail (Rail 1) at its connection to the centre post (Post 2), where load was applied using a manually operated hydraulic jack with its base bolted to a steel reaction frame. The hydraulic jack was fitted with a 10 kN capacity load cell, which was connected to a load readout. The steel reaction frame was bolted to the laboratory floor.

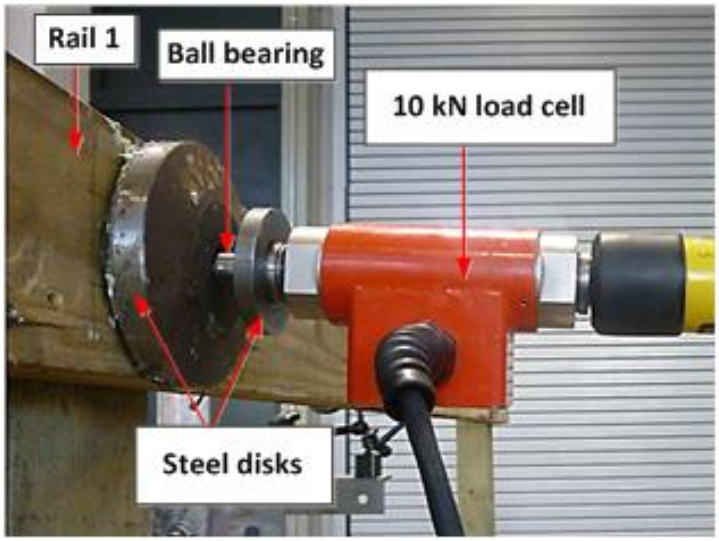

Figure 5.12: Close-up view of the loading arrangement on the two-bay timber fence

5.4.2. Test Setup, Instrumentation and Test Procedure for the Load Tests on Two-Bay PVC Fence

Load tests were carried out on a two-bay PVC post and rail fence that comprised of three posts and two rails, as shown in Figure 5.13. The rails were slotted through the cut-outs of the posts. Figure 5.14 shows an Illustrative diagram of the PVC rail-to-post connection. The details of the base connections for the PVC posts have been described in Section 5.2.2.

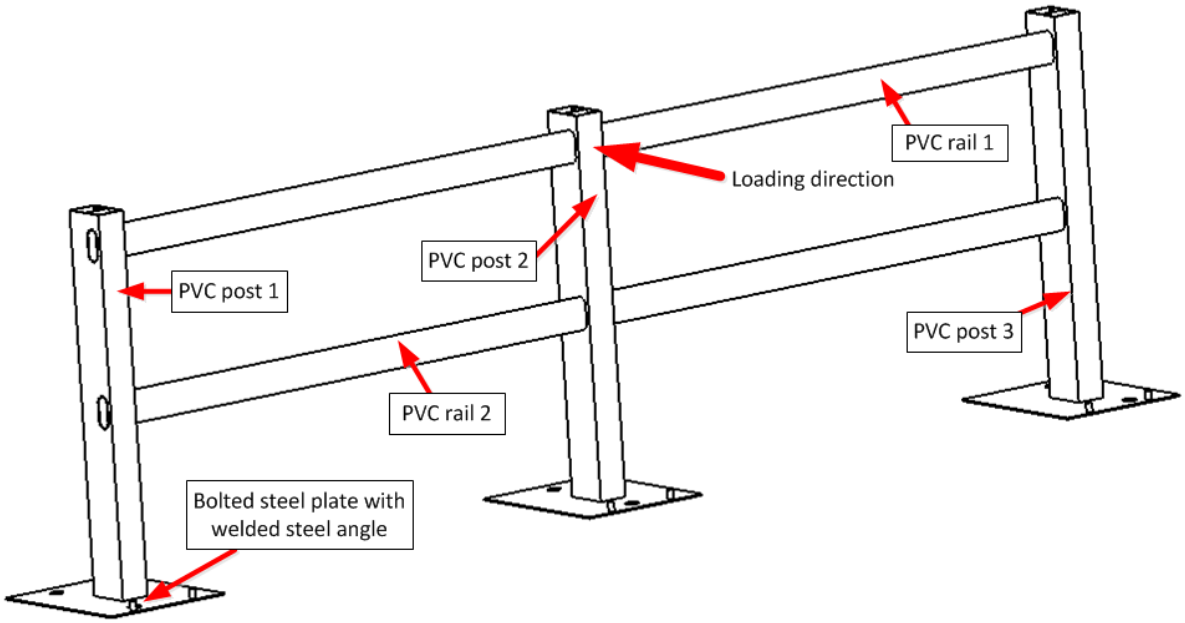

Figure 5.13: Illustrative diagram of the test setup for the two-bay PVC post and rail fence

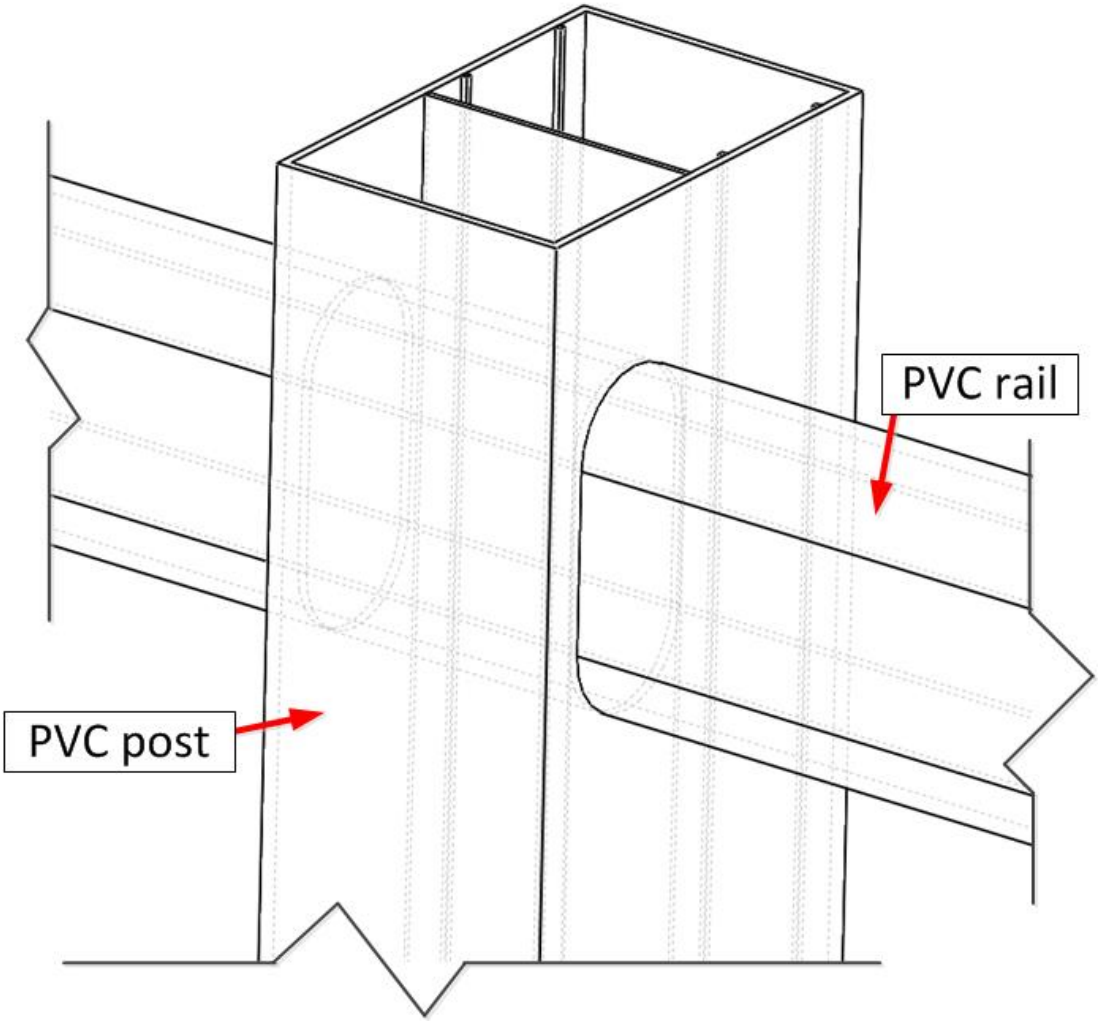

Figure 5.14: Illustrative diagram of the PVC rail-to-post connection

Two sets of load tests were carried out on the PVC post and rail fence, with the difference being their overall geometry. The overall geometry of the first and second set of tests is given in Figure 5.15 and Figure 5.16, respectively. The overall geometry of the first set of load tests is the same as that typically used for equestrian PVC fencing. In the second set of tests, the spacing between the PVC posts was reduced from 2000 mm to 1800 mm so that the distance between the PVC posts was the same as that of the timber fence tested as described in Section 5.4.1. Hence, the second set of load-deflection responses of the PVC fence could be compared with those of the timber fence. It is, however, worth highlighting that the heights of the timber and PVC posts were marginally different (cf. Figure 5.10 and Figure 5.16).

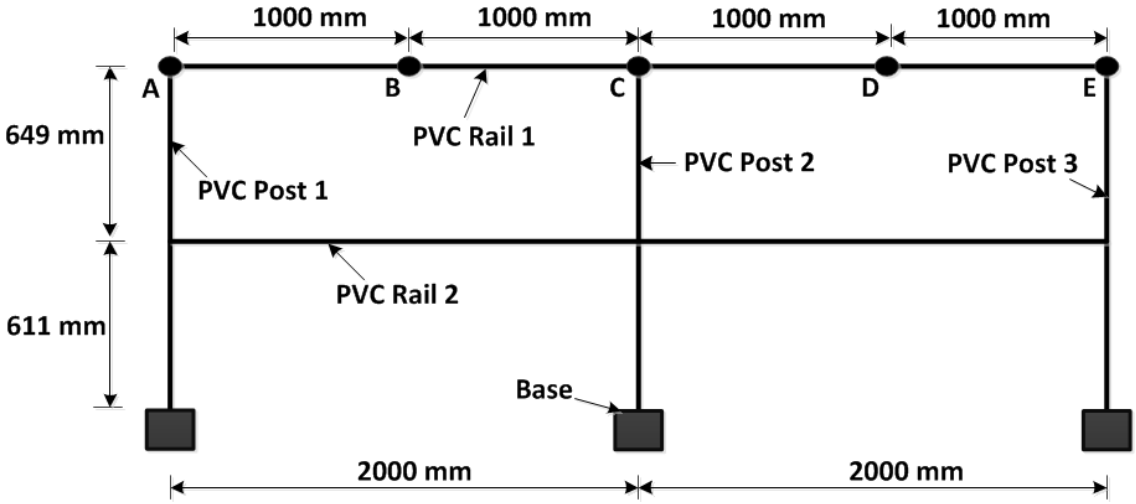

Figure 5.15: Overall geometry of the PVC post and rail fence (post spacing = 2000 mm)

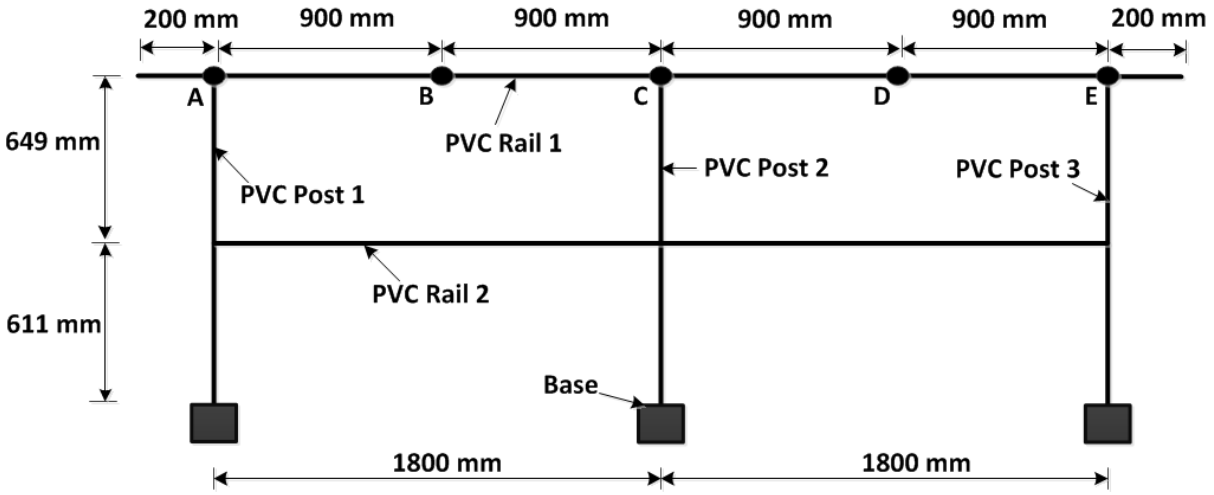

Figure 5.16: Overall geometry of the PVC post and rail fence (post spacing = 1800 mm)

For both sets of load tests, the PVC fence was tested under static incremental loading up to a maximum load of 600 N. Figure 5.17 shows the loading arrangement for the first set of load tests on the two-bay PVC fence. The load was applied normal to the plane at the top of the centre post (Node C) of the two-bay PVC fence, and subsequently at the mid-bay points (Nodes B and D in Figure 5.15 and Figure 5.16). A line load was applied on the PVC post (105 mm below the top of the centre post) through a circular steel rod attached to a 2.5 kN load cell. Figure 5.18 and Figure 5.19 show close-up views of the loading arrangement on the PVC fence at Nodes C and B, respectively. It should be noted that the circular steel rod attached to the load cell was rotated 90^{o} so that a line load could be applied to the top rails at the

mid-bay points (Nodes B and D). The loads were applied in increments of 100 N up to a maximum load of 600 N. Three dial gauges were placed in contact with the back of the posts (Nodes A, C and E), and two dial gauges in contact with the back of the top rail at mid-bay points (Nodes B and D) to record horizontal deflections corresponding to each load increment. The test procedure was repeated three times.

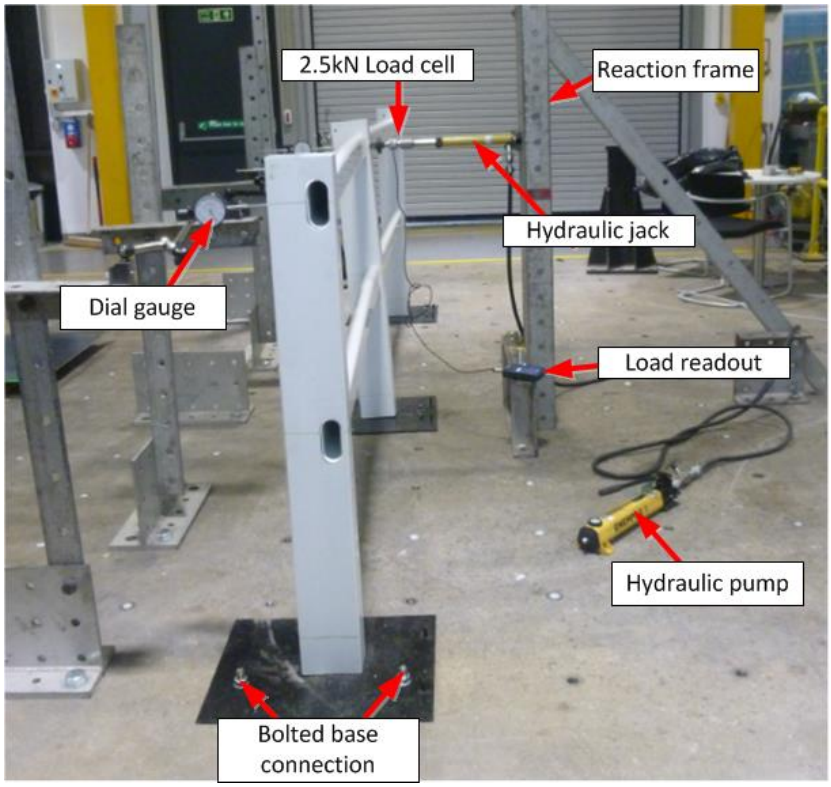

Figure 5.17: Load test on the two-bay PVC fence with a 2000 mm post spacing (First set of load tests)

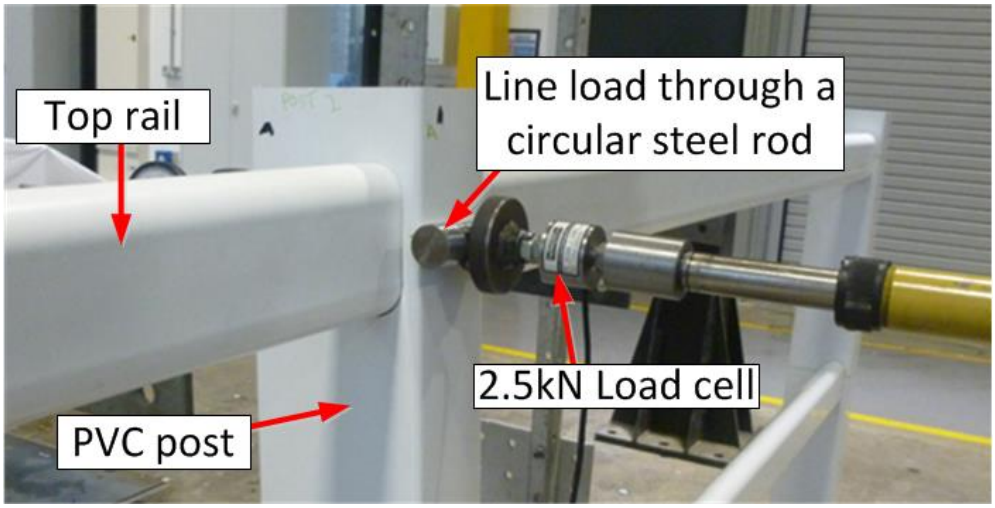

Figure 5.18: Close-up view of the loading arrangement on the PVC fence (load applied at Node C)

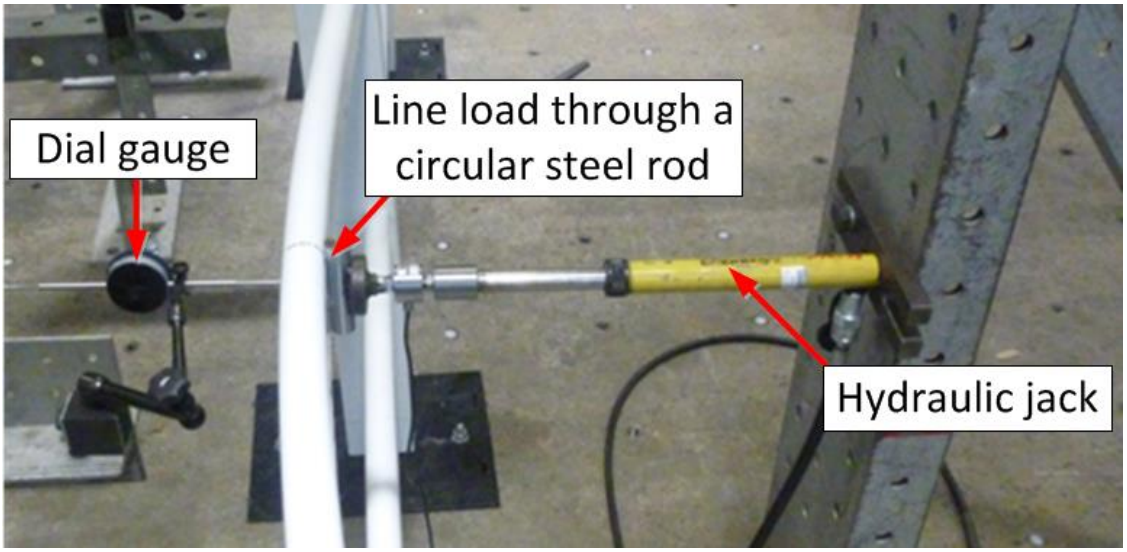

Figure 5.19: Close-up view of the loading arrangement on the PVC fence at the mid-bay point (load applied at Node B)

5.5. Results and Discussion of Tip-Loaded Cantilever Bending Tests on Timber and PVC Posts

5.5.1. Results and Discussion of Tip-Loaded Cantilever Bending Test on the Timber Post

The average deflection values were used to determine the rotational stiffness of the bolted joint at the base of the timber post. The load-deflection data for the three repeat cantilever tests are given in Appendix 9. The average deflection at the back of the timber post at the maximum load of 80 kg (785 N) was 20.6 mm; hence dividing this load by the corresponding average deflection gave a transverse stiffness of 38.1 N/mm. A moment-rotation plot for the timber post is shown in Figure 5.20. A regression line was fitted to the plot and the rotational stiffness, K of the bolted joint at the base of the timber post was determined as 3 x 10^5 Nm/rad.

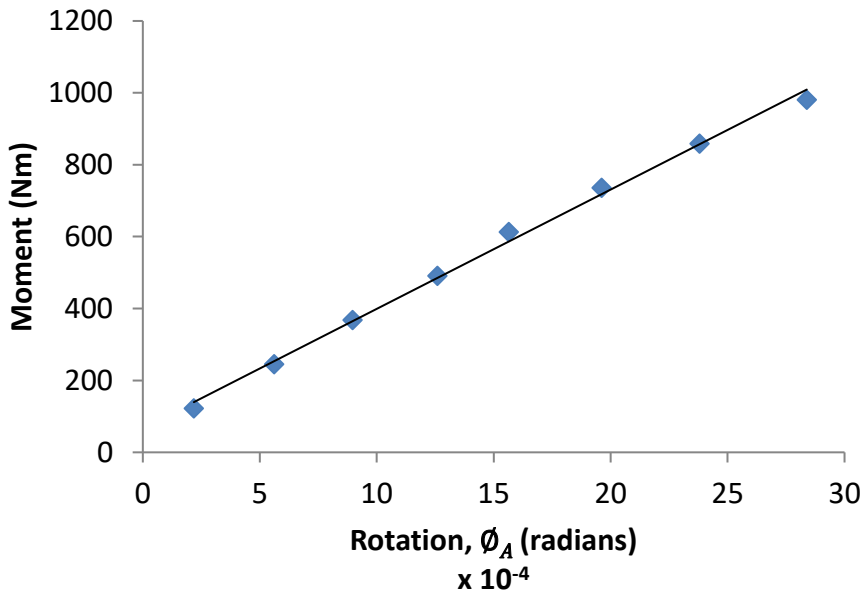

Figure 5.20: A plot of moment against rotation for the tip-loaded cantilever beam

5.5.2. Results and Discussion of Tip-loaded Cantilever Bending Test on the PVC Post

Three repeat tests were carried out on the PVC post, and the average deflection values were used to plot its load-deflection response shown in Figure 5.21.

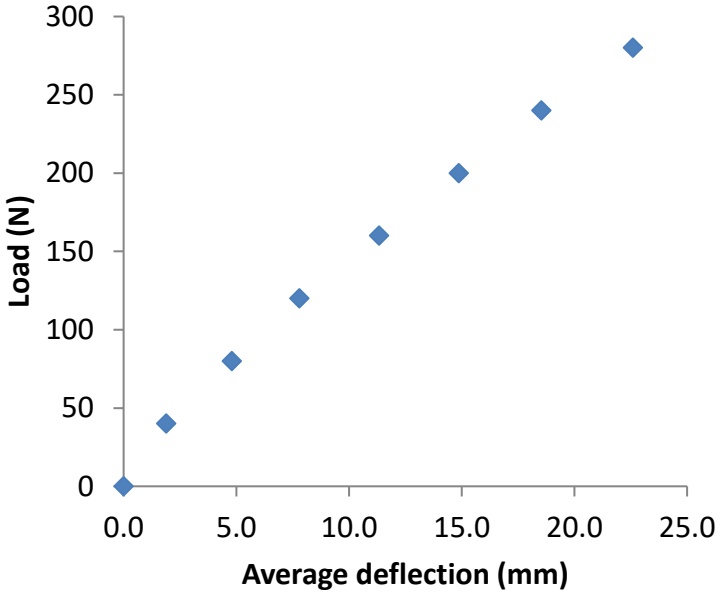

Figure 5.21: Load versus average deflection response for cantilever test on PVC post

The load-deflection data for the tip-loaded cantilever bending test on the PVC post is given in Appendix 9 and shows good repeatability. Figure 5.21 shows a linear load-deflection response. The average deflection at the back of the PVC post at the maximum load of 280 N was 22.6 mm; hence dividing this load by the corresponding average deflection gave a transverse stiffness of 12.4 N/mm.

5.6. Results and Discussion of the Load Tests on the Timber and PVC Fencing Structures

5.6.1. Results and Discussion of the Load Tests on the Two-Bay Timber Fence

The results of the three repeat load tests on the two-bay timber fence showed good repeatability and are given in Appendix 10. Figure 5.22 shows a plot of the load versus average deflection responses at Nodes A – C of the two-bay timber fence. The load-deflection plots for the three Nodes A – C show linear responses. The timber fence supported a maximum load of 1400 N without showing any signs of damage. The average transverse deflections at a maximum load of 1400 N at Nodes A - C are given in Table 5.2.

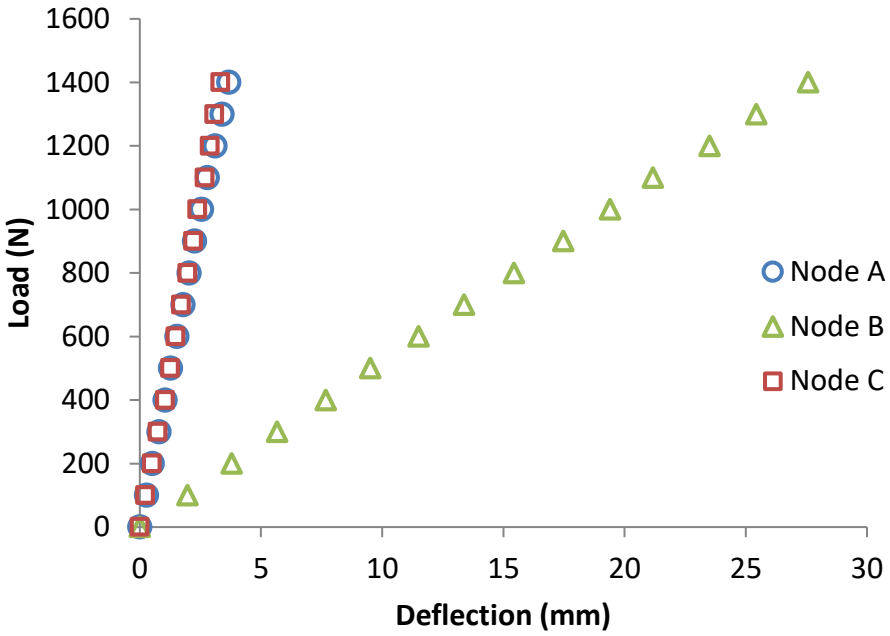

Figure 5.22: Load versus average deflection responses at Nodes A – C of the two-bay timber fence

As expected, Node B (being the loading point), had the largest deflection of 27.6 mm for an applied maximum load of 1400 N. Nodes A and C had significantly lower average transverse deflections of 3.7 mm and 3.3 mm, respectively, reflecting the limited load distribution effects produced by the rails. The difference between the average deflections at Nodes A and C is small, and may also be attributed to the differences in the flexural moduli of the timber post and rail sections. As the rails only partially re-distribute the load applied at the centre post (Node B) to the two outer posts (Nodes A and C), the transverse stiffness of the two-bay timber fence was determined by dividing the maximum load of 1400 N by the average transverse deflection at Node B. Therefore, the transverse stiffness for the two-bay timber fence was 50.7 N/mm.

Table 5.2: Traverse deflection at Nodes A – C of the two-bay timber fence at the maximum load of 1400 N

Node	Transverse deflection [mm]
A	3.7
B	27.6
C	3.3

5.6.2. Results and Discussion of the Load Tests on the Two-Bay PVC Fence

Figure 5.23 and Figure 5.24 show images of the deformations of the PVC fence with a post spacing of 2000 mm, when subjected to a maximum load of 600 N applied at Nodes B and C, respectively.

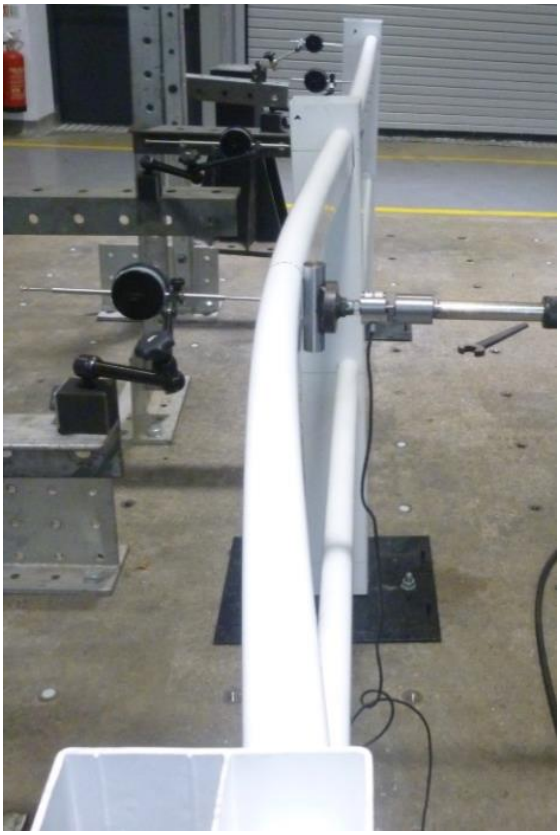

Figure 5.23: The two-bay PVC fence with a post spacing of 2000 mm supporting a maximum load of 600 N applied at Node B (mid-bay point)

Figure 5.24: The two-bay PVC fence with a post spacing of 2000 mm supporting a maximum load of 600 N applied at Node C (top of the centre post)

It is worth noting that there was a small upward movement of the bottom of the centre PVC post from the bolted steel plate (with welded steel angles and circular steel studs) when

loading was applied at the top of the centre post (see Figure 5.25). A similar situation was observed with the centre post and the outer post closer to the loading point when loading was applied at the mid-bay points.

Figure 5.25: Image showing separation between the base of the centre PVC post and steel plate when a load of 600 N was applied at the top of the former (Node C)

The load-deflection data for both sets of load tests on the PVC fence are given in Appendix 10. Figure 5.26, Figure 5.27 and Figure 5.28 show plots of the load versus average deflection responses at Nodes A – E of the two-bay PVC fence with a post spacing of 2000 mm loaded at Nodes B, C and D respectively.

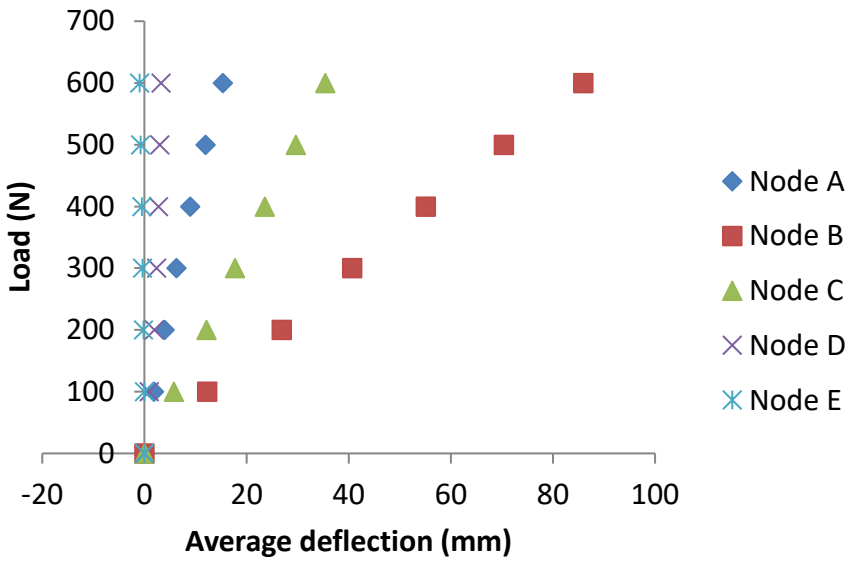

Figure 5.26: Load versus average deflection responses at Nodes A – E of the two-bay PVC fence loaded at Node B (post spacing = 2000 mm)

The results for both sets of tests on the PVC fence were linear and showed good repeatability. The two-bay PVC fence also supported a maximum load of 600 N without showing any signs of damage. The load versus average deflection responses at Nodes A – E of the two-bay PVC fence with a post spacing of 1800 mm loaded at Nodes B, C and D are

also given in Appendix 10; their overall features are similar to those of Figure 5.26, Figure 5.27 and Figure 5.28, though, of course, the magnitudes of the deflections were different.

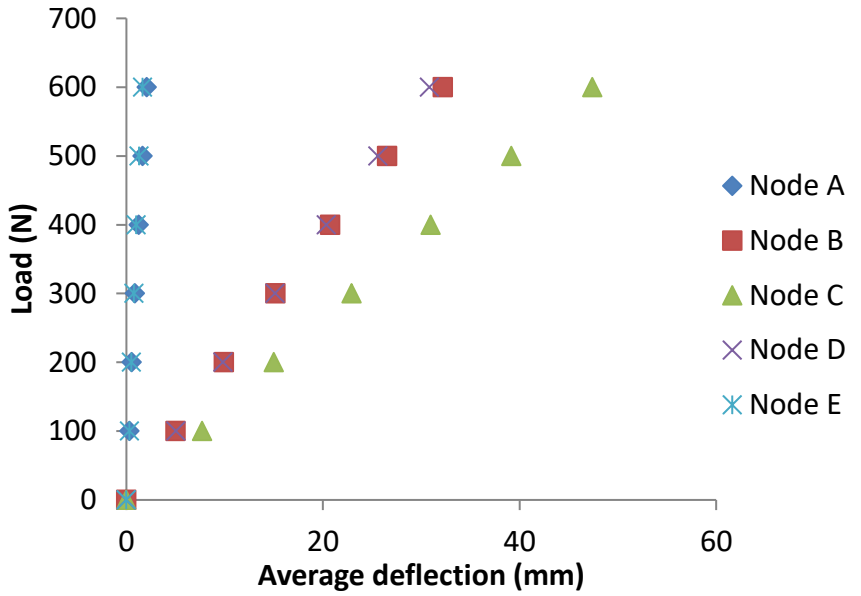

Figure 5.27: Load versus average deflection responses at Nodes A – E of the two-bay PVC fence loaded at Node C (post spacing = 2000 mm)

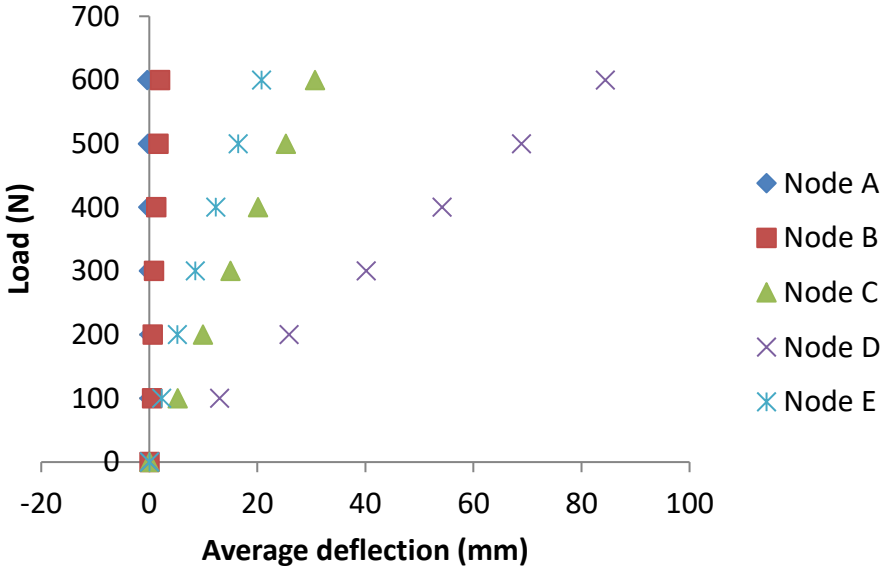

Figure 5.28: Load versus average deflection responses at Nodes A – E of the two-bay PVC fence loaded at Node D (post spacing = 2000 mm)

The average transverse deflections at the maximum load of 600 N at Nodes A – E are given in Table 5.3. As expected, the largest deflections occurred at the nodes where the loading was applied. For the first set of load tests (2000 mm post spacing), the largest deflections corresponding to the applied maximum load of 600 N applied at Nodes B, C and D were 85.9

mm, 47.4 mm and 84.4 mm, respectively (see Table 5.3). These results show that when the same load magnitude (600 N) was applied at the mid-bay points (Nodes B and D) and the top of the centre post (Node C), the corresponding deflections at the former were approximately 80 % greater than the latter. Similarly, the largest deflections corresponding to the applied maximum load of 600 N at Nodes B, C and D obtained from the second set of load tests (1800 mm post spacing) were 65.8 mm, 42.9 mm and 68.9 mm, respectively. These results also reflect that greater deflections were obtained when the fence was loaded at mid-bay points (Node B and D) compared to when loaded at the top of the centre post (Node C). Node A had a small deflection of 0.2 mm in the opposite direction to the loading when the maximum load of 600 N was applied at Node D. A similar situation was observed when the same load of 600 N was applied at Node B; the deflection at Node E was about 0.9 mm in the opposite direction to the loading.

Table 5.3: Transverse deflections of the two-bay PVC fence at Nodes A - C at the maximum load of 600 N

Test	Loading point	Average transverse deflection [mm]				
		Node A	Node B	Node C	Node D	Node E
First set	Node B	15.4	85.9	35.4	3.3	- 0.9
	Node C	2.1	32.2	47.4	30.8	1.6
	Node D	- 0.2	2.0	30.6	84.4	20.8
Second set	Node B	23.1	65.8	30.3	5.9	- 0.7
	Node C	5.1	29.1	42.9	26.5	4.4
	Node D	- 0.1	5.1	28.9	68.9	27.9

When load was applied at Node B (mid-bay point), the deflection at Node A was 56 % lower than that of Node C (located at the top of the centre post) in the first set of tests. When subjected to the same loading in the second set of tests, the deflection at Node A was 24 % lower than that of Node C. Furthermore, when load was applied at the other mid-bay point (Node D), the deflections at Node E were about 32 % and 4 % lower than those at Node C for the first and second set of tests, respectively. These test results show that when loading was applied at the mid-bay points, the deflections at the top of the centre post were greater than the deflections at the outer post closer to the loading point. However, it was expected that the deflections at the centre post would be less than those at the outer post (closer to the mid-bay loading point) due to the stiffness support provided to the former post as a

result of the structural continuity across the other bay. These differences may be due to variable contact between the inner faces of the PVC posts and the welded steel angle which may have led to different joint stiffnesses at the bases of the PVC posts. It may also be as a result of the separations between the bases of the centre and outer posts (closer to the loading point) from the bolted steel plate when loaded at the mid-bay points (see Figure 5.25).

For both sets of tests, when load was applied at Node C (located at the top of the centre post), the deflections at Node A were approximately 31 % and 16 % greater than those at Node E for the first and second set of tests, respectively. It would be expected that the deflections of these nodes at opposite ends of the top rail should be equal. On the other hand, the deflections at Node B were approximately 5 % and 10 % greater than those at Node D for the first and second set of tests, respectively reflecting a smaller difference compared to those at Nodes A and E. Furthermore, it was expected that the deflection at Node A when the load was applied at Node B should be the same as that of Node E when the load was applied at Node D. However in the first set of tests, when a load of 600 N was applied at Node B, the deflection at Node A was 15.4 mm, which is approximately 26 % lower than the deflection at Node E (20.8 mm) when the same load was applied at Node D. Similarly, the deflection at Node A was about 17 % lower than the deflection at Node E when a load of 600 N was applied at Nodes B and D, respectively in the second set of tests. These differences can be attributed to the presence of small clearances leading to relative movement (minor slip) at the interface between the rail cut-outs of the PVC posts and the edges/faces of the PVC rails. Thus, these slips may have led to limited load distribution across the full two-bay PVC fence.

An applied maximum load of 600 N at Node B gave 85.9 mm and 65.8 mm maximum deflections in the first and second set of tests, respectively, reflecting a 23 % difference. Similarly, deflections of 84.4 mm and 68.9 mm at Node D were obtained from the first and second set of tests, respectively when subjected to a maximum load of 600 N at Node D; these values show that the latter was about 18 % smaller than the former. The transverse deflections recorded at Node C which correspond to the maximum load of 600 N applied at Node C were used to determine the relative transverse stiffnesses for both sets of load tests on the two-bay PVC fence. The transverse deflections were 47.4 mm and 42.9 mm for the

first and second set of tests, respectively. Dividing the maximum load of 600 N applied at Node C by the transverse deflection at the same node, gave transverse stiffnesses of 12.7 N/mm and 14 N/mm for the first and second set of tests, respectively. The test results showed that a reduction in the distance between the PVC posts from 2000 mm to 1800 mm resulted in an approximate 10 % increase in the relative transverse stiffness. It is also worth noting that in comparison with the transverse stiffness obtained from the cantilever test on the PVC post (12.4 N/mm), it is evident that the transverse stiffness of the two-bay PVC fence (with a post spacing of 2000 mm) is only about 2 % greater than the former. This reflects that the relative transverse stiffness was not significantly increased with the additional PVC posts and rails.

5.7. Comparison of the Transverse Stiffnesses of the Representative Two-Bay Timber and PVC Fencing Structures

The two-bay timber and PVC fences supported maximum loads of 1400 N and 600 N, respectively, without any apparent or visible damage, and their load-deflection responses were linear and showed good repeatability. The deflections at the top of the centre posts corresponding to the applied maximum loads were used to obtain a measure of the relative transverse stiffnesses for the two-bay timber fence and PVC fences. The second set of load tests on the PVC fence had a post spacing (1800 mm) equal to that of the two-bay timber fence, however, there was a limitation due to the heights of the timber and PVC posts being marginally different. Nevertheless, comparisons of the transverse stiffnesses were made between the timber fence and the results from the second set of load tests on the PVC fence. The relative transverse stiffnesses for the two-bay timber and PVC fences were 50.7 N/mm and 14.0 N/mm, respectively. It is also worth highlighting that the PVC fence had steel reinforcements (a steel plate with 600 mm long welded steel angles) for increased strength and stiffness. However, from the foregoing transverse stiffnesses, it is evident, that the transverse stiffness of the two-bay timber fence is approximately 262 % greater than that of the PVC fence.

5.8. Chapter Summary

Experimental tests have been carried out to determine the load-deflection responses of two-bay timber and PVC fences. The test setup, instrumentation and analysis techniques

have been described, and images of the test setups have also been presented. Results obtained from the experimental tests have been presented, discussed and analysed.

The two-bay timber and PVC fences' transverse stiffnesses were determined by dividing the maximum loads applied at the top of the centre posts by the corresponding average transverse deflections. The analyses showed that the two-bay timber and PVC fences had relative transverse stiffnesses of 51 N/mm and 14 N/mm, respectively, reflecting that the former is significantly stiffer than the latter. These relative transverse stiffness values were based on three repeat load tests on the fencing structures which showed very good repeatability. Furthermore, the layout of the PVC fence was modified to ensure that it had the same post spacing as the timber fence, however, the heights of the timber and PVC posts were marginally different.

It should be noted that the transverse stiffness of the fencing structures is dependent on the mechanical and geometric properties of the structural members (posts and rails) and joints. Hence, there are limitations; as bases of the posts are typically concreted into the ground in practice, the base joint stiffnesses may vary and depend on several environmental factors (i.e. moisture content, temperature). There are also limitations with the rail-to-post connections such as the location and/or number of nails on timber fences as well as the relative movement (slip) at the interface between the cut-outs of the PVC posts and the PVC rails. In addition, as reported earlier in Chapter 4, there were large differences in the flexural moduli of the timber sections (compared to PVC) and the mechanical properties of timber are dependent on several factors (such as the presence of knots). Consequently, a sensitivity analysis (using ANSYS FEA) was carried out in Chapter 6 to investigate the effect of varying the experimentally determined flexural moduli of the ungraded timber posts and rails. This analysis in Chapter 6 was therefore used to estimate the lower and upper bound transverse stiffnesses of the two-bay timber fence. In summary, as there have been no load tests reported on timber or PVC fencing in the open literature and no current structural load-bearing standards for equestrian fencing, these experimental results provide useful benchmarks for assessing the structural stiffness requirements of the novel waste carpet structural composites.

6. Finite Element (FE) Modelling of Timber and PVC Fencing Structures

6.1. Introduction

This chapter describes the Finite Element (FE) modelling and analysis carried out using ANSYS software to investigate the load-deformation responses of two-bay timber and PVC fences. The overall geometry, loading and boundary conditions of the fencing structures that were explored in the experimental testing in Chapter 5 formed the basis of the FE analyses carried out in this chapter. The aim of the FE analyses is to determine how accurately the load-deformation responses of the fencing structures can be predicted without the need of an experimental setup. This is because physical experimental testing can be both costly and time-consuming. Thus, the FE analyses described in this chapter were carried out to supplement the experimental work described in Chapters 4 and 5.

For both the timber and PVC fencing structures, a relatively simple FE modelling of the load-deflection responses of their respective posts was initially carried out. The results were compared with those of the experimental tip-loaded cantilever bending tests (described in Chapter 5) and used to validate the FE analysis technique. Thereafter, details of the FE analyses carried out on the two-bay timber and PVC fencing structures are presented, compared and validated with the experimental results given in Chapter 5. The FE models and analyses can then be used to investigate the load-deformation response of a fencing structure comprised of novel waste carpet structural composites, and evaluate its transverse stiffness characteristics relative to those of similar timber and PVC fences.

6.2. Background to ANSYS FE Modelling of Beams and Structures

FE analysis may be used to solve a broad range of engineering problems ranging from relatively simple elastic analysis to complex nonlinear deformations of large structures. Advances in technology have led to the development of modern FE software packages (i.e. ANSYS and ABAQUS) to model and analyse complex engineering structural challenges and problems in a fast and cost-effective manner. These software packages can be used to

develop FE models, which can be used to investigate and determine several properties (i.e. deformations, strains, stresses and reaction forces) of beams and structures.

The FE modelling for this study was carried out using ANSYS Workbench (ANSYS Workbench Release 15). ANSYS Workbench is an FE program which comprises of several applications used for static and dynamic analysis. ANSYS DesignModeler - an application of ANSYS Workbench can be used for creating geometry and editing existing Computer-Aided Design (CAD) models. Other common CAD tools used for designing geometries include SolidWorks and Pro/Engineer; these geometries can then be imported into ANSYS Mechanical (also an application of ANSYS Workbench) to carry out mechanical and structural simulations. ANSYS Mechanical is also used for defining mesh optimisation, boundary conditions and analysis of results. There is a range of finite elements (such as beam, solid, shell and contact elements) in ANSYS which are based on different equations and theories for the analysis of various types of beams of structures. Each element type has a unique number and prefix that identifies the element category (i.e. BEAM188) (Madenci and Guven, 2006).

Solid elements such as SOLID185, which is a 3D eight-node structural element with three degrees of freedom (UX, UY, UZ) at each node, are commonly used for three-dimensional (3D) modelling of solid structures (Satasivam and Bai, 2014, Ibrahim et al., 2016, Pakala and Kodur, 2016). The use of solid elements results in very good accuracy but increases computational time. It is, however, more computationally efficient to model and analyse thin to moderately-thick beam-type structures using shell elements compared to solid elements (Zhu et al., 2014). A common shell element used in ANSYS is SHELL181, which is a four-node element based on first-order-shear-deformation theory (Zhang et al., 2013). SHELL181 has six degrees of freedom at each node which are: three translational (U_X, U_Y, U_Z) and three rotational (ROTX, ROTY and ROTZ) displacements. Contacts between parts/faces of a structure in ANSYS are modelled using pairs of elements, i.e. CONTA174 and TARGE170 elements (Pakala and Kodur, 2016). These elements are used to represent contact and sliding between surfaces, and account for friction and large deformations (geometric nonlinearity) (ANSYS Workbench Release 15). It is worth noting that incorporating several contacts between different parts of a structure in ANSYS results in substantial complexity, increased computational time and convergence problems. These convergence problems are also due to frictional effects which cause nonlinearities and more iteration steps.

BEAM188 elements are commonly used to represent beams and are based on Timoshenko beam theory which takes shear-deformation into account (Yan et al., 2016). The BEAM188 element is defined by two nodes and is suitable for linear, large rotation and large nonlinear applications (ANSYS, 2016, Jishi et al., 2016). The BEAM188 element utilises a cubic interpolation function, hence increasing the number of elements does not significantly affect deformation results. They are also more computationally efficient than solid or shell elements. MPC184 elements (Multi-Point Constraint), defined by two coincident nodes are also used for modelling joints in ANSYS. The BEAM188 and MPC184 elements both have six degrees of freedom per node. The six degrees of freedom comprise three translational (U_X, U_Y, U_Z) and three rotational (ROTX, ROTY and ROTZ) displacements (see Figure 6.1). Hence, different types of joints can be represented by imposing the appropriate kinematic constraints on the degrees of freedom. The translational and rotational stiffnesses can be specified as coefficients of a 6 x 6 stiffness matrix.

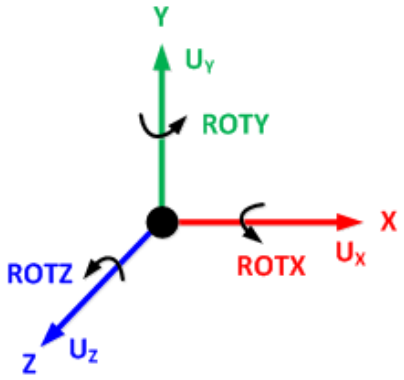

Figure 6.1: A sketch showing the six degrees of freedom at a node

For this study, as the two-bay timber and PVC fencing structures mainly resist bending in service; only the longitudinal post/rail elastic properties significantly affect the FE simulation results. The longitudinal elastic flexural moduli of the posts and rails of the fencing structures have been determined and given in Chapter 4. Hence, for simplicity, isotropic linear elastic material models were used in the FE analyses. Isotropic linear elastic material models were also chosen because the mechanical properties of the materials in their transverse directions were not determined from experimental tests described in Chapter 4.

Two different FE analyses were carried out on the timber structure; a cantilever semi-rigid beam analysis was carried out to validate the FE analysis technique, and the results were

compared with the experimental tip-loaded cantilever bending test results from Chapter 5. The other FE analysis was the modelling of the two-bay timber fence, which was compared with the results of the experimental load tests given in Chapter 5. Additional FE analyses were also carried out on the PVC post and two-bay PVC post and rail fence. The FE results for the PVC fence were also validated by comparison with the results of the experimental load tests given in Chapter 5.

6.3. Cantilever Beam FE Model and Analyses

6.3.1. Cantilever Beam FE Model and Analysis of the Timber post

A line body utilising BEAM188 element was used to represent the timber post for computational efficiency. MPC184 element (Multi-Point Constraint) was used to represent the bolted base joint at Point A (see Figure 6.2). A semi-rigid joint was created at Point A by rigidly fixing the three translational (U_X, U_Y, U_Z) and two rotational (ROTX and ROTY) degrees of freedom, leaving only one degree of freedom (rotation about the z-axis, ROTZ) illustrated in Figure 6.3. The details of the timber post used in the cantilever FE model are given in Table 6.1.

The flexural modulus of the timber post was 8.1 GPa (see Table 4.5 in Chapter 4), and a Poisson's ratio of 0.3 was assumed used in the FE model (Kretschmann, 2010). A rotational stiffness of 3 x 10^5 Nm/rad, which was obtained from the experimental tip-loaded cantilever test described in Section 5.3.1 of Chapter 5, was used to represent the rotational stiffness about the z-axis at Point A. Similar to the experimental work described in Section 5.3.1, a load of 785 N was applied at Point B in the negative Y-direction as illustrated in Figure 6.2a. Figure 6.2b shows an image illustrating a normal view from Point A to B. It should be appreciated that the coordinate system at Point B is the same as that at Point A.

Figure 6.2: FE cantilever semi-rigid beam analysis model showing the coordinate system: (a) Side view (b) Normal view from Point A to B

Table 6.1: Details of the timber post used in the cantilever FE model

Span [mm]	Width [mm]	Depth [mm]	Second moment of area about plane of flexure [mm^4]	Flexural modulus [GPa]	Poisson's ratio
1250	120	72	3,732,480	8.1	0.3

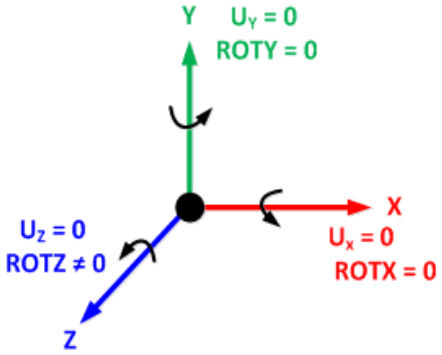

Figure 6.3: Boundary conditions at Point A of the timber FE cantilever semi-rigid analysis model

6.3.2. Cantilever Beam FE Model and Analysis of the PVC post

Due to the relatively more complex geometry and hollow sections of the PVC fence (compared to the timber fence), the geometry of the PVC post was created with the SolidWorks CAD software and imported into ANSYS for analysis. The geometric details of the PVC post and the steel plate with pairs of welded steel angles have been described previously in Figure 5.2 and Figure 5.3 of Chapter 5.The pairs of steel angles welded to the 4.5 mm thick steel plate was 600 mm long. The overall length of the PVC post was 1260 mm. The automesh function in ANSYS was used to generate SHELL181 elements to model the PVC post and the pairs of welded steel angles at its base (see Figure 6.4). The global mesh relevance option in ANSYS was set to 100. The relevance option controls the fineness of the mesh for the entire model, and ranges from −100 (for coarse mesh and high speed computation) to 100 (for fine mesh and high accuracy solutions). The contact between the inner wall of the PVC post (highlighted in red in Figure 6.5) and the face of one of the steel angles welded to the flat steel plate (highlighted in blue in Figure 6.5) was modelled using contact elements (CONTA174 and TARGE170) and defined with a coefficient of friction of 0.3 (Pakala et al., 2012, ANSYS Workbench Release 15). These contact elements are typically used to represent contact and sliding between faces in ANSYS (Tsavdaridis and Papadopoulos, 2016).

The experimentally determined flexural modulus of the PVC post used in the FE model was 1.3 GPa (see Chapter 4), and the flexural modulus of the steel plate with welded steel angles was assumed to be 210 GPa (Callister and Rethwisch, 2008). Additional mechanical properties of the PVC post provided by the manufacturer (Duralock Performance Fencing) are given in Appendix 1. The Poisson's ratio for the PVC post and welded steel angles of 0.3 was assumed in the FE model (Green, 2006). Similar to the loading and boundary conditions of the experimental test in Section 5.3.2, a line load of 280 N was applied 105 mm below the top of the PVC post, and the holes on the steel plate with welded steel angles were rigidly fixed (see Figure 6.4). Preliminary study on the effect of mesh refinement on solution convergence for the PVC post showed that the deflection results do not change significantly as the number of elements was increased beyond 6,000 elements, hence a total of 6,231 elements were used for this FE analysis.

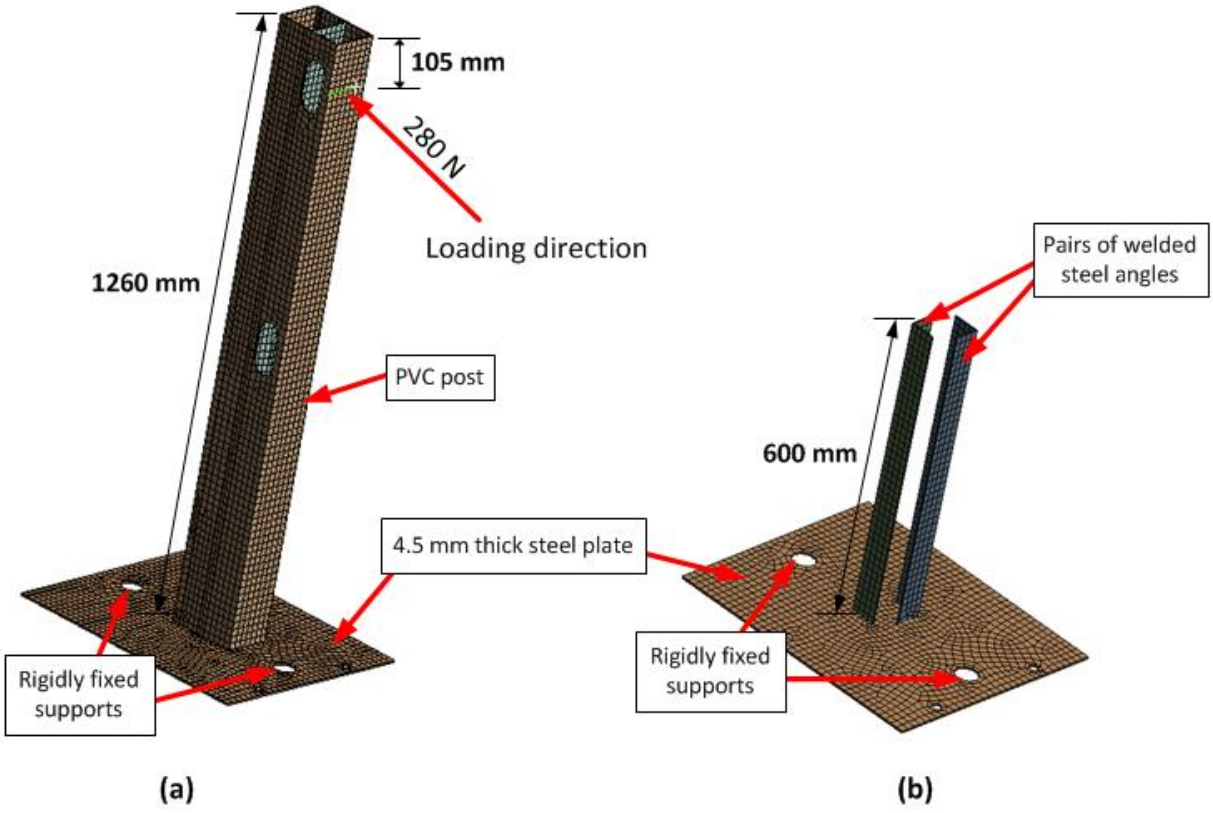

Figure 6.4: Loading and boundary conditions of the FE cantilever model of the PVC post: (a) PVC post assembly and (b) steel plate with pairs of welded steel angles

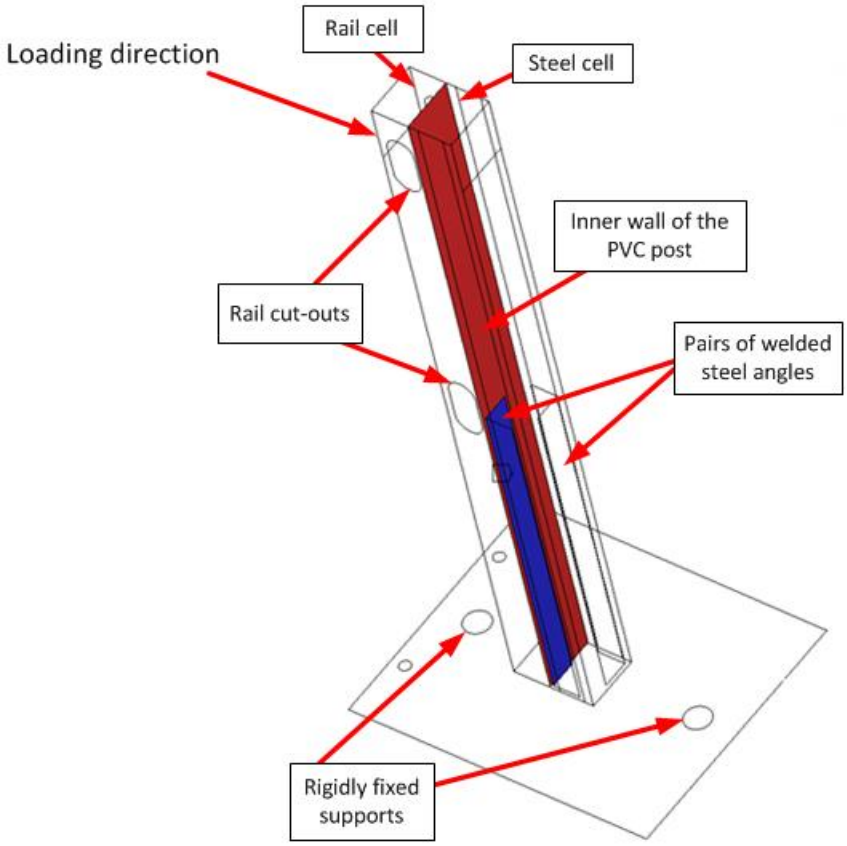

Figure 6.5: Image illustrating the contact between the inner wall of the PVC post and the face of one of the steel angles welded to the flat steel plate

6.4. Analysis and Discussion of the Cantilever Beam FE Models and the Experimental Results

Table 6.2 gives a comparison between the FE models and experimental deflections of the tip-loaded cantilever timber and PVC posts; the deflections predicted by the FE models are about 2 – 4 % greater than the experimental test results. The result shows that the FE model deflection for the tip-loaded cantilever timber post is about 2 % greater than that obtained from the experimental test for a maximum load of 785 N applied at its top. The ratio between the cantilever PVC FE model and experimental deflection was 1.04, based on an applied load of 280 N at the top of the PVC post (see Table 6.2); this result shows that the predicted deflection is only about 4 % greater than the test result. In general, the cantilever beam FE results have been compared with the experimental test results and shown to be in very good agreement. These results and analyses have also validated the FE technique.

Table 6.2: Comparison of cantilever FE models with the experimental results for maximum loads applied at the top of the timber and PVC posts

Post	Maximum load [N]	Deflection [mm]		Ratio of FE model / Experimental result
		Experimental test result	FE model	
Timber	785	20.6	21.1	1.02
PVC	280	22.6	23.6	1.04

6.5. Two-Bay Fence FE Model Setup and Analysis

6.5.1. FE Modelling and Analysis of the Timber Fencing Structure

Line bodies utilising BEAM188 elements were used to represent the timber posts and rails for computational efficiency. Figure 6.6 shows the overall geometry, nodes and member labels of the two-bay timber fence FE model. All the nodes have the same coordinate system as highlighted at Node E in Figure 6.6. MPC184 elements were used to represent the bolted base joints (see Nodes D – F in Figure 6.6). The corresponding flexural moduli for each post and rail obtained from the three-point bending tests (given in Chapter 4) were used in the FE models (see Table 6.3). The average widths and depths of the rectangular cross-section timber posts and rails are also given in Table 6.3. A Poisson ratio of 0.3 was assumed for the timber posts and rails in the FE models (Kretschmann, 2010).

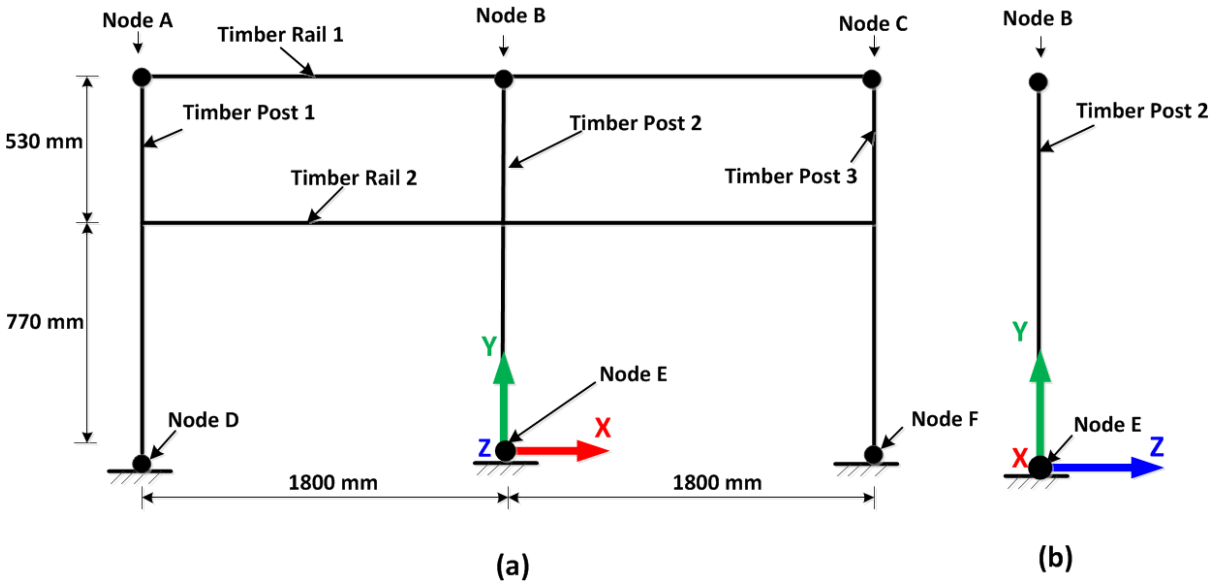

Figure 6.6: Overall geometry of the two-bay timber fence FE model: (a) Front-view (b) Edge-view from Post 2 to 3

Table 6.3: Geometric and mechanical properties of the timber posts and rails used in the FE model

Post/rail	Average width [mm]	Average depth [mm]	Second moment of area about plane of flexure [mm^4]	Flexural modulus [GPa]	Poisson's ratio
Timber Post 1	122	71	3,638,762	10.7	0.3
Timber Post 2				8.1	
Timber Post 3				9.5	
Timber Rail 1	93	37	392,561	9.1	
Timber Rail 2				13.5	

Loading was applied at Node B in the negative Z-direction (see Figure 6.6). Two different FE models were created to simulate the load-deformation response of the two-bay timber fence, and the displacements from each model were evaluated and compared with the experimentally measured displacements. Table 6.4 gives details of the two types of joints used at the base of the posts in the FE Models 1 and 2 of the timber fence.

Table 6.4: Joint details used at the base of the posts in FE Models 1 and 2 of the two-bay timber fence

Model	Description
1	All the six nodal displacements were set to zero.
2	The rotational stiffness with respect to rotations about the x-axis was 3×10^5 Nm/rad and the other five nodal displacements were set to zero.

6.5.2. FE Modelling and Analysis of the PVC Fencing Structure

Figure 6.7 shows the overall geometry, nodes and member labels of the two-bay PVC fence model. Sketches of the cross-section of the PVC post and rail are shown in Figure 5.2 and Figure 5.3 (in Chapter 5). The details of the PVC posts and rails used in the FE model are given in Table 6.5. It should be noted that the flexural moduli of the PVC posts and rails were taken from the three-point bending tests described in Chapter 4. The flexural modulus of the 600 mm long welded steel angles was assumed to be 210 GPa (Callister and Rethwisch, 2008). A Poisson's ratio for the welded steel angles, PVC posts and rails of 0.3 was also used in the FE model (Green, 2006).

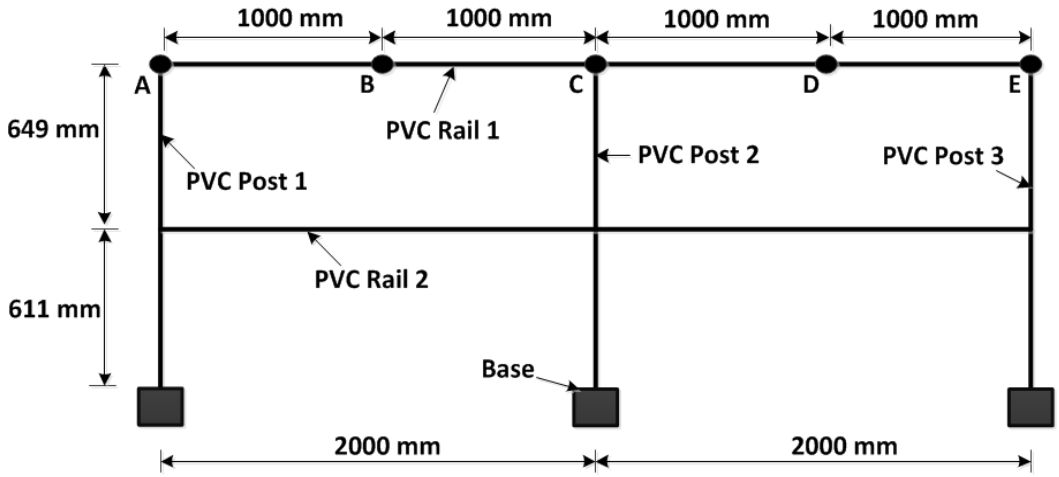

Figure 6.7: Overall geometry of the two-bay PVC fence FE model

Table 6.5: Details of the PVC posts and rails used in the FE model

Post/rail	Second moment of area about plane of flexure [mm^4]	Flexural modulus [GPa]	Poisson's ratio
PVC Post (1 – 3)	4,769,499	1.3	0.3
PVC Rail (1 – 2)	400,126	2.7	

Similar to the description given in Section 6.3.2, the global mesh relevance option in ANSYS was set to 100, and the automesh function was used to generate SHELL181 elements to model the welded steel angles and the PVC posts and rails. The contact between the inner wall of the PVC post and the face of one of the steel angles welded to the flat steel plate (shown previously in Figure 6.5) was modelled using CONTA174 and TARGE170 elements, and defined with a coefficient of friction of 0.3. The six rail-to-post connections on the two-bay PVC fence were also modelled using CONTA174 and TARGE170 elements. Complete contacts between the cut-outs in the PVC posts (highlighted in green in Figure 6.8) and the faces of the PVC rails posts (highlighted in red in Figure 6.8) were defined with a coefficient of friction of 0.3 (Pakala et al., 2012, ANSYS Workbench Release 15). The pairs of holes on the steel plates with welded steel angles were rigidly fixed (shown previously in Figure 6.4). Similar to the load tests described in Chapter 5, a load of 600 N was applied at Nodes B, C and D (see Figure 6.7) normal to the plane of the PVC fence.

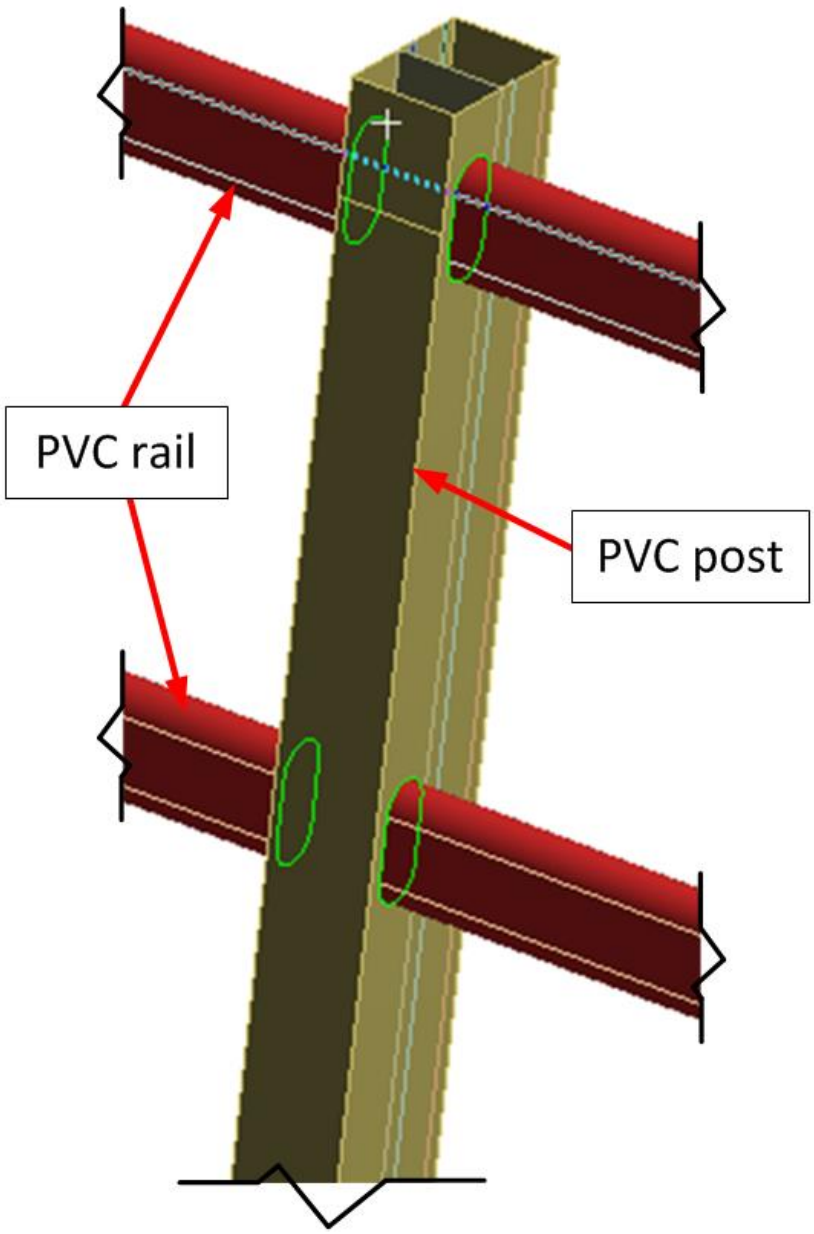

Figure 6.8: An image of the FE model of the PVC rail-to-post connections

The effect of mesh refinement on solution convergence for the two-bay PVC fence analysis was carried out. Figure 6.9 shows a plot of the deflection at Node B versus the total number of elements (after an applied load of 600 N at Node B). The plot shows that the deflection results do not change significantly as the number of elements is increased beyond 10,000 elements. Hence, the FE model with a total number of 10,153 elements (see Figure 6.10) was used for the analysis of the two-bay PVC fence.

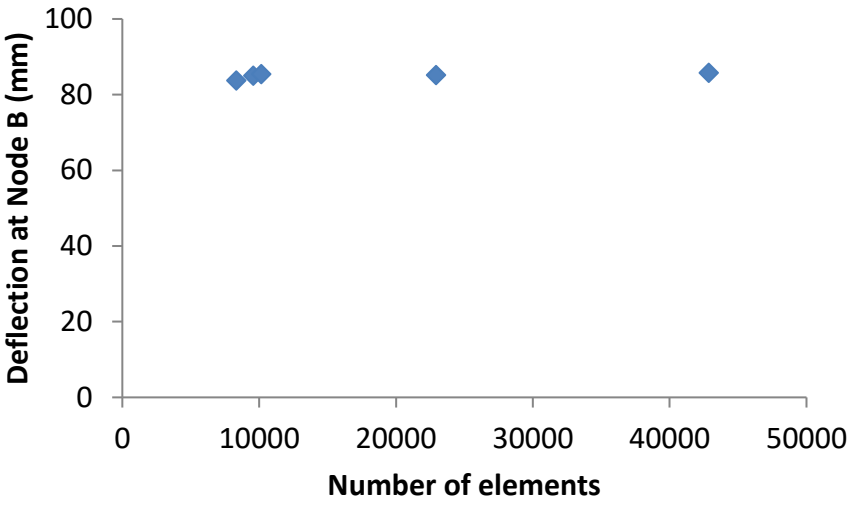

Figure 6.9: Mesh refinement study showing a plot of deflection (at Node B) against the number of elements

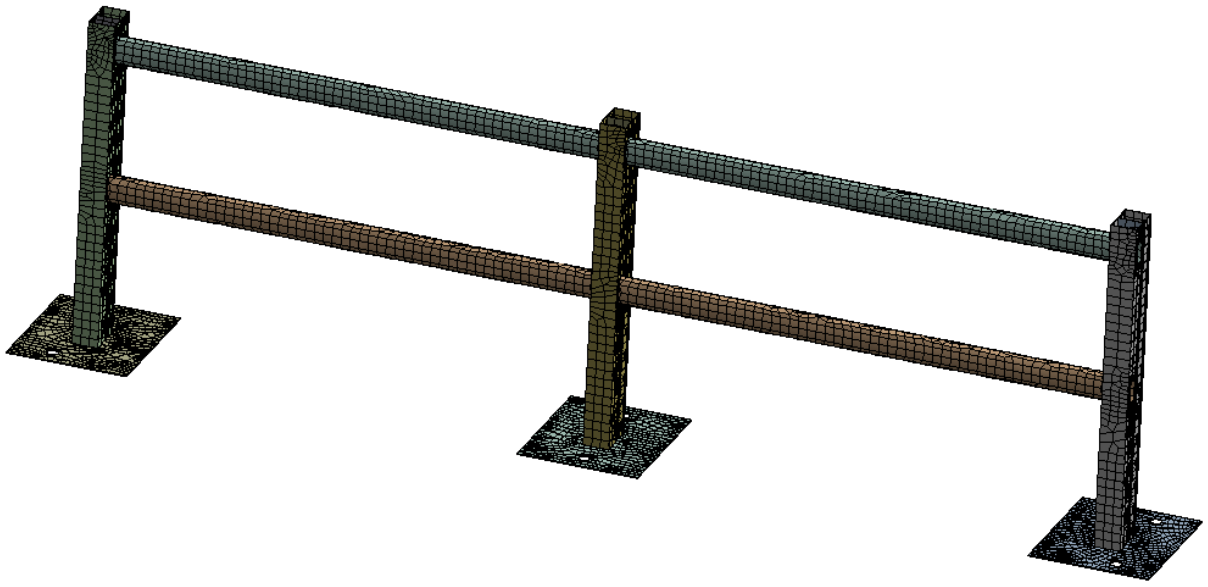

Figure 6.10: Mesh used in the FE model of the two-bay PVC fence

6.6. Analysis and Discussion of the Timber and PVC Fencing Structures' FE Models and the Experimental Results

6.6.1. Analysis and Discussion of the Two-Bay Timber Fence FE Models and Experimental Results

Table 6.6 shows the results of the FE Models 1 and 2 of the two-bay timber fence compared with the experimental deflections for a load of 1400 N applied at the top of Post 2 (Node B in Figure 6.6). As expected, the largest deflection was at Node B (being the loading point). The ratios between the deflections predicted by FE Model 1 and those measured by experimental testing for Nodes A, B and C are 0.76, 0.82 and 0.78, respectively. The ratios between the deflections predicted by FE Model 2 and the experimentally determined deflections for Nodes A, B and C are 1.11, 0.97 and 1.18, respectively. This analysis shows that the results predicted by FE Model 2 are in better agreement with the experimental deflections for Nodes A - C. This is because Model 1 assumed perfectly rigid supports at the base joints of the timber fence, which simplified the FE model. However, this resulted in a greater discrepancy between the Model 1 and experimental deflections. Model 2, on the other hand, utilised the rotational stiffness of the base joints obtained from the tip-loaded cantilever tests (see Section 5.3.1).

Table 6.6: Comparison of two-bay timber fence FE Models 1 and 2 with the experimental results for a maximum load of 1400 N applied at the top of Post 2

Node	Average deflection [mm]	Deflection [mm]		Ratio of FE model to experimental deflection	
	Experimental test result	FE Model 1	FE Model 2	FE Model 1 / Experimental result	FE Model 2 / Experimental result
A	3.7	2.8	4.1	0.76	1.11
B	27.6	22.5	26.7	0.82	0.97
C	3.3	2.6	3.9	0.78	1.18

Figure 6.11 shows a contour plot (from Model 2) of the transverse deflection of the two-bay timber fence for an applied load of 1400 N. Compared with the experimentally measured deflection at Node A, the deflections from FE Models 1 and 2 are 24 % lower and 11 %

higher, respectively. Furthermore, in comparison with the experimental deflections, FE Models 1 and 2 deflections at Node C are 22 % lower and 18 % higher, respectively. The Node B deflections obtained from FE Models 1 and 2 are lower than the experimental deflections by 18 % and 3 %, respectively. These analyses show that the deflections derived from FE Models 1 and 2 for Node B are in better agreement with the experimental values than those at Nodes A and C. The relatively poorer agreement between the deflections at the outer posts (Nodes A and C) compared to that of the centre post (Node B) may be due to the fact that the FE models assumed perfectly rigid rail-to-post joints, thus producing greater transfer from the centre post to the outer posts. However, in reality, the rail-to-post nailed joints are not perfectly rigid.

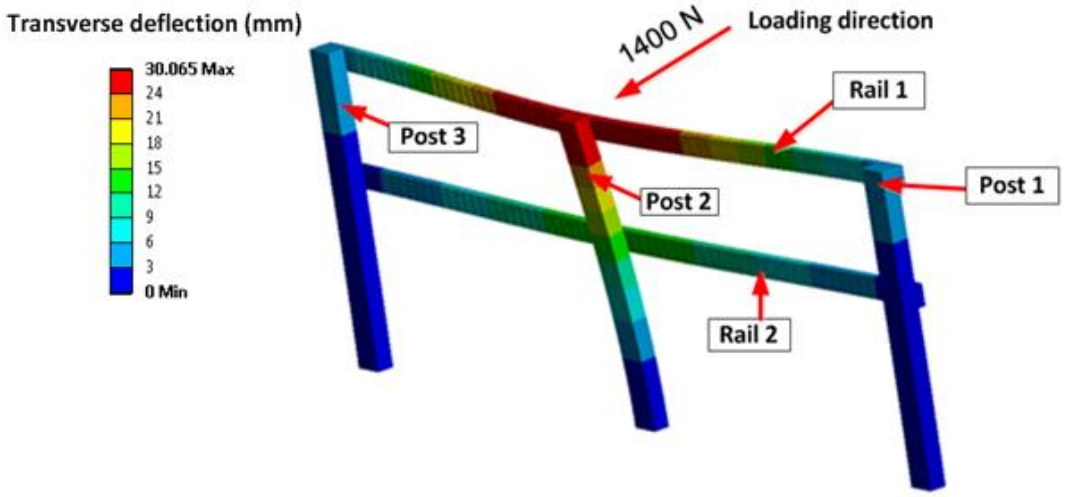

Figure 6.11: FE Model 2 Contour plot showing the transverse deflection of the two-bay timber fence under a load of 1400 N applied at the top of Post 2

Due to the variable nature of timber, a sensitivity analysis was carried out to investigate the effect of using the lowest and highest flexural moduli obtained from the three-point bending tests on the timber posts and rails. The lowest and highest flexural moduli were used as the elastic moduli in FE Model 2 for each of the posts and rails of the two-bay timber fence. The deflections at Nodes A and C were equal. The deflections obtained from using the lowest flexural modulus (8.1 GPa) was 4 mm at Nodes A and C, whereas, using the highest flexural modulus of 13.5 GPa gave a 2.9 mm deflection (see Table 6.7).

Table 6.7: Comparison between using the lowest and highest flexural moduli in FE Model 2 with the experimental test results for an applied load of 1400 N at the top of Post 2

Node	Average deflection [mm]	Deflection from FE Model 2 [mm]	
	Experimental test result	Lowest modulus (8.1 GPa)	Highest modulus (13.5 GPa)
A and C	3.7	4	2.9
B	27.6	28.5	18.9

Using the lowest and highest flexural moduli in FE Model 2, transverse deflections at Node B of 28.5 mm and 18.9 mm, respectively were obtained. These transverse deflections at Node B also correspond to transverse stiffnesses of 49.1 N/mm and 74.1 N/mm (based on an applied load of 1400 N), which represent lower and upper bound transverse stiffnesses of the two-bay timber fence.

6.6.2. Analysis and Discussion of the Two-Bay PVC Fence FE Models and Experimental Results

Figure 6.12 shows a contour plot of the transverse deflection of the two-bay PVC fence for an applied load of 600 N applied at the top of the centre post (Node C in Figure 6.7). The deformation modes predicted by the FE analysis are in good agreement with those observed in the experimental tests.

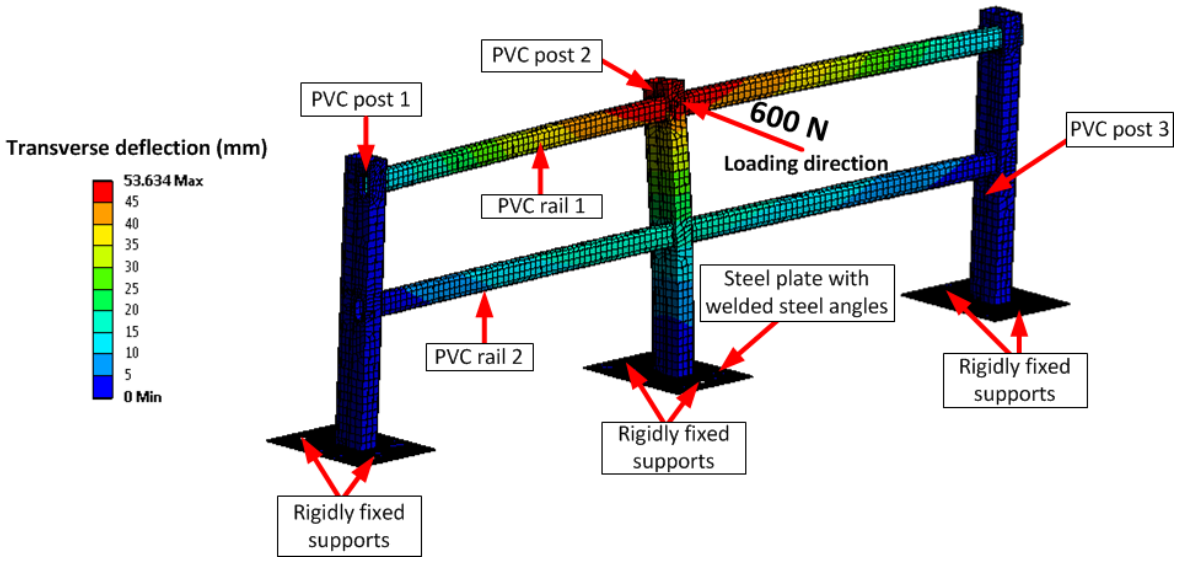

Figure 6.12: Contour plot showing the transverse deflection of the two-bay PVC fence for a maximum load of 600 N applied at the top of post 2 (Node C)

When the load was applied at Node C (top of the centre post), the deformation mode predicted by the FE analysis is shown in Figure 6.12, and this compares well with the experimental mode shown in Figure 5.24 (from Chapter 5). Similarly, the deformation mode observed from the experimental load tests (cf. Figure 5.23 from Chapter 5) on the two-bay PVC fence is identical to those shown in Figure 6.13 and Figure 6.14 when a maximum load of 600 N was applied at Nodes B and D, respectively.

Table 6.8 shows the results of the FE model of the two-bay PVC fence compared with the experimental transverse deflections for a load of 600 N applied at the top of the centre post (Node C) and mid-bay points (Nodes B and D). It is evident that the FE model and test values are in good agreement. When the load was applied at Node C (top of the centre post), the FE model deflection at Node C is 10 % lower than the experimental deflection. The FE deflections at Nodes B and D are almost equal to the experimental deflections when the load was applied at Node C, whereas, greater discrepancies of about 20 % are shown at Nodes A and E (outer posts). However, it should be appreciated that the actual differences in the deflections predicted by the FE model and the average experimental tests results were 0.5 mm and 0.3 mm for Nodes A and E, respectively, which are rather small. In general, the deflections predicted by the FE model at Nodes A – E when the load was applied at Node C, vary from approximately 10 % lower to 20 % higher than the experimental deflections (see Table 6.8).

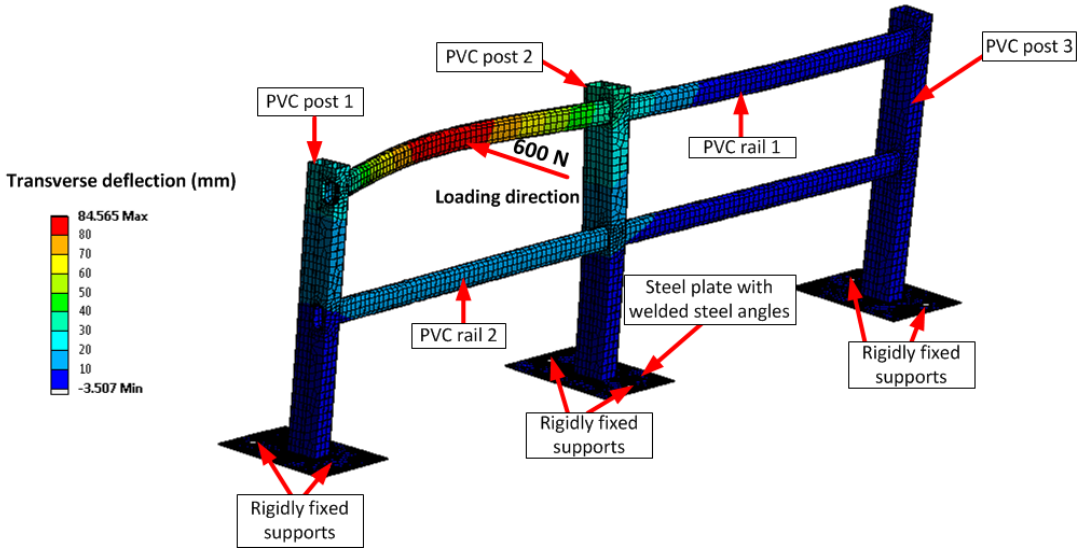

Figure 6.13: Contour plot showing the transverse deflection of the two-bay PVC fence for a maximum load of 600 N applied at Node B (mid-bay point)

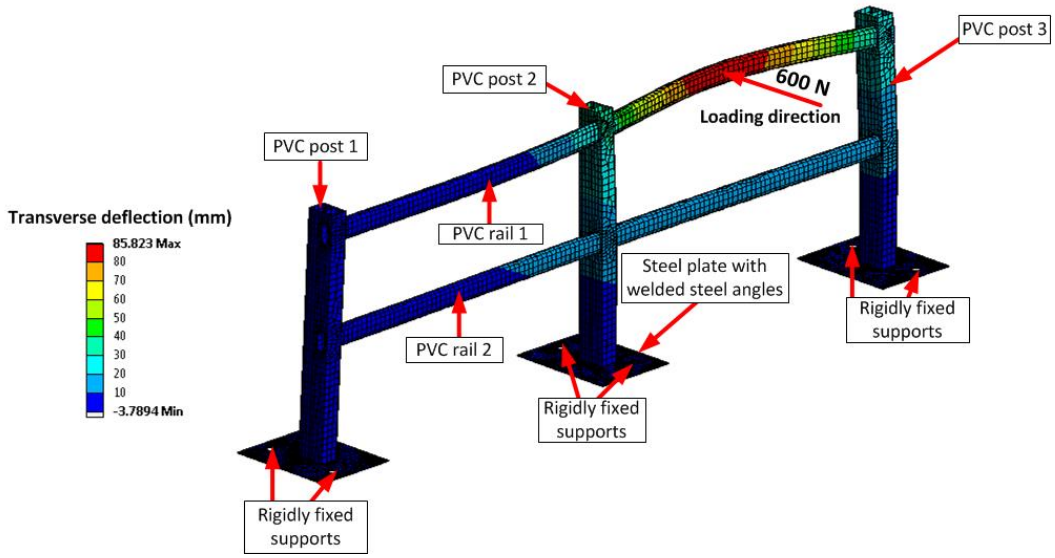

Figure 6.14: Contour plot showing the transverse deflection of the two-bay PVC fence for a maximum load of 600 N applied at Node D (mid-bay point)

Table 6.8: Comparison of two-bay PVC fence FE model with the experimental transverse deflections at Nodes A – E for a maximum load of 600 N applied at Nodes B – D

Analysis	Loading point	Transverse deflection [mm]				
		Node A	Node B	Node C	Node D	Node E
FE model	Node B	21.0	83.0	30.5	2.5	- 0.7
	Node C	2.6	31.9	44.4	30.9	1.9
	Node D	- 0.8	2.4	30.3	84.1	22.2
Experimental test result	Node B	15.4	85.9	35.4	3.3	- 0.9
	Node C	2.1	32.2	47.4	30.8	1.6
	Node D	- 0.2	2.0	30.6	84.4	20.8
FE model / Experimental deflection	**Node B**	**1.4**	**1.0***	**0.9**	**0.8**	**0.8**
	Node C	**1.2**	**1.0**	**0.9***	**1.0**	**1.2**
	Node D	**4.0**	**1.2**	**1.0**	**1.0***	**1.1**

* represents the deflection values at the same respective loading Node

The ratios between the FE model and the experimental deflections at the respective loading Nodes B, C and D are 1.0, 0.9 and 1.0, respectively. This shows that the deflections predicted by the FE analyses at the respective loading Nodes (asterisked in Table 6.8) show very good agreement with the experimental deflections.

The deflections at Nodes B and D when load was applied at these respective nodes were 83.0 mm and 84.1 mm, respectively, which are very close to each other, as expected. Also, it was expected that the deflection at Node A when the load was applied at Node B should be

the same as that of Node E when the load was applied at Node D. The deflections obtained from the FE model at Node A when load applied at Node B was 21.0 mm, which is also reasonably close to the deflection at Node E (22.2 mm) when load was applied at Node D. Similarly, the deflection at Node C should be the same when load was applied at Nodes B and D. When load was applied at Nodes B and D, the deflections predicted by the FE model at Node C were 30.5 mm and 30.3 mm, respectively showing almost equal values.

In general, when load was applied at Nodes B and D, It can be seen that the predicted FE deflections are in good agreement with experimental deflections, except for the corresponding deflections at Node A (see Table 6.8). The ratios between the FE model and the experimental deflection at Node A, when load was applied at Nodes B and D were 1.4 and 4.0, respectively. The relatively poorer agreement between the deflections at Node A when load was applied at Nodes B and D can be attributed to the fact the FE model of the PVC fence assumed that the cut-outs in the PVC posts were in complete contact with the faces/edges of the PVC rails (see Figure 6.15b), thus allowing a greater redistribution of load to the outer posts of the two-bay PVC fence. However, in practice, there were small clearances between the cut-outs and the faces/edges leading to relative movement (minor slip) at the PVC rail-to-post connections which limited load re-distribution effects across each bay of the two-bay PVC fence (see Figure 6.15a).

It is also worth noting that the experimental deflections at Node A (when load was applied at Node D) for Tests 1 – 3 were 0 mm, - 0.3 mm and - 0.4 mm, respectively (see Appendix 10). It is, therefore, evident that the aforementioned deflections are very small, and the differences between the experimental test results are presumably due to bedding-in effects. Furthermore, the actual difference between the predicted FE model and the average experimental deflection at Node A when load was applied at Node D was only 0.6 mm, even though the percentage difference appears significant.

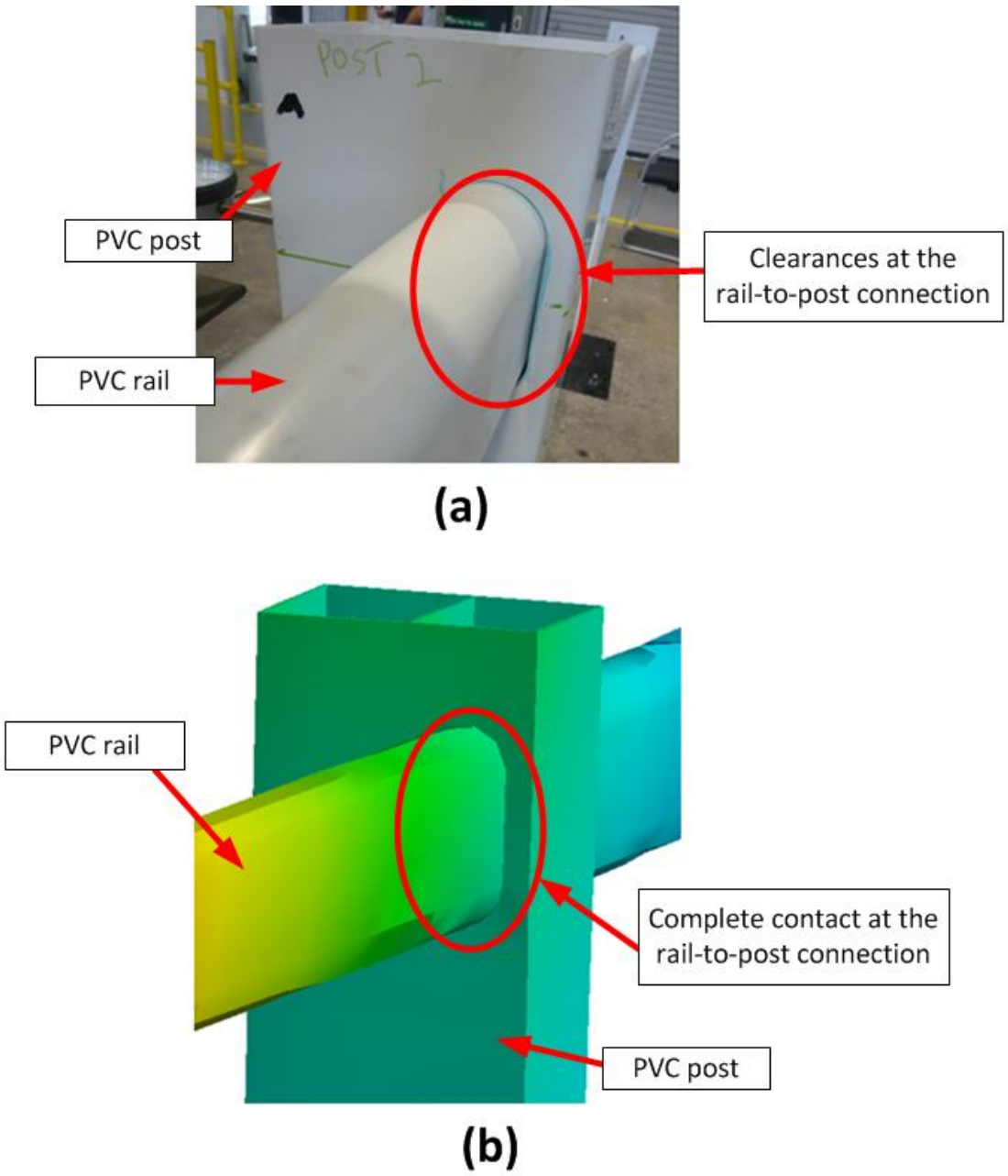

Figure 6.15: Images showing the (a) Experimental and (b) FE rail-to-post connections

6.7. Chapter Summary

Finite Element (FE) analyses of the two-bay timber and PVC post and rail fencing structures have been carried out, and compared with the experimental test results. Good correlation between the FE analyses and experimental test results has been demonstrated. Isotropic linear elastic FE models using ANSYS were able to predict the load-deformation responses of two-bay timber and PVC fences for reasonably large transverse deflections.

Line bodies utilising BEAM188 elements were used to represent the timber posts and rails for computational efficiency and the bolted base joints were represented with MPC184 elements (Multi-Point Constraint). Two FE models for the two-bay timber fence were analysed. FE Model 1 used rigidly fixed joints at the base of the timber posts, whereas, FE Model 2 used semi-rigid base joints with a joint rotational stiffness of 3 x 10^5 Nm/rad. The deflections predicted by FE Model 1 varied from about 18 - 24 % lower than those from the experimental tests, whereas, the deflections predicted by FE Model 2 vary from about 3 % lower to 18 % higher than the experimental deflections. The study showed that modelling a semi-rigid joint with a specified rotational stiffness (rather than rigidly fixed joints), improved the FE model of the cantilever beam and two-bay timber fence. The FE analyses have also shown that beam elements can predict the load-deformation response of the two-bay timber fence accurately.

SHELL181 elements were used to model the PVC posts and rails and the steel plate with welded steel angles. The six rail-to-post connections were modelled with CONTA174 and TARGE170 elements using ANSYS. Line loads were applied at the top of the centre post and the mid-bay points of the two-bay PVC fence. The ratios of the FE model to the experimental deflections at the loading nodes range from 0.9 to 1.0, reflecting good to excellent correlation with the experimental results at the respective loading nodes. When the maximum load of 600 N was applied at the top of the centre PVC post, the deflections predicted from the FE analysis varied from about 10 % lower to 20 % higher than the experimental deflections. On the other hand, greater differences between the predicted FE and experimental deflections were observed at the rail-to-post connection on the outer PVC posts when load was applied at the mid-bay points. This discrepancy has been discussed and is due to limited load re-distribution effects (across the two-bay fence during the experimental load tests) due to the presence of small clearances leading to relative movement (slip) at the interface between the cut-outs of the PVC posts and the edges/faces of the PVC rails. In contrast, the FE analysis assumed full interaction at the rail-to-post connections of the two-bay PVC fence model.

As reported in Chapter 5, the experimentally determined relative transverse stiffnesses of the two-bay timber and PVC fences were 51 N/mm and 14 N/mm, respectively. However, there were large differences in the flexural moduli of the timber sections (compared to

PVC). The experimental results in Chapter 4 showed that the average flexural modulus of the timber posts and rails varies from 8.1 - 13.5 GPa. Hence, a sensitivity analysis was carried out to investigate the effect of varying the flexural modulus of the post and rail sections of the two-bay timber fence. The findings from the FE analyses showed that using flexural moduli of 8.1 GPa and 13.5 GPa resulted in transverse stiffnesses of 49.1 N/mm and 74.1 N/mm, respectively, which represent lower and upper bound transverse stiffnesses of the two-bay timber fence.

A limitation with the FE analyses was the assumption of perfectly rigid rail-to-post joints, regardless of the fact that rail-to-post nailed joints (of the timber fence) have rotational stiffnesses. Similarly, as the FE analyses assumed full interaction at the rail-to-post connections of the two-bay PVC fence model, a more comprehensive FE analyses would be required to understand and model rail-to-post connections more accurately. In addition, although timber is an orthotropic and inhomogeneous structural material, simplified isotropic linear elastic FE models were created to simulate the structural behaviour of a two-bay timber fence. Further experimental testing would, therefore, be required to determine the mechanical properties in their transverse directions, and thus lead to the development of improved FE models.

In summary, FE analyses have been carried out to complement the physical testing work reported in Chapters 4 and 5, and this has found merit in predicting the load-deformation responses of the described two-bay timber and PVC fencing structures to a quantified degree of accuracy. Furthermore, the FE analyses may thus provide useful benchmarks for assessing and evaluating the transverse stiffness and load-deformation response of a fencing structure comprised of novel waste carpet structural composites.

7. Finite Element (FE) Modelling of Novel Carpet Structural Composite Fencing Structures

7.1. Introduction

This chapter describes the Finite Element (FE) modelling and analysis of a fencing structure comprised of novel waste carpet structural composite posts and rails. As the flexural modulus is a vital structural property and part of the information used in evaluating the load-deformation response of a fencing structure, the flexural moduli of the novel waste carpet structural Composites (A – C) have been determined and were given in Chapter 4. The test results from Chapter 4 showed that the average flexural modulus for Composite C (2.6 GPa) was significantly greater than those of the other novel waste carpet structural Composites A (0.047 GPa) and B (0.185 GPa). Nevertheless, the overall average flexural modulus for Composite C (2.6 GPa) is only about a quarter of that of timber (10 GPa) and very close to that of PVC (2.7 GPa).

Therefore, this chapter aims to investigate and optimise the load-deformation response of a novel waste carpet structural composite (Composite C) fence relative to those of similar timber and PVC fences. As there are no current load-bearing standards for equestrian fencing, the experimental results of the load tests carried out on the fencing structures in Chapter 5, act as the benchmark data. Analyses are carried out using the two-bay timber fence FE model developed using the ANSYS software described in Chapter 6. The comparisons and validations of the two-bay timber FE model with the experimental test results have shown that the FE model can be used with confidence to investigate the load-deformation response of a fencing structure comprised of novel structural composites. Thus, FE analyses are carried out and evaluated using the elastic properties of the Composite C material and the geometric properties of the two-bay timber fence. Thereafter, geometric optimisations and structural analyses via changes to the rectangular cross-sections of the Composite C posts and rails and their overall layout, are carried out and evaluated to achieve stiffness properties similar to those of the equestrian timber and PVC fences.

7.2. Investigation of the Load-Deformation Response of a Fencing Structure Comprised of Novel Waste Carpet Structural Composites

The deflections at the top of the centre posts corresponding to the applied maximum loads of 1400 N and 600 N were used to obtain a measure of the relative transverse stiffnesses for the two-bay timber and PVC fences, respectively. From the experimental tests described in Chapter 5, the relative transverse stiffnesses for the two-bay timber and PVC fences were 50.7 N/mm and 14.0 N/mm, respectively, reflecting that the former is significantly stiffer than the latter.

The FE model used to evaluate the load-deformation response of the two-bay timber fence was used for the investigation of the structural response of the fencing structure comprised of Composite C posts and rails. Composite C was chosen because it had a significantly greater flexural modulus of (2.6 GPa) compared to Composites A and B. The loading, boundary conditions, overall geometry and post/rail cross-section dimensions for the Composite C fence model were the same as that of the two-bay timber fence. Table 7.1 give details of the Composite C posts and rails used in the FE model, and the overall geometry of the two-bay Composite C fence FE model is given in Figure 7.1.

As the mechanical properties of the Composite C materials in their transverse directions were not determined from the experimental tests described in Chapter 4, isotropic linear elastic material models were used in the FE analyses. Furthermore, the fencing structures mainly resist bending in service; therefore, only the longitudinal post/rail elastic properties significantly affect the FE deflection results. The elastic flexural modulus and Poisson's ratio used for the Composite C posts and rails were 2.6 GPa and 0.3, respectively (see Chapter 4). BEAM188 elements were used to represent the Composite C posts and rails, and MPC184 elements were used to represent the joints at the base of the Composite C posts. The rotational stiffness with respect to the x-axis was 3×10^5 Nm/rad and the other five nodal displacements were set to zero at the base joints (see Nodes D – F in Figure 7.1). A load of 1400 N was applied at Node B (top of the centre post) in the negative z-direction (see Figure 7.1).

The FE analysis showed a deflection of 80.4 mm at the top of the centre post, based on an applied load of 1400 N at Node B. Based on the deflection and load applied at the top of the centre post, the relative transverse stiffness of the two-bay Composite C fence FE model was evaluated to be 17.4 N/mm. The aforementioned relative transverse stiffness of the two-bay Composite C fence FE model is compared with the experimentally derived transverse stiffnesses of the two-bay timber and PVC fences (see Chapter 5) in Figure 7.2. The results show that the transverse stiffness of the two-bay Composite C fence is 24.3 % greater than a similar PVC fence. On the other hand, it is evident that the relative transverse stiffness of the two-bay timber fence is about three times greater than a similar Composite C fence. This was expected as the experimentally derived flexural moduli of the timber posts and rails varied from 8.1 GPa – 13.5 GPa, and are significantly greater than the average flexural modulus of the Composite C material (2.6 GPa) (see Chapter 4).

Table 7.1: Details of the Composite C posts and rails used in the FE model

Composite C post/rail	Average width [mm]	Average depth [mm]	Second moment of area about plane of flexure [mm^4]	Flexural modulus [GPa]	Poisson's ratio
Post	122	71	3,638,762	2.6	0.3
Rail	93	37	392,561		

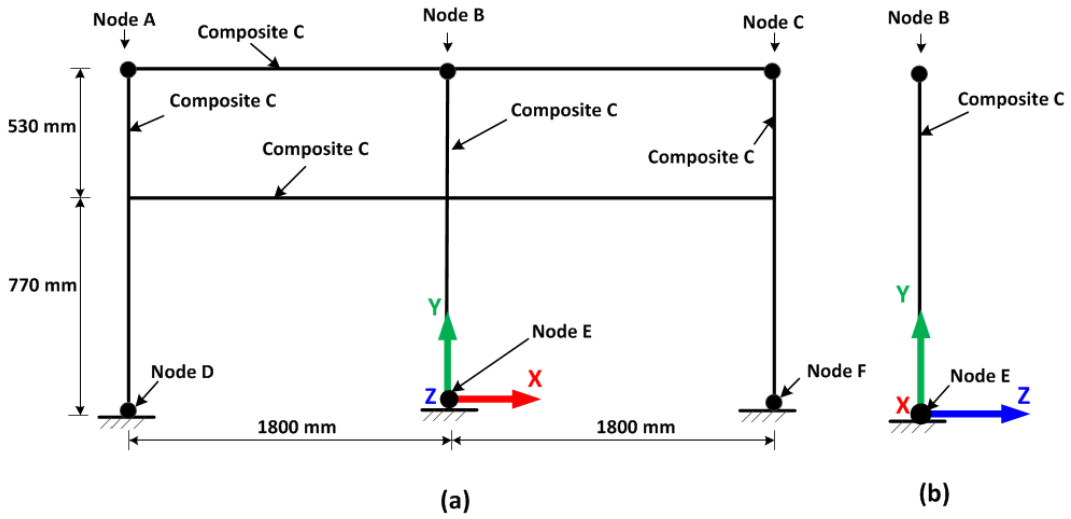

Figure 7.1: Overall geometry of the two-bay Composite C fence FE model: (a) Front-view (b) Edge-view from Node B to Node C

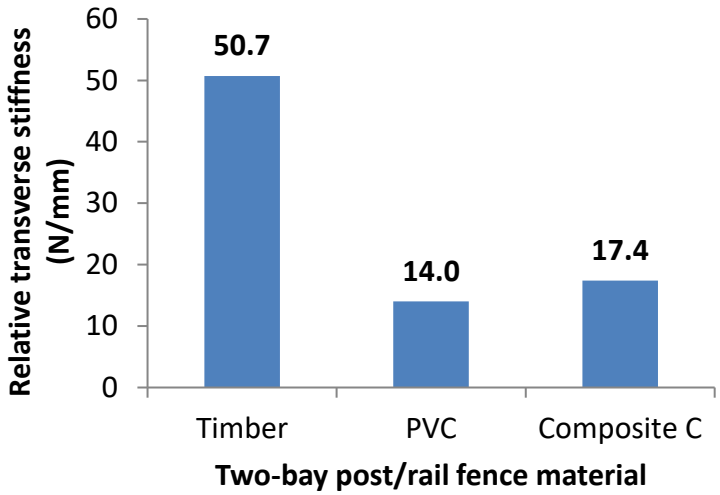

Figure 7.2: Comparison of the relative transverse stiffnesses of two-bay timber, PVC and Composite C fences

7.3. Design Optimisation and Structural Analyses

As a result of the relatively lower transverse stiffness of the two-bay Composite C fence compared to the timber fence, this section focusses on the design optimisation of the carpet composite (Composite C) posts and rails and the overall geometric layout of the structure to achieve a transverse stiffness similar to that of the timber fence. It should be noted that the ANSYS FE model described in Section 7.2 was used to carry out these optimisations and structural analyses.

7.3.1. Geometric Optimisation of the Cross-Sections of the Composite C Posts and Rails

An increase in the second moment of area of the members of a structure gives an increase in its overall stiffness (see Equation (1) in Chapter 4). Therefore, the second moment of area about the plane of flexure for the Composite C posts and rails were increased by increasing the depth of their respective cross-sections, whilst their widths remained constant (see Figure 7.3). The depths of the Composite C posts and rails were increased by a factor of two; the depth of the former was increased from 71 to 142 mm, and the latter from to 37 to 74 mm (in increments of 5 mm). It should be appreciated that the depths of the posts and rails were increased independently, not simultaneously. Figure 7.4 shows a plot of the maximum deflection against the depths of the Composite C posts and rails based on an applied load of 1400 N at the top of the centre post.

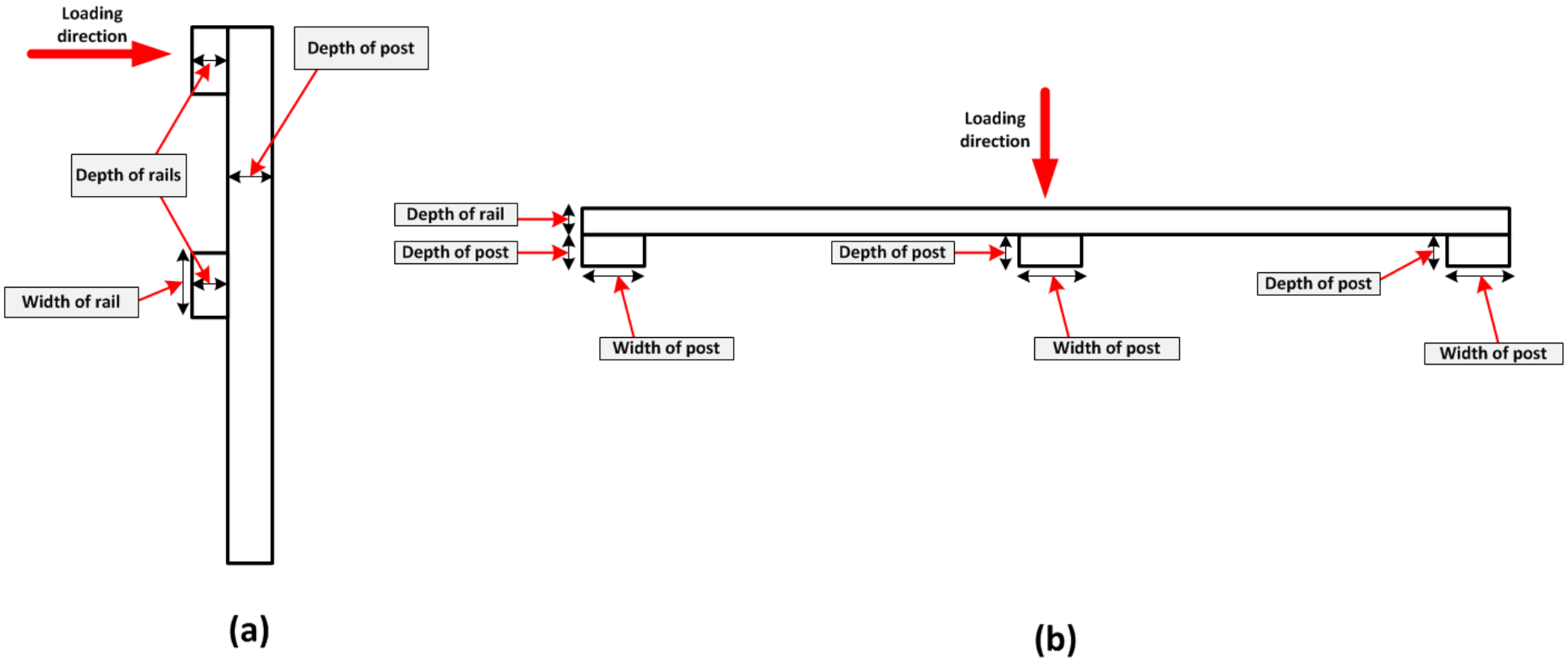

Figure 7.3: Sketches showing the depths and widths of the Composite C posts and rails that were optimised: (a) Edge-view and (b) Plan-view

Figure 7.4 shows that the maximum deflection gradually decreases towards an asymptotic value as the depths of the respective posts and rails increases. The analyses show that doubling the depths of each of the three posts of the two-bay Composite C fence reduced the maximum deflection from 80.4 to 19.5 mm, whereas doubling the depths of the two rails reduced the maximum deflection from 80.4 to 54.7 mm. These analyses thus reflect that an increase in the depths of the respective posts and rails by a factor of 2 gave reductions in the maximum deflections of 76 % and 32 %, respectively (see Figure 7.4). It is thus evident that increasing the second moment of area of the posts led to a greater reduction in the maximum deflection compared to increasing those of the rails. Therefore, increasing the flexural stiffnesses of the posts compared to the rails leads to a greater increase in the overall transverse stiffness of the fence structure.

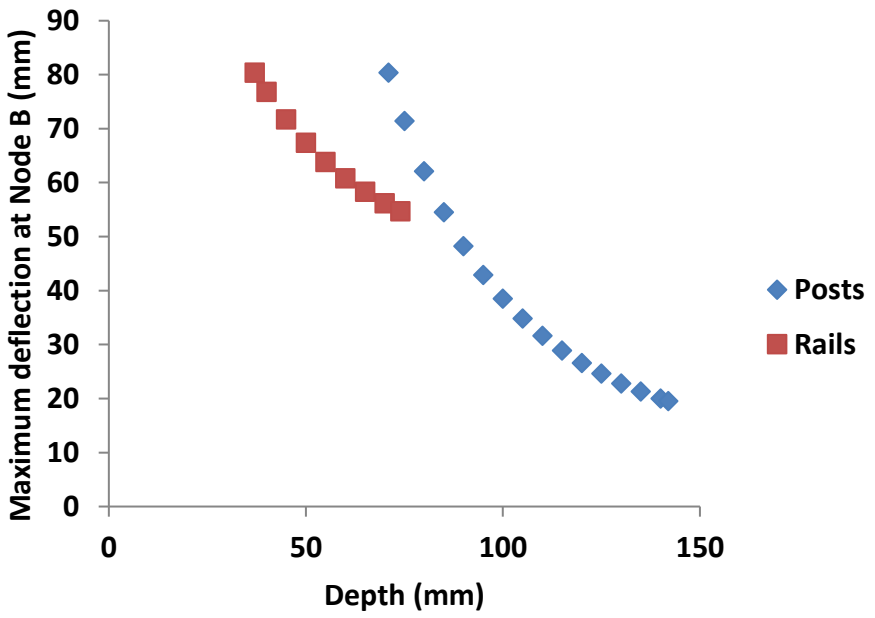

Figure 7.4: A plot of the maximum deflection against the depths of the Composite C posts and rails based on an applied load of 1400 N at the top of the centre post

7.3.2. Structural Optimisation through an Increase in the Number of the Composite C Posts and Rails of the Fencing Structure

An investigation was carried out into the effect of increasing the number of the Composite C posts and rails on the maximum deflection of the fencing structure when a load of 1400 N was applied at the top of the centre post. Sketches of the different geometric layouts comprising 2 – 5 rails and 3 – 9 posts are given in Figure 7.5 and Figure 7.6, respectively. Figure 7.5(a) – (d) were two-bay fencing structures with two, three, four and five rails, respectively. It should be noted that the spacing between the rails was reduced from 530 mm (from Figure 7.1) to 300 mm (see Figure 7.5); this was done to fit in five rails with equal distances (300 mm) between them. However, the adjustment of the geometric layout from Figure 7.1 to Figure 7.5a only resulted in a maximum deflection of 78 mm which is 3 % lower than the former, reflecting only a minor difference. On the other hand, although the overall boundary dimensions remained as 1300 by 3600 mm, the geometric layouts given in Figure 7.6 had different numbers of bays which varied in increments of two from two – eight. The cross-sections of the Composite C posts and rails were kept constant (see Table 7.1).

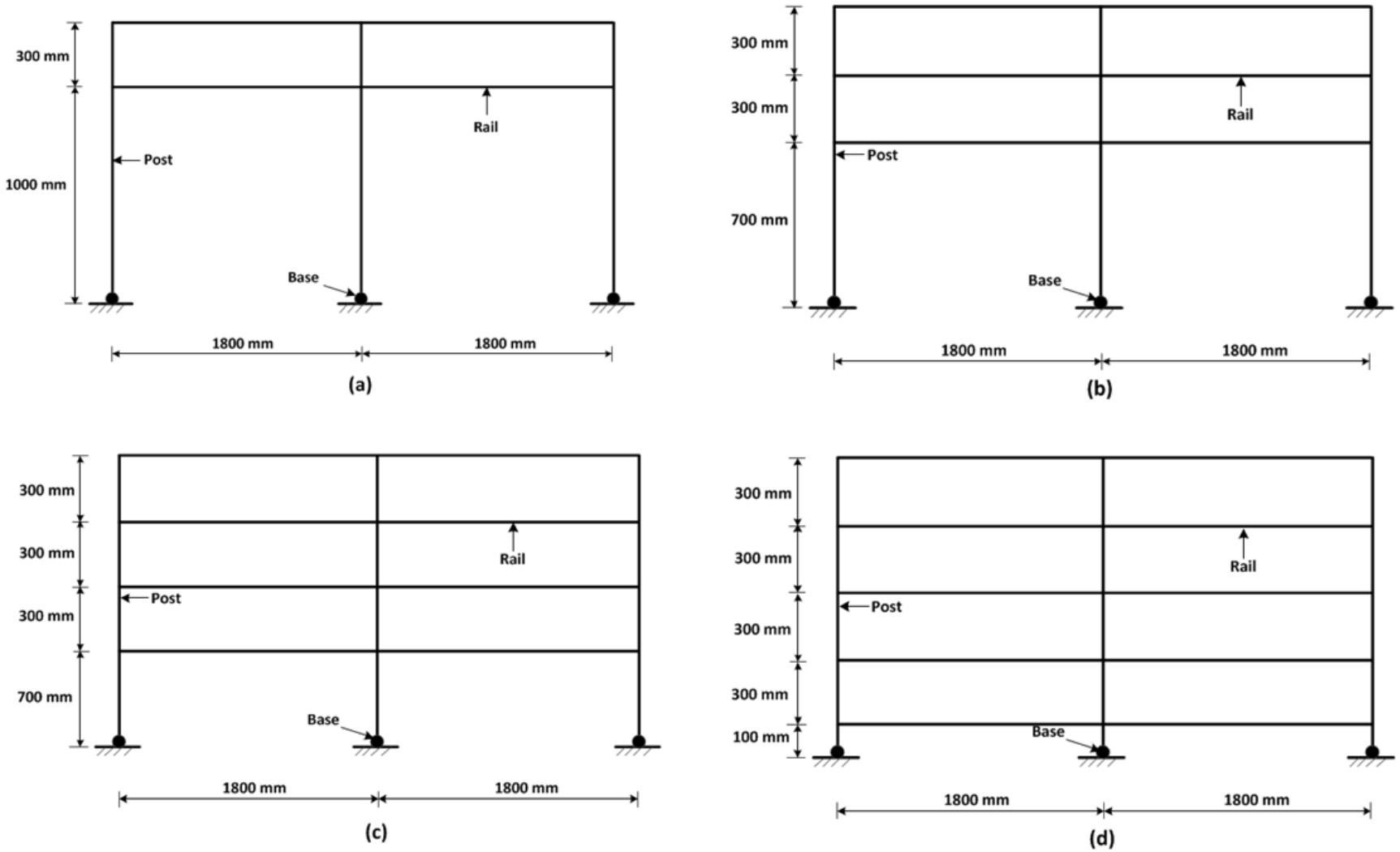

Figure 7.5: Details of the geometric layout with three posts and: (a) two rails (b) three rails (c) four rails and (d) five rails [not drawn to scale]

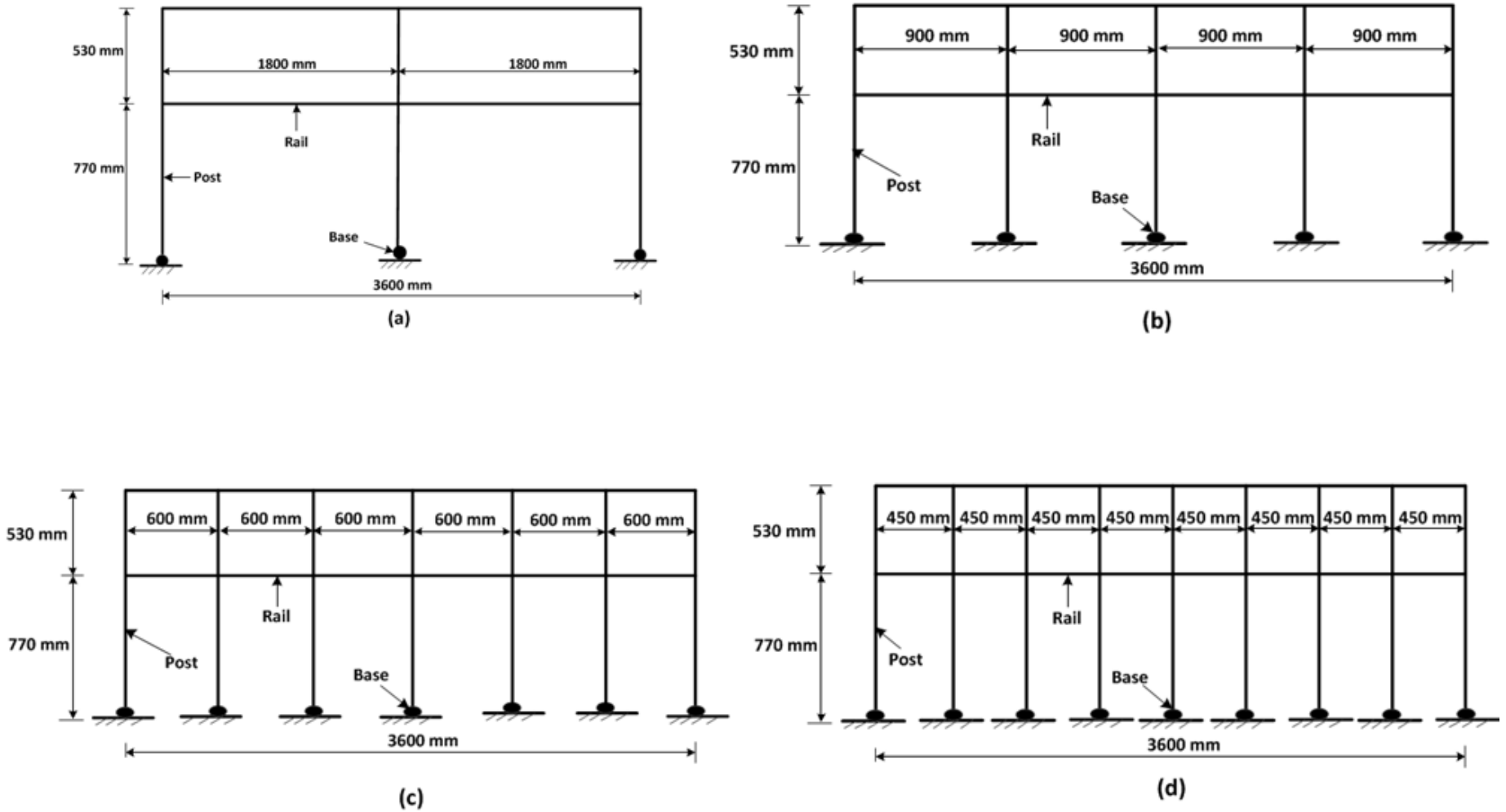

Figure 7.6: Details of the geometric layout with two rails and (a) three posts (b) five posts (c) seven posts (d) nine posts [not drawn to scale]

Figure 7.7 shows a plot of the maximum deflection against the number of the rails (2 – 5) based on an applied load of 1400 N at the top of the centre post. The result shows a gradual but insignificant reduction (approximately 6 %) in the maximum deflection from 78 to 73.6 mm, when the number of rails was increased from 2 – 5 rails. Figure 7.8 shows a plot of the maximum deflection against the number of posts (3 – 9); the result also shows that an increase in the number of the posts led to a significant reduction in the maximum deflection.

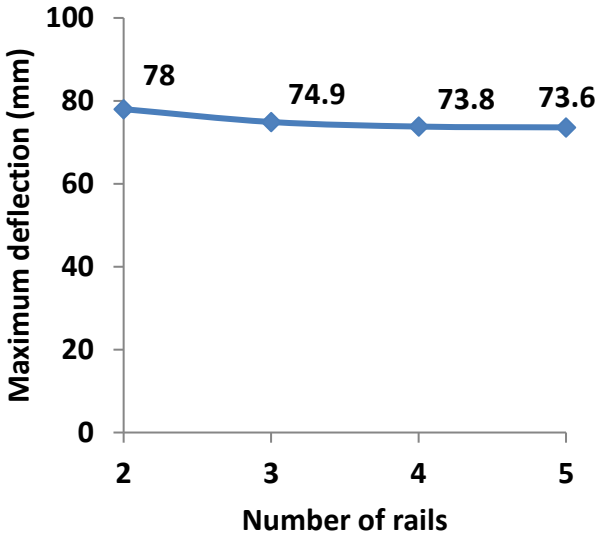

Figure 7.7: A plot of the maximum deflection against the number of the rails for an applied load of 1400 N at the top of the centre post

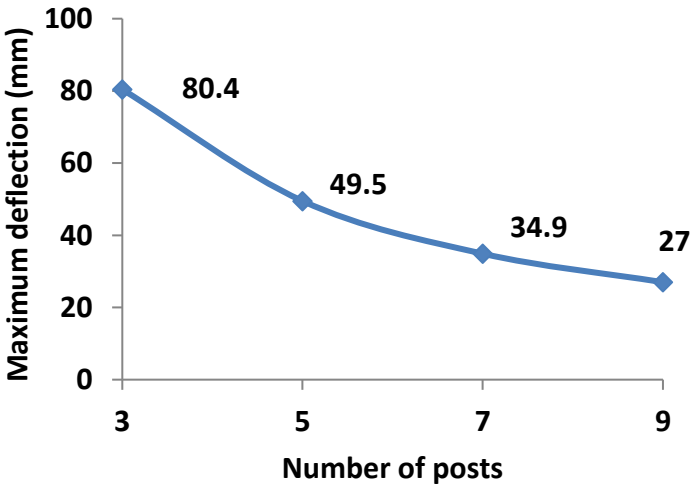

Figure 7.8: A plot of the maximum deflection against the number of the posts for an applied load of 1400 N at the top of the centre post

An increase in the number of Composite C posts from 3 to 9 posts led to a 66 % reduction in the maximum deflection, i.e. from 80.4 to 27 mm. It is evident that additional posts resulted in a greater reduction in the maximum deflection compared to an increase in the number of the rails. Furthermore, based on the maximum deflection of 27 mm at an applied load of 1400 N (at the top of the centre post), the transverse stiffness for the geometric layouts with 9 posts (see Figure 7.6) was 51.9 N/mm which is slightly greater than that of the two-bay timber fence of 50.7 N/mm. On the other hand, the transverse stiffnesses for the geometric layouts with 3, 5 and 7 posts were 17.4, 28.3 and 40.1 N/mm, respectively. The aforementioned transverse stiffnesses are lower than that of the timber fence, but are greater than that of the PVC fence.

7.3.3. Optimisation of the Cross-Sections of the Composite C Posts in the Geometric Layouts with 3, 5 and 7 Posts

Additional structural optimisations were carried out by increasing the depth of the Composite C posts by a factor of 2 (i.e. 71 to 142 mm) in increments of 5 mm for the geometric layouts with 3, 5 and 7 posts. The aim was to achieve a maximum transverse deflection similar to that of the timber fence, which was 27.6 mm and corresponds to a relative transverse stiffness of 50.7 N/mm. It should, therefore, be appreciated that there was no need to optimise the cross-section of the Composite C posts in the geometric layout with 9 posts (see Figure 7.6d), as it had a relative transverse stiffness of 51.9 N/mm (marginally greater than that of the timber fence). Figure 7.9 shows a plot of the maximum deflection against the depth of the posts for the geometric layouts with 3, 5 and 7 posts.

It should be noted that these maximum deflections are based on an applied load of 1400 N at the top of the centre post. The plots in Figure 7.9 all show a gradual reduction in the maximum deflection towards an asymptotic value. Increasing the depths of the posts by a factor of 2 (i.e. 71 to 142 mm) resulted in maximum deflections of 19.5, 14.4 and 10.3 mm for the geometric layouts with 3, 5 and 7 posts, respectively. These deflections also correspond to relative transverse stiffnesses of 71.8, 97.2 and 135.9 N/mm for the geometric layouts with 3, 5 and 7 posts, respectively. These aforementioned transverse stiffnesses are significantly greater than that of the timber fence, and thus, lead to a significant rise in the total masses of the Composite C posts and rails.

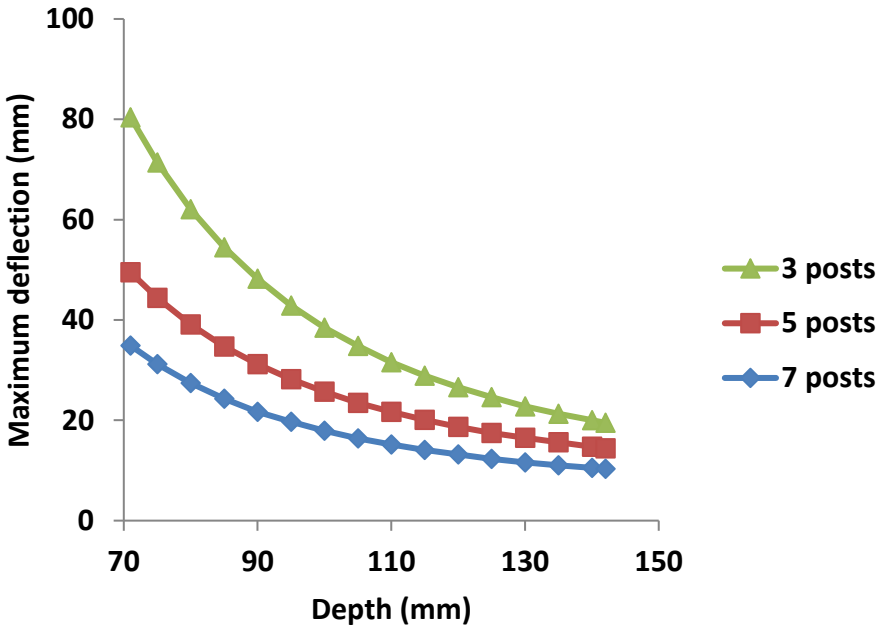

Figure 7.9: A plot of the maximum deflection against the depths of the posts for the geometric layouts with 3, 5 and 7 posts

In view of this, Table 7.2 gives the results of further structural analyses carried out to examine the maximum deflections and transverse stiffnesses for each depth increment. The analyses show that a 69 % increase in the depth of the Composite C posts for the geometric layout with 3 posts (shown in Figure 7.6a) resulted in a maximum deflection of 26.6 mm and corresponds to a transverse stiffness of 52.6 N/mm (see Table 7.2). Therefore, a width of 122 mm and depth of 120 mm of the rectangular cross-section posts (as opposed to 122 mm by 71 mm) gives a relative transverse stiffness of 52.6 N/mm, which is slightly greater than that of the timber fence (50.7 N/mm). Furthermore, a 41 % and 13 % increase in the depth of the Composite C posts for the geometric layouts with 5 and 7 posts, (shown in Figure 7.6b and c) respectively, also resulted to transverse stiffnesses marginally greater than that of the timber fence (see Table 7.2). Therefore, for the geometric layout with 5 posts (Figure 7.6b), the rectangular cross-section dimensions of the posts may be 122 mm (width) by 100 mm (depth) without any changes to the cross-sections of the rails given in Table 7.1. Similarly, for the geometric layout with 7 posts (Figure 7.6c), the depths of the posts may be increased to 80 mm, to give a transverse stiffness approximately equal to that of the two-bay timber fence, whilst the width of the posts and cross-section dimensions of the rails remain the same as those given in Table 7.1.

Table 7.2: Maximum deflections and transverse stiffnesses for different depths (71 – 142 mm) and number of posts (3, 5 and 7) based on an applied load of 1400 N at the top of the centre post

Width [mm]	Depth [mm]	Percentage increase in depth [%]	3 posts		5 posts		7 posts	
			Maximum deflection [mm]	Transverse stiffness [N/mm]	Maximum deflection [mm]	Transverse stiffness [N/mm]	Maximum deflection [mm]	Transverse stiffness [N/mm]
122	71	0	80.4	17.4	49.5	28.3	34.9	40.1
	75	6	71.4	19.6	44.4	31.5	31.2	44.9
	80	13	62.1	22.5	39.1	35.8	**27.4**	**51.1**
	85	20	54.5	25.7	34.7	40.3	24.3	57.6
	90	27	48.2	29.0	31.2	44.9	21.7	64.5
	95	34	42.9	32.6	28.2	49.6	19.7	71.1
	100	41	38.5	36.4	**25.7**	**54.5**	17.9	78.2
	105	48	34.8	40.2	23.5	59.6	16.4	85.4
	110	55	31.6	44.3	21.7	64.5	15.2	92.1
	115	62	28.9	48.4	20.1	69.7	14.1	99.3
	120	69	**26.6**	**52.6**	18.7	74.9	13.2	106.1
	125	76	24.6	56.9	17.5	80.0	12.3	113.8
	130	83	22.8	61.4	16.5	84.8	11.6	120.7
	135	90	21.3	65.7	15.6	89.7	11	127.3
	140	97	20.0	70.0	14.7	95.2	10.5	133.3
	142	100	19.5	71.8	14.4	97.2	10.3	135.9

The highlighted values (in green) give maximum deflections less than and transverse stiffnesses greater than those of the timber fence.
The dimensions of the geometric layout with maximum deflections and transverse stiffnesses highlighted in *bold* were used for further analyses in Section 7.4.

7.4. Comparison of the Number and Masses of Timber, PVC and Composite C Posts and Rails Required for a Typical Equestrian Fencing Arena

Four different geometric layouts have been optimised, and the analyses show that they give relative transverse stiffnesses very close to that of the timber fence. Therefore, it is of interest to determine and compare the total masses of their respective posts and rails. The details of the respective rectangular cross-sectional dimensions for the four geometric layouts (determined from Table 7.2) are also given in Table 7.3. The masses of the Composite C posts and rails were determined using the average density of Composite C (1275 kg/m^3).

Table 7.3: Total mass of Composite C posts and rails for four geometric layouts

Geometric layout	Composite C post/rail	Dimension [width x depth x length] [mm]	Number	Total mass [kg]	
Figure 7.6a	Post	122 x 120 x 1300	3	73	**105**
	Rail	93 x 37 x 3600	2	32	
Figure 7.6b	Post	122 x 100 x 1300	5	101	**133**
	Rail	93 x 37 x 3600	2	32	
Figure 7.6c	Post	122 x 80 x 1300	7	113	**145**
	Rail	93 x 37 x 3600	2	32	
Figure 7.6d	Post	122 x 71 x 1300	9	129	**161**
	Rail	93 x 37 x 3600	2	32	

The total mass of the Composite C posts and rails of the geometric layout in Figure 7.6d is 53.3 % greater than that of Figure 7.6a. The results in Table 7.3 also show that the geometric layout in Figure 7.6a has the lowest mass compared to the masses of the layouts in Figure 7.6b – d. Hence, from the point of view of added mass, it is more efficient to increase the relative transverse stiffness of the fencing structure, by increasing the depths of the posts' cross-sections rather than the number of the posts. Hence, the geometric layout in Figure 7.6a is proposed for the design of an equestrian fencing arena comprised of Composite C posts and rails.

In order to estimate the total mass of the Composite C posts and rails used for typical equestrian fences, an indicative number of timber and PVC posts and rails used for typical equestrian fences were obtained via prior communications with Equestrian Surfaces Ltd. Therefore, as the geometric layout in Figure 7.6a was chosen for further analyses, the number of Composite C posts and rails required for an equestrian fencing arena is the same as that of the timber posts and rails. More precisely, the cross-section dimensions of the Composite C rails and overall geometry of the fencing structure are the same as those of a typical equestrian timber fence. However, the cross-section dimensions for the Composite C posts are larger than those of the timber posts. The optimisation in Section 7.3.3 has shown that a 69 % increase in the depth of the cross-section of the Composite C posts (from 71 mm to 120 mm) gives a similar transverse stiffness to that of the timber fence. Using the aforementioned values, the number and total masses of the timber, PVC, Composite C posts and rails required for a typical equestrian fencing arena were evaluated and compared in Table 7.4, which shows that the total mass of the Composite C posts and rails is more than three times that of the timber posts and rails.

Table 7.4: Numbers and total masses of timber, PVC and Composite C posts and rails used for a typical equestrian fencing arena

Two-bay post/rail fence material		**Dimension [width x depth x length] [mm]**	**Average density* [kg/m^3]**	**Mass [kg]**	**Number**	**Total mass [kg]**	
Timber	Post	122 x 71 x 1300	521	5.9	75	443	**1052**
	Rail	93 x 37 x 3600	465	5.8	105	609	
PVC	Post	150 x 100 x 1300	1484	3.3	60	198	**639**
	Rail	108 x 50 x 4000	1175	4.9	90	441	
Composite C	Post	122 x 120 x 1300	1275	24.3	75	1823	**3482**
	Rail	93 x 37 x 3600	1275	15.8	105	1659	

*** - measured mass densities from Chapter 3**

Furthermore, the total mass of the PVC posts and rails is about 20 % of the total mass of the Composite C posts and rails used for a typical equestrian fencing arena. However, it is worth noting that PVC fences commonly utilise steel reinforcement to increase the overall stiffness and strength of the posts. The mass of the flat steel plate with two welded steel angles used to support the PVC posts in the load tests carried out on a representative two-bay PVC fence

(described in Chapter 5) was 14.8 kg. Based on the number of PVC posts, the total mass of the flat steel plates with two welded steel angles is 888 kg (60 x 14.8 kg). This shows that the total mass of the PVC posts and rails including the welded steel angles is 1527 kg, which is about 45 % greater than the total mass of the timber posts and rails (1052 kg) and about 44 % of the total mass of the Composite C posts and rails (3482 kg).

7.5. Comparison of the Embodied Energy for Composite C, Timber and PVC

As described earlier in Chapter 2, embodied energy mainly involves the energy involved in the processing of the materials until it is ready for use. Therefore, this section discusses the embodied energy for the Composite C and subsequently compared with those of PVC and timber obtained by Hammond and Jones (2011).

The power requirement and throughput of the UNTHA VR140 granulator were used to determine the energy consumed for the initial shredding process to be 0.07 MJ/kg (UNTHA, 2015). This value (0.07 MJ/kg) is also very close to that given by Shuaib and Mativenga (2016) and Witik et al. (2011), of 0.09 MJ/kg as the energy intensity for shredding waste as a pre-recycling process. Shuaib and Mativenga (2016) also stated that the shredding stage is not as energy intensive as subsequent recycling processes (i.e. extrusion, pressing). According to Song et al. (2009), the energy intensity for the hydraulic press and high-temperature extrusion processing stages are 12 MJ/kg and 19 MJ/kg respectively. Therefore, calculations based on the aforementioned energy intensities for the processing stages, were used to determine the embodied energy of the Composite C material.

The embodied energy of the Composite C material was thus evaluated to be 31.1 MJ/kg and according to Hammond and Jones (2011), the embodied energy for wood and PVC are 10 MJ/kg and 77.2 MJ/kg respectively. These results show that the embodied energy for PVC is greater than that of the Composite C material by 2.5. This is because PVC involves more production processes which are energy intensive, and are also typically derived from non-renewable fossil fuels. On the other hand, the embodied energy for the Composite C material is about a factor of three greater than that of wood (10 MJ/kg). Although the embodied energy for the Composite C material is greater than that of wood, it should however be highlighted that the embodied energy for the latter mainly involves the

processes (i.e. cutting, drying) required to process a tree trunk into a useful structural material and that global forest loss is occurring at a high rate of 13.7 million hectares per year and accounts for 12 % of global CO_2 emissions (Van der Werf et al., 2009). Given the aforementioned points, the sustainable production of Composite C, as an alternative to timber and PVC, thereby helps with the preservation of natural resources (i.e. non-renewable fossil fuel), decreased deforestation and diversion of carpet waste from landfill and incineration.

7.6. Assembly of the Novel Carpet Structural Composite Fencing Structures

Connections are important factors to be considered in the design of fencing structures. This is because connections are critical components that can affect the overall stiffness, strength and serviceability of fencing structures. Structural members can be connected by mechanical fasteners (such as nails, bolts, screws) or with the use of an adhesive or a combination of both mechanical fasteners and an adhesive (Baker, 2000). More precisely, the use of nails is the most common type of fasteners used in fencing structures (TRADA, 2012a). This is partly because nail fasteners are relatively easier to assemble (or disassemble) and are less sensitive to thermal, water and other environmental conditions compared to adhesive joints (Strong, 2008). Furthermore, mechanical fastening is usually the lower-cost assembly option compared to adhesive bonding because of its simplicity and low-cost tooling requirements (Baker, 2000).

Therefore, as a result of the aforementioned benefits (i.e. simplicity) of nailed connections in timber fencing structures, the use of nail fasteners is proposed for the assembly of the post and rail sections of the novel carpet composite fencing structure. Furthermore, the novel waste carpet composite posts can be concreted into the ground to serve as rigid supports for the rails. Additionally, other factors to consider in the design of the rail-to-post connection for the novel carpet composite fencing structure include the shape, size and material of the fastener, spacing between each fastener and the distance from each fastener to an end or edge of the post/rail to prevent structural failure at the location of the connections. As the connections of the structure were out of the scope for this research study, further research will be needed to investigate the suitability and properties of the

mechanical fasteners to be applied in practice alongside a good measure of sound engineering judgement.

7.7. Chapter Summary

The elastic properties of the waste carpet structural composite (Composite C) were used to carry out FE analyses (using ANSYS software) on post and rail fencing structures to investigate and compare the load-deformation responses with those of similar timber and PVC fences.

The loading, boundary conditions, overall geometry and post/rail cross-section dimensions for the Composite C fence model were the same as that of the two-bay timber fence described in Chapter 5. The initial results showed that using the original cross-sections of the timber posts and rails and the overall geometry of the timber fence, the relative transverse stiffness of the Composite C fence was 17.4 N/mm. This relative transverse stiffness (17.4 N/mm) is approximately 23 % greater than that of a similar PVC fence, and only about a third of that of a similar timber fence. However, structural analyses and design optimisations have shown that changes to the cross-sections of the waste carpet structural composite (Composite C) posts/rails and their overall geometric layout resulted in an increase in the relative transverse stiffness. The study also shows that additional posts and rails increased the overall transverse stiffness of the fencing structure. Furthermore, geometric optimisations of the cross-sections of the posts and/or increase in the number of posts led to a greater rise in the relative transverse stiffness of the fencing structure compared to similar optimisations of the rails.

The study also shows that a 69 % increase in the depth of the cross-section of the Composite C posts (from 71 to 120 mm) resulted in a transverse stiffness similar to that of the timber fence, which is greater than that of the PVC fence by a factor of 3.8. This relative transverse stiffness of 52.6 N/mm was achieved with a lower mass compared to alternative geometric layouts which involved increasing the number of posts to achieve a similar transverse stiffness.

Also, the analyses carried out in this chapter showed that the number of Composite C posts and rails required for a typical equestrian fencing arena is the same as that of the timber

posts and rails. However, the cross-section dimensions for the Composite C posts are larger than those of the timber posts. The total mass of the timber, PVC and Composite C posts and rails required for a typical equestrian fencing arena were compared. The results showed that the total mass of the Composite C posts and rails is more than three times greater than that of the timber posts and rails. Also, the total mass of the Composite C posts and rails is greater than that of the PVC posts and rails (with welded steel angle reinforcement) by a factor of 2.

8. Conclusions and Recommendations for Further Research

8.1. Conclusions

This research was in collaboration with a small local industry (ECO2 Enterprises) and sought to develop and characterise structural materials from carpet waste, which can be used for equestrian fencing. The benefits of this novel approach include the reduction of carpet waste sent to landfill annually and the replacement of common equestrian timber and PVC fencing materials.

A comprehensive literature review of waste carpet structural composites alongside timber and PVC materials was carried out. The review showed that about 400,000 tonnes of carpet waste are disposed to UK landfill sites annually due to the difficulty associated with processing them into feasible alternative commodities. Furthermore, there are limited studies that have investigated the viability of using carpet waste within structural composites, and estimates from the literature indicate that a tonne of recycled carpet waste saves 4.2 tonnes CO_2 emissions. The literature studies have focussed on carpets with synthetic fibres/man-made face fibres (i.e. nylon, polypropylene etc.) and isolated those with natural face fibres (i.e. wool). Also, some of the manufacturing processes for the carpet structural composites included the addition of glass fibres and comprised of energy intensive stages which may be uneconomical and therefore reduces the environmental benefits.

The literature review also showed that there is no legislative requirement for the load-bearing characteristics for equestrian fencing. However, timber and PVC are very common materials used for equestrian fencing. The flexural modulus is an important property used in evaluating the stiffness of fencing structures. Timber is anisotropic, and its flexural moduli in the longitudinal direction (parallel-to-the-grain) and tangential/radial direction (perpendicular-to-the-grain) range from 7 – 20 GPa and 0.23 – 1.33 GPa, respectively. Hence, timber is typically loaded parallel-to-the-grain. On the other hand, PVC has a lower flexural modulus of about 2.5 GPa; therefore, PVC equestrian fencing structures typically utilise steel reinforcement to increase the stiffness and strength of the post. Furthermore, the production of PVC involves multi-stage processes which are energy intensive, and its

raw materials are derived from non-renewable fossil fuels. Although timber possesses greater environmental benefits compared to rigid PVC, global forest loss is also occurring at a high rate of 13.7 million hectares (137,000 km^2) per year and deforestation accounts for about 12 % of global CO_2 emissions. Timber is also susceptible to degradation, and its mechanical properties vary widely and are affected by several factors i.e. presence of knots, moisture content, species type etc.

Given the challenges associated with carpet waste and fabrication of waste carpet structural composites reported in the literature, prototype Composites A – C were manufactured from carpet waste. Composites A and B consisted of a polyurethane polymer matrix enclosing a bonded carpet strip core. The polyurethane formulation for Composite B included 2 wt. % CoatForce10 (CF10) fibre filler. The manufacturing process for Composite C included shredding, granulation and extrusion of strips of carpet waste, before being moulded with no second phase polymer addition. The manufacturing processing options for the prototype novel waste carpet structural Composites A – C may be used for carpets with synthetic/man-made and/or natural face fibres. In addition, the manufacturing processes did not involve mechanical separation of the carpet fibres. Therefore, this approach may be used to manufacture structural composites containing substantial volumes of carpet waste.

Experimental tests were carried out to determine the mechanical properties of the prototype novel waste carpet structural Composites A – C, timber and PVC equestrian fencing materials. As polyurethane was used as the matrix for the waste carpet structural Composites A and B, three-point bending tests were carried out to determine the relative flexural properties of unfilled polyurethane and 9 wt. % CF10 fibre filled polyurethane beams; the average flexural moduli for the former and latter were 114 MPa and 159 MPa, respectively, reflecting a 40 % increase in the flexural modulus due to the filler. Also, the average flexural strengths for the unfilled and filled (with 9 % CF10 fibre addition) polyurethane beams were 4 MPa and 4.3 MPa, respectively, which are reasonably close.

An element of this study involved the investigation of the mechanical properties of bonded single-lap joints of waste wool carpet strips at different orientations (Tuft-to-Tuft, Tuft-to-Back, Back-to-Back). Tensile tests were carried out on a limited number of samples of these bonded carpet strips to determine their ultimate shear strengths. The test results showed

that the Back-to-Back orientations had the highest shear strength, whereas the Tuft-to-Tuft orientation had the lowest shear strength. This information helps to define the suitability of the orientation of the bonded carpets strips to be used in the novel waste carpet structural composite. Based on the limited study, the test results, therefore, indicate that the Back-to-Back bonded joint orientation may be most suitable for inclusion in the fabrication of waste carpet structural composites. However, further testing of more bonded lap joints of waste wool carpet strips would be required to fully understand their properties as a sandwich core in structural composites.

The experimentally derived flexural moduli of timber and PVC were compared with those of the novel waste carpet structural Composites A – C. The results showed that the average flexural modulus of Composite C was significantly greater than those of Composites A (0.047 GPa) and B (0.185 GPa). In addition, the average flexural moduli of Composite C (2.6 GPa) and PVC (2.7 GPa) are reasonably close. Nevertheless, the overall average flexural modulus for Composite C is only about a quarter of that of timber which ranges from 8.1 – 13.5 GPa. The average flexural strength for Composite C was 29.2 MPa. Scanning Electron Microscopy (SEM) images also showed that the failure modes and variations in the mechanical properties of the Composite C materials may be attributed to the presence of flaws (such as voids), impurities and dirt particles in the raw material (waste carpet), processing conditions, as well as the type and source of carpet waste used.

The average elastic tensile modulus of Composite C was 2.7 GPa, and the average tensile strength was 14.5 MPa. Similarly, uniaxial tensile tests were carried out on PVC coupons, and their average tensile modulus (elastic) and strength was 3.4 GPa and 44.6 MPa, respectively. The experimental uniaxial tensile test results showed that the average tensile modulus of PVC is about 26 % greater than that of Composite C. Also, the average tensile strength of the PVC coupons is about three times greater than that of the Composite C material. Furthermore, compression tests carried out on timber sections showed that the average compressive strengths parallel-to- and perpendicular-to-the-grain were 26.7 and 1.7 MPa, respectively; these results also demonstrate that timber is highly orthotropic and has significantly greater compressive strength parallel-to-the-grain compared to perpendicular-to-the-grain.

This project also investigated experimental load tests and Finite Element (FE) modelling of two-bay timber and PVC post and rail fences which are representative of typical multi-bay fencing systems. The load tests and FE analyses were evaluated to determine the load-deformation responses of the two bay timber and PVC fences. Isotropic linear elastic FE models using ANSYS were able to predict the load-deformation responses of the fencing structures for reasonably large transverse deflections. BEAM188 elements were used to represent the timber posts and rails for computational efficiency and the bolted base joints were represented with MPC184 elements (Multi-Point Constraint). SHELL181 elements were used to model the two-bay PVC fencing structure. The six rail-to-post connections were modelled with CONTA174 and TARGE170 elements. In general, good correlation between the FE analyses and experimental test results was demonstrated. Furthermore, computationally efficient beam and shell elements were able to predict accurately the load-deformation responses of the two-bay timber and PVC fencing structures, respectively. The FE analyses also showed that modelling a semi-rigid joint with a specified rotational stiffness (rather than rigidly fixed joints), improved the FE model of the two-bay timber fence. The load tests on the two-bay timber and PVC fences were evaluated to give relative transverse stiffnesses of 50.7 N/mm and 14.0 N/mm, respectively, which demonstrated that the former is about 262 % stiffer than the latter. These aforementioned results were also used as the benchmark data for equestrian fencing structures and for assessing the stiffness requirements of the novel waste carpet structural composites (Composite C).

Furthermore, this study investigated the novel waste carpet structural composites (Composite C) as the posts/rails of an equestrian fencing structure. Composite C was chosen because it had a significantly greater flexural modulus compared to Composites A and B. The FE model for the timber fence was used to analyse the load-deformation response of Composite C post and rail fences, whilst varying their geometric layouts and the cross-sections of the posts and rails. Using the average flexural modulus of Composite C (2.6 GPa), and the overall geometry of the timber fence, the relative transverse stiffness of the two-bay Composite C post and rail fence was 17.4 N/mm, which is 23 % greater than that of the PVC fence, and about 66 % lower than that of a similar timber fence.

Therefore, design optimisation via geometric changes to the Composite C fence was carried out to achieve a relative transverse stiffness similar to that of a timber fence. The research

demonstrated that additional posts and rails increased the overall transverse stiffness of the Composite C fence. Furthermore, geometric optimisations of the cross-sections of the posts and/or increasing the number of the posts led to a greater increase in the relative transverse stiffness of the fencing structure compared to similar optimisations of the rails. In addition, from the point of view of added mass, it is more efficient to increase the relative transverse stiffness of the fencing structure, by increasing the depth of the posts' cross-sections rather than that of the rails and/or number of the posts/rails. More precisely, the study showed that a 69 % increase in the depth (from 71 to 120 mm) of the Composite C posts resulted in a transverse stiffness similar to that of the timber fence. The analysis thus demonstrates that the number of Composite C posts and rails required for a typical equestrian fencing arena is the same as that of the timber posts and rails.

In general, structural analyses and testing have shown that changes to the cross-sections of the Composite C posts/rails and their layout demonstrate the potential of recycled carpet waste composites as alternatives to common structural materials (i.e. timber and PVC) for equestrian fencing structures. Furthermore, this study has demonstrated the prospect of a viable remediation pathway for carpet waste, and the possibility of economic and environmental benefits.

8.2. Recommendations for Further Research

Following the study reported in this thesis, the following investigations are suggested for future research:

8.2.1. Optimisation of the Design and Manufacturing Processing Conditions for Waste Carpet Structural Composites

The results of the experimental tests showed variation in the mechanical properties of the prototype composites partly due to the processing conditions. Although the use of modern automated equipment may reduce the presence of flaws and geometric imperfections, there is a need for further research on the use of suitable compatibilizers or binding agents to enhance the miscibility and compatibility of the different carpet constituents and eliminate the presence of flaws, defects and voids, leading to more consistent mechanical properties of the waste carpet structural composites. Furthermore, there were limitations in the number of prototype samples manufactured and tested. Therefore, in order to further

characterise the mechanical properties of the novel composites, it is essential to carry out more repeat tests on more prototype samples. This will give an indication of their repeatability as well as an improved understanding of the waste carpet structural composites and their suitability for use as equestrian fencing materials.

The analysis in Chapter 7 also showed that the total mass of the Composite C posts and rails required for a typical equestrian fencing arena is significantly greater than those of timber and PVC. For this reason, it is worth exploring the option of designing the Composite C posts and rails as sandwich components to reduce their overall mass. This is because sandwich composites have high flexural stiffness with a relatively lower mass alongside good energy absorption capabilities. Their advantages also include efficient material usage, which, in turn, may maximise economic and environmental benefits.

As the waste carpet structural composites are intended to be used in an outdoor environment, further research with a view to understanding the effect of different environmental conditions (i.e. temperature changes and ultra violet (UV) degradation) on their mechanical properties and failure modes should be undertaken. In addition, developing an understanding of their resistance to moisture, weathering and biological attack is important and may also involve investigations of suitable stabilisers or preservatives to prolong service life.

8.2.2. Further Study on the Experimental and Finite Element Analyses of Fencing Structures

More repeats of the experimental tests on the equestrian fencing structures at different loading orientations are essential in developing a more comprehensive understanding of these structures. Finite Element analyses were carried out in this study to complement the physical testing. For simplicity and based on the material properties available, the post and rail sections of the FE models were modelled as linear elastic isotropic materials. However, more repeat tests to determine additional material properties of the posts and rails in their transverse directions will contribute to the development of improved FE models of the fencing structures.

In addition, the evaluation of a suitable failure criterion (based on the materials' strengths) in the FE models is vital and useful in predicting the failure initiation and propagation in the posts and rails. Other assumptions made in the FE analyses include perfectly rigid rail-to-post nailed joints of the timber fence and full interaction at the rail-to-post connections of the PVC fence model. Therefore, additional experimental testing to characterise the mechanical properties of rail-to-post connections would be useful in the design of equestrian fencing structures. Furthermore, as all joints possess finite rather than infinite stiffnesses, further study would also be required, to model these connections more precisely.

8.2.3. Experimental Load Tests on a Novel Waste Carpet Structural Composite Post and Rail Fencing Structure

The comparisons and validations of the two-bay timber FE model with the experimental test results showed that the FE model could be used satisfactorily to investigate the load-deformation response of a fencing structure comprised of novel waste carpet structural composites. However, experimental load tests including static, collapse and impact testing of the fencing structures are important and should form part of any future research. In addition, as equestrian fencing structures typically resist different types of combined loading (i.e. impact and bending); further work is essential in evaluating and quantifying the loading conditions of other practical scenarios that these structures may undergo whilst in service. These analyses will further enhance the understanding of the structural response of fencing structures, and possibly lead to useful structural design guidance.

8.2.4. Economic and Life Cycle Assessment

Estimates from the literature indicate that each tonne of recycled carpet saves 4.2 tonnes of CO_2 emissions, which suggests that this recycling approach offers environmental benefits and possibly economic benefits. However, life cycle assessments may vary considerably and depend on the processing stages involved in the production of the recycled novel waste carpet structural composites.

Therefore, as the rationale for this research is partly to reduce carpet waste going to landfill, and also replace timber and PVC materials, it is important to undertake detailed economic cost and life cycle assessments of waste carpet structural composite fencing systems from

initial production through to the point of installation, and provide comparisons with alternative structural systems (i.e. timber and PVC fencing). In order to comprehensively assess the life cycle of these novel materials, it is essential to consider important factors such as the type and quantity of raw materials, energy input and resulting emissions from the manufacturing processes, transportation cost, service life and end-of-life stage. Furthermore, as sustainability remains a major goal of the current economic and environmental agenda, it is also vital to consider emerging market and economic opportunities (such as job creation) and the geographical impact that may occur as a result of the successful application of the recycling approach proposed in this thesis.

References

ABATE, K. 2007. Formulating for Extruding Rigid PVC Fenestration Products. *The Chemist,* 84**,** 2-11.

ABRAMOFF, M. D., MAGALHAES, P. J. & RAM, S. J. 2004. Image Processing with ImageJ. *Biophotonics International,* 11**,** 36 - 42.

AGARWAL, S. & GUPTA, R. K. 2011. Plastics in Buildings and Construction. *In:* KUTZ, M. (ed.) *Applied Plastics Engineering Handbook.* Oxford: William Andrew Publishing.

AKOVALI, G. 2012. Plastic Materials: Polyvinyl Chloride (PVC). *In:* PACHECO-TORGAL, F., JALALI, S. & FUCIC, A. (eds.) *Toxicity of Building Materials.* Oxford: Woodhead Publishing.

ALOMAYRI, T., ASSAEDI, H., SHAIKH, F. U. A. & LOW, I. M. 2014. Effect of water absorption on the mechanical properties of cotton fabric- reinforced geopolymer composites. *Journal of Asian Ceramic Societies,* 2**,** 223-230.

AMERICAN CHEMISTRY COUNCIL. 2008. *The Economic Benefits of Polyvinyl Chloride in the United States and Canada*

[Online]. Available: http://www.pvc.org/upload/documents/The_Economics_of_PVC.pdf [Accessed 17th February 2016].

ANSYS. 2016. *BEAM188 3-D Linear Finite Strain Beam* [Online]. Available: http://www.ansys.stuba.sk/html/elem_55/chapter4/ES4-188.htm [Accessed 2nd July 2016].

ANSYS WORKBENCH RELEASE 15 User's Guide ANSYS Inc.

ASHBY, M. F. & JONES, D. R. H. 2006. *Engineering materials 2 : an introduction to microstructures, processing and design,* Oxford, Butterworth-Heinemann.

ASIF, M. 2009. Sustainability of timber,wood and bamboo in construction. *In:* KHATIB, J. (ed.) *Sustainability of Construction Materials.* Cambridge: Woodhead Publishing Limited.

ASIF, M., DAVIDSON, A. & MUNEER, T. 2002. Life Cycle of Window Materials - A Comparative Assessment. Millennium School of Engineering Napier University, Edinburgh.

ASTM F964 2013. Standard Specification for Rigid Poly (Vinyl Chloride) (PVC) Exterior Profiles Used for Fencing and Railing. West Conshohocken, PA: ASTM International.

ASTM F1999 2006. Standard Practice for Installation of Rigid Poly(Vinyl Chloride) (PVC) Fence Systems. West Conshohocken, PA: ASTM International.

ASTM STANDARD D143 2009. Standard Test Methods for Small Clear Specimens of Timber. West Conshohocken, PA: ASTM International.

BAJRACHARYA, R. M., MANALO, A. C., KARUNASENA, W. & LAU, K.-T. 2016. Characterisation of recycled mixed plastic solid wastes: Coupon and full- scale investigation. *Waste management (New York, N.Y.),* 48**,** 72.

BAKER, A. A. 2000. *Composite Materials for Aircraft Structures [electronic resource]*, Reston : American Institute of Aeronautics and Astronautics.

BAKIS, C. E., BANK, L. C., BROWN, V., COSENZA, E., DAVALOS, J., LESKO, J., MACHIDA, A., RIZKALLA, S. & TRIANTAFILLOU, T. C. 2002. Fiber- reinforced polymer composites for construction- state-of-the- art review. *J. Compos. Constr.*

BERENGUER, E., FERREIRA, J., GARDNER, T. A., ARAGÃO, L. E. O. C., DE CAMARGO, P. B., CERRI, C. E., DURIGAN, M., OLIVEIRA, R. C. D., VIEIRA, I. C. G. & BARLOW, J. 2014. A large-scale field assessment of carbon stocks in human-modified tropical forests. *Global change biology.* [Online]. Available: http://dx.doi.org/10.1111/gcb.12627.

BERTO, J. 2003. *Fencing system*. US patent application 6585234 B2.

BHS. 2014. *GUIDELINES FOR THE KEEPING OF HORSES:STABLE SIZES, PASTURE ACREAGES AND FENCING* [Online]. The British Horse Society. Available: http://www.bhs.org.uk/~/media/BHS/Files/PDF%20Documents/Guide%20for%20the%20Keeping%20of%20Horses.ashx [Accessed 1 August 2014].

BIEHL, M., PRATER, E. & REALFF, M. J. 2007. Assessing performance and uncertainty in developing carpet reverse logistics systems. *Computers & Operations Research,* 34**,** 443-463.

BIRD, L. 2013. *Carpets - Moving from Waste to Resource* [Online]. Carpet Recycling UK. Available: http://www.carpetrecyclinguk.com/downloads/Carpet_Recycling_UK_Annual_Report_and_2020_Vision_Jane_Gardner_Carpet_Recycling_UK.pdf [Accessed 23 May 2014].

BIRD, L. 2014. *Carpet Recycling UK Conference* [Online]. Carpet Recycling UK. Available: http://www.carpetrecyclinguk.com/downloads/27_percent_landfil_diversion_how_t

he UK exceeded its targets two years early Laurance Bird and Jane Gardner Carpet Recycling UK.pdf [Accessed 26 July 2014].

BLUNDELL, E. 2010. *The effects of dressage competitions on the mechanical properties of a synthetic equestrian arena surface.* MSc, University of Central Lancashire.

BOLDEN, J., ABU-LEBDEH, T. & FINI, E. 2013. Utilization of recycled and waste materials in various construction applications *American Journal of Environmental Sciences,* 9**,** 14-24.

BRAUN, D. 2002. Recycling of PVC. *Progress in Polymer Science,* 27**,** 2171-2195.

BRITISH PLASTICS FEDERATION. 2015. *Polyvinyl Chloride PVC* [Online]. Available: http://www.bpf.co.uk/plastipedia/polymers/pvc.aspx [Accessed 4 February 2016].

BS 1722-7 2006. Fences. Specification for wooden post and rail fences. London: British standards Institution.

BS 14122-3 2016. Safety of machinery. Permanent means of access to machinery. Stairs, stepladders and guard-rails London: British Standards Institution.

BS EN 178 2013. Plastics - Determination of flexural properties London: British Standards Institution.

BS EN 338 2009. Structural timber. Strength classes. London: British Standards Institution.

BS EN 408 2010. Timber structures. Structural timber and glued laminated timber. Determination of some physical and mechanical properties. London: British Standards Institution.

BS EN 1995 2004. Eurocode 5: Design of timber structures. London: British Standards Institution.

BS EN 12620 2002. Aggregates for concrete. London: British Standard Institution.

CALLISTER, W. D. & RETHWISCH, D. G. 2007. *Materials science and engineering: an introduction,* New York, Wiley.

CALLISTER, W. D. & RETHWISCH, D. G. 2008. *Fundamentals of Materials Science and Engineering: An Integrated Approach,* New Jersey, Wiley.

CAMBRIDGE ENGINEERING SELECTOR 3.1 2000. Granta Design Limited ed. Cambridge, UK.

CAO, X., JAMES LEE, L., WIDYA, T. & MACOSKO, C. 2005. Polyurethane/clay nanocomposites foams: processing, structure and properties. *Polymer,* 46**,** 775-783.

CARBON RIVER. 2010. *An analysis of carbon emissions for different end of life scenarios for virgin, recycled and low grade wood fibre* [Online]. Available:

http://www.appgwoodpanelindustry.org/docs/WPIF%20CarbonRiver%20Report%20Final.pdf [Accessed 1 July 2014].

CARPET RECYCLING UK. 2010. *Carpet Recycling and Government Policy* [Online]. Available: http://www.carpetrecyclinguk.com/downloads/Carpet_Recycling_and_Government_Policy_Jan%202010.pdf [Accessed 5 May 2014].

CERESANA RESEARCH 2014. Global demand for PVC to rise by about 3.2%/ year to 2021. *Additives for Polymers,* 2014**,** 10-11.

DA SILVA, A. & KYRIAKIDES, S. 2007. Compressive response and failure of balsa wood. *International Journal of Solids and Structures,* 44**,** 8685-8717.

DAVID, D. J., DICKERSON, J. L., SINCOCK, T. F. & WILLIAMS, S. R. 1996. *Thermoplastic composition and method for producing thermoplastic composition by melt blending carpet*. US patent application 5,498,667.

DEPARTMENT FOR ENVIRONMENT FOOD AND RURAL AFFAIRS. 2009. *Code of Practice for the Welfare of Horses, Ponies, Donkeys and their Hybrids* [Online]. Available: https://www.gov.uk/government/uploads/system/uploads/attachment_data/file/69389/pb13334-cop-horse-091204.pdf [Accessed 5 July 2014].

DEPARTMENT FOR ENVIRONMENT FOOD AND RURAL AFFAIRS. 2011. *Applying the Waste Hierarchy: evidence summary* [Online]. Available: https://www.gov.uk/government/uploads/system/uploads/attachment_data/file/69404/pb13529-waste-hierarchy-summary.pdf [Accessed 1 June 2014].

DEPARTMENT FOR ENVIRONMENT FOOD AND RURAL AFFAIRS. 2013. *Statistics on waste managed by local authorities in England in 2012/13* [Online]. Available: https://www.gov.uk/government/uploads/system/uploads/attachment_data/file/255610/Statistics_Notice1.pdf [Accessed 25 January 2014].

DEPARTMENT FOR ENVIRONMENT FOOD AND RURAL AFFAIRS. 2014. *Reducing and managing waste* [Online]. Available: https://www.gov.uk/government/policies/reducing-and-managing-waste [Accessed 30 August 2014].

DEPARTMENT FOR ENVIRONMENT FOOD AND RURAL AFFAIRS. 2015. *UK Statistics on Waste* [Online]. Available: https://www.gov.uk/government/uploads/system/uploads/attachment_data/file/48

7916/UK_Statistics_on_Waste_statistical_notice_15_12_2015_update_f2.pdf [Accessed 3rd March 2016].

DONG, S. B., ALPDOGAN, C. & TACIROGLU, E. 2010. Much ado about shear correction factors in Timoshenko beam theory. *International Journal of Solids and Structures,* 47**,** 1651-1665.

DURALOCK PERFORMANCE FENCING. 2014. *Installation guides* [Online]. Available: http://www.duralock.com/en/about-us/installation-guides [Accessed 15 June 2014].

EASTERLING, K. E., HARRYSSON, R., GIBSON, L. J. & ASHBY, M. F. 1982. On the Mechanics of Balsa and Other Woods. *Proceedings of the Royal Society of London. Series A, Mathematical and Physical Sciences (1934-1990),* 383**,** 31-41.

EUROPEAN COMMISSION. 2010. *Green Public Procurement - Windows Technical Background Report* [Online]. Available: http://ec.europa.eu/environment/gpp/pdf/windows_GPP_background_report.pdf [Accessed 4th March 2016].

EUROPEAN COUNCIL OF VINYL MANUFACTURERS. 2014. *How is PVC used?* [Online]. Available: http://www.pvc.org/en/p/how-is-pvc-used [Accessed 7th February 2016].

EUROPEAN UNION. 2010. *Being wise with waste: the EU's approach to waste management* [Online]. Available: http://ec.europa.eu/environment/waste/pdf/WASTE%20BROCHURE.pdf [Accessed 25 January 2014].

FATAHI, B., KHABBAZ, H. & FATAHI, B. 2012. Mechanical characteristics of soft clay treated with fibre and cement. *Geosynthetics International,* 19**,** 252-262.

FISHBEIN, B. K. 2000. Carpet take-back: EPR American style. *Environmental Quality Management,* 10**,** 25-36.

FREEDONIA 2012. Fencing: United States. Ohio: The Freedonia Group, Inc.

GARDNER, J. 2016. *Recycle your carpets, save on disposal costs, gain green credentials* [Online]. Available: http://www.carpetrecyclinguk.com/downloads/Recycle_your_carpets_save_on_disposal_costs_gain_green_credentials_Jane_Gardner_Carpet_Recycling_UK_20_09.pdf [Accessed 17 February 2017].

GAY, S. W. 2011. Fencing Materials For Livestock Systems. Virginia: Virginia State University.

GERMAN, R. L. 1992. *Fence Rail Connection*. US patent application 771,639.

GIESEKAM, J., BARRETT, J., TAYLOR, P. & OWEN, A. 2014. The greenhouse gas emissions and mitigation options for materials used in UK construction. *Energy & Buildings*.

GLASS, S. V. & ZELINKA, S. L. 2010. Moisture Relations and Physical Properties of Wood. *In:* ROSS, R. (ed.) *Wood Handbook - Wood as an Engineering Material.* Madison, WI: U.S. Department of Agriculture Forest Service, Forest Products Laboratory.

GOWAYED, Y. A., VAIDYANATHAN, R. & EL-HALWAGI, M. 1995. Synthesis of composite materials from waste fabrics and plastics. *Journal of Elastomers and Plastics,* 27**,** 79-90.

GREEN, S. M. 2006. Deformation of materials. *Current Orthopaedics,* 20**,** 9 - 15.

HAMMOND, G. & JONES, C. 2011. Inventory of Carbon and Energy (ICE) Version 2.0. University of Bath, Bath.

HAYLES, C. S. 2015. Environmentally sustainable interior design: A snapshot of current supply of and demand for green, sustainable or Fair Trade products for interior design practice. *International Journal of Sustainable Built Environment,* 4**,** 100-108.

HELMS, M. M. & HERVANI, A. A. 2006. Reverse logistics for recycling: challenges facing the carpet industry. *Greening the supply chain.* Springer London.

HUGO, A. M., SCELSI, L., HODZIC, A., JONES, F. R. & DWYER-JOYCE, R. 2011. Development of recycled polymer composites for structural applications. *Plastics, rubber, and composites : PRC.,* 40**,** 317-323.

HUYNEN, E. 2008. *Product Data Sheet CoatForce CF10* [Online]. Available: http://www.lapinusfibres.com/files/Lapinus%20Fibres%20Files/ProductDataSheets/CoatingAdditives/CoatForceCF10.pdf [Accessed 25 March 2014 2014].

IBRAHIM, A. M. A., FAHMY, M. F. M. & WU, Z. 2016. 3D finite element modeling of bond-controlled behavior of steel and basalt FRP- reinforced concrete square bridge columns under lateral loading. *Composite Structures,* 143**,** 33-52.

IMETRUM. Available: http://www.imetrum.com/ [Accessed 25 April 2016].

ISOPESCU, D., STANILA, O., ASTANEI, I. & CORDUBAN, C. 2012. Experimental Analysis of Wood Mechanical Properties from Bending, Tensile and Compression Tests. *Romanian Journal of Materials,* 42**,** 204-219.

JAIN, A., PANDEY, G., SINGH, A. K., RAJAGOPALAN, V., VAIDYANATHAN, R. & SINGH, R. P. 2012. Fabrication of structural composites from waste carpet. *Advances in Polymer Technology,* 31**,** 380-389.

JISHI, H. Z., UMER, R. & CANTWELL, W. J. 2016. The fabrication and mechanical properties of novel composite lattice structures. *Materials & Design,* 91**,** 286-293.

KALPAKJIAN, S. 1984. *Manufacturing processes for engineering materials,* Massachusetts, Addison-Wesley.

KIZILTAS, A. & GARDNER, D. J. Utilization of carpet waste as matrix in natural fiber-filled engineering thermoplastic composites for automotive applications SPE automotive composites conference and exhibition, 11 - 13 September 2012 Troy Michigan.

KLINE, K. H. 2014. *Safe Fencing for Horses* [Online]. Available: http://livestocktrail.illinois.edu/uploads/horsenet/papers/Safe_fencing.pdf [Accessed 12 August 2014].

KOTLIAR, A. M. 1999. Woodlike properties from carpet and textile fibrous waste: mitigating the coming landfill crisis. *Polymer-Plastics Technology and Engineering,* 38**,** 513-531.

KRETSCHMANN, D. 2010. Mechanical Properties of Wood. *In:* ROSS, R. (ed.) *Wood Handbook - Wood as an Engineering Material.* Madison, WI: U.S. Department of Agriculture Forest Service, Forest Products Laboratory.

LAVE, L., CONWAY-SCHEMPF, N., HARVEY, J., HART, D., BEE, T. & MACCRACKEN, C. 1998. Recycling postconsumer nylon carpet. *Journal of Industrial Ecology,* 2**,** 117-126.

LEBOW, S. T. 2010. Wood Preservation. *In:* ROSS, R. (ed.) *Wood Handbook - Wood as an Engineering Material.* Madison, WI: U.S. Department of Agriculture Forest Service, Forest Products Laboratory.

LEMIEUX, P., STEWART, E., REALFF, M. & MULHOLLAND, J. A. 2004. Emissions study of co-firing waste carpet in a rotary kiln. *Journal of Environment Management,* 70**,** 27-33.

MADENCI, E. & GUVEN, I. 2006. *The finite element method and applications in engineering using ANSYS,* New York, Springer.

MANSFIELD. 2012. *Mansfield Sand keeps riders riding all year round with Premier Fibre* [Online]. Available: http://prblog.freestyleuk.com/2012_04_01_archive.html [Accessed 20th September 2016].

MARKARIAN, J. 2008. Extruder developments drive productivity improvements for rigid PVC. *Plastics, Additives and Compounding,* 10**,** 22-26.

MARTIN, J. 2006. Pultruded composites compete with traditional construction materials. *Reinforced Plastics,* 50**,** 20-27.

MATUANA, L. M. 2015. The Use of Wood Fibers as Reinforcements in Composites. *In:* FARUK, O. & SAIN, M. (eds.) *Biofiber Reinforcement in Composite Materials.* Cambridge: Woodhead Publishing.

MIHUT, C., CAPTAIN, D. K., GADALA-MARIA, F. & AMIRIDIS, M. D. 2001. Review: Recycling of nylon from carpet waste. *Polymer Engineering and Science,* 41**,** 1457-1470.

MIRAFTAB, M., HORROCKS, R. & WOODS, C. 1999. Carpet waste, an expensive luxury we must do without! . *Autex Research Journal,* 1**,** 1-7.

MIRAFTAB, M. & LICKFOLD, A. 2008. Utilization of Carpet Waste in Reinforcement of Substandard Soils. *Journal of industrial textiles,* 38**,** 167-174.

MIRAFTAB, M. & MIRZABABAEI, M. Carpet waste utilisation, an awakening realisation: a review. 2nd International Symposium on Fiber Recycling 11-12 May 2009 Atlanta, Georgia.

MIRAFTAB, M., RUSHFORTH, I. & HOROSHENKOV, K. 2005. Acoustic underlay manufactured from carpet tile wastes. Part 1: Effect of variation in granular/fibre dry ratio, binder concentration, and waste particle size on impact sound insulation of the produced underlays. *Autex Research Journal,* 5**,** 96-105.

MOORE, N. 2015. *Timber Utilisation Statistics 2015* [Online]. Available: http://www.forestry.gov.uk/pdf/Timber_Utilisation_Report_2015.pdf/$FILE/Timber_Utilisation_Report_2015.pdf [Accessed 8th February 2016].

MURALISRINIVASAN, N. 2011. *Update on Troubleshooting the PVC Extrusion Process,* Shropshire, iSmithers Rapra Technology.

MURDOCK, D. E., MANCOSH, D. & PRZYBYLINSKI, J. P. 2011. *Carpet waste composite*. 7923477 B2.

MURRAY, J., FROST, J. & WANG, Y. 2000. Behavior of a Sandy Silt Reinforced with Discontinuous Recycled Fiber Inclusions. *Transportation Research Record,* 1714**,** 9-17.

MUZZY, J. Recycling Post-Consumer Carpet. 9th Annual Conference on Recycling of Fibrous Textile and Carpet Waste, 23-25 February 2006 Atlanta, Georgia.

PAKALA, P. & KODUR, V. 2016. Effect of concrete slab on the behavior of fire exposed subframe assemblies with bolted double angle connections. *Engineering Structures,* 107**,** 101-115.

PAKALA, P., KODUR, V. & DWAIKAT, M. 2012. Critical factors influencing the fire performance of bolted double angle connections. *Engineering Structures,* 42**,** 106-114.

PALENIK, S. 1999. Microscopical Examination of Fibres. *In:* ROBERTSON, J. & GRIEVE, M. (eds.) *Forensic Examination of Fibres.* 2nd ed. London: Taylor and Francis.

PATRICK, S. G. 2005. *Practical Guide to Polyvinyl Chloride,* Shropshire, Rapra Technology Limited.

PEOPLES, R. 2006. Carpet stewardship in the United States - a commitment to sustainability. *In:* WANG, Y. (ed.) *Recycling in Textiles.* Cambridge: Woodhead Publishing.

PLASTICSEUROPE. 2015. *Plastics - The Facts 2015, An Analysis of European Plastics Production, Demand and Waste data* [Online]. Brussels: PlasticsEurope Association of Plastics Manufacturers. Available: http://www.plasticseurope.org/Document/plastics---the-facts-2015.aspx [Accessed 4th February 2016].

PORTEOUS, J. & KERMANI, A. 2007. *Structural timber design to Eurocode 5,* Oxford, Blackwell.

READ, D. J., FREER-SMITH, P. H., MORISON, J. I. L., HANLEY, N., WEST, C. C. & SNOWDON, P. 2009. *Combating Climate Change. A Role of UK Forestry. An Assessment of the Potential of the UK's trees and woodlands to mitigate and adapt to climate change* [Online]. Edinburgh. Available: http://www.forestry.gov.uk/pdf/SynthesisUKAssessmentfinal.pdf/$FILE/SynthesisUKAssessmentfinal.pdf [Accessed].

REALFF, M. J., LEMIEUX, P., LUCERO, S., MULHOLLAND, J. & SMITH, P. B. 2005. Characterization of transient puff emissions from the burning of carpet waste charges in a rotary kiln combustor. *IEE 47th Cement Industry Technical Conference.* Kansas city.

RECYCLING INTERNATIONAL. 2015. *Europe records PVC recycling growth in 2014* [Online]. Available: http://www.recyclinginternational.com/recycling-news/8742/plastic-and-rubber/europe/europe-records-pvc-recycling-growth-2014 [Accessed 3rd March 2016].

RUSHFORTH, I., HOROSHENKOV, K., MIRAFTAB, M. & SWIFT, M. 2005. Impact sound insulation and viscoelastic properties of underlay manufactured from recycled carpet waste. *Applied Acoustics,* 66**,** 731-749.

SANDBERG, D., HALLER, P. & NAVI, P. 2013. Thermo- hydro and thermo- hydro- mechanical wood processing: An opportunity for future environmentally friendly wood products. Taylor & Francis Group.

SATASIVAM, S. & BAI, Y. 2014. Mechanical performance of bolted modular GFRP composite sandwich structures using standard and blind bolts. *Composite Structures,* 117**,** 59-70.

SHEIKH-AHMAD, J. Y. 2009. *Machining of polymer composites,* New York, Springer.

SHUAIB, N. A. & MATIVENGA, P. T. 2016. Energy demand in mechanical recycling of glass fibre reinforced thermoset plastic composites. *Journal of Cleaner Production,* 120**,** 198-206.

SIDDIQUE, R., KHATIB, J. & KAUR, I. 2008. Use of recycled plastic in concrete: A review. *Waste Management,* 28**,** 1835-1852.

SIMS, G., JOHNSON, A. & HILL, R. 1987. Mechanical and structural properties of a GRP pultruded section. *Composite Structures,* 8**,** 173-187.

SINGH, N., HUI, D., SINGH, R., AHUJA, I. P. S., FEO, L. & FRATERNALI, F. 2016. Recycling of plastic solid waste: A state of art review and future applications. *Composites Part B Engineering*.

SMITH , M. 2013. Use of Recycled and Reclaimed Timbers. *In:* RICHARDSON, A. (ed.) *Reuse of Materials and Byproducts in Construction* London: Springer.

SMITH, M., BULL, J. W., MORRIS, T. & UNDERWOOD, C. 2013. Strength Prediction of Recovered Softwood Beams for Structural Reuse. *In:* TOPPING, B. H. V. & IVANYI, P. (eds.) *Fourteenth International Conference on Civil, Structural and Environmental Engineering Computing.* Sardinia Italy Civil - Comp Press.

SONG, Y. S., YOUN, J. R. & GUTOWSKI, T. G. 2009. Life cycle energy analysis of fiber-reinforced composites. *Composites. Part A. Applied science and manufacturing.,* 40**,** 1257-1265.

STRONG, A. B. 2008. *Fundamentals of composites manufacturing : materials, methods and applications,* Dearborn, Michigan, Society of Manufacturing Engineers.

TAYLOR, G. D. 1994. *Materials in Construction,* Essex, England, Longman Scientific & Technical.

THE CARPET AND RUG INSTITUTE. 2003. *THE CARPET PRIMER* [Online]. Available: http://www.carpet-rug.org/Documents/Publications/029_The_Carpet_Primer.aspx [Accessed 5 April 2014].

THERMO SCIENTIFIC. 2010. *Thermo Scientific Microphazir PC Handheld Carpet Fiber Identification* [Online]. Available: http://www.thermoscientific.com/content/dam/tfs/ATG/CAD/CAD%20Documents/Product%20Manuals%20&%20Specifications/Portable%20Analyzers%20for%20Material%20ID/Handheld%20NIR/microPHAZIRPC-Carpet-analyzer.pdf [Accessed 2nd September 2015].

TOUSEY, T. T. 2011. Utilizing Waste Materials as a Source of Alternative Energy: Benefits and Challenges. *In:* RAO, K. R. (ed.) *Energy and Power Generation Handbook: Established and Emerging Technologies.* New York: ASME press.

TRADA 1993. Timber fencing. *In:* TIMBER RESEARCH AND DEVELOPMENT ASSOCIATION (ed.). High Wycombe: TRADA Technology.

TRADA 2003. Design of structural timber connections. *In:* TIMBER RESEARCH AND DEVELOPMENT ASSOCIATION (ed.). High Wycombe: TRADA Technology.

TRADA 2011. Environmental aspects of wood: Wood waste and reuse. *In:* TIMBER RESEARCH AND DEVELOPMENT ASSOCIATION (ed.). High Wycombe TRADA Technology.

TRADA 2012a. Fasteners for structural timber: nails, staples, screws, dowels and bolts *In:* TIMBER RESEARCH AND DEVELOPMENT ASSOCIATION (ed.). High Wycombe: TRADA Technology.

TRADA. 2012b. *Timber Species* [Online]. Available: https://www.trada.co.uk/publications/download/?id=B3FE77B4-1257-442B-89DA-4253E934F9FF [Accessed 8th January 2014].

TSAVDARIDIS, K. D. & PAPADOPOULOS, T. 2016. A FE parametric study of RWS beam-to-column bolted connections with cellular beams. *Journal of Constructional Steel Research,* 116**,** 92-113.

TURVEY, G. 2015. Experimental investigation of the load–deformation behaviour of pultruded GFRP modular and custom safety barriers. *Composite Structures,* 133**,** 659-666.

UCAR, M. & WANG, Y. 2011. Utilization of recycled post consumer carpet waste fibers as reinforcement in lightweight cementitious composites. *International Journal of Clothing Science and Technology,* 23**,** 242-248.

UDDIN, M. F., MAHFUZ, H., ZAINUDDIN, S. & JEELANI, S. Anisotropic behavior of rigid polyurethane foam with acicular nanoparticles infusion under high strain rate compression,''. CD Proceedings of 20th technical conference of the American Society for Composites, Philadelphia, PA, Paper, 2005. 1-15.

UK GOVERNMENT. 2016. *Landfill Tax: increase in rates* [Online]. Available: https://www.gov.uk/government/publications/landfill-tax-increase-in-rates/landfill-tax-increase-in-rates [Accessed 17 February 2017].

UNITED NATIONS ENVIRONMENT PROGRAMME. 2002. *gas emissions from waste disposal* [Online]. Available: http://www.grid.unep.ch/waste/html_file/42-43_climate_change.html [Accessed 31 July 2014].

UNITED STATES ENVIRONMENTAL PROTECTION AGENCY. 2003. *Background Document for Life-Cycle Greenhouse Gas Emission Factors for Carpet and Personal Computers* [Online]. Available: http://www.epa.gov/climatechange/wycd/waste/downloads/CarpetPCReport_11_21.pdf [Accessed 1 August 2014].

UNTHA. 2015. *UNTHA SHREDDING TECHNOLOGY VR 140* [Online]. Available: http://pdf.directindustry.com/pdf/untha-shredding-technology/vr60-vr80-vr100-vr120-vr140-vr160/7823-300815.html [Accessed 2nd September 2015].

USDA 2011. Pasture management - Guide for Horse Owners. *In:* AGRICULTURE, U. S. D. O. (ed.). Columbia: United States Department of Agriculture Natural Resources Conservation Service

VAIDYANATHAN, R., SINGH, R. P. & LEY, T. 2013. Recycled Carpet Materials for Infrastructure Applications. Oklahoma: Oklahoma Transportation Centre.

VAN DER WERF, G. R., MORTON, D. C., DEFRIES, R. S., OLIVIER, J. G., KASIBHATLA, P. S., JACKSON, R. B., COLLATZ, G. J. & RANDERSON, J. 2009. CO2 emissions from forest loss. *Nature Geoscience,* 2**,** 737-738.

VINYLPLUS. 2015. *PVC Recycling Technologies* [Online]. Available: http://www.vinylplus.eu/uploads/2015-12-10_Recycling-Technologies-English.pdf [Accessed 4th March 2016].

WANG, Y. 2006a. Carpet recycling technologies. *In:* WANG, Y. (ed.) *Recycling in Textiles.* Cambridge: Woodhead Publishing.

WANG, Y. 2006b. Utilization of recycled carpet waste fibers for reinforcement of concrete and soil. *In:* WANG, Y. (ed.) *Recycling in Textiles.* Cambridge: Woodhead Publishing.

WANG, Y. 2010. Fiber and textile waste utilization. *Waste and Biomass Valorization,* 1**,** 135-143.

WANG, Y., ZHANG, Y., POLK, M., KUMAR, S. & MUZZY, J. 2003. Recycling of carpet and textile fibres. *In:* ANDRADY, L. (ed.) *Plastics and the Environment: A Handbook.* New York: John Wiley & Sons.

WANG, Y., ZUREICK, A. H., CHO, B. S. & SCOTT, D. 1994. Properties of fibre reinforced concrete using recycled fibres from carpet industrial waste. *Journal of Materials Science,* 29**,** 4191-4199.

WASTE AND RESOURCES ACTION PROGRAMME. 2011. *Market Situation Report : Realising the value of recovered wood* [Online]. Available: http://www2.wrap.org.uk/downloads/Wood_MSR_Final_Aug_2011.2d751694.11101.pdf [Accessed 9 August 2014].

WASTE AND RESOURCES ACTION PROGRAMME. 2012. *Composition and re-use potential of household bulky textiles in the UK* [Online]. Oxon. Available: http://www.wrap.org.uk/sites/files/wrap/Textiles%20-%20bulky%20waste%20summary.pdf [Accessed 13 August 2014].

WASTE AND RESOURCES ACTION PROGRAMME. 2014. *Collecting and shredding carpets from Household Waste Recycling Centres* [Online]. Available: http://www.wrap.org.uk/sites/files/wrap/Collection%20of%20carpets%20from%20HWRCs%20by%20reprocessor_0.pdf [Accessed 1 August 2014].

WIEDENHOEFT, A. 2010. Structure and Function of Wood. *In:* ROSS, R. (ed.) *Wood Handbook - Wood as an Engineering Material.* Madison, WI: U.S. Department of Agriculture Forest Service, Forest Products Laboratory.

WITIK, R. A., PAYET, J., MICHAUD, V., LUDWIG, C. & MÅNSON, J.-A. E. 2011. Assessing the life cycle costs and environmental performance of lightweight materials in automobile applications. *Composites Part A,* 42**,** 1694-1709.

WOOLLEY, T. & KIMMINS, S. 2000. *Green Building Handbook,* London, Taylor and Francis Group.

WWF. 2005. *Window of Opportunity - The environmental and economic benefits of specifying timber window frames* [Online]. Available: http://assets.wwf.org.uk/downloads/windows_0305.pdf?_ga=1.254747469.4382160.1457193984 [Accessed 8th March 2016].

XANTHOS, M. & DEY, S. K. 2001. *Wood substitute composition and process for producing same*. US patent application 6,211,275 B1.

XANTHOS, M., DEY, S. K., MITRA, S., YILMAZER, U. & FENG, C. 2002. Prototypes for building applications based on thermoplastic composites containing mixed waste plastics. *Polymer composites,* 23**,** 153-163.

YAN, J., QIN, F., CAO, Z., FAN, F. & MO, Y. L. 2016. Mechanism of coupled instability of single- layer reticulated domes. *Engineering Structures,* 114**,** 158-170.

YANG, H.-S., KIM, H.-J., PARK, H.-J., LEE, B.-J. & HWANG, T.-S. 2006. Water absorption behavior and mechanical properties of lignocellulosic filler– polyolefin bio-composites. *Composite Structures,* 72**,** 429-437.

YANG, T.-C., NOGUCHI, T., ISSHIKI, M. & WU, J.-H. 2014. Effect of titanium dioxide on chemical and molecular changes in PVC sidings during QUV accelerated weathering. *Polymer Degradation and Stability,* 104**,** 33-39.

YOUNG, D. C., CHLYSTEK, S. J., MALLOY, R. & RIOS, I. 1998. *Recycling of carpet scrap*. US patent application 5,719,198.

YU, J., SUN, L., MA, C., QIAO, Y. & YAO, H. 2016. Thermal degradation of PVC: A review. *Waste management,* 48**,** 300-314.

ZHANG, C., GROSS, J. L. & MCALLISTER, T. P. 2013. Lateral torsional buckling of steel W-beams subjected to localized fires. *Journal of Constructional Steel Research,* 88**,** 330-338.

ZHANG, Y., MUZZY, J. D. & KUMAR, S. 1999. Recycling carpet waste by injection and compression molding. *Polymer-Plastics Technology and Engineering,* 38**,** 485-498.

ZHOU, Y., STRAWDER, G. & JEELANI, S. Fabrication and characterization of neat and nanophased polyurethane foam. SPE Automotive and Composites Divisions–7th Annual Automotive Composites Conference and Exhibition, ACCE 2007–Driving Performance and Productivity, 2007. 11-13.

ZHU, L., ZHAO, Y., LI, S., HUANG, Y. & BAN, L. 2014. Numerical analysis of the axial strength of CHS T-joints reinforced with external stiffeners. *Thin-Walled Structures,* 85**,** 481-488.

Appendices

Appendix 1: Mechanical properties of PVC (Duralock Performance Fencing)

DURALOCK
PERFORMANCE FENCING
Duralock (UK) Ltd, 6A Enstone Business Park,
Enstone, Chipping Norton,
Oxfordshire, OX7 4NP, England
Tel: +44 (0) 1608 678238 Fax: +44 (0) 1608 677170
Website: www.duralock.com e-mail: info@duralock.com

DURALOCK TECHNICAL RACERAIL SPECIFICATION
TROPICAL VIRGIN PVCu

Rail profile nominally 108 x 50, with wall thickness c. 3.01mm
Nominal weight 1.3kg/metre top & bottom

Post profile nominally 150 x 100, with wall thickness c. 3.0mm
Nominal weight 2.3kg/metre

Typical extrusion material:

Titanium Dioxide	7%
5 kg Vicat softening point	78 to 82°C
Relative density	range 1.42 to 1.48
Flexural modulus	range 2373 to 2510 Mpa
Impact type	high (12-20 KJ/M^2)
Coefficient of thermal expansion	6 x 10^{-5}/deg C
Rockwell hardness R scale	115 deg
Tensile strength	45-50 MN/M^2
Thermal conductivity	0.16 W/Mk

Falling weight test, minus 10° C (-10C)
(2 metres height/5kg weight 25mm radius) NO BREAKS

Appendix 2: Product data sheet for CoatForce (CF10) fibre

Product Data Sheet

CoatForce® CF10

Engineered mineral fibre (Note Q)

Lapinus®
intelligent fibres

lapinus@lapinusfibres.com
www.lapinusfibres.com

CoatForce® CF10 is a high quality engineered mineral fibre. Its fibre length results in an excellent dispersion in various matrix materials e.g. water- and solvent based resins, bitumen. CoatForce® CF10 gives excellent mechanical properties to various paint and coating systems.

All CoatForce® products are worldwide exonerated from classification as a carcinogen.

Chemical Analysis

	Min.	Max.
SiO_2	37 %wt	42 %wt
Al_2O_3	18 %wt	23 %wt
CaO+MgO	34 %wt	39 %wt
FeO	0 %wt	1 %wt
K_2O+Na_2O		3 %wt
Others		3 %wt

Typical average fibre diameter

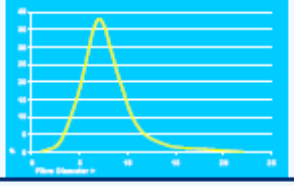

Typical average fibre length

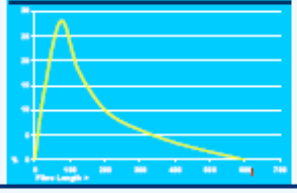

ADVANTAGES OF COATFORCE® CF10

- CoatForce® CF10 shows in various applications added values in improvement of mechanical properties and rheological behaviour.
- CoatForce® CF10 has an off-white colour and very low shot content.
- CoatForce® CF10 is worldwide safe to use with respect to Health and Safety regulations.

Parameter	Average/Tolerance		Testmethod
Non-Fibrous Material	Norm.	Max.	TV 316
	N > 125 µm	0.1%wt	0.2%wt
Fibre Length	125 ± 25 micron		TV 305
Ignition Loss	max. 0.3 %wt		TV 302
Moisture Content	max. 0.1 %wt		TV 302
Fibre diameter (mass wt. av.)	approx. 7 micron		TV 165
Fibre diameter (num. av.)	approx. 5 micron		TV 165
Specific surface area	approx. 0.22 m2/g		TV 165
Hardness	6 Moh		
Melting Point	> 700 °C		Furnace, Visual
Specific Density	2.71 ± 0.1 g/cm3		
Colour	off-white		Visual
Oil absorption	approx 20 g/100 g		ASTM D281

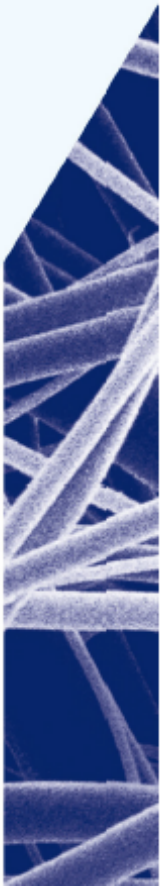

Author: E. Huynen
Issue: July 2008 (03)

Replaces Issue: March 2006 (02)
ISO 9001 LF007.F08

Appendix 3: Width and depth measurements of Composite A – C

Width and depth measurements of Composites A and B

Beam	Width [mm]	Depth [mm]
Composite A	93	46
	109	48
	112	52
	118	54
Average	**108**	**50**
Composite B	104	99
	114	101
	116	102
	118	110
Average	**113**	**103**

Width and depth measurements of Composite C_PP (C_PP1 – C_PP9), Composite C_PPW (C_PPW1 – C_PPW9), Composite C_SF (C_SF1 – C_SF9) and Composite C_SFW (C_SFW1 – C_SFW9)

Sample label	Width [mm]	Depth [mm]	Sample label	Width [mm]	Depth [mm]	Sample label	Width [mm]	Depth [mm]	Sample label	Width [mm]	Depth [mm]
C_PP1	37.4	11.8	C_PPW1	38.7	8.8	C_SF1	38.1	11.2	C_SFW1	38.2	12
	37.9	11.3		38.9	10.5		38.5	11.5		39.2	11.8
	38.3	10.3		38.5	11.3		38.8	11.6		39.7	10.2
	38	9.7		37.0	11.4		38.5	11.4		39.2	8.9
C_PP2	38	11.7	C_PPW2	38.1	8.9	C_SF2	38.2	10.4	C_SFW2	38.9	12.1
	38	11.5		38.9	10.2		38.7	11		39.4	11.1
	38	10		39.0	11.1		39.1	11.1		38.8	9.9
	38.1	10.2		38.9	11.4		39.5	10.6		38.5	8.2
C_PP3	38.9	9.4	C_PPW3	39.7	11.5	C_SF3	38.3	10.8	C_SFW3	38.3	11.6
	38.6	10.4		39.0	11.1		38.8	11.2		39.1	11.2
	37.8	11.3		38.0	9.8		38.7	11		39.4	10.3
	36.9	11		37.3	9.0		39.1	10.8		39.2	8.5
C_PP4	38.4	8.8	C_PPW4	37.8	12.2	C_SF4	38.8	8.9	C_SFW4	37.8	12.6
	38.2	10.5		38.2	11.6		39.3	11.2		38.1	11.7
	35.6	11.2		38.4	10.9		39.3	11.7		37.7	10.8
	34	11.1		38.5	9.4		39.2	12.3		36.9	9
C_PP5	38.7	8.8	C_PPW5	38.1	12.8	C_SF5	39	9	C_SFW5	38.7	12.7
	39	10.3		38.7	11.6		39	10.2		38.9	11.7
	39.3	11		39.3	10.6		38.7	11.3		38.6	10.6
	37.9	11.2		39.3	9.8		38.4	12.2		37.9	9
C_PP6	38.1	11.6	C_PPW6	38.5	9.1	C_SF6	38.4	12	C_SFW6	38.5	12.5
	38.4	11		39.2	10.9		39.1	11.6		38.9	11.5
	38.6	10		39.4	11.7		39.7	10.3		39.7	10.5
	38	8.9		39.2	12.1		39.3	9		39.5	9.6
C_PP7	39.4	11.4	C_PPW7	38.2	8.9	C_SF7	38.9	9.6	C_SFW7	38.3	12.2
	39.4	10.8		39.2	10.3		39.3	11.3		39	11.4
	39.2	9.6		39.2	11.5		39.4	11.6		38.4	10.1
	38.6	8.7		39.2	12.0		38.6	12.1		37.9	8.3
C_PP8	39.4	11.3	C_PPW8	38.0	9.2	C_SF8	38.8	9.3	C_SFW8	39.1	8.6
	39.4	10.9		38.9	10.3		39	10.6		39.6	10.4
	39.2	10		39.3	11.3		38.9	11.5		39.2	11.7
	38.5	8.5		38.9	11.7		38.8	11.6		38.8	11.8
C_PP9	38.2	8.9	C_PPW9	38.7	9.0	C_SF9	38.8	9.2	C_SFW9	39	12.1
	38.2	10		39.5	10.2		39	10.7		38.9	11.3
	38.1	10.8		39.1	11.4		39	11.4		39.2	9.9
	37.3	11		38.9	11.8		38.8	12.2		39.1	8.6
Overall Average	**38**	**10**	**Overall Average**	**39**	**11**	**Overall Average**	**39**	**11**	**Overall Average**	**39**	**11**

Appendix 4: Image of a test rig showing Composite A loaded in three-point bending

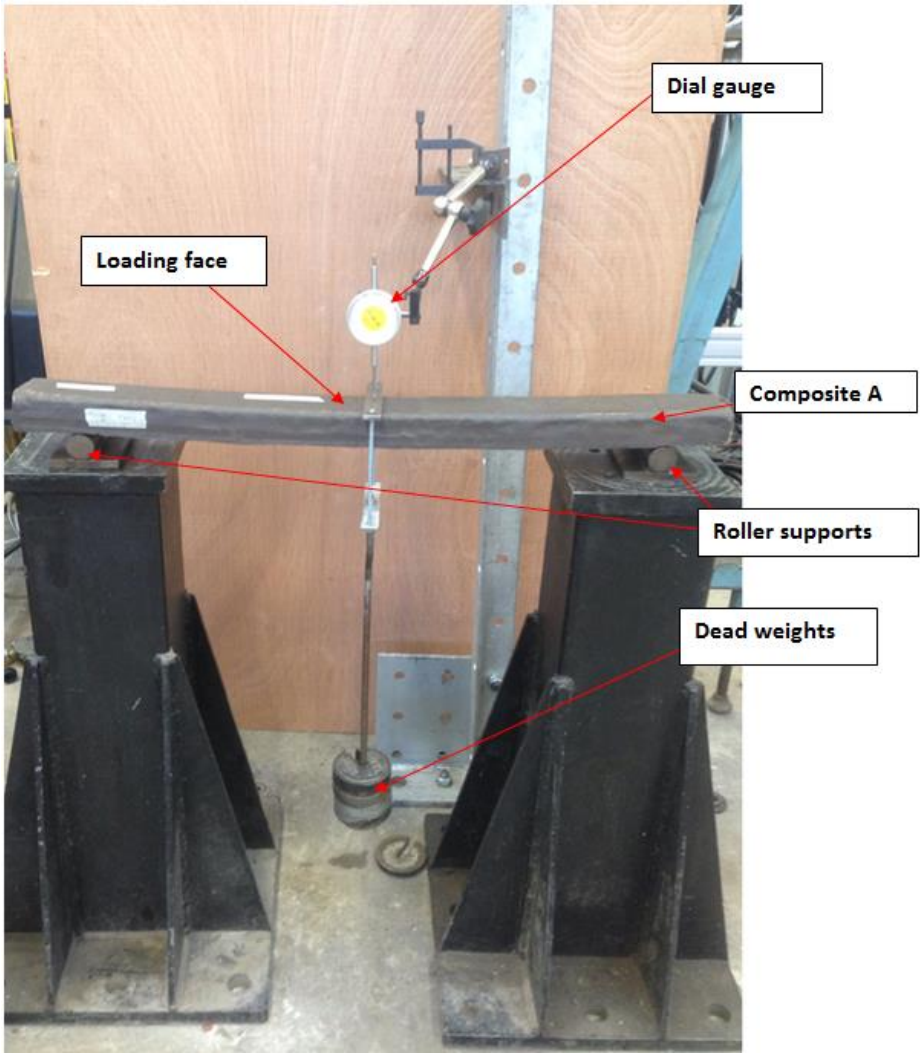

Appendix 5: Three-point bending test results

Three-point bending test results for Composites A and B

Beam	Load [N]	Centre deflection [mm]		
		Test 1	Test 2	Test 3
Composite A	0	0	0	0
	9.82	2.17	1.58	1.48
	19.62	4.6	3.48	3.31
	29.42	6.15	5.61	5.28
	39.22	8.7	7.97	7.5
Composite B	0	0	0	0
	14.79	0.3	0.25	0.26
	34.41	1.06	1.15	1.2
	54.03	2.15	2.09	2.2
	73.65	3.23	3.1	3.23
	93.27	4.3	4.15	4.32

Three-point bending test results for Timber Post 1

Load [kg]	Load [N]	Centre deflection [mm]			Average centre deflection [mm]
		Test 1	Test 2	Test 3	
1.5	15	0	0	0	0
11.5	113	0.16	0.19	0.19	0.18
21.5	211	0.32	0.35	0.36	0.34
31.5	309	0.47	0.49	0.49	0.48
41.5	407	0.6	0.65	0.63	0.63
51.5	505	0.75	0.8	0.79	0.78
61.5	603	0.89	0.95	0.92	0.92
71.5	701	1.03	1.08	1.06	1.06
81.5	800	1.17	1.22	1.19	1.19
91.5	898	1.32	1.37	1.35	1.35
101.5	996	1.47	1.51	1.5	1.49

Three-point bending test results for Timber Post 2

Load [kg]	Load [N]	Centre deflection [mm]			Average centre deflection [mm]
		Test 1	Test 2	Test 3	
1.5	15	0	0	0	0
11.5	113	0.2	0.32	0.17	0.23
21.5	211	0.39	0.53	0.35	0.42
31.5	309	0.58	0.73	0.53	0.61
41.5	407	0.8	0.9	0.7	0.80
51.5	505	1	1.1	0.86	0.99
61.5	603	1.18	1.27	1.05	1.17
71.5	701	1.39	1.44	1.22	1.35
81.5	800	1.58	1.62	1.39	1.53
91.5	898	1.76	1.8	1.56	1.71
101.5	996	1.93	2	1.75	1.89

Three-point bending test results for Timber Post 3

Load [kg]	Load [N]	Centre deflection [mm]			Average centre deflection [mm]
		Test 1	Test 2	Test 3	
1.5	15	0	0	0	0
11.5	113	0.15	0.2	0.17	0.17
21.5	211	0.3	0.38	0.35	0.34
31.5	309	0.45	0.54	0.51	0.50
41.5	407	0.61	0.7	0.66	0.66
51.5	505	0.76	0.86	0.8	0.81
61.5	603	0.91	1.00	0.96	0.96
71.5	701	1.06	1.16	1.1	1.11
81.5	800	1.22	1.31	1.25	1.26
91.5	898	1.38	1.48	1.38	1.41
101.5	996	1.55	1.63	1.53	1.57

Three-point bending test results for Timber Rail 1

Load [kg]	Load [N]	Centre deflection [mm]			Average centre deflection [mm]
		Test 1	Test 2	Test 3	
1.5	15	0	0	0	0
3.5	34	2.45	2.52	2.49	2.49
5.5	54	5	5.1	5.05	5.05
7.5	74	7.6	7.7	7.65	7.65
9.5	93	10.2	10.3	10.22	10.24
11.5	113	13	12.8	12.78	12.86

Three-point bending test results for Timber Rail 2

Load [kg]	Load [N]	Centre deflection [mm]			Average centre deflection [mm]
		Test 1	Test 2	Test 3	
1.5	15	0	0	0	0
3.5	34	1.77	1.75	1.75	1.76
5.5	54	3.6	3.5	3.55	3.55
7.5	74	5.4	5.35	5.4	5.38
9.5	93	7.21	7.17	7.22	7.20
11.5	113	9.07	9	9.05	9.04

Three-point bending test results for Timber Post 4

Span [mm]	Centre deflection [mm]	Load [N]		
		Test 1	Test 2	Test 3
1500	0.5	270	273	**290**
	1	515	530	**540**
	1.5	760	770	**770**
	2	994	1006	**1020**
973	0.5	1250	1020	**1300**
	1	2180	1900	**2230**
	1.5	3160	2920	**3230**
	2	4100	3900	**4200**
774	0.5	1700	1540	**1700**
	1	3300	3125	**3110**
	1.5	4630	4720	**4730**
	2	5890	6100	**6300**
662	0.5	2280	2160	**2300**
	1	4280	4250	**4300**
	1.5	6400	6400	**6500**
	2	8300	8400	**8600**

Three-point bending test results for PVC Post 1 (Loading Orientation A)

Load [kg]	Load [N]	Centre deflection [mm]			Average centre deflection [mm]
		Test 1	Test 2	Test 3	
1.5	15	0	0	0	0
11.5	113	0.6	0.6	0.5	0.6
21.5	211	1.1	1.1	1.0	1.1
31.5	309	1.4	1.4	1.3	1.4
41.5	407	1.7	1.7	1.6	1.7
51.5	505	2.0	2.0	1.9	2.0

Three-point bending test results for PVC Post 2 (Loading Orientation A)

Load [kg]	Load [N]	Centre deflection [mm]			Average centre deflection [mm]
		Test 1	Test 2	Test 3	
1.5	15	0	0	0	0
11.5	113	0.7	0.7	0.6	0.7
21.5	211	1.0	1.0	1.0	1.0
31.5	309	1.3	1.3	1.3	1.3
41.5	407	1.6	1.6	1.5	1.6
51.5	505	1.9	1.9	1.8	1.9

Three-point bending test results for PVC Post 3 (Loading Orientation A)

Load [kg]	Load [N]	Centre deflection [mm]			Average centre deflection [mm]
		Test 1	Test 2	Test 3	
1.5	15	0	0	0	0
11.5	113	0.6	0.6	0.6	0.6
21.5	211	1.1	1.1	1.1	1.1
31.5	309	1.4	1.4	1.3	1.4
41.5	407	1.7	1.7	1.7	1.7
51.5	505	2.0	2.0	2.0	2.0

Three-point bending test results for PVC Post 1 (Loading Orientation B)

Load [kg]	Load [N]	Centre deflection [mm]			Average centre deflection [mm]
		Test 1	Test 2	Test 3	
1.5	15	0	0	0	0
11.5	113	0.3	0.2	0.3	0.3
21.5	211	0.6	0.5	0.6	0.6
31.5	309	0.8	0.7	0.9	0.8
41.5	407	1.1	1.0	1.1	1.1
51.5	505	1.4	1.3	1.4	1.4

Three-point bending test results for PVC Post 2 (Loading Orientation B)

Load [kg]	Load [N]	Centre deflection [mm]			Average centre deflection [mm]
		Test 1	Test 2	Test 3	
1.5	15	0	0	0	0
11.5	113	0.3	0.3	0.3	0.3
21.5	211	0.7	0.7	0.7	0.7
31.5	309	1.0	1.0	1.0	1.0
41.5	407	1.2	1.2	1.2	1.2
51.5	505	1.5	1.5	1.5	1.5

Three-point bending test results for PVC Post 3 (Loading Orientation B)

Load [kg]	Load [N]	Centre deflection [mm]			Average centre deflection [mm]
		Test 1	Test 2	Test 3	
1.5	15	0	0	0	0
11.5	113	0.3	0.3	0.3	0.3
21.5	211	0.7	0.6	0.6	0.6
31.5	309	1.0	0.9	0.9	0.9
41.5	407	1.2	1.2	1.2	1.2
51.5	505	1.5	1.4	1.4	1.4

Three-point bending test results for PVC Rail 1

Load [kg]	Load [N]	Centre deflection [mm]			Average centre deflection [mm]
		Test 1	Test 2	Test 3	
1.5	15	0	0	0	0
2.5	25	6.9	6.8	7.0	6.9
3.5	34	14.5	14.2	14.3	14.3
4.5	44	22.0	21.8	21.7	21.8
5.5	54	29.2	29.2	29.1	29.2
6.5	64	36.7	36.6	36.5	36.6

Three-point bending test results for PVC Rail 2

Load [kg]	Load [N]	Centre deflection [mm]			Average centre deflection [mm]
		Test 1	Test 2	Test 3	
1.5	15	0	0	0	0
2.5	25	7.2	7.1	7.1	7.1
3.5	34	14.7	14.5	14.4	14.5
4.5	44	22.5	22.3	22.2	22.3
5.5	54	30.0	29.9	30.0	30.0
6.5	64	37.5	37.7	37.6	37.6

Three-point bending test results for PVC Rail 3

Load [kg]	Load [N]	Centre deflection [mm]			Average centre deflection [mm]
		Test 1	Test 2	Test 3	
1.5	15	0	0	0	0
2.5	25	7.2	7.1	7.1	7.1
3.5	34	14.9	14.5	14.6	14.7
4.5	44	22.7	22.4	22.3	22.5
5.5	54	30.4	30.2	30.2	30.3
6.5	64	38.2	38.0	38.2	38.1

Transverse stiffnesses and flexural moduli for 36 Composite C beams

Beam (C_PP)	Transverse stiffness [N/mm]	Flexural modulus [MPa]	Beam (C_PPW)	Transverse stiffness [N/mm]	Flexural modulus [MPa]	Beam (C_SF)	Transverse stiffness [N/mm]	Flexural modulus [MPa]	Beam (C_SFW)	Transverse stiffness [N/mm]	Flexural modulus [MPa]
C_PP1	29.4	2143	C_PPW1	29.0	2262	C_SF1	38.5	2319	C_SFW1	32.8	2352
C_PP2	30.3	2156	C_PPW2	31.3	2483	C_SF2	31.7	2253	C_SFW2	35.1	2833
C_PP3	29.9	2329	C_PPW3	32.8	2656	C_SF3	35.1	2386	C_SFW3	41.6	3277
C_PP4	27.0	2270	C_PPW4	39.2	2645	C_SF4	31.3	2062	C_SFW4	42.6	2920
C_PP5	32.8	2659	C_PPW5	43.5	2754	C_SF5	32.8	2403	C_SFW5	48.8	3289
C_PP6	29.0	2345	C_PPW6	40.7	2742	C_SF6	33.3	2384	C_SFW6	48.8	3215
C_PP7	26.4	2245	C_PPW7	36.9	2692	C_SF7	32.8	2094	C_SFW7	42.6	3312
C_PP8	30.8	2583	C_PPW8	35.1	2608	C_SF8	30.8	2204	C_SFW8	40.8	3001
C_PP9	25.0	2161	C_PPW9	38.5	2861	C_SF9	32.8	2266	C_SFW9	42.6	3280
Overall Average	**29**	**2321**	**Overall Average**	**36**	**2634**	**Overall Average**	**33**	**2263**	**Overall Average**	**42**	**3053**

Maximum flexural loads and flexural strengths for 20 Composite C beams

Beam (C_PP)	Maximum flexural load [N]	Flexural strength [MPa]	Beam (C_PPW)	Maximum flexural load [N]	Flexural strength [MPa]	Beam (C_SF)	Maximum flexural load [N]	Flexural strength [MPa]	Beam (C_SFW)	Maximum flexural load [N]	Flexural strength [MPa]
C_PP1	417.3	34.1	C_PPW1	361.0	30.8	C_SF1	318.1	22.8	C_SFW1	342.8	27.5
C_PP2	336.1	27.0	C_PPW2	357.3	30.7	C_SF2	341.3	27.2	C_SFW2	315.8	27.4
C_PP3	345.2	29.5	C_PPW3	379.0	33.1	C_SF3	338.3	26.2	C_SFW3	366.4	31.3
C_PP4	346.4	31.5	C_PPW4	414.9	32.1	C_SF4	333.1	25.2	C_SFW4	281.7	22.2
C_PP5	422.3	36.8	C_PPW5	383.4	28.3	C_SF5	343.0	27.9	C_SFW5	414.6	32.0
Overall average	**373.5**	**31.8**	**Overall average**	**379.1**	**31.0**	**Overall average**	**334.8**	**25.9**	**Overall average**	**344.3**	**28.1**

Energies absorbed in three-point bending for 20 Composite C beams

Beam (C_PP)	Energy absorbed [J]	Beam (C_PPW)	Energy absorbed [J]	Beam (C_SF)	Energy absorbed [J]	Beam (C_SFW)	Energy absorbed [J]
C_PP1	6.0	C_PPW1	6.1	C_SF1	3.0	C_SFW1	4.8
C_PP2	3.0	C_PPW2	5.0	C_SF2	4.6	C_SFW2	4.2
C_PP3	3.2	C_PPW3	5.4	C_SF3	3.4	C_SFW3	5.6
C_PP4	4.5	C_PPW4	7.3	C_SF4	4.6	C_SFW4	2.8
C_PP5	7.0	C_PPW5	4.3	C_SF5	5.1	C_SFW5	7.1
Overall average	**4.7**	**Overall average**	**5.6**	**Overall average**	**4.1**	**Overall average**	**4.9**
Standard deviation	**1.7**	**Standard deviation**	**1.1**	**Standard deviation**	**0.9**	**Standard deviation**	**1.6**
CV* (%)	**37**	**CV* (%)**	**20**	**CV* (%)**	**22**	**CV* (%)**	**33**
Overall average energy absorbed in bending for Composite C					**4.9 J**		

CV* - Coefficient of variation

Appendix 6: Image showing PVC post loaded in three-point bending

Loading Orientation A

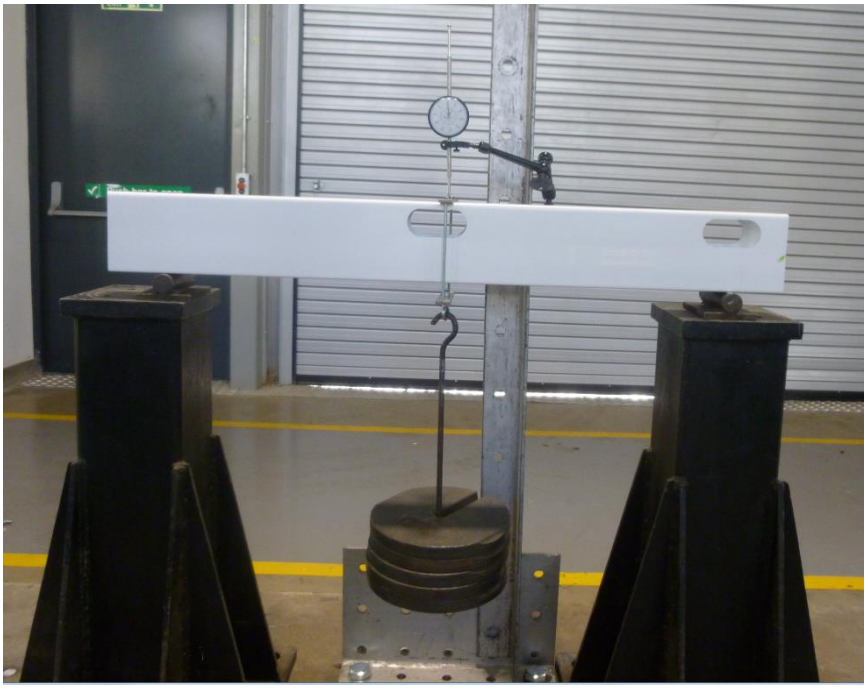

Loading Orientation B

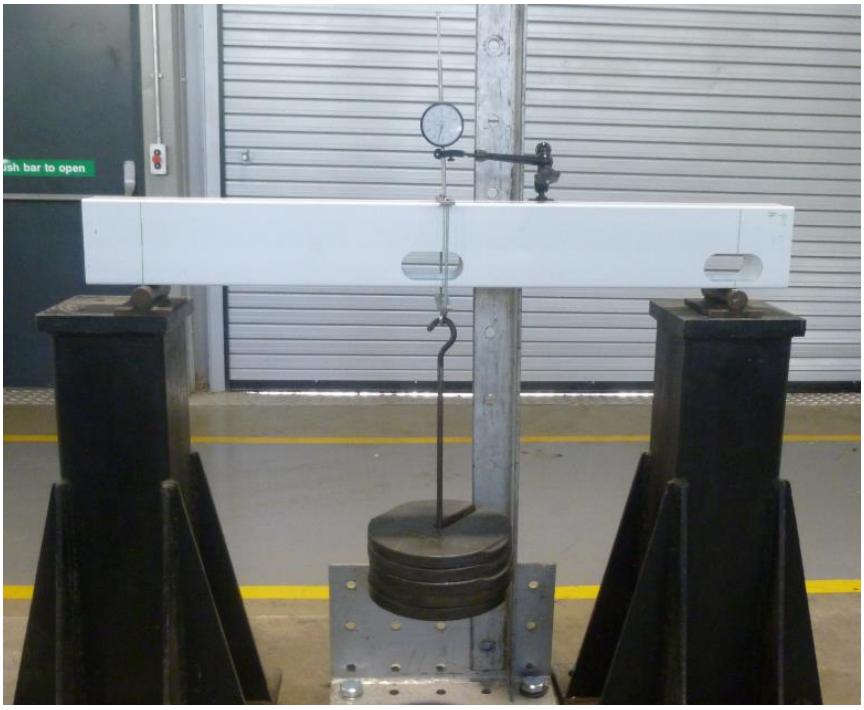

Appendix 7: Uniaxial tensile test results for Composite C materials

Maximum tensile loads, strengths, moduli and energies absorbed for 16 Composite C specimens

Beam	Maximum tensile load [N]	Tensile strength [MPa]	Tensile modulus [GPa]	Energy absorbed [J]
C_PP6	7713	19.4	*N/A*	*N/A*
C_PP7	7483	18.9	2814	2.4
C_PP8	6506	16.3	2786	1.3
C_PP9	6478	16.7	3225	1.3
Average	**7045**	**17.8**	**2942**	**1.7**
C_PPW6	5470	12.7	2325	1.8
C_PPW7	6622	15.9	2995	2.4
C_PPW8	5535	13.5	2702	1.2
C_PPW9	6167	14.9	2681	2.0
Average	**5949**	**14.2**	**2676**	**1.9**
C_SF6	5478	13.1	1992	2.3
C_SF7	5819	13.3	*N/A*	*N/A*
C_SF8	4608	11.0	2645	0.6
C_SF9	5794	13.7	2358	1.6
Average	**5425**	**12.8**	**2332**	**1.5**
C_SFW6	5441	12.6	2577	1.2
C_SFW7	5400	13.4	3100	1.0
C_SFW8	5346	12.9	2407	1.6
C_SFW9	5688	13.9	3045	1.7
Average	**5469**	**13.2**	**2782**	**1.4**

Appendix 8: Width measurements of carpet joint specimens

Width measurements for carpet joint specimens of Series 1 and Series 2

Single-lap joint configuration	Specimen label	Series 1		Series 2	
		Width [w] [mm]	Average width [w] [mm]	Width [w] [mm]	Average width [w] [mm]
Tuft-to-Tuft	T2T_1	101	101.3	60	56.3
		101		58	
		100		55	
		103		52	
	T2T_2	104	100	55	56.3
		100		55	
		101		56	
		95		59	
	T2T_3	99	102.3	58	58.3
		106		58	
		103		60	
		101		57	
Tuft-to-Back	T2B_1	95	97.8	56	56.5
		97		57	
		97		58	
		102		55	
	T2B_2	92	99.3	56	53.5
		106		56	
		97		51	
		102		51	
	T2B_3	99	100.8	50	53.5
		105		51	
		98		59	
		101		54	
Back-to-Back	B2B_1	101	99.5	51	54.3
		96		55	
		100		49	
		101		52	
	B2B_2	98	99.3	57	57.3
		103		54	
		97		56	
		99		62	
	B2B_3	98	101.5	55	54.3
		104		51	
		103		57	
		101		54	
Overall Average			**100.2**	**55.1**	

Appendix 9: Results of the tip-loaded cantilever test on timber and PVC posts

Results of the tip-loaded cantilever test on Timber post (span = 1250 mm)

Load [kg]	Load [N]	Tip deflection [mm] Test 1	Test 2	Test 3	Average deflection [mm]	Moment [M_A] [Nm]	Flexural modulus [E] [MPa]	Rotational stiffness [K] [x 10^5] [Nm/rad]	Angle at Joint [$\emptyset_A$] [x 10^{-4}] [rad]
10	98.1	2.4	2.4	2.5	2.40	123	8111	5.6	2.18
20	196	4.9	5	5	4.96	245		4.4	5.62
30	294	7.4	7.6	7.6	7.50	368		4.1	8.97
40	392	10	10.1	10.2	10.08	491		3.9	12.59
50	491	12.6	12.6	12.7	12.59	613		3.9	15.65
60	589	15.2	15.3	15.3	15.22	736		3.7	19.62
70	687	17.8	18	17.8	17.87	858		3.6	23.80
80	785	20.6	20.5	20.6	20.57	981		3.5	28.38

Results of the tip-loaded cantilever test on PVC post

Load [N]	Deflection [mm]	Deflection [mm]	Deflection [mm]	Average deflection [mm]
0	0	0	0	0.0
40	1.9	1.9	1.9	1.9
80	4.6	5	4.8	4.8
120	7.8	7.8	7.8	7.8
160	11.2	11.5	11.3	11.3
200	14.8	14.8	15	14.9
240	18.4	18.6	18.6	18.5
280	22.4	22.7	22.7	22.6

Appendix 10: Results of the load tests on two-bay timber and PVC fencing structures

Results of the load tests on two-bay timber fence

Load [N]	Deflection at Node A [mm]			Deflection at Node B [mm]			Deflection at Node C [mm]			Average deflection at Node A [mm]	Average deflection at Node B [mm]	Average deflection at Node C [mm]
	Test 1	Test 2	Test 3	Test 1	Test 2	Test 3	Test 1	Test 2	Test 3			
0	0	0	0	0	0	0	0	0	0	0	0	0
100	0.3	0.25	0.25	1.9	2	2	0.2	0.22	0.25	0.27	1.97	0.22
200	0.5	0.55	0.5	3.85	4	3.5	0.5	0.54	0.45	0.52	3.78	0.50
300	0.8	0.75	0.8	5.7	5.6	5.7	0.7	0.74	0.75	0.78	5.67	0.73
400	1.1	1.0	1.0	7.9	7.8	7.3	1.1	1.0	1.0	1.03	7.67	1.03
500	1.3	1.3	1.2	9.7	9.7	9.1	1.2	1.28	1.25	1.27	9.50	1.24
600	1.55	1.52	1.52	11.4	11.5	11.6	1.35	1.52	1.55	1.53	11.50	1.47
700	1.8	1.8	1.73	13.5	13.5	13.1	1.58	1.8	1.73	1.78	13.37	1.70
800	2.1	2.1	1.9	15.4	15.8	15.1	1.8	2.1	2.0	2.03	15.43	1.97
900	2.3	2.3	2.15	17.6	17.6	17.2	2.0	2.3	2.3	2.25	17.47	2.20
1000	2.65	2.6	2.4	19.9	19.3	19	2.2	2.5	2.4	2.55	19.40	2.37
1100	2.9	2.85	2.6	21.5	21.2	20.8	2.6	2.72	2.7	2.78	21.17	2.67
1200	3.2	3.25	2.85	23.7	24	22.8	2.9	2.95	2.82	3.10	23.50	2.89
1300	3.5	3.45	3.2	26	25.2	25.1	3.1	3.03	3.1	3.38	25.43	3.08
1400	3.8	3.68	3.5	28	27.2	27.5	3.4	3.22	3.35	3.66	27.57	3.32

Results of the load tests on two-bay PVC fence loaded at Node B (post spacing = 2000 mm)

Two-bay PVC fence (post spacing = 2000 mm)																				
Load [N]	**Node A**				**Node B (loading point)**				**Node C**				**Node D**				**Node E**			
	Test 1	**Test 2**	**Test 3**	**Average**	**Test 1**	**Test 2**	**Test 3**	**Average**	**Test 1**	**Test 2**	**Test 3**	**Average**	**Test 1**	**Test 2**	**Test 3**	**Average**	**Test 1**	**Test 2**	**Test 3**	**Average**
0	0	0	0	**0**	0	0	0	**0**	0	0	0	**0**	0	0	0	**0**	0	0	0	**0**
100	1.7	2	2	**1.9**	13	12.1	11.9	**12.3**	5.8	5.9	5.7	**5.8**	0.7	1.2	1.1	**1.0**	0	0	0	**0.0**
200	3.7	4	4.2	**4.0**	26.5	27	27.3	**26.9**	11.6	12.4	12.5	**12.2**	1.5	2.2	2.2	**2.0**	-0.1	-0.2	-0.2	**-0.2**
300	6	6.4	6.5	**6.3**	40.2	41	41	**40.7**	17.2	18	18.2	**17.8**	2	2.6	2.6	**2.4**	-0.3	-0.3	-0.4	**-0.3**
400	8.6	9.1	9.3	**9.0**	54.7	55.1	55.6	**55.1**	23	23.8	24	**23.6**	2.4	3	3	**2.8**	-0.5	-0.5	-0.5	**-0.5**
500	11.5	12.3	12.3	**12.0**	69.8	70.8	70.7	**70.4**	29	30	30	**29.7**	2.6	3.3	3.3	**3.1**	-0.7	-0.7	-0.8	**-0.7**
600	15	15.6	15.6	**15.4**	85.7	86.2	85.9	**85.9**	34.9	35.8	35.6	**35.4**	2.8	3.5	3.5	**3.3**	-1	-0.9	-0.9	**-0.9**

Results of the load tests on two-bay PVC fence loaded at Node C (post spacing = 2000 mm)

Two-bay PVC fence (post spacing = 2000 mm)																				
Load (N)	**Node A**				**Node B**				**Node C (loading point)**				**Node D**				**Node E**			
	Test 1	**Test 2**	**Test 3**	**Average**	**Test 1**	**Test 2**	**Test 3**	**Average**	**Test 1**	**Test 2**	**Test 3**	**Average**	**Test 1**	**Test 2**	**Test 3**	**Average**	**Test 1**	**Test 2**	**Test 3**	**Average**
0	0	0	0	**0**	0	0	0	**0**	0	0	0	**0**	0	0	0	**0**	0	0	0	**0**
100	0.3	0.3	0.3	**0.3**	5	4.8	5.2	**5.0**	7.7	7.4	8	**7.7**	5.3	4.4	5.4	**5.0**	0.3	0.3	0.3	**0.3**
200	0.5	0.6	0.5	**0.5**	9.9	9.9	10	**9.9**	15	14.8	15.2	**15.0**	10.2	9.2	10.1	**9.8**	0.5	0.5	0.5	**0.5**
300	0.9	0.9	0.8	**0.9**	15.1	15.3	15.1	**15.2**	22.9	22.8	23	**22.9**	15.5	14.5	15.4	**15.1**	0.7	0.8	0.8	**0.8**
400	1.3	1.3	1.2	**1.3**	20.9	20.7	20.6	**20.7**	31.1	30.8	31	**31.0**	20.8	19.7	20.5	**20.3**	1	1	1	**1.0**
500	1.7	1.6	1.6	**1.6**	26.8	26.4	26.4	**26.5**	39.3	39	39.2	**39.2**	26	24.9	25.9	**25.6**	1.3	1.3	1.3	**1.3**
600	2.1	2.1	2	**2.1**	32.2	32.2	32.2	**32.2**	47.4	47.4	47.4	**47.4**	31.2	30.3	31	**30.8**	1.6	1.7	1.6	**1.6**

Results of the load tests on two-bay PVC fence loaded at Node D (post spacing = 2000 mm)

Two-bay PVC fence (post spacing = 2000 mm)																				
Load [N]	**Node A**				**Node B**				**Node C**				**Node D (loading point)**				**Node E**			
	Test 1	**Test 2**	**Test 3**	**Average**	**Test 1**	**Test 2**	**Test 3**	**Average**	**Test 1**	**Test 2**	**Test 3**	**Average**	**Test 1**	**Test 2**	**Test 3**	**Average**	**Test 1**	**Test 2**	**Test 3**	**Average**
0	0	0	0	**0**	0	0	0	**0**	0	0	0	**0**	0	0	0	**0**	0	0	0	**0**
100	0	0	0	**0.0**	0.5	0.5	0.5	**0.5**	5.2	5.3	5.2	**5.2**	13.2	13	12.7	**13.0**	2.3	2.3	2.2	**2.3**
200	0	-0.1	0	**0.0**	0.7	0.6	0.6	**0.6**	10	10	9.8	**9.9**	26	26	25.5	**25.8**	5.3	5.2	5.1	**5.2**
300	0	-0.15	-0.1	**-0.1**	0.9	0.75	0.8	**0.8**	15.2	14.9	15	**15.0**	40.5	39.8	40	**40.1**	8.7	8.4	8.4	**8.5**
400	0	-0.25	-0.2	**-0.2**	1.3	1.3	1.2	**1.3**	20.3	20	20	**20.1**	54.5	54	54	**54.2**	12.5	12.2	12.2	**12.3**
500	0	-0.3	-0.3	**-0.2**	1.7	1.7	1.7	**1.7**	25.5	25.1	25.2	**25.3**	69	68.5	69	**68.8**	16.7	16.3	16.3	**16.4**
600	0	-0.3	-0.4	**-0.2**	2.1	2	1.9	**2.0**	31.1	30.5	30.3	**30.6**	85	84.1	84.1	**84.4**	21.2	20.6	20.5	**20.8**

Results of the load tests on two-bay PVC fence loaded at Node B (post spacing = 1800 mm)

Two-bay PVC fence (post spacing = 1800 mm)																				
Load (N)	**Node A**				**Node B (loading point)**				**Node C**				**Node D**				**Node E**			
	Test 1	**Test 2**	**Test 3**	**Average**	**Test 1**	**Test 2**	**Test 3**	**Average**	**Test 1**	**Test 2**	**Test 3**	**Average**	**Test 1**	**Test 2**	**Test 3**	**Average**	**Test 1**	**Test 2**	**Test 3**	**Average**
0	**0**	**0**	**0**	**0**	**0**	**0**	**0**	**0**	**0**	**0**	**0**	**0**	**0**	**0**	**0**	**0**	**0**	**0**	**0**	**0**
100	3.3	3.4	3.5	**3.4**	10	10.8	10.8	**10.5**	4.7	5	5.1	**4.9**	1	1.3	1.1	**1.1**	0	-0.05	0	**0.0**
200	7.0	7.4	7	**7.1**	21.7	21.9	21.6	**21.7**	10.5	10.5	10.2	**10.4**	2.4	2.5	2.3	**2.4**	-0.2	-0.15	-0.1	**-0.2**
300	10.4	11.2	10.3	**10.6**	32	32.5	31.4	**32.0**	15	15.3	14.7	**15.0**	3.3	3.4	3	**3.2**	-0.4	-0.35	-0.27	**-0.3**
400	14.3	15.3	14.2	**14.6**	42.7	44.1	42.7	**43.2**	20	20.6	20	**20.2**	4.2	4.2	4	**4.1**	-0.5	-0.5	-0.5	**-0.5**
500	18.4	19.7	18.5	**18.9**	53.7	55.8	53.9	**54.5**	25.2	25.9	25	**25.4**	5.1	5.2	5	**5.1**	-0.6	-0.6	-0.6	**-0.6**
600	22.7	23.7	22.8	**23.1**	65.2	66.8	65.5	**65.8**	30.2	30.8	30	**30.3**	5.9	6	5.8	**5.9**	-0.7	-0.67	-0.65	**-0.7**

Results of the load tests on two-bay PVC fence loaded at Node C (post spacing = 1800 mm)

Two-bay PVC fence (post spacing = 1800 mm)																				
Load (N)	**Node A**				**Node B**				**Node C (loading point)**				**Node D**				**Node E**			
	Test 1	**Test 2**	**Test 3**	**Average**	**Test 1**	**Test 2**	**Test 3**	**Average**	**Test 1**	**Test 2**	**Test 3**	**Average**	**Test 1**	**Test 2**	**Test 3**	**Average**	**Test 1**	**Test 2**	**Test 3**	**Average**
0	0	0	0	**0**	0	0	0	**0**	0	0	0	**0**	0	0	0	**0**	0	0	0	**0**
100	1	0.9	0.7	**0.9**	5.5	5	4.5	**5.0**	8	7.6	7	**7.5**	5.1	4.8	4.6	**4.8**	0.6	0.8	0.6	**0.7**
200	1.7	1.5	1.5	**1.6**	9.7	9.2	9	**9.3**	14.5	14.2	13.9	**14.2**	9.3	9.1	9	**9.1**	1.1	1.2	1.1	**1.1**
300	2.4	2.4	2.3	**2.4**	14.6	14.3	13.8	**14.2**	21.8	21.3	21	**21.4**	13.8	13.5	13.4	**13.6**	1.8	1.9	1.8	**1.8**
400	3.3	3.2	3.2	**3.2**	19.4	19	19.1	**19.2**	29	28.4	28.7	**28.7**	18	17.7	18	**17.9**	2.6	2.6	2.6	**2.6**
500	4.2	4	4	**4.1**	24.1	23.8	23.4	**23.8**	35.6	35.4	35.1	**35.4**	22	21.8	21.9	**21.9**	3.4	3.4	3.4	**3.4**
600	5.4	5	5	**5.1**	29.6	28.9	28.7	**29.1**	43.4	42.7	42.7	**42.9**	26.8	26.2	26.4	**26.5**	4.6	4.3	4.4	**4.4**

Results of the load tests on two-bay PVC fence loaded at Node D (post spacing = 1800 mm)

Two-bay PVC fence (post spacing = 1800 mm)																				
Load (N)	**Node A**				**Node B**				**Node C**				**Node D (loading point)**				**Node E**			
	Test 1	**Test 2**	**Test 3**	**Average**	**Test 1**	**Test 2**	**Test 3**	**Average**	**Test 1**	**Test 2**	**Test 3**	**Average**	**Test 1**	**Test 2**	**Test 3**	**Average**	**Test 1**	**Test 2**	**Test 3**	**Average**
0	**0**	**0**	**0**	**0**	**0**	**0**	**0**	**0**	**0**	**0**	**0**	**0**	**0**	**0**	**0**	**0**	**0**	**0**	**0**	**0**
100	0	0.1	0.15	**0.1**	0.5	0.8	1.2	**0.8**	4.3	5.1	5.5	**5.0**	10.8	11.5	12	**11.4**	3.2	3.7	4.1	**3.7**
200	-0.05	0.1	0.15	**0.1**	1.5	1.4	1.6	**1.5**	9.5	9.3	9.5	**9.4**	22.3	22.3	22.7	**22.4**	7.8	8	8.6	**8.1**
300	-0.05	0.1	0.15	**0.1**	2.3	2.3	2.4	**2.3**	14.2	14.3	14.2	**14.2**	33.5	34	34	**33.8**	12.6	13.1	13.5	**13.1**
400	-0.1	0.1	0.5	**0.2**	3.3	3.1	3.2	**3.2**	19.1	18.8	18.8	**18.9**	45	45.1	45.1	**45.1**	17.4	17.9	18.3	**17.9**
500	-0.1	0.1	0.5	**0.2**	4.3	4	4.1	**4.1**	24.3	23.4	23.5	**23.7**	56.9	56.3	56.5	**56.6**	22.4	22.6	23.1	**22.7**
600	-0.25	-0.1	0.1	**-0.1**	5.2	4.9	5.1	**5.1**	29.7	28.5	28.5	**28.9**	69.6	68.5	68.5	**68.9**	27.7	27.8	28.2	**27.9**

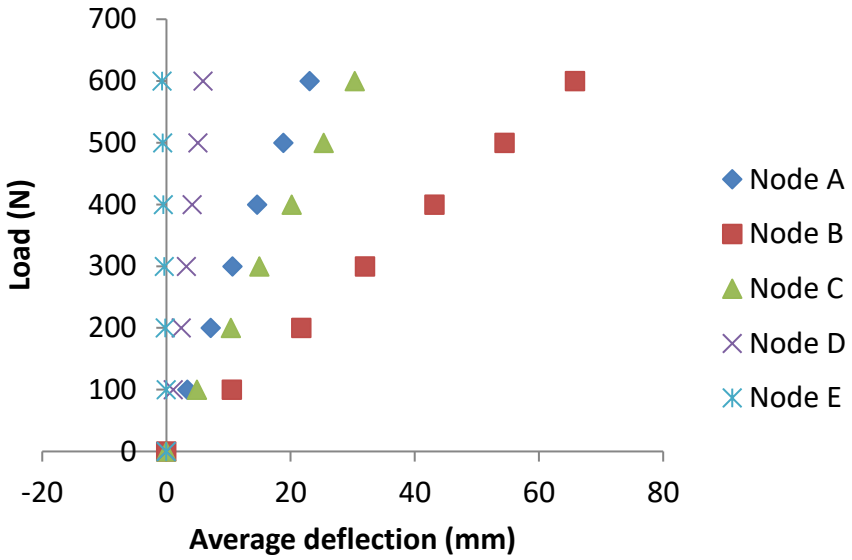

Load versus average deflection responses at Nodes A – E of the two-bay PVC fence loaded at Node B (post spacing = 1800 mm)

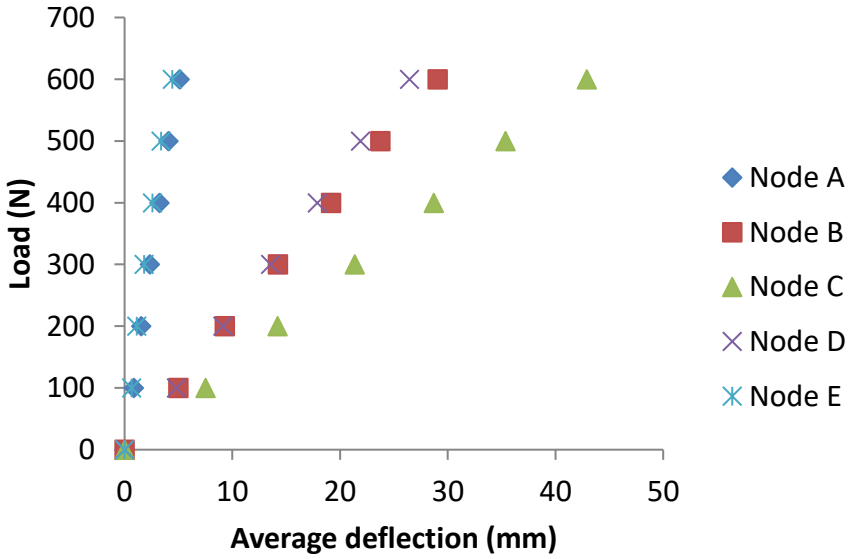

Load versus average deflection responses at Nodes A – E of the two-bay PVC fence loaded at Node C (post spacing = 1800 mm)

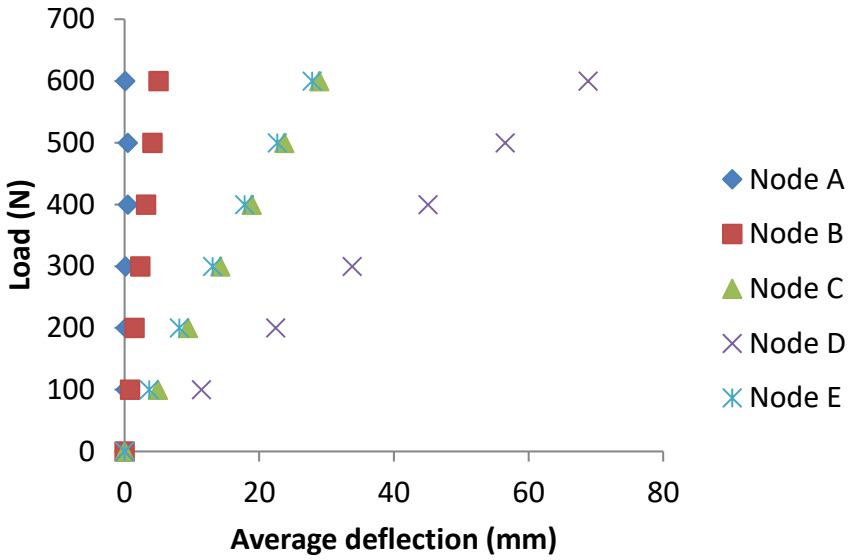

Load versus average deflection responses at Nodes A – E of the two-bay PVC fence loaded at Node D (post spacing = 1800 mm)